# DOCTORAL THESIS

Title Chemical Modulation of Identified *Hit* Compounds as Apoptosis Inhibitors


Presented by Miriam Corredor Sánchez

Centre Institute of Advanced Chemistry of Catalunya (CSIC)
IQS (URL)

Departments Chemical and Biomolecular Nanotechnology (IQAC, CSIC)
Organic Chemistry (IQS)

Directed by Prof. Àngel Messeguer and Dr. Ignacio Alfonso

Tutored by Dr. Jordi Teixidó

**Als meus pares i a en Llorenç**

# Acknowledgments

This thesis would not have been possible without the help of so many people in so many ways and I would like to mention some of them:

Al professor Àngel Messeguer, director d'aquesta tesi per confiar en mi des del primer moment i haver-me donat l'oportunitat de desenvolupar un projecte d'investigació tan interessant. Gràcies pels consells donats i els ànims quan semblava no haver-hi llum, també per les paraules de reconeixement en els bons moments.

Al Dr. Ignacio Alfonso, co-director de ésta tesis. Gracias Nacho porque sin tu ayuda no sé si ahora estaría terminando éste largo periodo. Gracias por estar siempre dispuesto a escuchar mis infinitos problemas, tanto los graves como los que yo veía graves y tener las soluciones para todos ellos.

Al Dr. Jordi Bujons, per haver volgut formar part d'aquest treball, col·laborar amb tota la part teòrica i per resoldre els dubtes computacionals o bioquímics que sempre em sorgien.

To Dr. Dietmar Appelhans from the Leibniz Institute of Polymer Research in Dresden for accepting me in his research group and proposing interesting possibilities to try with my molecules. I also would like to thank my colleagues in the IPF, to Robert and Jens for making the office an entertaining place. To Sandra for becoming a nice friend and a great help in the IPF. To Burak, Hendrik, Francesco and Emrah for the lunch times, trips and the amazing time we spent together. To Franka and Tina for the "klein" beers, parties, weird theaters and nice bi-language conversations. Specially to Damien, for your help in the laboratory, for introducing to me the friends' group and for finding activities to make the life in a foreign country much better.

Al Dr. Jordi Teixidó per haver acceptat ser tutor d'aquesta feina i per interessar-se sempre per mi personal i professionalment.

Al grupo del Prof. Enrique Pérez-Payá por la realización de los ensayos biológicos de los compuestos, especialmente a Mar y Mónica.

A tota la gent que ha compartit el dia dia amb mi al laboratori. Primerament, els que ja no hi són: A Carina y Cristina por ayudarme a la adaptación cuando llegué y compartir cafés, bromas y problemas juntos. A Fede, por tus días de alegría despreocupada. A Miquel por tus ganas de ayudar y estar ahí cuando surge cualquier problema y te pedía heelp. A Dani por ser un mercenario de la química y compartir problemas con la fase sólida. A la Gloria perquè has estat molt important des de que vaig entrar al laboratori i amb els anys l'amistat s'ha fet més gran. Els caps de setmana de visita per Deutschland van ser increibles i les xerrades amb una bona cervesa alemana no van tenir preu, només espero que amb la distancia no perdem tot el que teníem. A Chris por tu positivismo ante la vida, mostrarme tu manera de verla y por seguir ahí

después de tanto tiempo. De los que se han ido me queda Ana, que fuiste de las últimas en venir, pero con el poco tiempo que has estado en el 309 has dejado una gran huella.

A tota la gent del LAB309 que encara comparteix les meves alegries i les meves penes. A tots gràcies pels esmorzars, dinars diaris i també pels sopars de laboratori, festes i congressos compartits, perquè sense vosaltres no hagués estat el mateix. A Esther, por las charlas a primera hora sobre cualquier tema, por el frikismo y por los problemas del lab compartidos. A la Laura, t'agraeixo la teva alegria diaria, perquè encara que les coses no surtin, sempre tens punts de vista positius i el teu riure s'encomana encara que jo tingui un mal dia. A Cristian por ser como eres, porque entre tanta chica no es fácil y tu siempre estás dispuesto a escuchar. Gracias también por esos desayunos mañaneros que sino me moriría de hambre... A en Joan i l'Enrico per la vostra paciència amb les lloques del lab Nord, pels cafès i els tuppers compartits and to Inci because it has been fantastic to meet you and to share and keep sharing nice days in the lab.

Gracias a Asun y Sandra, casi no tengo palabras para agradeceros todo lo que habeis hecho por mi durante éstos años. A las dos por nuestras confidencias personales, por ayudarme y escucharme en los problemas de la vida o de la química, así como compartir conmigo los vuestros. Asun, gracias porque desde que llegaste al lab nos transmitiste tu alegría y nos enseñaste que hay que vivir motivados cada día y no solo los fines de semana. Gracias por confiar conmigo y porque sé que estás ahí cuando te necesito. A Sandra, porque durante la tesis me has ayudado muchísimo con tu experiencia en temas parecidos, con los mismos problemas químicos y biológicos… Gracias también por tu sinceridad, tu opinión aceptada cuando es algo bueno o algo malo, pero sé que siempre es por mi bien. Y ahora que somos VISION, me alegro que seas tú mi compañera con experiencia, alguien que me ayuda en todo sin pedir nada a cambio.

A la gent de la meva uni per haver seguit el meu progrés des de que vam acabar la carrera juntes. A la Jessi pels cafès de diumenge tarda posant-nos al dia i donant-me sempre la opinió sincera que tant necessito. A la Marta perquè sempre has estat molt important i m'encanta que encara seguim comptant l'una amb l'altra, tant dins com fora del CSIC. A la Marina, la Ingrid i la Txell pels sopars o dinars compartits amb la resta i per no desconnectar-nos del tot.

A l'Alba, t'agraeixo moltíssim que durant les teves curtes visites a Barcelona traiéssis sempre temps per quedar amb mi i poder mantenir l'amistat que es va consolidar a finals de la carrera i que des de llavors és tant important per mi.

A les meves amigues de sempre, l'Anna, la Ru, la Eli, la Roser, la Rosi, la Nunu, la Lídia i la Gemma, perquè tot i que hem crescut i ens anem distanciant, els moments que trobem per estar juntes sempre valen la pena.

A en Xevi per compartir amb nosaltres la teva manera de ser, per ser el millor vecinuu que podriem tenir i per haver-nos fet la distància més fàcil. A l'Ori, l'Anni, la Gina i en Jordi per totes

les quedades de divendres, i els sopars i copes de dissabtes que permeten desconnectar del dia a dia.

A en Llorenç i l'Ana per preocupar-se per mi i interessar-se sempre per la meva vida. A en Gerard i la Grace per totes les hores compartides, pels sopars al pis, findes a Capafonts i perquè sou genials.

Als meus pares, perquè sense ells res de tot això hagués estat possible, perquè són les persones que més confien en mi i creuen que puc fer qualsevol cosa. Per ajudar-me en tot sense demanar res. Sou els millors que podria tenir. Gràcies.

Finalment vull agrair a la persona que comparteix amb mi el dia a dia. Gràcies Llu per haver-me donat el teu suport tot aquest temps per arribar a aquest punt. Per aguantar les queixes en mals dies, motivar-me o ajudar-me a relativitzar els problemes i fer-me buscar solucions. També per alegrar-te dels meus èxits i valorar-me sempre.

Thanks to all of you, because although it has not been easy, finally, we've managed it.

# SUMMARY

Apoptosis is a biological process relevant to different human diseases stated that is regulated through protein-protein interactions and complex formation. In this context, one point of regulation is the formation of the multiprotein complex known as apoptosome. Consequently, this complex is of interest for the development of apoptosis modulators. In our group, it has been previously reported a peptidomimetic compound bearing a 3-substituted-piperazine-2,5-dione moiety as a potent apoptotic inhibitor. Structural studies of this compound showed the presence of *cis/trans* isomers of the exocyclic tertiary amide bond in slow exchange, which should be of high relevance for off-target interaction in front of the biological target. This information encouraged us to perform an isosteric replacement of the amide bond by a 1,2,3-triazole moiety, where different substitution patterns would mimic different amide rotamers. The syntheses of these restricted analogs have been carried out using the Ugi multicomponent reaction followed by an intramolecular cyclization. Unexpectedly, for one of the proposed structures, a novel β-lactam compound was formed.

All synthesized compounds showed to efficiently inhibit apoptosis, *in vitro* and in cellular extracts, with slight differences for the corresponding regioisomers. Noticeably, the compound bearing the new β-lactam scaffold showed the highest inhibitory activity. On the other hand, computational studies also support the hypothesis that these new families of inhibitors exert their action by binding to Apaf-1, one of the components of the apoptosome complex.

Due to the formation of the unexpected β-lactam scaffold, a reactivity study has been carried out to explain the course of the intramolecular cyclization of the Ugi adducts. In order to be able to modulate this cyclization, a small library of compounds bearing both heterocyclic scaffolds has been synthesized and their activities as apoptosis inhibitors have been evaluated.

Moreover, couplings between some of the apoptosome inhibitors and different glycodendrimer moieties have been carried out to improve the properties of our compounds as drug candidates.

As a conclusion, a new family of compounds has been designed, synthesized and characterized, and most of them showed good apoptosis inhibitory activities *in vitro* and in cellular extracts. We deem that the reduction of the conformational freedom achieved in this new family of inhibitors could be fundamental to increase the selectivity, which is a highly important condition when regulating such a delicate process

# Index

## Abbreviations

| | |
|---|---|
| AIDS | Acquired immunodeficiency syndrome |
| DNA | Deoxyribonucleic acid |
| ATP | Adenosine triphosphate |
| dATP | Deoxyadenosine triphosphate |
| ADP | Adenosine diphosphate |
| dADP | Deoxyadenosine diphosphate |
| CARD | Caspase Recruitment Domain |
| Apaf-1 | Apoptosis Protease-Activating Factor-1 |
| NOD | Nucleotide-binding Oligomerization Domain |
| HTS | High Throughput Screening |
| DKP | Diketopiperazine |
| HOMO | Highest Occupied Molecular Orbital |
| LUMO | Lowest Unoccupied Molecular Orbital |
| CuAAC | Copper Azide-Alkyne Cycloaddition |
| RuAAC | Ruthenium Azide-Alkyne Cycloaddition |
| Ugi-4CC | Ugi 4 Components Coupling |
| MCR | Multicomponent Reaction |
| Boc | *tert*-Butyloxycarbonyl |
| NMR | Nuclear Magnetic Resonance |
| DCM | Dichloromethane |
| IBX | 2-Iodoxybenzoic acid |
| DMF | Dimethylformamide |
| ACN | Acetonitrile |
| HSQC | Heteronuclear Single Quantum Coherence |
| HMBC | Heteronuclear Multiple Bond Correlation |
| TLC | Thin Layer Chromatography |
| THF | Tetrahydrofuran |
| NOESY | Nuclear Overhauser Effect Spectroscopy |
| $IC_{50}$ | Drug Concentration causing 50% inhibition |
| NBD | Nucleotide Binding Site |
| RBDD | Receptor-Base Drug Design |

| | |
|---|---|
| MM/GBSA | Molecular Mechanics /Generalized Born Surface Area |
| PDB | Protein Data Bank |
| IFD | Induced Fit Docking |
| HMQC | Heteronuclear Multiple-Quantum Correlation |
| GIAO | Gauge-Invariant Atomic Orbital |
| 2,4-diCl-phen | 2,4-Dichlorophenethyl |
| Bn | Benzyl |
| *p*-F-phen | *p*-Fluorophenethyl |
| CIGAR | Constant time Inverse-detection Gradient Accordion Rescaled |
| EtOAc | Ethyl Acetate |
| HPLC | High-performance Liquid Chromatography |
| HRMS | High-Resolution Mass Spectrmetry |
| TFA | Trifluoroacetic acid |
| βLac | β-Lactam |
| DBU | 1,8-Diazabicyclo[5.4.0]undec-7-ene |
| TS | Transition State |
| PEI | Polyethyleneimine |
| PPI | Poly(propylene imine) |
| HOBt | Hydroxybenzotriazole |
| DIPEA | N,N-Diisopropylethylamine |
| EDC | 1-Ethyl-3-(3-dimethylaminopropyl)carbodiimie |
| PEG | Polyethylene Glycol |
| LILBID-MS | Laser Induced Liquid Bead Ion Desorption |
| BOP | Benzotriazol-1-yl-oxy-tris(dimethylamino)phosphonium hexafluorophosphate |
| TEA | Triethylamine |
| NHS | *N*-Hydroxysuccinimide |
| EDTA | Ethylenediaminetetraacetic acid |
| EGTA | Ethylene Glycol Tetraacetic Acid |
| DTT | Dithiothreitol |
| PMSF | Phenylmethylsulfonyl fluoride |
| DAB/Am64 | Polypropylenimine tetrahexacontaamine Dendrimer, Generation 5.0 |

# 0. Introduction

## 0.1. Apoptosis

Apoptosis is a fundamental mechanism of programmed cell death that is physiologically and genetically regulated and plays a central role in development, normal cell turnover and immune system function.[5] Defects in appropriate suppression of apoptosis are observed in cancer pathogenesis[6] and autoimmune disorders,[7] while anomalous induced apoptosis plays an important role in acquired immunodeficiency disease (AIDS),[8] neurodegenerative and heart diseases.[9, 10]

Diverse apoptotic stimuli, including activation of cell surface death receptors, anti-cancer agents, irradiation, lack of survival factors, and ischemia,[11] induce signalling cascades that activate the caspase family of cysteine aspartyl proteases. The mechanism of apoptosis is executed by a family of highly conserved proteases known as caspases.[12] These caspases are essential to the apoptotic process, as they are required for the initiation and execution of programmed cell death. Effector caspases (e.g., caspases-3 and-7) are responsible for the disassembly of cellular components,[13] while initiator caspases (e.g., caspases-8,-9 and -10) are responsible for the activation of effector caspases. Defined apoptotic signals activate the mitochondria-mediated or intrinsic pathway that uses caspase-9 as its initiator. Caspase-9 activation is triggered by the release to the cytoplasm of propapototic proteins from the mitochondrial inter-membrane space, cytochrome *c* and Smac/Diablo,[14,15] when apoptosis-inducing signals, such as DNA damage or metabolic dysfunction are perceived by the cell.[16]

### 0.1.1. Apoptosome

The formation of the macromolecular complex named apoptosome is a key event in this intrinsic apoptosis pathway. The apoptosome is a holoenzyme multiprotein complex formed by cytochrome *c*-activated Apaf-1 (apoptosis protease-activating factor), dATP, and procaspase-9.[17] When cytochrome *c* is released from the mitochondria, it binds to Apaf.1 triggering a conformational change and the hydrolysis of the Apaf-1 bound dATP/ATP. In a process dependent on the hydrolysis of ATP or dATP to ADP or dADP respectively, the Apaf-1-cytochrome *c* heterodimers[15, 18] assemble into a seven Apaf-1/cytochrome *c*-based wheel-like apoptosome, where the Apaf-1 caspase recruitment domain (CARD) is now accessible to bind to the CARD domain of procaspase-9.[18-20] Then, the activated caspase-9 cleaves and activates executioner caspases such as caspase-3.[5, 21] (Figure 0.1).

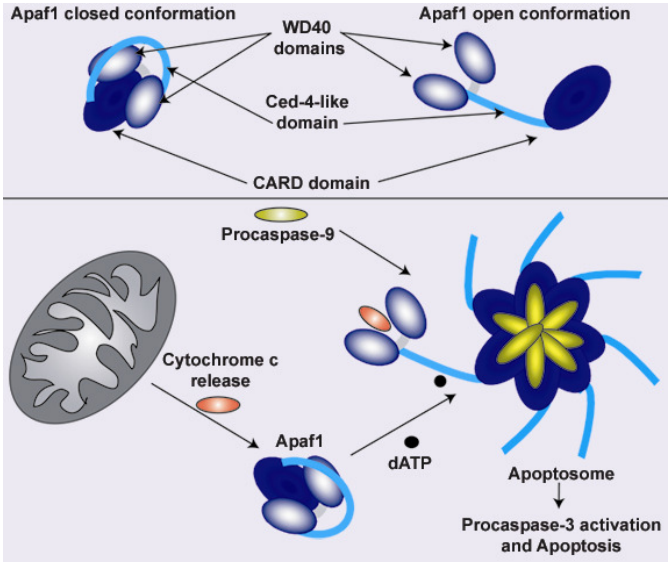


**Figure 0.1:** Conformational changes in the Apaf-1 molecules lead to the apoptosome formation and activation of the apoptotic cascade.[22]

Apaf-1 is a rather large cytoplasmatic protein (~130 kDa) that carries multiple functional domains. First an *N*-terminal caspase activation recruitment domain (CARD). Then, a CED4 homology domain (which includes the dATP/ATP-binding motif), which is responsible for Apaf-1 conformational changes and it is called NOD (Nucleotide oligomerization domain). Finally, the C-terminal WD40 repeats domain, which alllows interactions with Cyt *c* and promotes the oligomerization.[23] This domain can bind the CARD domain but it can probably interact with other apoptotic regulator proteins as well.[22]

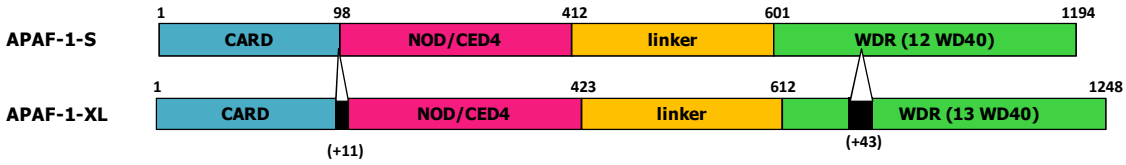


**Figure 0.2:** Structural domains and Apaf-1-S and Apaf-1-XL isoforms.

In cells, before the release of cytochrome *c* from the mytochondria, Apaf-1 remains in an inactive or closed conformation, because the WD40 domain blocks the CARD domain as a negative mechanism of autoregulation.[24] As already explained, the cytochrome *c* induces a conformation change in Apaf-1 to an open conformation which exhibits an oligomerization surface and shows the CARD domain. The dATP union to Apaf-1 in this open conformation is then available and induces a second conformational change in Apaf-1 that helps the oligomerization to form the apoptosome.

### 0.1.2. Apoptosis as therapeutic target

Defects in the regulation of apoptosis are at the root of a variety of diseases. When cells acquire resistance to induction and execution of apoptosis it frequently correlates with cancer or autoimmune disease. Thus, important efforts to new anti-cancer therapies rely on inducing apoptosis. In contrast, tissue infarction, ischemia-reperfusion damage, degenerative diseases, and AIDS showed in common excessive apoptosis-mediated unwanted cell death.[25, 26] To identify molecules that could ameliorate disease-associated excessive apoptosis, drug discovery efforts initially targeted the inhibition of caspase activity, particularly the effector caspase-3.[27] However, caspase-3 inhibitors have encountered problems in their pharmacological development. Peptidomimetic inhibitors bearing such requirements have been identified, but they are not compatible with achieving potent cell-based activity.[28] The activity of most of the caspase inhibitors is greatly attenuated, and even in the presence of cell extracts the reduction in potency is, in most cases, up to two orders of magnitude in comparison to isolated caspases.[29] Thus, there is a considerable need for more selective, stable and cell permeable caspase inhibitors.

Alternatively, protein-protein interactions upstream of caspase activation can also be relevant points of intervention for the development of modulators of apoptosis pathways. Recent data proposed the formation of the multiprotein complex apoptosome as an interesting target for the development of apoptotic modulators.[17, 30-32] Understanding the mechanism of functional activation of the apoptosome has helped to define prospective targets for treating deregulated apoptosis that is associated with human pathologies.[33] Inappropriate apoptosome activity has been shown to play a role in neurodegenerative disorders and its supression by biological tools provided resistance to apoptosis induction.[34, 35] Inactivation of the apoptosome might provide a therapeutic avenue for treating not only neurodegenerative but other pathological disorders as ischemia, cardiac and renal failure.

As previously mentioned, the chemical modulation of the apoptosome represents potential pathways for the development of new therapeutic strategies. In this context, Apaf-1 has to be considered as an attractive target for the development of such modulators; however, small molecules that regulate Apaf-1 have yet to be discovered. Before mitochondrial-dependent apoptosis induction, Apaf-1 is monomeric, inactive and the CARD domain is not accessible. [15] Only upon cytochrome *c* release, Apaf-1 is activated by dATP/ATP-dADP/ADP exchange and forms the apoptosome.[18, 19] With these precedents, the pharmacological target Apaf-1 can be dually seen as a “classical” ATP hydrolase or, alternatively, as a protein-protein interaction-based target. To our knowledge, no successful attempts to inhibit the hydrolase activity with small molecules have been reported. The studies carried out since this project started were addressed to the protein-protein interaction-based formation of the apoptoosme. As Apaf-1 was a new target, the drug discovery process was based in the screening of large collections of compound libraries in a suitable high throughput screening (HTS) format. Fortunately, the group

of Dr. Enrique Pérez-Payá (CIPF, Valencia) developed an efficient *in vitro* and *ex-vivo* methodology for identifying molecules inhibiting the apoptosome formation.[27].

## 0.2. Peptidomimetics as potential *hits*

Oligomers of *N*-alkylglycines, also known as peptoids, constitute a family of non-natural molecules attractive for the drug discovery process due to their broad variety of biological activities and to the proteolytic stability that they exhibit.[36-38] They are structuraly differenced from peptides because the side chains are linked to the nitrogen atom of the amide bond and not to the α carbon. (Figure 0.3)


**Figure 0.3:** Structure of a peptoid and a peptide, where $R^1$, $R^2$ and $R^3$ represent the diversity introduced by their side chains.

This structural difference confers to peptoids a higher stablity to the hydrolysis and less polarity, features that are translated to a high resistance to proteases and a better intestinal absorption. Although peptoids can adopt secondary structures depending on their size and the residues linked to the backbone nitrogens,[39] in general they are highly flexible molecules and have higher conformational freedom than peptides.[40] In peptoids the *cis* conformation of the amide bonds that connect the monomer residues can be more highly populated than in peptides.[41, 42] Nevertheless, not all the *cis/trans* conformational isomers of the different amide bonds present in a defined peptoid will be biologically active in front of a specific target due to the high specifity of the ligand-receptor interaction.

Taking advantatge that short peptoids have been subject of intensive research due to their potential interest in drug discovery, the group of Rabenstein reported the use of NMR tecniques to study the *cis/trans* isomerization derived from the rotation of the amide bonds of small peptoid models.[43] These authors observed a slow *cis/trans* exchange rate for even the most labile of the amide bonds between the two-C terminal residues. This feature can be of importance with respect to the on/off rate for the ligand-receptor binding or when facing undesired interactions with other targets causing some secondary effects. Thus, peptoid *hits* require some structural optimization. One possibility is the generation of rings in the structure, such as six or seven-membered ring cycles to constrain the conformational mobility.

2,5-Diketopiperazines (DKP) are peptidomimetic structures bearing a six-membered heterocycle and are characterized for possessing a relatively rigid skeleton where different pharmacophoric groups can be attached. (Figure 0.4).

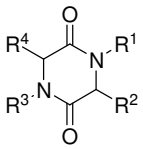

**Figure 0.4:** DKP structure.

The DKPs show selectivity in the recognition of opioid receptors[44] and some other uses were identified, such as ligands of the neurokinin-2 receptor or competitive antagonists of the natural product substance P in the neurokinin-1 receptor.[45] Combinatorial libraries based on DKP skeletons compounds as collagenase-1[46, 47] inhibitors or bradykinins antagonists[48] have also been described. More recently, new bioactive compounds agonists of the FSH receptor,[49] and potential and selectives antagonists of the oxytocin recetor[50, 51] have been identified.

The formation of DKPs has been considered in some cases an undesired secondary reaction when performing some peptidic sequences. They would be formed after an intramolecular attack of the *N*-terminal amino group to the carbonyl group of the second residue causing the excision of the peptidic chain. (Figure 0.5)[52]

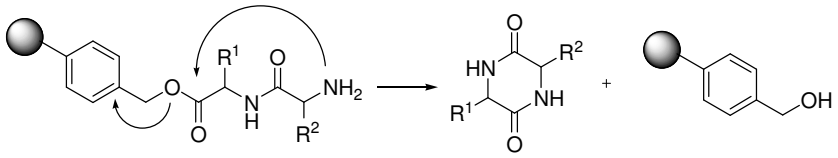

**Figure 0.5:** DKP formation through the intramolecular attack of the *N*-terminal group.

The formation of the DKPs has been widely studied.[52] Different procedures can be followed, such as the synthesis of the lineal dipeptide using conventional coupling agents, the coupling of deprotected aminoacids catalized by acylases[53] or the Ugi multicomponent rection.[54, 55]

Scott *et al.*[56] developed a new route for the synthesis of non-peptidic DKPs libraries where initially α-bromocarboxylic acids were coupled to the polymeric support followed by a nucleophylic substitution with a variety of amines. (Figure 0.6) This strategy was developed later in our research group for the identification of selective inhibitors to the acetylcholinesterase from a DKPs library.[57]

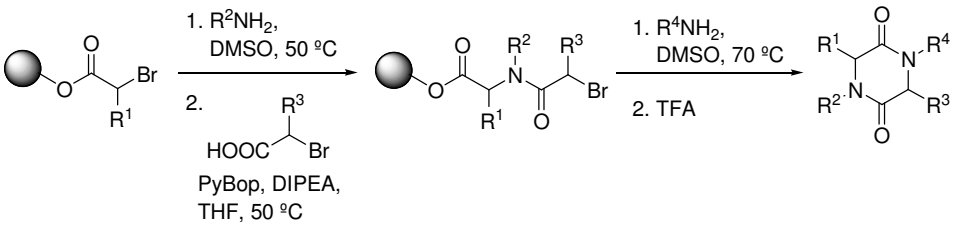


**Figure 0.6:** Synthesis of DKPs using α-bromocarboxylic acids and primary amines.

## 0.3. Group background

A library of *N*-alkylglycines[58] was assayed to find molecules that inhibit the apoptosome formation with a methodology that was established in the laboratory of Prof. Enrique Pérez-Payá using a reconstitutive apoptosome assay. This screening lead to the identification of a *hit* peptoid called N15-20-15. (Figure 0.7)

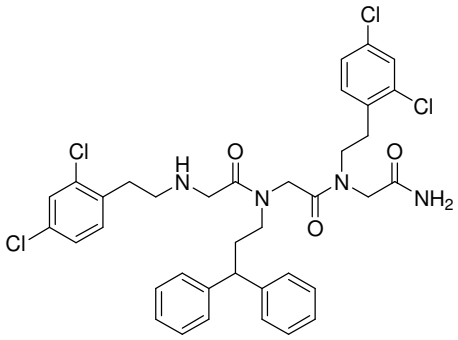

N15-20-15C

**Figure 0.7:** *Hit* peptoid identified as inhibitor of the apoptosome formation.

In contrast with the wide possibilities of identifying *hits* againts pharmaceutical targets the high conformational flexibility given for the free rotation of the amide bonds of peptoids can generate selectivity problems because of undesired off-target interactions. In our casee, this drawback was counterbalanced by a second-generation of peptidomimetics in which the original conformational flexibility was restricted to a certain extent. The formal cyclization through selected points of the peptoid molecule leads to constrained analogues that improved their potency and selectivity.[59]

The hydrophobicity of this compound also caused some problems in the biological assays reproducibility and new analogues of N15-20-15C were designed and synthesized. The analogues synthesized contained a charged residue and the solubility in the *in vitro* assays was improved and the therapeutic potency was demonstrated.[27] Despite this improvement, these compounds showed problems in the cellular extracts assays and high cytotoxicity; thus, some strategies were designed to facilitate the internalization of the compounds into the cell. First of all, the synthesis of peptide-peptoid conjugates to improve the efficiency in translocating the

plasmatic membrane. Secondly, the synthesis of conformationally restricted analoges derived from this peptoid to delimit its flexibility and to avoid inespecific interactions; and finally the synthesis of polymer-drug conjugates to improve the intracellular biodisponibility of the inhibitors. This last strategy is explained in Chapter 4.

The first strategy was developed in the laboratory of Prof. Enrique Pérez-Payá. The peptoid was linked to two penetrating peptides previoulsy described due to their capacity to facilitate the cellular internalization (TAT-peptoid and PEN-peptoid).[60, 61,62] Both compounds showed activity in cellular extracts, but the antiapoptotic activity was not reproducible when working in cell lines, in addition to show inespecific cellular toxicity.[63]

Covalent constraints have been explored in peptoid research mainly by employing macrocyclization between side chains,[64] head-to-tail strategies[65] or Ugi four- and three component reactions.[66] In our group, from the different possibilities contemplated to obtain constrained peptidomimetics derived from the identified peptoid *hits*, those approaches that generated the novel 7-substituted perhydro-1,4-diazepine-2,5-dione (**A**) and the 3-substituted 1,4-piperazine-2,5-dione (**B**) derivatives were selected (Figure 0.8). In these systems, two of the three tertiary amide bonds present in the molecules are forced to adopt the *cis* configuration by the heterocycle formation. Both compounds were shown to be potent inhibitors of the apoptosome formation and capable of decreasing cell death in different cellular models of apoptosis.[5]

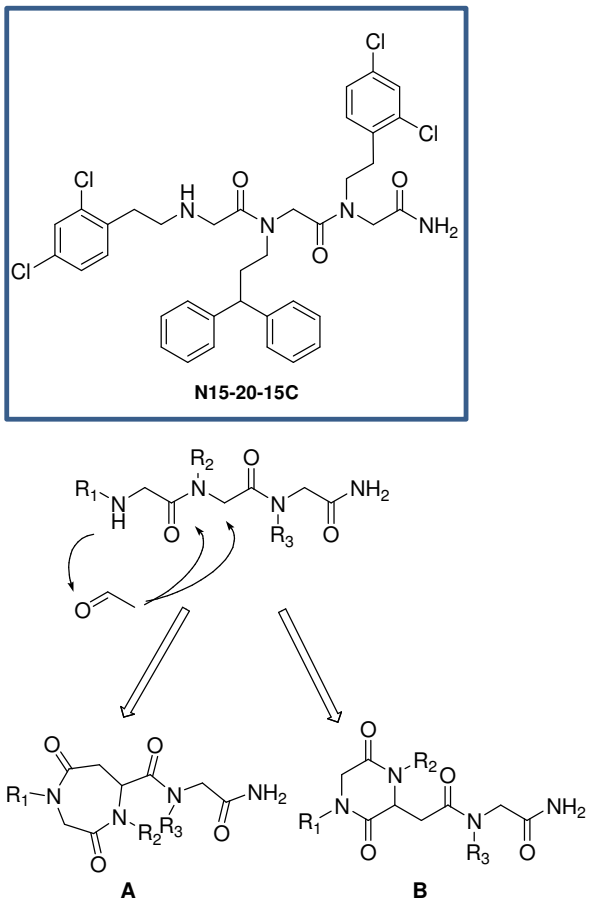


**Figure 0.8:** Peptoid **N15-20-15C** identified as inhibitor of the formation of the apoptosome its formal chemical modulation to generate the heterocyclic analogues **A** and **B**.[59]

Our group reported an efficient solid-phase-based synthetic approach to the peptidomimetic families of **A** and **B**.[59] (Figure 0.8). Moreover, an NMR-based structural study of compounds **QM31** and **1** (Figure 0.9) in different solvents was carried out to determine the thermodynamic and kinetic parameters that define the relative stability of the *cis/trans* conformers potentially present in the exocyclic amide bond. Such amide bond is the only one that still shows conformational flexibility when compared to the original peptoid *hit*. The conformation of compounds **A-B** in solution was important in order to understand their biological activity, as well as for the future re-design and optimization of the next generation of inhibitors that are presented in this thesis.

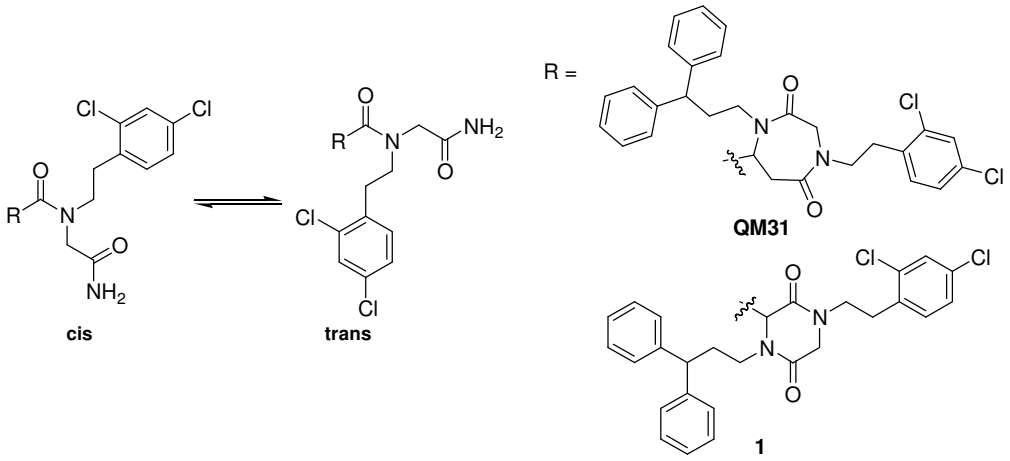


**Figure 0.9:** Dynamic process responsible for the conformational behavior of compounds **QM31** and **1**. [59]

The conformational studies showed a large population of *cis* amide isomers. It has been recently reported that the *trans* configurations in peptoids are predominant in solution, although important proportions of the *cis* rotamers are also present.[43] In addition, the *trans* (*cis*) configuration is favored even more when the other amide bonds have *trans* (*cis*) disposition. In these peptidomimetic systems two amide bonds are frozen in a *cis* configuration due to the constraints of the corresponding cyclic structure. Accordingly, an increased proportion of the *cis* rotamer should be expected for the free exocyclic amide bond and is exactly what was observed. It was demonstrated that the *cis/trans* ratio is highly affected by the polarity of the solvent due to the possibility of establishing an intramolecular H-bonding pattern.[59]

These studies showed that the *cis/trans* isomerization of the amide bond is slow in the NMR time scale. Thus, the binding phenomena must be faster than the amide bond rotation and, accordingly, both rotamers would look like different molecules to the biomolecular receptor[59].

Therefore, as both isomers could act as different molecules when interacting with the Apaf-1 protein, the main objective of this thesis was to design and synthesize conformational restricted analogues refered to the free amide bond of compound **1** and test their activity as apoptotic modulators. From this general objective that is explained in detail in chapter 1, some other interesting points appeared during the course of this doctoral research and they are also developed and explained in next chapters.

# 1. Design, synthesis and characterization of new apoptotis inhibitors

## 1.1. Introduction

### 1.1.1. Triazole as amide bond mimetic

The biological function of peptides and proteins is defined by their ability to adopt well-defined conformations that complement those of their corresponding binding partner or receptor. The ability to access to peptidomimetics that mimic and/or stabilize such secondary structure then allows the study of the associated biological process, with an opportunity for drug design.[67] In this context, replacement of the amide bond with isosters has been a continuous goal in many laboratories.

Successful replacements will provide improved stability, lipophilicity and absorption. Many peptide surrogates have been introduced already. However, the discovery of new peptide surrogates with easier syntheses is an important achievement that could open new opportunities for the study of amide-containing molecules and the development of inhibitors with novel physicochemical properties.[68]

During the last decade, structural mimics of *cis* amides in peptides and proteins have been reported, among them pseudo-prolines[69,70], disubstituted tetrazoles[71] and triazoles[72,73]. Disubstituted 1,2,3-triazoles have been shown to be viable surrogates for *cis* and *trans*- amide bonds, depending on their substitution pattern.[74] (Figure 1.1).[75]

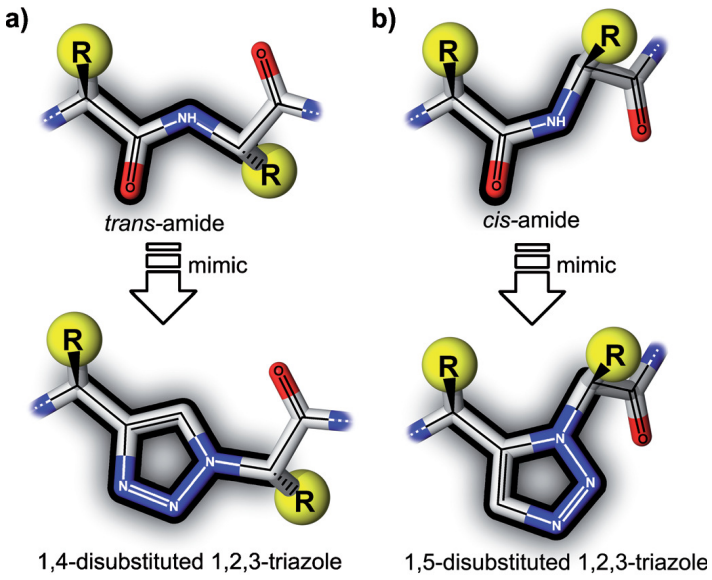


**Figure 1.1**: Representation of triazolyl amide mimics incorporated into a generic peptide backbone.[75]

The triazole ring is an interesting structural motif, more than just a passive linker,[76] since it possesses a hydrogen bond donor and an acceptor, a large molecular dipole and also a metal binding site. It can interact with a wide variety of functionalities, e.g. hydrogen bonding partners

(e.g. amides or anions), molecular dipoles, and metal ions to generate many conformational and molecular recognition features.[77]

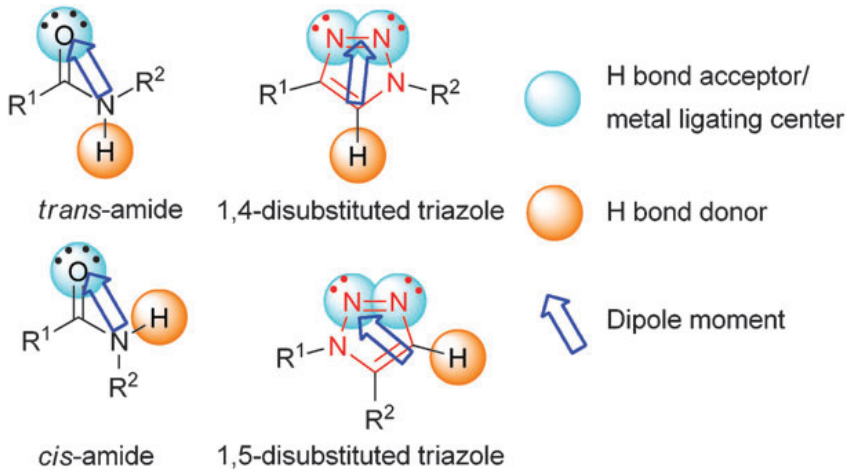


**Figure 1.2:** Comparison of structural features of 1,2,3-triazoles and secondary amides.[77]

For the common *trans*-amide, the $R^1$ to $R^2$ distance (3.9 Å) is slightly shorter than that of the 1,4-disubstituted triazole (5.0 Å), but the lone pairs on the carbonyl oxygen, functioning as hydrogen bonding acceptors, can be mimicked by those of the N-2 and N-3 atoms. Likewise, the hydrogen bonding donor capability of the N-H amide could be replaced by the triazole C-H bond.[78] Due to that difference in the distances, a $CH_2$ will be removed when synthesizing our triazoles; then the distances would be nearly the same. Strikingly similar structural features can also be identified between *cis*-amide and 1,5-disubstituted triazole. In this case, their $R^1$ to $R^2$ distances (2.4 Å) are essentially the same. Another point of interest is that the dipole moment of the triazole ring has been estimated to be 4.0-5.1 Debye,[79, 80] which is slightly higher than that of a secondary amide (3.8 Debye) [81]. For the two different lone pairs on the N atoms, theoretical calculations suggested that the N-3 lone pair has a higher basicity than the N-2 one in the gas phase.[80] This result suggests that the N-3 lone pair may be a better hydrogen bond acceptor and metal ligating center than N-2.

Thus, 1,2,3-triazoles offer an appealing motif in peptidomimetic research as a non-classical bioisoster of an amide[78, 82] because their structural and electronic features are similar to those of a peptide bond. In addition, general methods are now available for their synthesis.[67, 83, 84].

### 1.1.2. Click Chemistry and Triazole synthesis

Click chemistry is a term that was introduced by K. B. Sharpless in 2001 to describe reactions that fulfil a set of criteria. The reaction must be modular, wide in scope, render very high yields, generate only non-toxic by-products that can be removed by non-chromatographic methods, and be stereospecific. The required process characteristics include simple reaction

conditions, readily available starting materials, the use of no solvent or a solvent that is benign or easily removed, and simple product isolation. It is important to recognize that click reactions achieve their required characteristics by having a high thermodynamic driving force, usually higher than 20 kcal·mol$^{-1}$.[85]

Applications of click chemistry are increasingly found in all aspects of drug discovery; they range from lead finding through combinatorial chemistry and target-template *in vitro* chemistry, to proteomics and DNA research. Click chemistry features are beautifully represented among cycloaddition reactions involving heteroatoms, such as hetero-Diels-Alder and, particularly, 1,3-dipolar cycloadditions. These modular fusion reactions unite two unsaturated reactants and provide fast access to a wide variety of interesting five- and six-membered heterocycles. Among these reactions[86] the Huisgen dipolar cycloaddition is the most useful and reliable.

Huisgen's dipolar cycloaddition[87] of organic azides and alkynes is the most direct route to 1,2,3-triazoles. In the absence of a transition-metal catalyst, these reactions are not regioselective, relatively slow and require high temperatures and long reaction times to reach acceptable yields.[88]

Due to the fact that the reaction is highly exothermic (*ca*. -50 to 65 kcal/mol), its high activation barrier (25-26 kcal/mol for methyl azide and propyne)[89] results in exceedingly low reaction rates for unactivated reactants even at elevated temperature. Furthermore, since the difference in HOMO-LUMO energy levels for both azides and alkynes are of similar magnitude, both dipole-HOMO- and dipole-LUMO-controlled pathways operate in these cycloadditions. As a result, a mixture of regioisomeric 1,2,3-triazole products is usually formed when an alkyne is asymmetrically substituted (Scheme 1.1).[90]

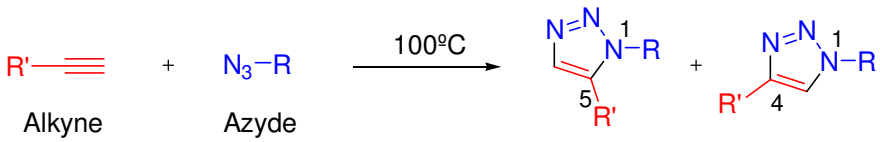


**Scheme 1.1:** Huisgen dipolar cycloaddition reaction.

Copper (I) catalysis discovered independently by the groups of Meldal[84] and Sharpless[85] accelerates the reaction to minutes and at much lower temperatures. The result of this copper catalyzed reaction is mostly, if not completely, a 1,4-triazole adduct (Scheme 1.2). The copper catalyzed reaction proceeds in both aqueous and organic solvents under simple experimental conditions. These features along with the unnecessary requirement of high temperatures makes this copper catalyzed azide-alkyne cycloaddition (CuAAC) a useful tool for synthetic chemists.[91] Moreover, the cycloaddition is thermodynamically favourable enough to be irreversible.

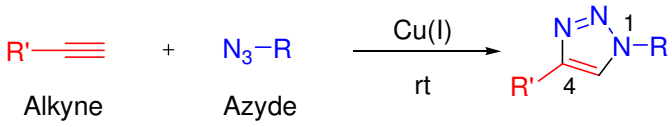


**Scheme 1.2:** Copper-Catalyzed Azide-Alkyne cycloaddition.

While a number of copper (I) sources can be used directly, it was found that the catalyst is better prepared *in situ* by reduction of Cu(II) salts, which are less costly and often purer than Cu(I) salts. As reducing agent, ascorbic acid and/or sodium ascorbate proved to be excellent for the preparation of a broad spectrum of 1,4-triazole products in high yields and purities at 0.25-2 mol% catalyst loading. [91]

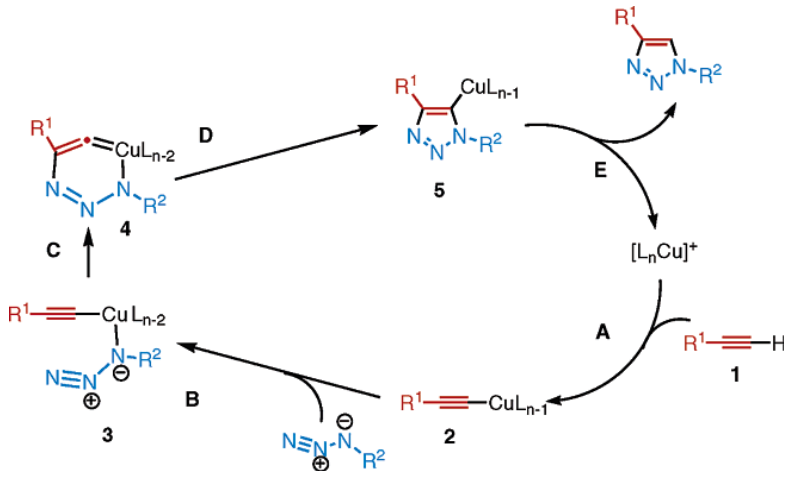


**Scheme 1.3:** Mechanism for the CuAAC.[89]

The mechanism proposed for the CuAAC begins with the formation of copper (I) acetylide, after which the azide displaces another ligand and binds to the metal. Then, an unusual six-membered copper (III) metallacycle is formed. The barrier for this process has been calculated to be considerably lower than the one for the uncatalyzed reaction. Ring contraction to a triazolyl-copper derivative is followed by protonolysis that delivers the triazole product and closes the catalytic cycle.[89]

As it has been shown, the copper-catalyzed 1,3-dipolar azide-alkyne cycloaddition (CuAAC) was an important advance in the chemistry of 1,2,3-triazoles. A significant rate acceleration ($10^7$ to $10^8$ compared to the uncatalyzed process), a remarkably broad scope, a tolerance to aqueous and oxidative conditions, and an exclusive regioselectivity have enabled a number of applications in the relatively short time since the reaction was discovered. Examples of these applications are found in: drug discovery,[79] bioconjugations,[92,93] polymer and material science[94,95] and related areas[96, 97] including supramolecular chemistry.[98-100]

While Cu (I) catalysis provides reliable means for the assembly of 1,4-disubstituted-1,2,3-triazoles, a general method for the generation of 1,5-disubstituted regioisomers was lacking. Although they can be synthesized by the reaction of bromomagnesium acetylides with organic azides,[101] this procedure lacks the scope and convenience of the CuAAC process.

In fact, 1,5-isomers have been only scarcely explored so far,[74,102] although Fokin and co-workers[90,103] recently reported that their preparation can be accomplished by a ruthenium-catalyzed azide-alkyne cycloaddition reaction (RuAAC). This reaction furnishes the triazole derivatives with a virtually total 1,5-regioselectivity.[104]

Catalytic transformations of alkynes mediated by ruthenium complexes were well-known. Therefore, ruthenium was a logical choice on the research for a catalyst of azide-alkyne cycloaddition. Different ruthenium complexes were tested by Jia and Fokin and co-workers. Acetate complex, $RuCl_2(PPh_3)_3$ or $RuHCl(CO)(PPh_3)_3$ were ineffective. In contrast, $CpRuCl(PPh_3)_2$ catalyst resulted in 50% conversion of the reactants to a mixture of 1,5- and 1,4-disubstituted triazoles. Then, a simple switch to the pentamethyl analogue, $Cp^*RuCl(PPh_3)_2$, resulted in the formation of only 1,5-regioisomer with complete conversion. Reactions with other [Cp*Ru] complexes gave similar results.[103]

The scope of the reaction was also studied and the fact that it is not very sensitive to the alkyne but to the nature of the azide was proved. Primary azides were more efficient than secondary ones, while tertiary azides reluctantly participated in the catalysis. These cycloadditions proceed well in aprotic organic solvents (benzene, toluene, THF, dioxane) whereas protic solvents have a detrimental effect on both yield and regioselectivity.

Since Cu (I) acetylides seem to be the intermediates in the CuAAC, this transformation is limited to terminal alkynes. The [Cp*RuCl] system is active with internal alkynes as well,[105] which suggests that ruthenium acetylides are not involved in the catalytic cycle. It was proposed that the neutral [Cp*RuCl] is the catalytically active species and the following mechanism was suggested.[90, 103]

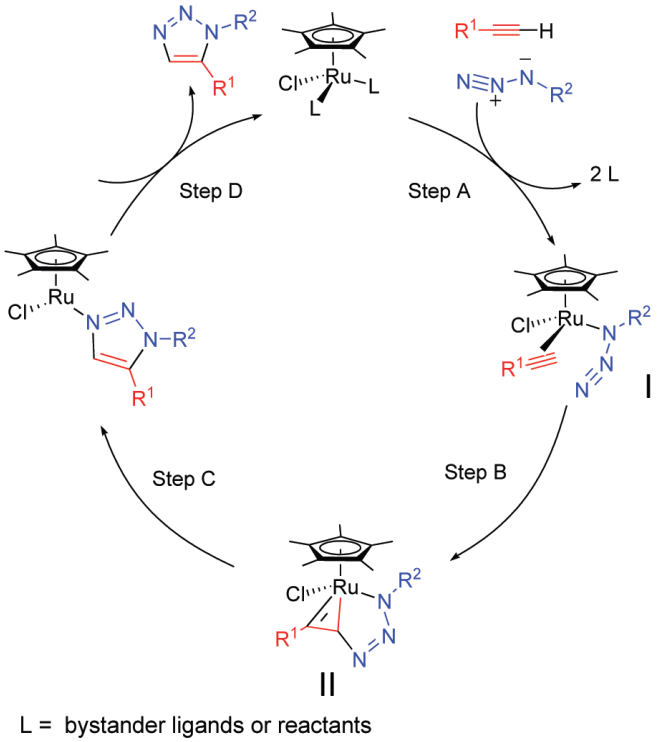


**Scheme 1.4:** Proposed intermediates in the catalytic cycle of RuAAC reaction.[90]

The displacement of the spectator ligands (step A) produces the activated complex **I**, which is converted, via the oxidative coupling of an alkyne and an azide (step B), to the ruthenacycle **II**. This step controls the 1,5-regioselectivity observed. The new C-N bond is formed between the most electronegative and less sterically-demanding carbon of the alkyne and the terminal nitrogen of the azide. The metallacycle intermediate then undergoes reductive elimination (step C) releasing the aromatic triazole product and regenerating the catalyst (step D) or the activated complex **I**.[90]

### 1.1.3. Ugi reaction

The Ugi reaction, or Ugi four-component coupling (Ugi 4-CC),[106-108] is perhaps the best known example of a multicomponent reaction (MCR). A MCR process is a one-pot reaction that forms products from three or more different starting compounds.[109] This reaction has been extensively studied since its discovery more than 50 years ago. The large range of structures accessible through this powerful reaction is continually expanding, through the ongoing development of variations of the MCR, together with an increasing number of elaborated postcondensation modifications and cascade processes.[110] It was first reported by Ivar Ugi in 1959[106] and along with the Passerini reaction, it is classified as an isocyanide-based multicomponent reaction.

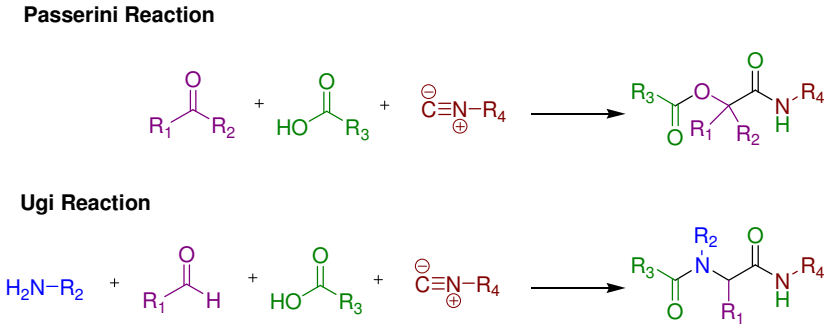


**Scheme 1.5:** Passerini and Ugi reaction.

The prototypical reaction (Scheme 1.5) results in the formation of an α-*N*-acylamino amide. The reaction is usually conducted in a polar protic solvent such as methanol, and some success in water has recently been shown.[111] Usually, non-polar halogenated solvents prove to be detrimental, as most amines are insoluble in those solvents, thus, favoring the occurrence of the Passerini reaction. The mild reaction conditions of the Ugi reaction allow for inclusion of a variety of functionality.

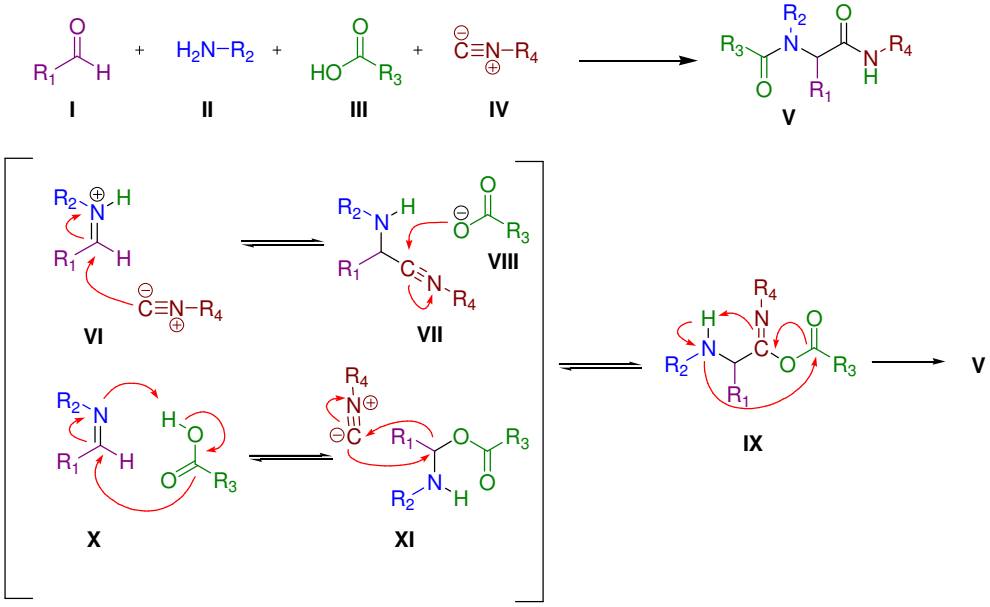


**Scheme 1.6:** Postulated mechanisms of the U-4CC.

Two possible mechanisms for the Ugi reaction have been postulated.[112] In both mechanisms, the first step involves condensation of aldehyde **I** and amine **II**, followed by protonation of the imine by **III** (Scheme 1.6). The debate is whether the next step involves introduction of the carboxylic acid to give **X**, causing isocyanide **IV** to react with **XI** via an $S_N2$ mechanism, or isocyanide **IV** first undergoes nucleophilic addition to imine **VI**, followed by the addition of carboxylate **VIII** to **VII**. Experiments supporting the formation of intermediate **VII** versus **XI** have not been performed. [113]

Major advances in the scope of the Ugi reaction have occurred only within the last 20 years, mainly because of the limited availability of isocyanides and poor stereocontrol. In the mid 1900's, only a few isocyanides were available. Today, about 380 isocyanides are commercially available[114] or easily synthesized.

Hulme *et al.*[54] described the synthesis in solution of DKPs using the Ugi reaction with the named Armstrong's convertible isonitrile (cyclohexenyl isocyanide)[115] followed by the deprotection of the Boc group and cyclization (Scheme 1.7). This approach can also be used in solid phase by anchoring the amine[116] or the icocyanide to the solid support.[117]

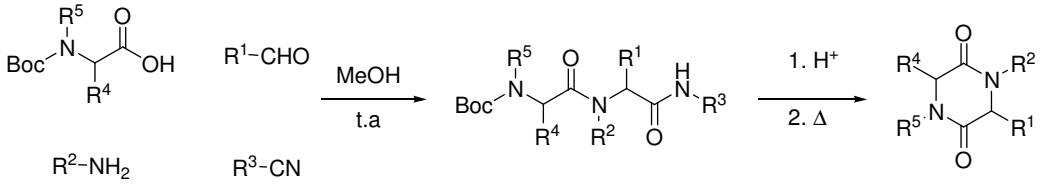


**Scheme 1.7:** DKPs synthesis through an Ugi multicomponent reaction.

Marcaccini *et al.*, also reported that the Ugi four-component condensation between amines, aromatic aldehydes, chloroacetic acid and isocyanides afforded the adducts which were cyclized to title DKPs upon treatment with ethanolic KOH under ultrasonication. (Scheme 1.8)

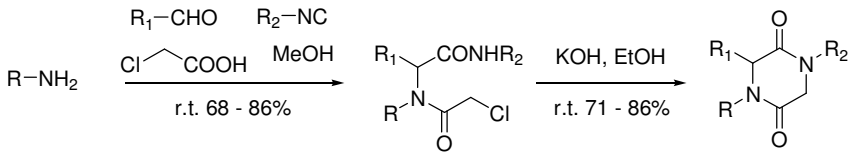


**Scheme 1.8:** DKPs synthesis through an Ugi multicomponent reaction followed by a base promoted cyclization.

## 1.2. Objectives

The conformational studies[59] of compound **1** (Figure 1.3) showed that the *cis/trans* isomerization of the amide bond is slow in the NMR timescale. Therefore, the binding phenomena must be faster than the amide bond rotation and, accordingly, both romaters would look like different molecules to the biomolecular receptor. The probable different biological activity of both rotamers exposed the possibility to freeze them separately.

In this regard, we hypothesized that the 1,4- and 1,5-disubstituted triazole moieties (**2a**, **2b**) could mimic the spatial disposition of the residues for the *cis* and *trans* configuration of **1**, respectively. As an intermediate situation, we also envisioned the preparation of the 2,4-disubstituted triazole derivative (**2c**).

In our case, the comparison is done between the peptoid moiety and the triazole, whereas in the previous examples (Figure 1.2), the amides compared were from peptides and the nomenclature is quite different. In the called *cis*-isomer in peptoid **1** (Figure 1.3), the substituent $R_2$ is in *trans* with respect to the DKP moiety, while the in **1**-*trans* $R_2$ is much nearer to the carbonyl of the DKP.

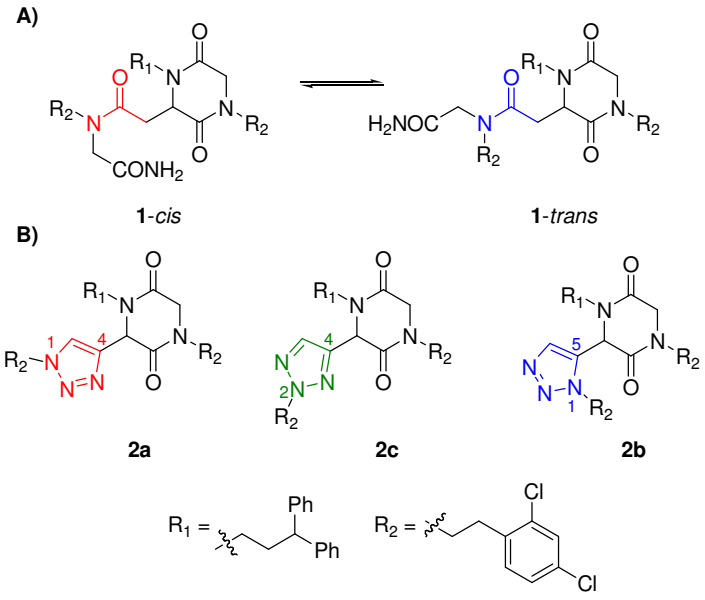


**Figure 1.3:** A) Structure of the apoptotic inhibitor 1. B) Proposed conformationally restricted analogs bearing the 1,2,3-triazole residue.

Taking all this into account, we planned the following aims:

1. To design and synthesize conformationally restricted analogs of **1** using 1,4-, 2,4- and 1,5- disubstituted triazole moieties to mimic the *cis* or *trans* isomer.

2. To evaluate the biological activity of these analogs as inhibitors of the apoptosome formation.

3. To study the mode of interaction of these compounds in the Apaf-1 protein by using a computational approach.

## 1.3. Results and discussion

For the syntheses of these conformationally restricted analogs (**2a-c)**, we planned a strategy (Scheme 1.9) based on the previously mentioned Ugi four-component coupling reaction (Ugi-4CC) [52,55,107,110,118,119] comprising a primary amine **4**, an aldehyde **5**, an isocyanide **6** and a carboxylic acid **7**, that are condensed to yield the single product **3**. After the formation of the open products, a base-promoted intramolecular cyclization would yield the final compounds **2**.

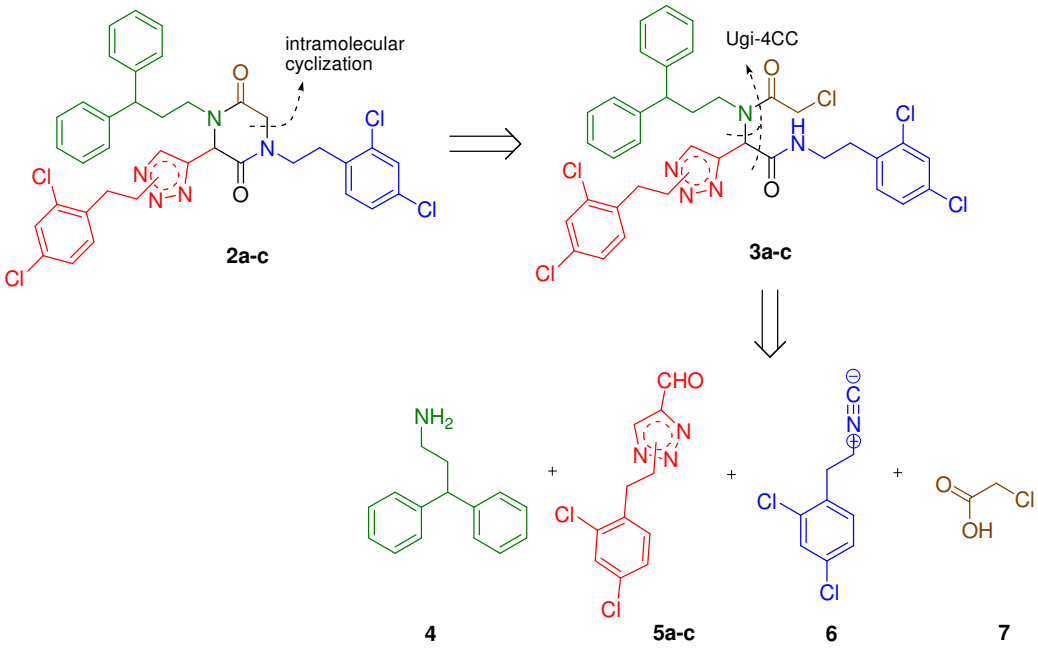


**Scheme 1.9:** Retrosynthesis of **2a-c** comprising an Ugi-4CC reaction followed by an intramolecular cyclization.

In the proposed scheme, the amine and the acid are commercially available, whereas the isocyanide and the aldehydes must be synthesised. The isocyanide was obtained as described in the literature. (Scheme 1.10)[120,121]

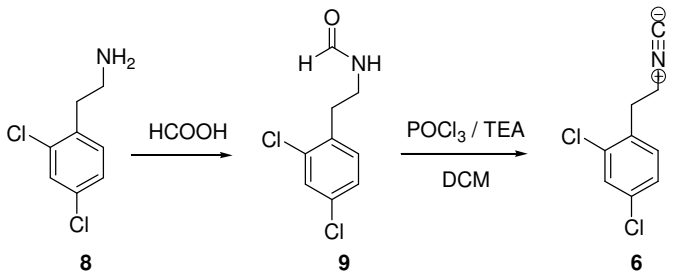


**Scheme 1.10:** Synthesis of isocyanide **6**.

First of all, we obtained the *N*-(2,4-dichlorophenethyl)formamide (**9**) from the reaction of 2-(2,4-dichlorophenyl)ethanamine (**8**) with formic acid under microwave activation; then, the desired isocyanide was obtained by treatment of the formamide intermediate with phosphoryl trichloride under anhydrous conditions. The first step was optimized using different conditions under microwave irradiation. But the limitant step is the dehydratation of the formamide because the phosphoryl trichloride is very sensitive and is hydrolyzed easily to the phosphoric acid, thus avoiding the desired reaction. The isocyanide was obtained as brown oil and as it was not possible to check it by mass-spectrometry, the disappearance of the amide signal in the $^{1}$H NMR and the changes in the chemical shifts of the protons linked to the nitrogen were enough to check that the product had been synthesized. The disgusting smell was also a clue to know that the isocyanide was obtained. (Figure 1.4) Since isocyanides are stable to strong base but sensitive to acid, some precautions had to be taken. Thus, in the presence of aqueous acid, isocyanides undergo hydrolysis back to the corresponding formamides. Moreover, some isocyanides can polymerize in the presence of acid and metal species.[122, 123] Actually, we observed this polymerization for the case of isocyanide **6** by the appearance of broad signals in the $^{1}$H NMR spectra. (Figure 1.4). In addition, due to the unpleasant smell and suspected toxicity of isocyanides, we tried the one-pot four-component reaction without any manipulation of isocyanide, as described by El Kaim *et al.*[124] Unfortunately, this strategy where the isocyanide is synthesized *in situ* while performing the Ugi coupling, did not work with our products. Therefore, the synthesis depicted in Scheme 1.10 was used for our required isocyanides.

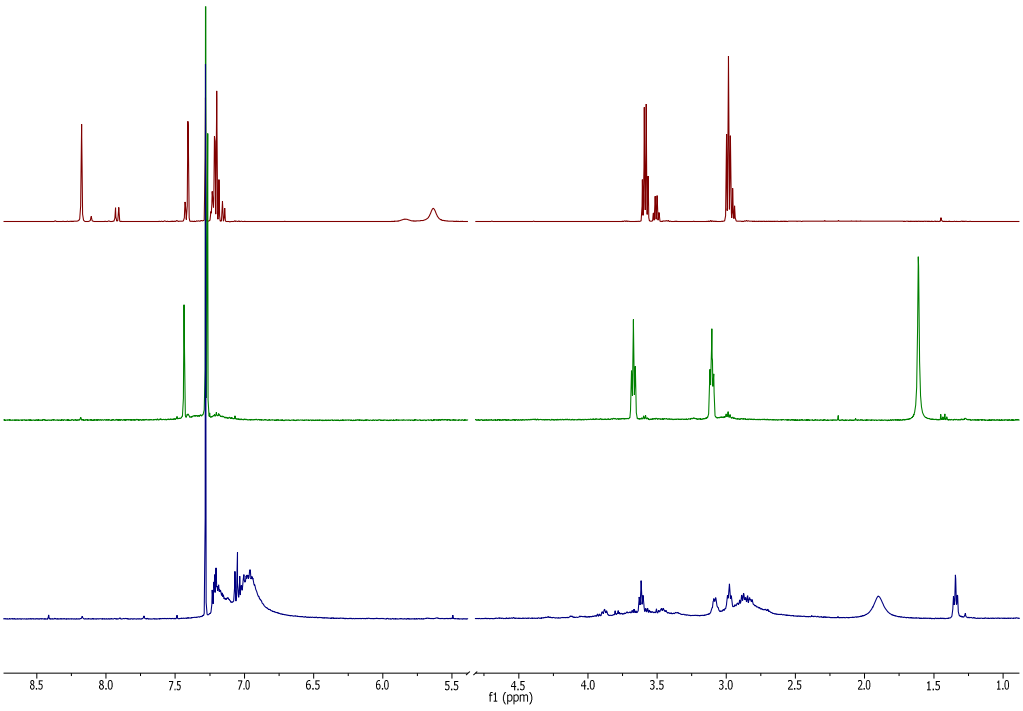


**Figure 1.4:** Comparison between the $^{1}$H NMR of the formamide intermediate (red), the isocyanide (green) and the polymer of the isocyanide (blue) accidentally formed.

### 1.3.1. Synthesis of aldehydes bearing the appropriate triazole pattern substitution

The key triazole aldehydes bearing different substitution patterns **5a-c** were synthesized by using modifications of synthetic methods described in the literature.

The first step was the tosylation of **10** with tosyl chloride and pyridine in DCM. The purified tosylate was subjected to azidation with sodium azide in anhydrous conditions and the crude reaction mixture was used without further purification. Since the 2,4-dichlorophenethyl bromide was commercially available, we could directly perform the azidation. Then, to synthesize the different regioisomers, the appropriate cycloaddition reactions were performed. (Scheme 1.11)

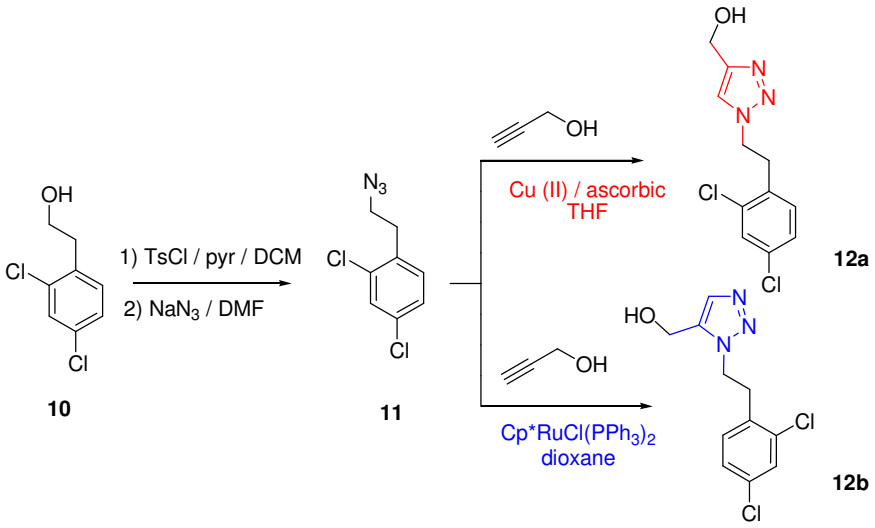


**Scheme 1.11:** Synthesis of the 1,4- and 1,5-disubstituted triazoles (**12a**, **12b**).

For the case of 1,4-disubstituted-1,2,3-triazole, the azide **11** was dissolved in THF and a solution of $CuSO_4$ / ascorbic acid in water was added and stirred under microwave activation leading to the desired triazole **12a**. It is worth mentioning that an extraction with $NaHCO_3$ was sometimes not enough for decomposing the complex of the triazole with the copper species, and an ammonia solution was then used. The formation of the triazole was observed by $^1H$ NMR because the triazole proton has a characteristic chemical shift at 7.4 ppm that is not present in the azide precursor. The product was also confirmed by high-resolution mass spectrometry where for $\mathbf{C_{11}H_{11}Cl_2N_3O}$ the calculated mass was 272.0357 $(M+H)^+$ and the experimental one was 272.0368. The yield of this reaction is quite satisfactory (60-70%).

For the case of 1,5-disubstituted 1,2,3-triazole (**12b**), the mentioned ruthenium catalyst was used (Scheme 1.11). In this case, the order of addition is important and, after several attempts, the optimal yield was obtained when a solution of alkyne and azide in dioxane was added to a dioxane solution of the catalyst. The desired triazole was obtained after a reverse-phase chromatographic purification. The selectivity of this catalyst is not as good as the copper one.

After two hours of reaction, the conversion was only 40%, but if the stirring was prolonged, the 1,4-isomer was also formed. Therefore, a compromise solution had to be reached. It is better to have a pure isomer with low yields than a mixture of the 1,4- and 1,5- compounds. Besides the low conversion, the final yield is decreased because of the further purification steps. The triphenylphosphine oxide that was formed during the reaction is not easy to remove by simple chromatographic column purification. Therefore, a semi preparative HPLC purification was used, leading to a 13% overall yield of the isolated compound.

These results may explain why CuAAC click reaction is used more frequently. The ruthenium catalysis is a less straighforward procedure, being more sensitive to experimental variables (time, temperature, traces of water). Moreover, it usually leads to lower yields and regioselectivity, as we have experimentally observed.

Finally, a simple oxidation with 2-iodoxybenzoic acid afforded in both cases the desired aldehydes **5a**, **5b** in good yields.(90-100%) (Scheme 1.12).

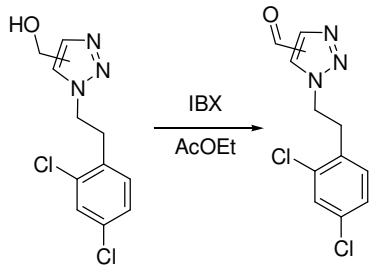


**12a,b** **5a,b**

**Scheme 1.12:** Oxidation of the triazoles **12** to the final aldehydes **5.**

On the other hand, although the 2-substituted-2*H*-1,2,3-triazoles can be obtained by alkylation of *NH*-1,2,3-triazoles with the suitable electrophilic reagents, a mixture of the isomeric products is often produced. Other possibilities are for example the oxidative cyclization of bishydrazones or bissemicarbazones[125] and the three-component Pd-catalyzed reaction that form 2-allyl-1,2,3-triazoles.[126] Despite these reports, a general and simple method for the stereoselective formation of the 2*H*-isomers is still not available. In 2008, Fokin and co-workers reported a three-component one-pot synthesis of 2-hydroxymethyl-2*H*-1,2,3-triazoles.[127] As shown in Scheme 1.13, the reaction afforded a mixture of two compounds.

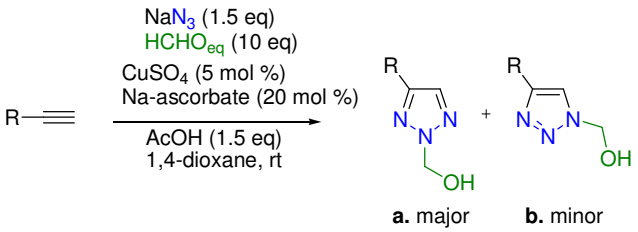


**Scheme 1.13:** Synthesis of *N*-hydroxymethyl-1,2,3-triazoles. [127]

These compounds are versatile intermediates that can be used for the preparation of N*H*-1,2,3-triazoles. In their method, formaldehyde, sodium azide and a terminal alkyne (propargyl alcohol in our case) react in a one-pot two-steps process under acid conditions. Azidomethanol formed *in situ* from protonated formaldehyde and sodium azide, is a likely intermediate. The subsequent copper (I)-catalyzed reaction with the alkyne provides the 1-hydroxymethyl-1*H*-1,2,3-triazole product. However, the instability of this derivative and its equilibrium with the N*H*-triazole and formaldehyde results in the rearrangement of the 1-hydroxymethyl triazole to the thermodynamically more stable 2-hydroxymethyl isomer. Thus, a mixture of the 1-hydroxymethyl-1,2,3-triazole (**b**) and the 2-hydroxymethyl (**a**) isomers are obtained, being the desired isomer (**a**) the major and the most stable one. In Scheme 1.14 the same reaction is depicted for our case. Basic hydrolysis of the *N*-hydroxymethylalcohol **13** led to the N*H*-compound **14**. Considering that **14** is used without further purification, the determination of the amount of product in the crude mixture is needed. *Tert*-butyl alcohol was used as an internal standard in $^1$H NMR ($D_2O$), the amount of product **14** calculated was around 20%.

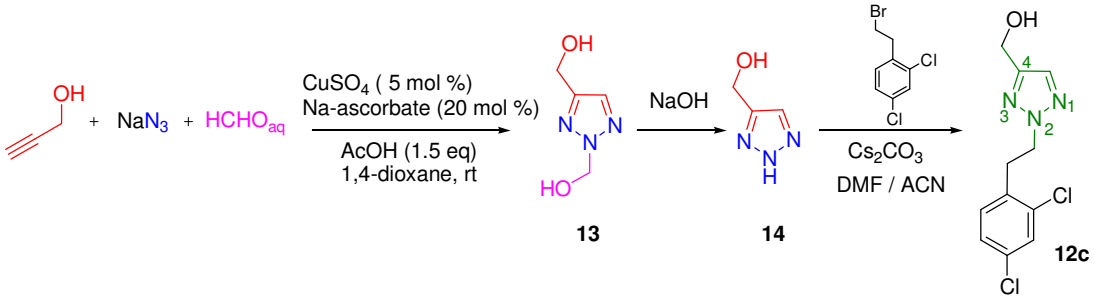


**Scheme 1.14:** Synthesis of the 2,4-disubstituted 1,2,3-triazole (**12c**).

Then the mixture was reacted with the corresponding bromo derivative to afford the 4-hydroxymethyl-2,4-disubstitued-triazole **12c** via a $S_N2$ reaction at N2 of the triazole **14** (Scheme 1.14). This reaction was performed in the presence of $Cs_2CO_3$ to avoid, as far as possible, the elimination side reaction. The process afforded a crude reaction mixture containing the desired triazole and small amounts of the 1,4- and 1,5-disubstituted triazoles, that were separated from the desired product by chromatographic purification (See Experimental Part). Then, compound

**12c** was also transformed into the corresponding aldehyde (**5c**) by oxidation with IBX with complete conversion.

The substitution patterns of the three isomeric triazoles were unambiguously established by a complete NMR assignment of the signals of **5a-c** and those of their corresponding alcohol precursors (**12a-c**), including the $^{15}N$ NMR signals from $^{1}H$-$^{15}N$ gHMBC 2D experiments (see Chapter 2 and Supp. Inf.).

### 1.3.2. Synthesis of the final products

Once all the reagents for the Ugi-4CC reaction were available, the reaction could be performed to obtain the open Ugi adducts. (Scheme 1.15).

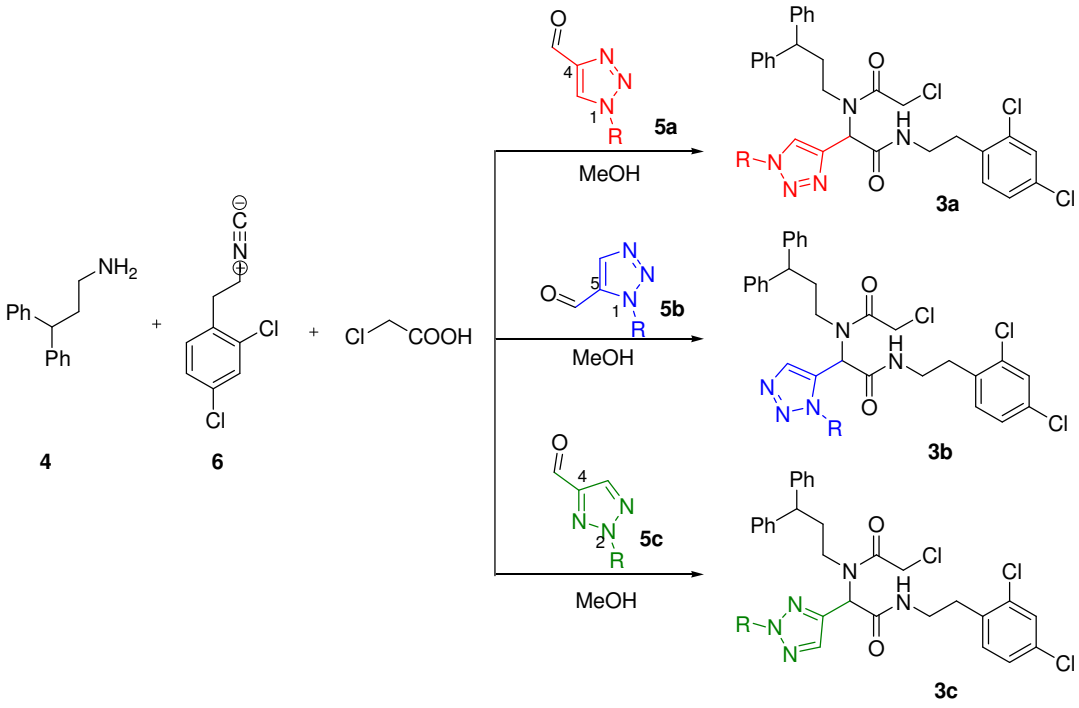


**Scheme 1.15:** Synthesis of the Ugi adducts (**3a-c**).

The Ugi reaction requires some considerations. It is favoured by high concentration of the reactants and is often necessary to add further solvent to achieve an efficient stirring. The order of addition of compounds is also important. Due to the low stability of isocyanides in acid medium, addition of the isocyanide to the acid (or vice versa) in the absence of the amine should be avoided. It is well known that the pre-formation of the imine has a beneficial effect on the multicomponent reaction. For this reason, the amine and the carbonyl compound are usually mixed and allowed to react for some time to ensure the formation of the imine before adding the other reagents.[108]

Considering that the formation of the imine is a key step for the progress of the overall reaction, it was monitored by $^1$H NMR. The imine was totally formed after 6 hours; afterwards, the addition of the isocyanide **6** and the carboxylic acid was done within 30 minutes. The addition of the acid before this period of time produced the hydrolysis of the imine and prevented the formation of the Ugi products **3**.

The Ugi reaction was monitored by NMR, by observing the formation of the CH (1) (5.41, 5.68, 5.39 ppm for **3a**, **3b** and **3c,** respectively) in **3**, the absence of the aldehyde (~10 ppm) and the imine protons (~8 ppm), and the formation of a NH bond (~6 ppm). The reported reaction time is 24 hours, but we have observed that the reaction course between the isomers is quite different. For the 1,4-disubstituted triazole **5a** and the 2,4-disubstituted triazole **5c**, the Ugi adducts **3a,c** were obtained after 24 hours under the established conditions. However, for **5b**, longer reaction times were needed (more than 48 hours controlled by NMR). The different reactivity observed could be due to the steric hindrance of the substituent in **5b** because of its proximity to the binding site and also because carbonyl compounds bearing electron-withdrawing groups, have shown diminished reactivity because of the lower basicity of the imine and consequent lower concentration of the iminium ion in solution.[108]

It has been reported that the Ugi-4CC adducts are usually less soluble than the starting products and that, in most cases, they precipitate in high yields and in almost pure form. [108] As we had not observed this precipitation with our products, some purification steps were required except for **3c,** where the crude reaction mixture was pure enough for characterization purposes and then to perform the following reaction. In the 1,4-disubstituted case, as the major impurity was the unreacted aldehyde **5a**, a resin scavenger AM-$NH_2$ was used to remove this reagent, whereas for **3b** a flash chromatography purification step was needed.

To afford the final DKP products from **3a-c**, two different base treatments were used due to the different reactivity of the structures (Scheme 1.16). For **3a**, a KOH /MeOH mixture was used and the desired product **2a** was formed with 58% yield; but when the same method was used for **3b**, the hydrolyzed product **15** (Figure 1.5) was obtained. Then, a NaH/THF system was assayed and the cyclic compound **2b** was isolated after preparative TLC purification, but with lower yield than the previous one (26%).

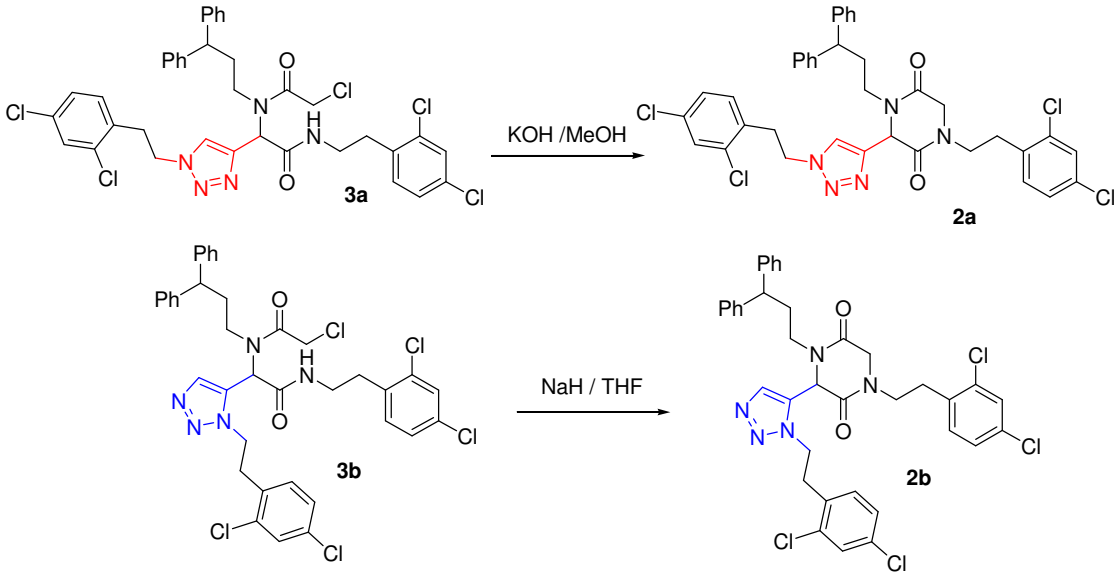


**Scheme 1.16:** Cyclization of **3a,b** to afford the final DKP products **2a,b.**

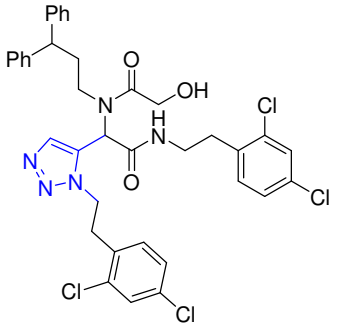


**Figure 1.5:** Product generated from the hydrolysis of **3b** with NaOH.

The course of the cyclization reactions was monitored by HPLC and NMR. In the chromatogram profile, both products eluted within 1 minute, although both of them are non-polar and exhibit long retention times (~18 min). (Supp. Inf.) The HPLC was performed using a gradient method from 20% to 100% $CH_3CN$ in 20 min. It was not possible to start with lower amounts of $CH_3CN$ because of the low solubility of our products.

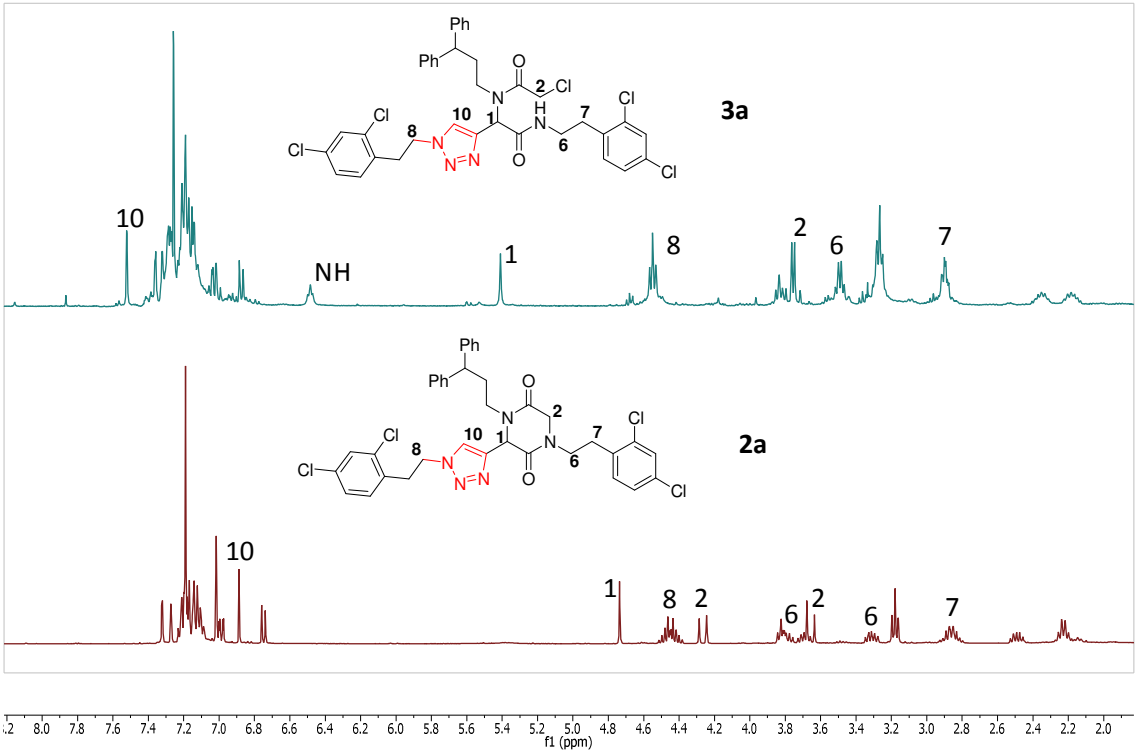


**Figure 1.6:** Comparison between the $^{1}$H NMR ($CDCl_3$, 500 MHz, 25 ºC) of the open and the cyclic compounds **3a** and **2a** respectively.

Figure 1.6 shows the $^{1}$H NMR spectra of the open product **3a** and of the diketopiperazine **2a**, where the differences observed between them were used to follow the cyclization. Thus, in **2a**, the NH signal (6.48 ppm) of the open product **3a** has disappeared. The shielding observed in H1 and H10 is another clue that a cycle is formed due to the increse of rigidity on the structure. Another noticeable change is the anisochrony of the two H2 in **2a**, which is also caused by the rigidity of the ring formation. A similar effect is observed in the protons of H6 that appear with different chemical shifts in **2a** but not in **3a**.

Moreover, the $^{13}$C NMR spectra show also slight differences between both structures; for instance, the carbonyl groups once the cycle is formed appear at lower chemical shift than in **3a**, and C2 changes from 40.7 to 51.0 ppm.

The changes observed for **3b** and **2b** are nearly the same than those mentioned above.

The use of any of the cyclization methods (NaOH/MeOH or NaH/THF), with intermediate **3c** led to an unexpected product. This compound had the same mass of **2c** in the ESI-MS spectrum (m/z = 720.14 for $MH^+$), but the $^{1}$H NMR spectrum showed some differences respect to the changes that were expected. The most surprising was the presence of an amide NH signal that should have disappeared when forming the DKP and that the CH (H1) of the chiral center of the DKP was absent, suggesting that the intramolecular cyclization had occurred in a

different way. In Figures 1.7 and 1.8, the $^{1}$H NMR spectra of the 1,4-disubstituted triazole DKP and the new compound can be compared.

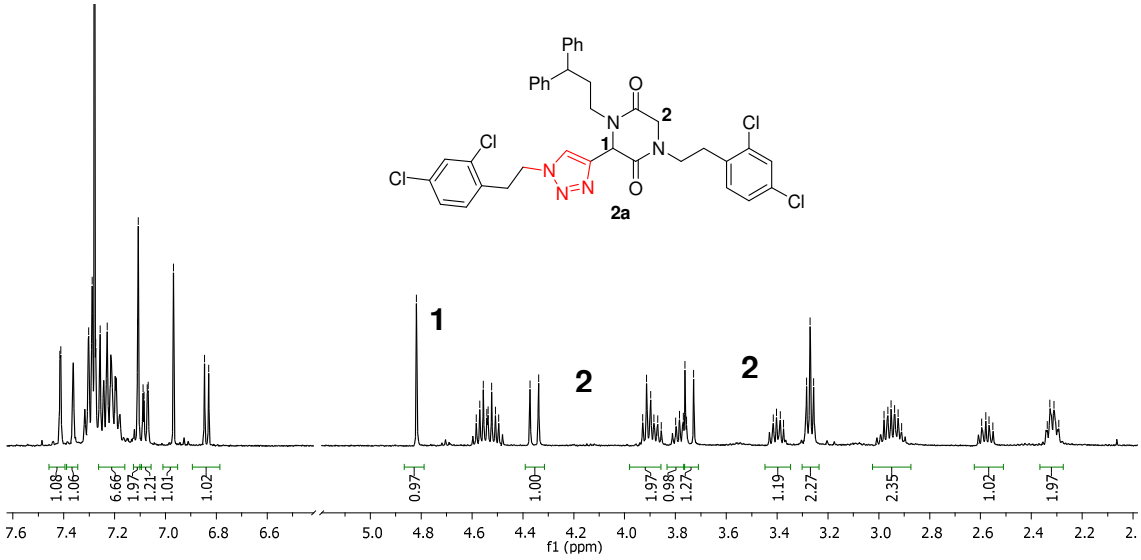


**Figure 1.7:** $^{1}$H NMR ($CDCl_3$, 500MHz, 25 ºC) of **2a**.

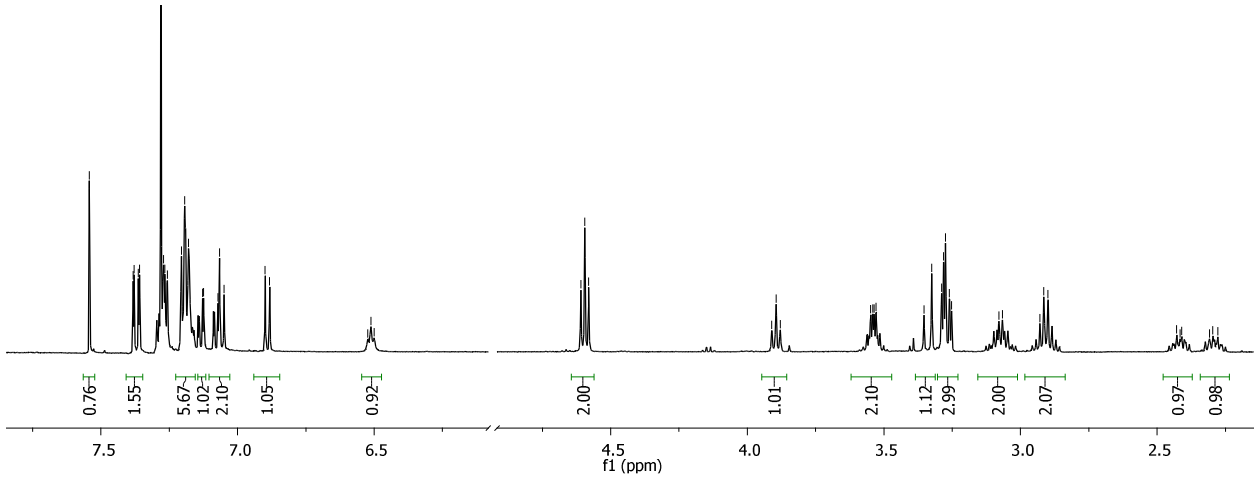


**Figure 1.8:** $^{1}$H NMR ($CDCl_3$, 500MHz, 25ºC) of the unknown product isolated from the cyclization reaction of **3c**.

To identify the unknown structure, it is useful to understand how the cyclization takes place and which other possible compounds are accessible with **3c** as a reagent in basic conditions. Thus, the possible anions formed after the addition of a base to the open compound **3c** are depicted in Scheme 1.17.

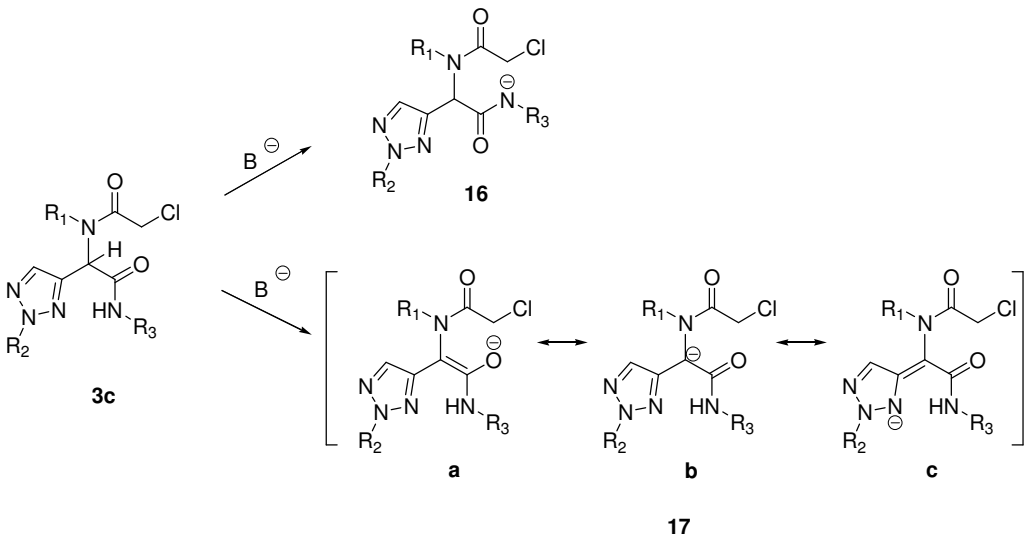

**Scheme 1.17:** Possible anions formed after adding base to **3c**.

First of all, it was proposed that the base removes the proton from the NH which would originate the anion **16** and as shown in Scheme 1.18, the final product would be the DKP **2c**. But, as commented above, this is not the way the cyclization took place.

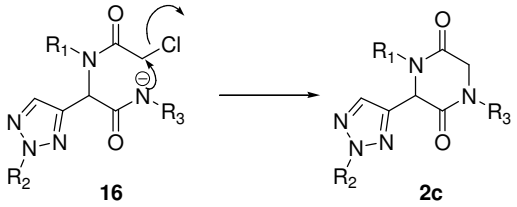

**Scheme 1.18:** Formation of the diketopiperazine **2c** from the anion **16**.

Observing the canonical structural resonance of **17** (Scheme 1.17), some compounds can be proposed. (Scheme 1.19).

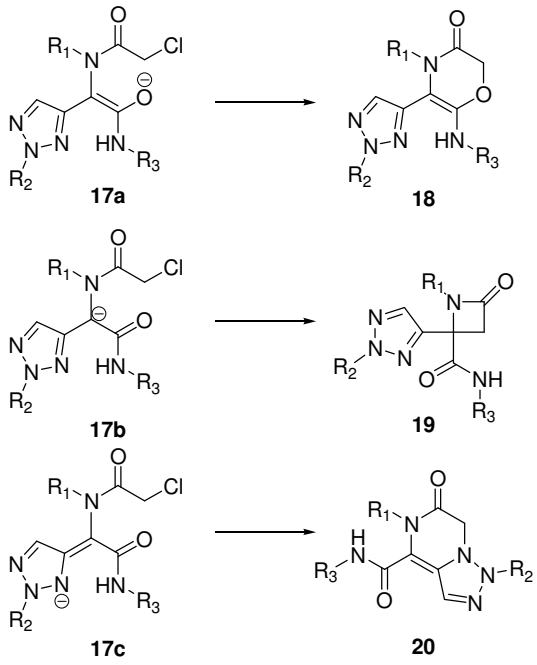


**Scheme 1.19:** Possible cyclization compounds formed from the different canonical resonance structure **16.**

One possibility would be compound **20** (Figure 1.9), where the cyclization has taken place through the nitrogen at position 3 of the triazole ($N_A$). This process would have afforded a new bicyclic compound bearing a rigid scaffold with a very similar disposition of the residues.

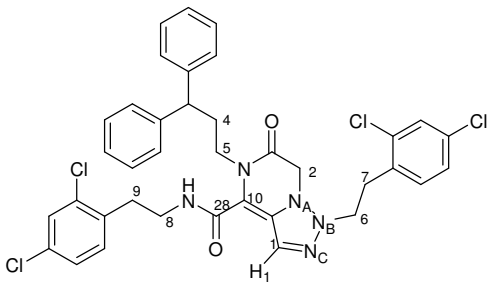

**Figure 1.9:** Compound **20**

We thought that this was the compound formed due to the correlations obtained in the $^{1}H$-$^{15}N$ HMBC NMR spectrum (Figure 1.10), where $N_B$ seems to correlate with H2, which is not possible in any of the other possibilities. As one of the protons of H7 has the same chemical shift than H2, the peak correlation that is observed in the spectrum is the correlation between $N_B$ and H7. This was confirmed with the synthesis of a benzylic substituent without H7 (See Chapter 3), where the mentioned correlation was not presented. Moreover, the N chemical shifts (referenced to $MeNO_2$) of this compound ($N_A$ = -55.9, $N_B$ = -124.2 and $N_C$ = -48.6 ppm) did not show large differences compared with the open compound **3c** (where, $N_A$ = -52.4, $N_B$ = -

125.3 and $N_C$ = -48.9 ppm). This fact was surprising because a shifted upfield was expected due to the alkylation suffered by $N_A$. Therefore, this cyclization possibility was discarded.

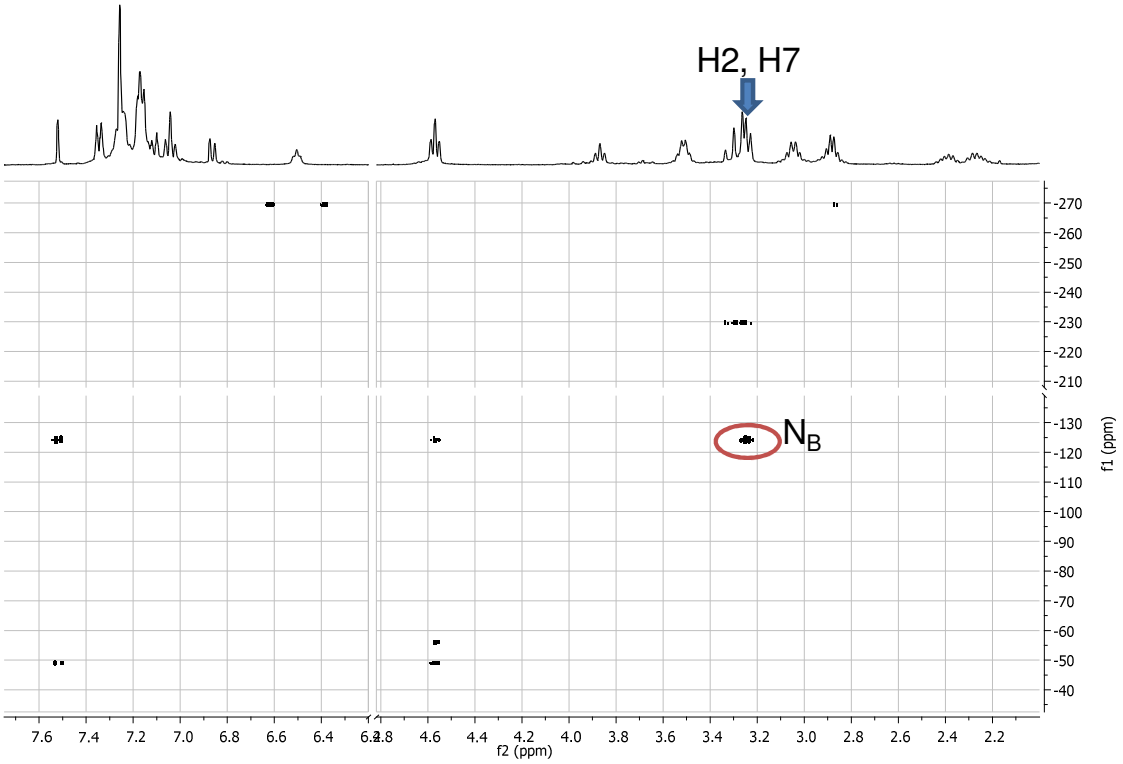


**Figure 1.10:** $^{1}H$-$^{15}N$ HMBC spectrum ($CDCl_3$, 500 MHz, at 25ºC referenced to $MeNO_2$) of the unknown cyclization compound.

Another possibility was derived from **17a** which is the cyclization through the oxygen of the amide bond, to give the compound **18**. (Figure 1.11)

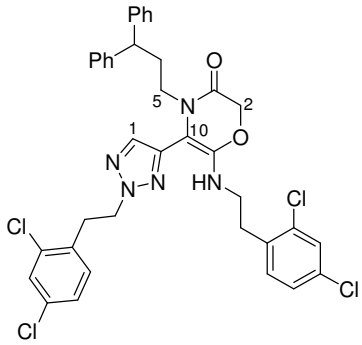


**Figure 1.11:** Compound **18**

In this case, the similar $^{15}N$ chemical shift in the triazole before and after the cyclization was in accordance with the proposed structure, because the N triazoles do not participate in the

reaction. However, the carbon at 58.9 ppm does not show correlations in the $^{1}H$-$^{13}C$ HSQC and as it correlates with H2 and H5 in the $^{1}H$-$^{13}C$ HMBC (Figure 1.12) it must be C10. This chemical shift is too low for a sp2 carbon; moreover, the correlation of C10 with H2 is through 4 bonds and is quite long distance to be able to observe its correlation peak.

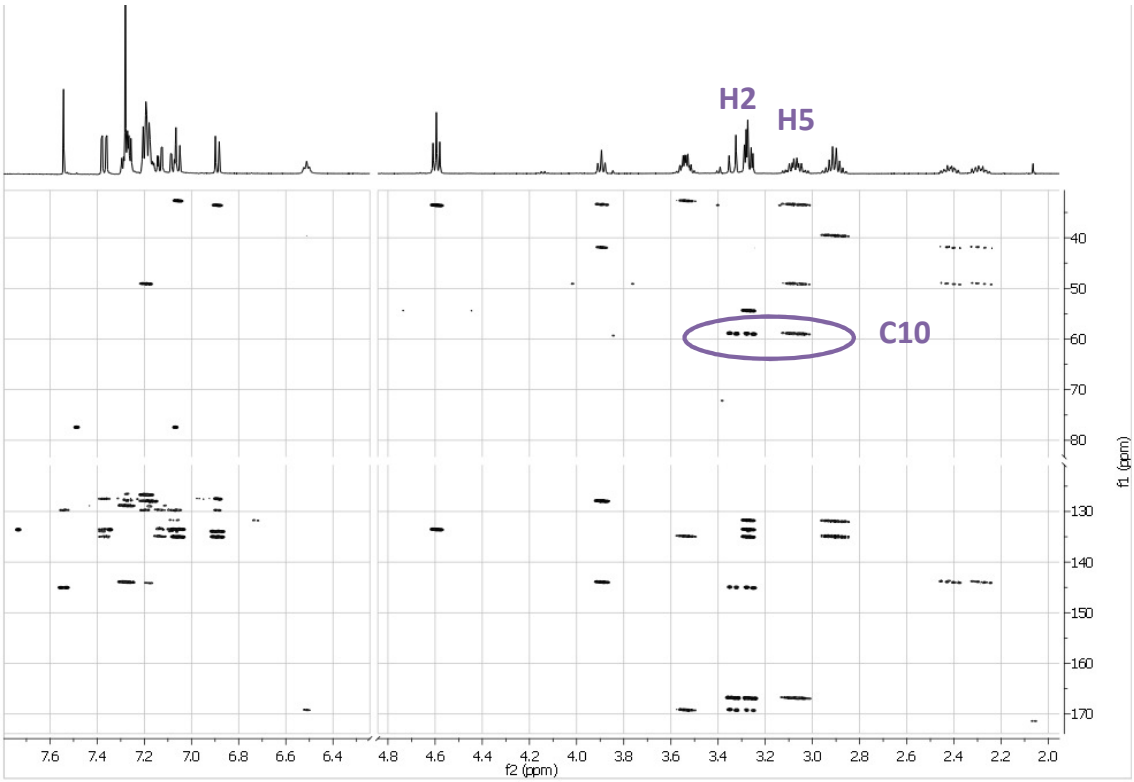


**Figure 1.12:** $^{1}H$-$^{13}C$ HMBC ($CDCl_3$, 500 MHz, 25 ºC) of the unknown cyclization compound.

Finally the third option, compound **19** (Figure 1.13) was considered. In this case, the cyclization has taken place through the CH contiguous to the triazole ring. In this structure, the nitrogen chemical shifts of the triazole will be very similar to those of the open compound **3c** ($N_A$ = -52.4, $N_B$ = -125.3 and $N_C$ = -48.9 ppm) as it was observed in the $^{15}N$ NMR. Moreover, the chemical shift of C10 is in accordance with the β-lactam structure, where a quaternary sp3 carbon appears at 58.9 ppm and it correlates with H2 and H5 in the $^{1}H$-$^{13}C$ HMBC. (Figure 1.12).

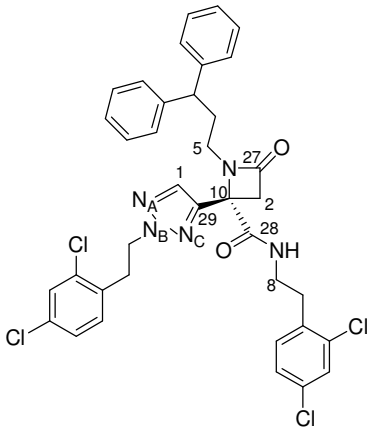


**Figure 1.13:** Compound **19**

With the $^{1}H$-$^{13}C$ HMBC (Figure 1.14), all the $^{13}C$ NMR signal of the structure can be assigned. For example, C29 is the quaternary carbon (no correlations in the $^{1}H$-$^{13}C$ HSQC) that correlates with H2. The carbonyl groups can also be assigned, where the one at 166.8 ppm is C27 (166.8 ppm) correlating with H5 and H2, whereas C28 (169.1 ppm) correlates with H8 and H2.

It is also important to mention that, in the diketopiperazines, the $^{13}C$ of the carbonyl groups appeared shifted upfield with respect to the open compound. However, the inverse phenomenon is observed for the β-lactam, and C28, which is outside the ring, shows a very high chemical shift.

In the NOESY amplification (Figure 1.15), the correlation through the space between one of the H2 with the proton of the triazole H1 and both of the H2 with the NH of the amide bond, are also in accordance to structure **19.** On the other hand, it can also be said that the amide bond has a free rotation because both of the protons in H2 are able to “see” the NH.

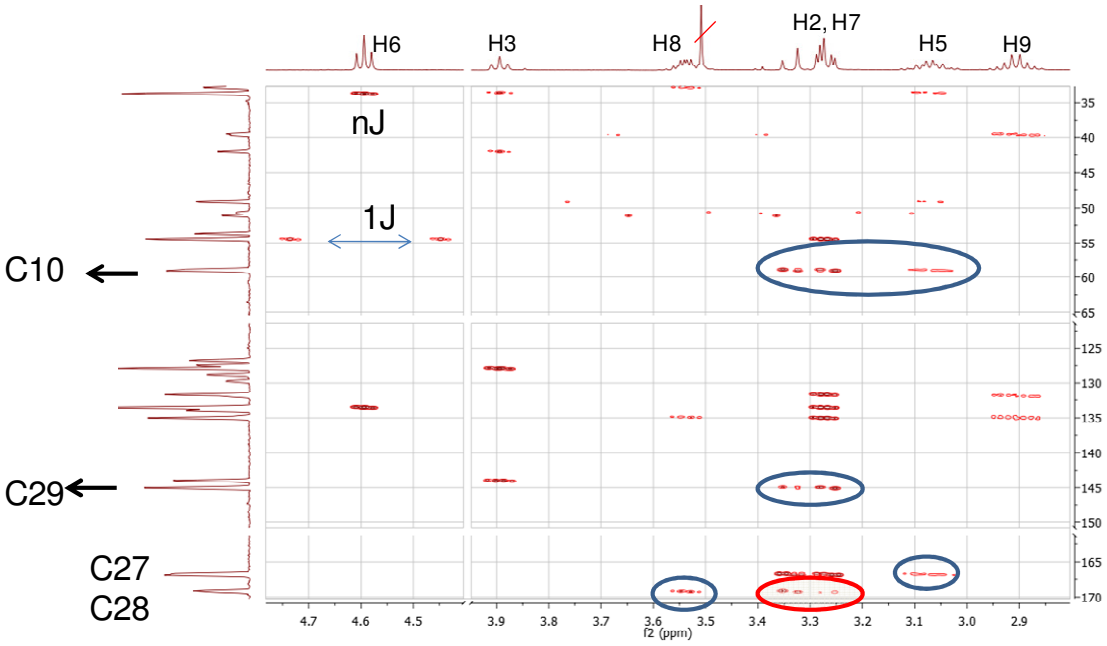


**Figure 1.14:** Amplification of the $^{1}H$-$^{13}C$ HMBC ($CDCl_3$, 500 MHz, 25 ºC) of the unknown cyclization compound.

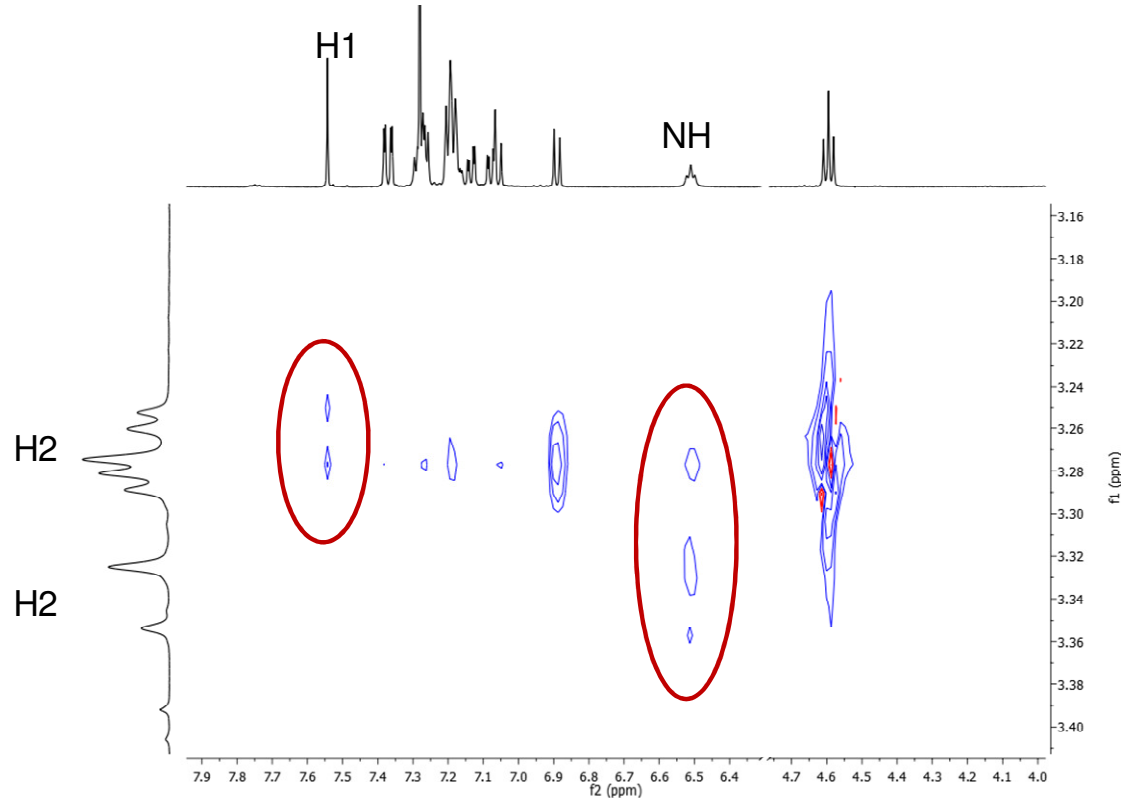


**Figure 1.15:** Amplification of the NOESY ($CDCl_3$, 500 MHz, 25ºC) of compound **19.**

After carefully analyzing again the NOESY, $^{1}H$-$^{13}C$ gHSQC/gHMBC, and $^{1}H$-$^{15}N$ gHMBC NMR spectra, as well as the FT-IR spectrum of the unknown structure, the proposed structure **19** was assigned. For the call of the FT-IR spectrum, (Figure 1.16) it is observed that in the case of **2a**, there is only one carbonyl absorption band (1670 $cm^{-1}$) because the two amides of the DKP are very similar. However, in the case of **19**, two carbonyl bands are observed. One of them (the one in the β-lactam ring) appears at higher wavenumber (1756 $cm^{-1}$), which means higher frequency due to the ring strain that reduces the conjugation of that carbonyl increasing the frequency in comparison with a secondary non-tensioned amide.[128] The carbonyl group of the other amide appears at 1679 $cm^{-1}$.

The formation of a similar two-step synthesis of β-lactams starting from isocyanides was also found in the literature,[55,118] but no reasonable explanation for the observed reactivity was reported. A deep study of this unexpected reaction will be discussed in Chapter 3.

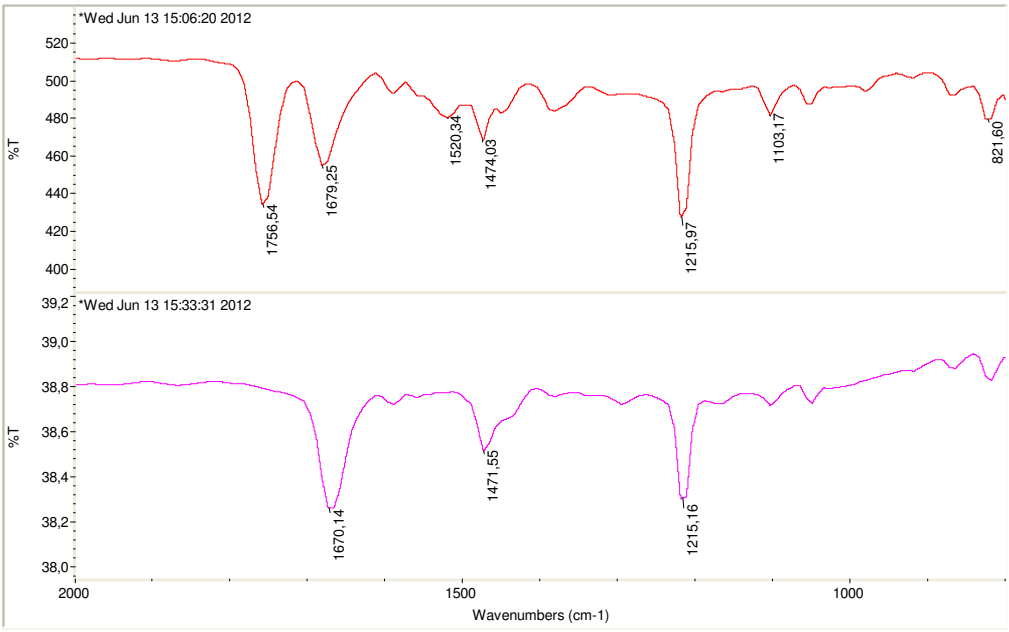


**Figure 1.16:** IR spectra of compounds **2a** and **19.**

### 1.3.3. Biological assays

The biological assays of compounds **2a**, **2b** and **19** were carried out in collaboration with the group of Prof. Enrique Pérez-Payá in Centro de Investigaciones Príncipe Felipe (Valencia) who had previously developed an efficient *in vitro* and *ex-vivo* methodology for measuring activity of molecules that inhibit the apoptosome formation.

All the compounds (**1**, **2a,b** and **19**) showed potent *in vitro* inhibition of the apoptosome-dependent activation of procaspase-9 activity (Figure 1.17 and Supp Info). Moreover, none of them was a direct inhibitor of the activity of recombinant caspase-9, which suggests that the most probable target is the apoptosome formation. As shown in Figure 1.17, a slight improvement of the activity was obtained in the triazole compounds, with non significant differences for the two regioisomers **2a** and **2b**. It is also worth mentioning that the β-lactam structure **19** exhibited the best activity. Similar inhibitory trends are observed in cellular extracts, although the standard deviations are quite high. Taken overall, this is an interesting starting point to further study this new scaffold for the design of optimized apoptosis inhibitors.

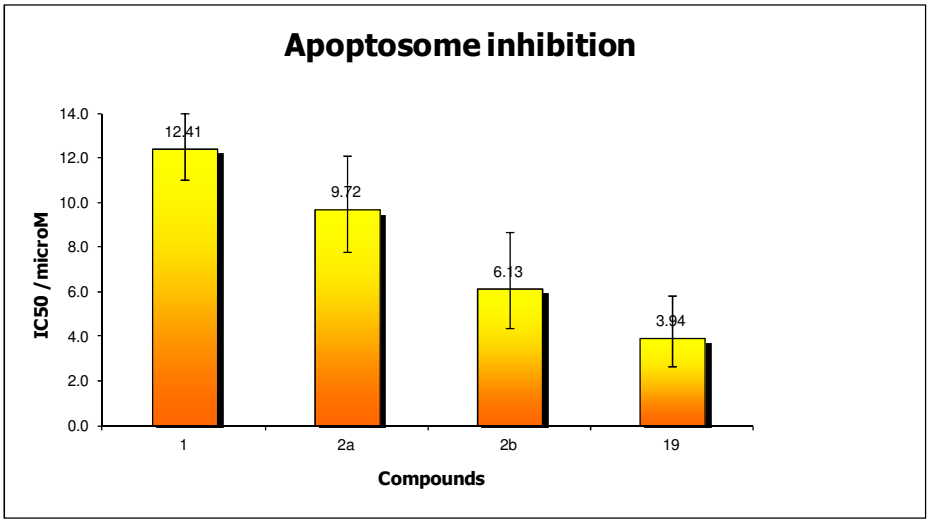


**Figure 1.17:** *In vitro* inhibitory activities of the apoptosome formation (for experimental details, see Experimental Part)

### 1.3.4. Computational studies

All the computational experiments were carried out in collaboration with Dr. Jordi Bujons.

As mentioned in the Introduction, the apoptotic protease-activating factor 1 (Apaf-1) controls caspase activation downstream to mitochondria. During apoptosis, Apaf-1 binds to cytochrome *c* and in the presence of ATP/dATP forms an apoptosome, leading to the recruitment and activation of the initiator caspase, caspase-9.[129] The mechanisms underlying Apaf-1 function are largely unknown and most of the structures of Apaf-1 found in the Protein Data Bank[130] are limited to the CARD domain. Riedl *et al.* published in 2005 the first structure of an Apaf-1 construct (Apaf-1 1-591) that involved the CARD and NOD domains (Figure 1.18).[1] This structure was representative of a significant part of the holo-Apaf-1 protein (1248 aa's in total) as to propose to carry out computational structure-based studies to determine potential modes of interaction of Apaf-1 ligands. It is significant to mention that with the structure of the protein, a molecule of ADP bound into a buried cavity was also detected. Consequently, this cavity was identified as the putative nucleotide binding site (NBD) where the ATP required for activation of the apoptosome would bind.

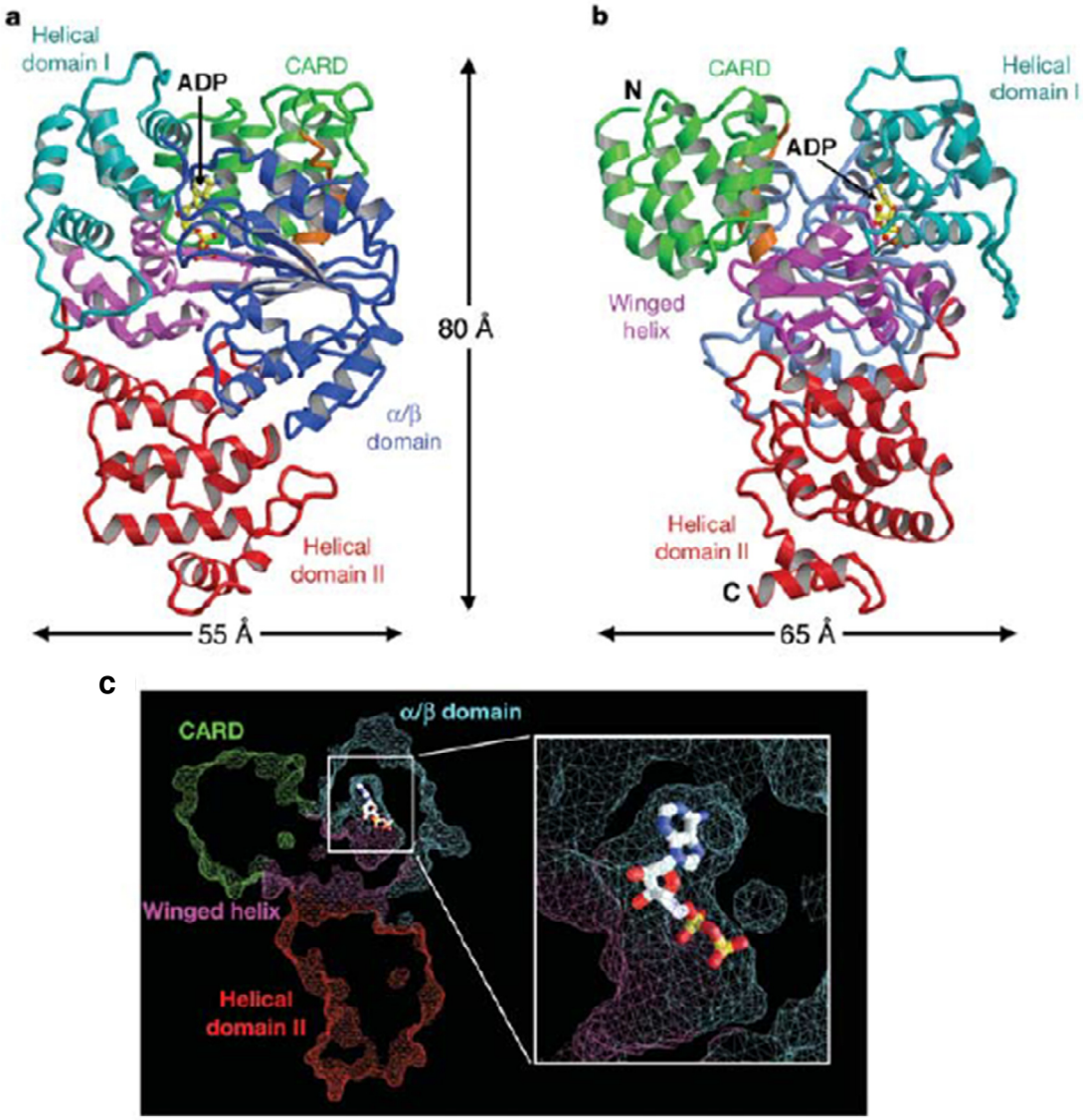


**Figure 1.10:** Overall structure of the WD40-deleted Apaf-1 bound to ADP. **a)** A ribbon diagram of the structure of Apaf-1 (residues 1-591) bound to ADP. Apaf-1 sequentially comprises five distinct domains: CARD (coloured green), an α/β fold (blue), helical domain I (cyan), a winged-helix domain (magenta) and helical domain II (red). These five domains pack against one another to generate a relatively compact structure. ADP binds to the hinge region between the α/β fold and helical domain I but is also coordinated by two critical residues from the winged-helix domain. **b)** The structure of Apaf-1 in another orientation. Relative to **a**, Apaf-1 is rotated 90º along a vertical axis within the plane of paper. **c)** A stereo view showing the binding of ADP in the Apaf-1 structure. (Modification of the Riedl's paper[1])

Molecular docking is one of the most widely used methodologies for receptor-base drug design (RBDD).[131] It allows to propose hypotheses of how ligands interact with target proteins and screen compound libraries to identify potential binder candidates, prior to experimental HTS.[132] Despite significant successes,[133] molecular docking still faces a lot of challenges, especially for efficiently exploring the conformational space of target proteins and ligands, and developing scoring functions to estimate the free energies of protein-ligand binding.

There are different available scoring functions,[134, 135,136] but in spite of the continuous efforts to improve them, their accuracy to rank the binding poses and to predict the binding free energies still remains unsatisfactory.[137]

Combining molecular mechanics and implicit solvation models, such as Molecular Mechanics/Generalized Born Surface Area (MM/GBSA) became popular in free energy calculations and molecular docking studies.[138-140] And some studies revealed that MM/GBSA performs well for both binding pose predictions and binding free energy estimations and is efficient to re-score the top-hit poses produced by other less accurate scoring functions.[141]

In order to identify possible sites of interaction on Apaf-1 for compound **QM31**, a related 7-membered cyclic analogue of **1**, preliminary blind docking screening targeting the reported human Apaf-1 1-591 (CARD-NOD) structure[1] was previously carried out in our research group. [142] This blind docking protocol involved: (i) a search for cavities in the Apaf-1 CARD-NOD structure to identify potential ligand binding sites, and (ii) a flexible docking of the ligand on to the different sites located.

The program SiteMap[143-145] was used to identify and score potential binding sites on the protein. The score provided by SiteMap is constructed and calibrated so that the average SiteScore for 157 investigated submicromolar sites is 1.0. Therefore, a score ≥ 1.0 suggests a site of particular promise, while a score ≤ 0.8 has been found to accurately distinguish between drug-binding and non-drug-binding sites. The best scored sites were used as targets for docking of the **QM31** ligand with the program Glide XP.[2-4]

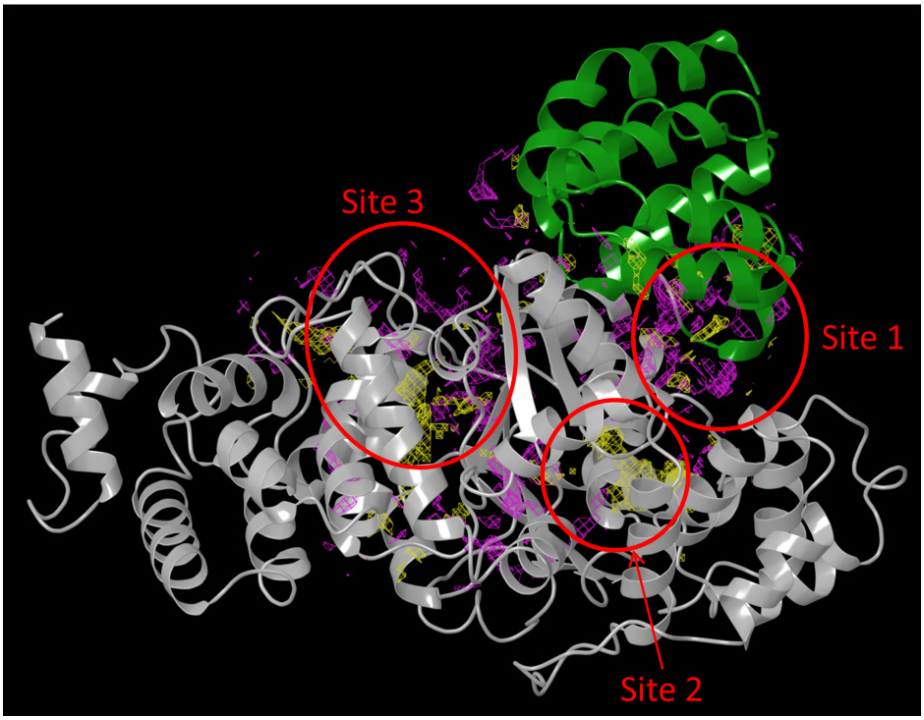


**Figure 1.19:** Human Apaf-1 CARD-NOD structure (PDB 1Z6T, Apaf-1 residues 1-591[1] showing the two domains (CARD in green, NOD in gray) and the computationally identified ligand binding sites, mapped as hydrophilic (magenta) and hydrophobic (yellow) mesh surfaces.

Figure 1.19 shows the best scored sites for interaction detected within the target structure and Table 1.1 summarizes the site scores. Thus, three main potential sites were identified. The first one (Site 1) is located on a large cleft at the CARD-NOD interface and is formed by helices α2, α3, α5, α7, α8, and the loop between residues 117-129. The second one (Site 2) is constituted by a relatively large cavity that coincides with the crystallographically identified ADP binding site (NBD), and implies helices α10, α15 and α17, sheets β2, β6 and β7, and loops between residues 117-129, 154-159 and 389-394. Finally, the third one (Site 3) is a nearly located cavity delimited by helices α12 and α25, sheets β2, β6 and β7, and loops between residues 207-219, 386-397 and 468-479. Docking at the three sites rendered plausible binding poses for **QM31** (Figure 1.20). The (*R*)-enantiomer was the best scored at all sites, although poses with similar conformations were also obtained for the (*S*)-enantiomer. At the most solvent exposed Site 1, binding was mainly stabilized through hydrogen-bond and π-cation interactions with different residues from the protein, while at the other two sites hydrophobic interactions were the main stabilizing contributions.

**Table 1.1:** Site scores for the best sites identified and docking scores for the best poses obtained for compound QM31. Residues that stabilize the docked poses through hydrogen-bonding, hydrophobic, π-cation or π-stacking interactions are listed.

| | Site score[a] | Docking score[b] | H-Bond | Hydrophobic | π-cation | π-stacking |
|---|---|---|---|---|---|---|
| Site 1 | 1.07 | -6.86 | Lys100<br>Arg122<br>Phe126<br>Arg428 | Ile106, Val124<br>Val125, Leu297 | Lys100<br>Arg111 | |
| Site 2 | 1.14 | -8.52 | Val124<br>Ser422 | Pro120, Pro123<br>Val124, Val127<br>Val 162, Ala165<br>Trp184, Ile294<br>Pro321, Leu322<br>Val419 | | Phe425<br>His438 |
| Site 3 | 1.07 | -7-71 | Gln477<br>Met481 | Leu216, Val393<br>Pro396, Pro475<br>Met481, Tyr482<br>Val517 | | |

[a] SiteMap scores ≥ 1.0 suggest sites with properties (hydrophobicity, hydrophilicity, H-bond donor or acceptor, and metal binding properties) of high suitability for ligand binding. [b] Glide XP docking scores in kcal $mol^{-1}$.

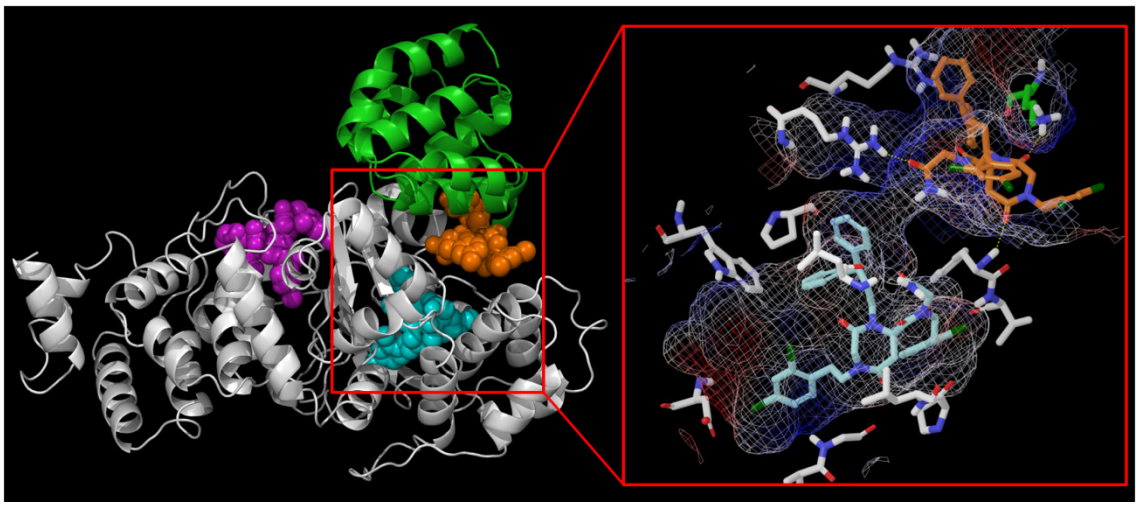

**Figure 1.20:** Human Apaf-1 CARD-NOD structure with the best docked poses determined for QM31 at the CARD-NOD interface (orange), the nucleotide binding site (cyan) and the third closely located site (purple). On the inset, the docked poses at the first two sites surrounded by interacting Apaf-1 residues, and a mesh representation of the protein surface that reveals a narrow channel connecting both sites, are shown.

Interestingly, in the reported crystal structure the first and the second binding sites (Sites 1 and 2) are connected through a narrow channel, which constitutes the only apparent entrance to the deeply buried nucleotide binding site (NBS), suggesting that access to this site requires unpacking of the CARD-NOD interface.[1] Thus, inhibitor binding at Site 1 could obstruct the access of dATP to the NBS by blocking the entrance to this channel and, possibly, by stabilizing Apaf-1 into a "locked" conformation that would hinder unpacking of the CARD-NOD interface. Alternatively, binding at Site 2 would directly block the NBS. Therefore, interaction with any of these sites, or both, would hamper dATP binding, and consequently would interfere with apoptosome formation. Furthermore, these two predicted binding sites on Apaf-1 were consistent with preliminary NMR and fluorescence experimental results that suggested the interaction between **QM31** and Apaf-1.

**Docking Analysis**

The above mentioned docking studies were extended to compounds **1**, **2a**, **2b** and **19**, however in this case only Sites 1 and 2 were considered since the relevance of the interaction at Site 3 for apoptosome inhibition was less clear. Since all the compounds have a single stereogenic center on their structures, independent docking runs were carried out for each enantiomer. Figure 1.21 shows the docking results obtained for compound **(*R*)-19**, on which the following discussion is focused. Figures 1.22 and 1.23 show the best poses of the other compounds, as well as the corresponding interaction diagrams.

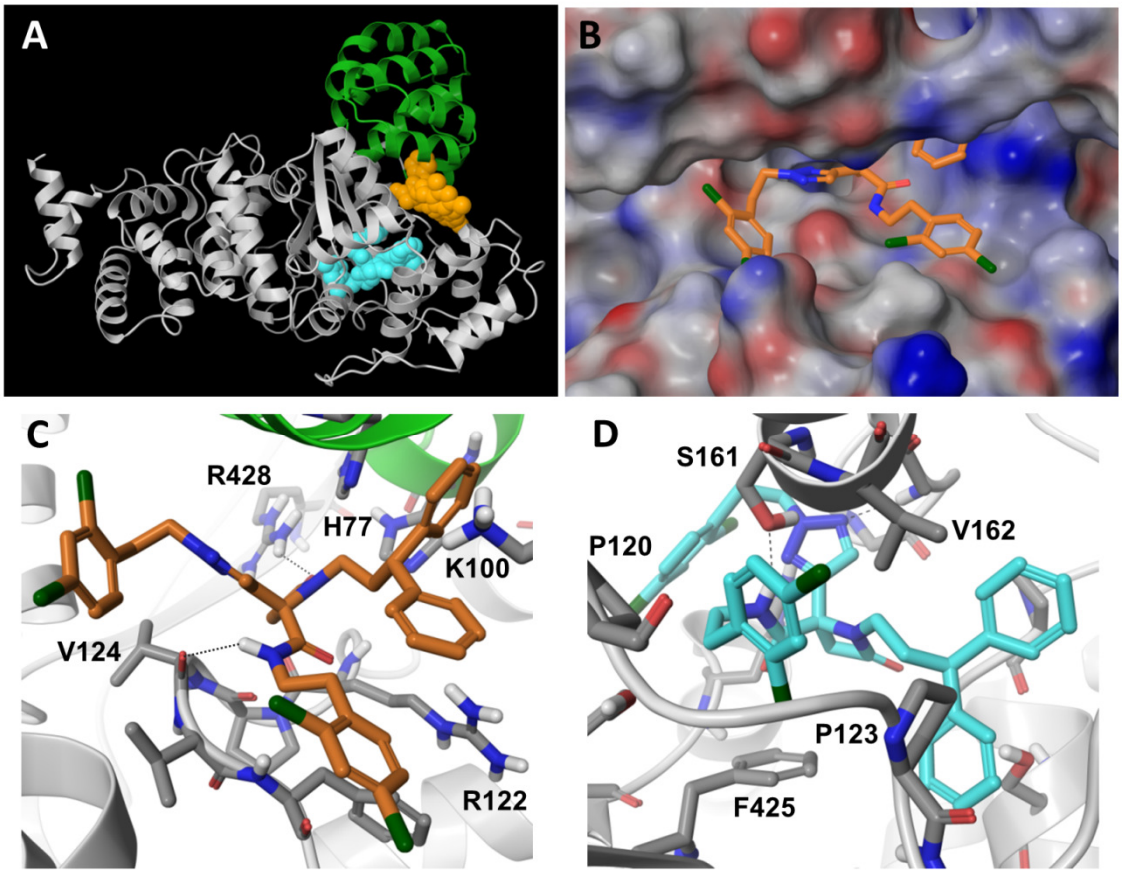


**Figure 1.21: A)** Best docked poses of compound **(R)-19** bound at the putative binding Sites 1 (orange) and 2 (cyan). **B)** View of **(R)-19** bound at the narrow cleft that constitutes Site 1. **C** and **D)** Detailed view of the above docked poses at the two sites surrounded by interacting Apaf-1 residues. Docking was performed with the program Glide XP.[2, 3 4]

According to our docking results, at Site 1 compound **(*R*)-19** is disposed along the cleft covering the entrance to the NBS access channel, with its diphenylmethyl moiety occupying a cavity formed by residues His28, Asp32, His77, Lys100, Arg111, and Arg122 (Figure 1.21B,C). The two aromatic rings of this moiety establish π-cation and π,π-stacking interactions with residues Lys100 and His77, respectively. All the other compounds similarly showed occupation of this cavity by their diphenylmethyl or one of their dichlorophenyl moieties, which were also stabilized by similar interactions with the cited residues (Figure 1.22). On the other hand, one of the dichlorophenyl substituents of **(*R*)-19** extents to the other side of the cleft and forms a π-cation interaction with residue Arg332, while the second dichlorophenyl group is oriented towards the more solvent exposed part and is disposed on top of a small hydrophobic patch on the surface of the protein, formed by residues Val125 and Leu297. Finally, the exocyclic amide as well as the carbonyl group of the β-lactam ring contribute to stabilize the docked pose of **(*R*)-19** by participating on hydrogen-bond interactions with residues Val124 and Arg428. Analysis of the docking poses obtained for the enantiomeric **(*S*)-19** and the rest of the compounds studied showed similar results (Figure 1.22). Hence, a common feature of the compounds bound at Site 1 was the formation of several π-cation interactions with different cationic residues (i.e. Lys100,

Arg111, Arg122 and Arg332), as well as hydrogen bond interactions with the polar side-chains or the backbone of close residues, while the contribution of hydrophobic interactions at this site was in general less important (Table 1.2), as already observed for **QM31**.

**Table 1.2:** Apaf-1 residues that participate in stabilizing the docked poses of compounds **1**, **2a**, **2b** and **19** through hydrogen-bonding, hydrophobic, π-cation or π-stacking interactions.

| | H-Bond | Hydrophobic | π-cation | π-stacking |
|---|---|---|---|---|
| Site 1 | Ser104<br>Arg122<br>Val124<br>Phe126<br>Arg428 | Tyr24 Ala74<br>Ile106 Pro123<br>Val124 Val125<br>Phe126 Leu297 | Lys100<br>Arg111<br>Arg122<br>Arg332 | His28<br>His77 |
| Site 2 | Gly157<br>Gly159<br>Ser161 | Pro120 Pro123<br>Val124 Val125<br>Phe126 Val127<br>Ala156 Val162<br>Ala165 Trp184<br>Ile294 Phe298<br>Pro321 Leu322<br>Val419 Phe425<br>Tyr436 | | Phe425<br>His438 |

Concerning the predicted binding Site 2, the residues that constitute this cavity are mainly hydrophobic in nature, particularly in the region close to the location of the purine ring of the bound ADP (ie. residues Pro123, Val125, Phe126, Val127, Val162, Ile294 and Pro321). The best docked pose obtained for compound **(*R*)-19** fills most of the cavity and partially overlaps with the crystallographically determined ADP molecule (Figure 1.21A,D), suggesting that both compounds would compete for binding at this Site. Its diphenylmethyl moiety occupies the same location as the purine system of ADP, while one of the dichlorophenyl rings is disposed in an approximately parallel orientation, surrounded by residues Pro120, Pro123, Val162 and Ala165, and the second one extents towards a more hydrophilic region of the cavity, constituted by the polar residues Lys160, Asp243, Asp244, Arg265, Asp392, His438 and Asp439. Finally, the triazole ring of **(*R*)-19** occupies the region where the diphosphate group of ADP binds, establishing a π,π-stacking interaction with His438 and a hydrogen bond with the backbone NH-group of Gly159, while the β-lactam is disposed close to the location of the ADP-ribose group. On the other hand, the best docked pose of the stereoisomer **(*S*)-19** shows an inverted geometry where the diphenylmethyl and dichlorophenyl moieties that were occupying the hydrophobic locations described above have switched places, while the second dichlorophenyl ring and the linked triazole still occupy the more hydrophilic region and the diphosphate binding site, respectively (Figure 1.23). The rest of the compounds considered show best docked poses

which are similar to that of **(*S*)-19,** with the exception of compound **(*S*)-1** which resembles more to **(*R*)-19**. The existence of these alternative docking geometries is derived from the flexibility of the compounds, as well as the large size of the cavity and the fact that the main stabilizing interactions with the protein are of hydrophobic, and therefore less specific, nature (Table 1.2).

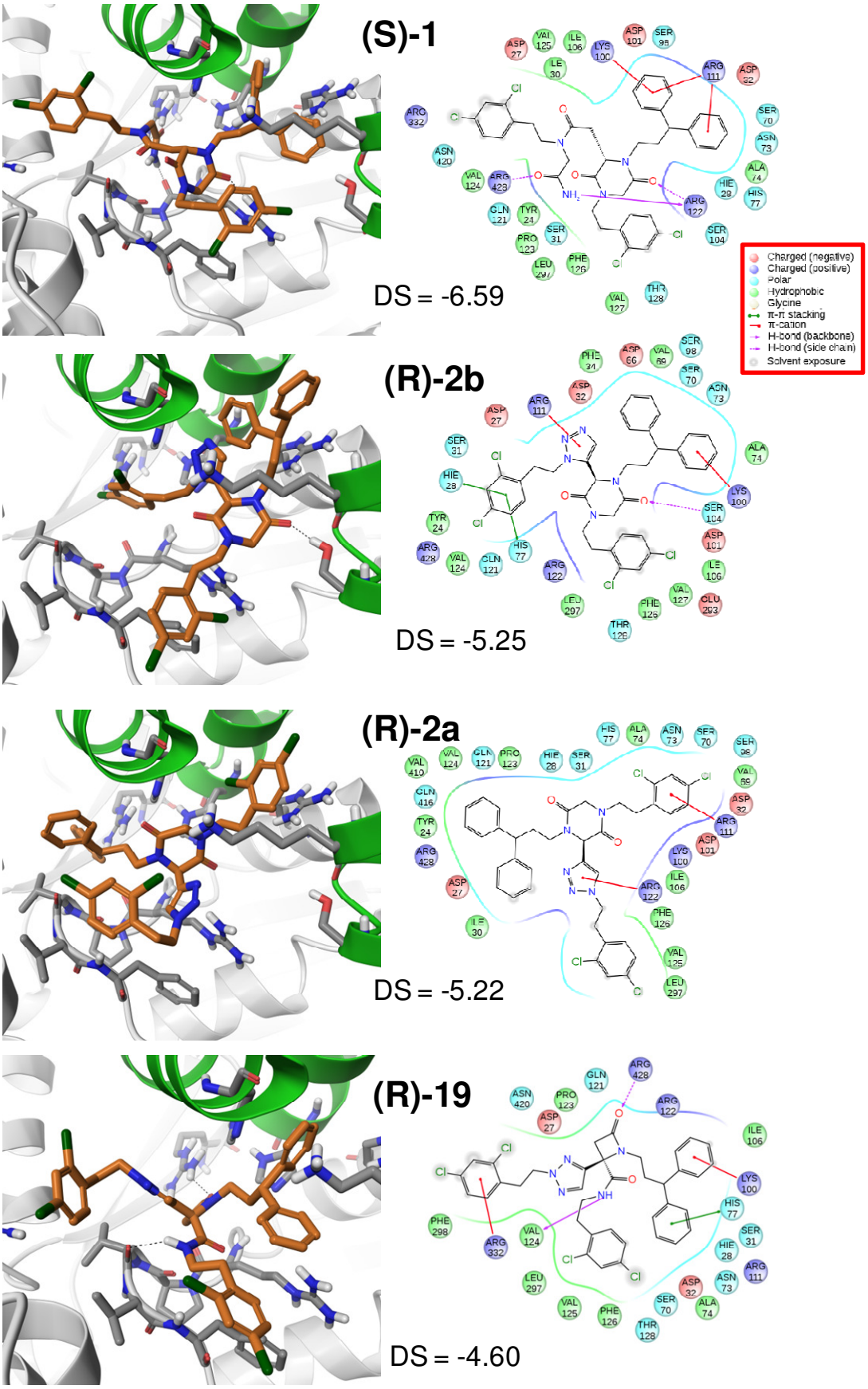


**Figure 1.22:** Best docked poses (left) and interaction diagrams (right) obtained for compound **1**, **2a**, **2b**, **19** bound at Site 1.

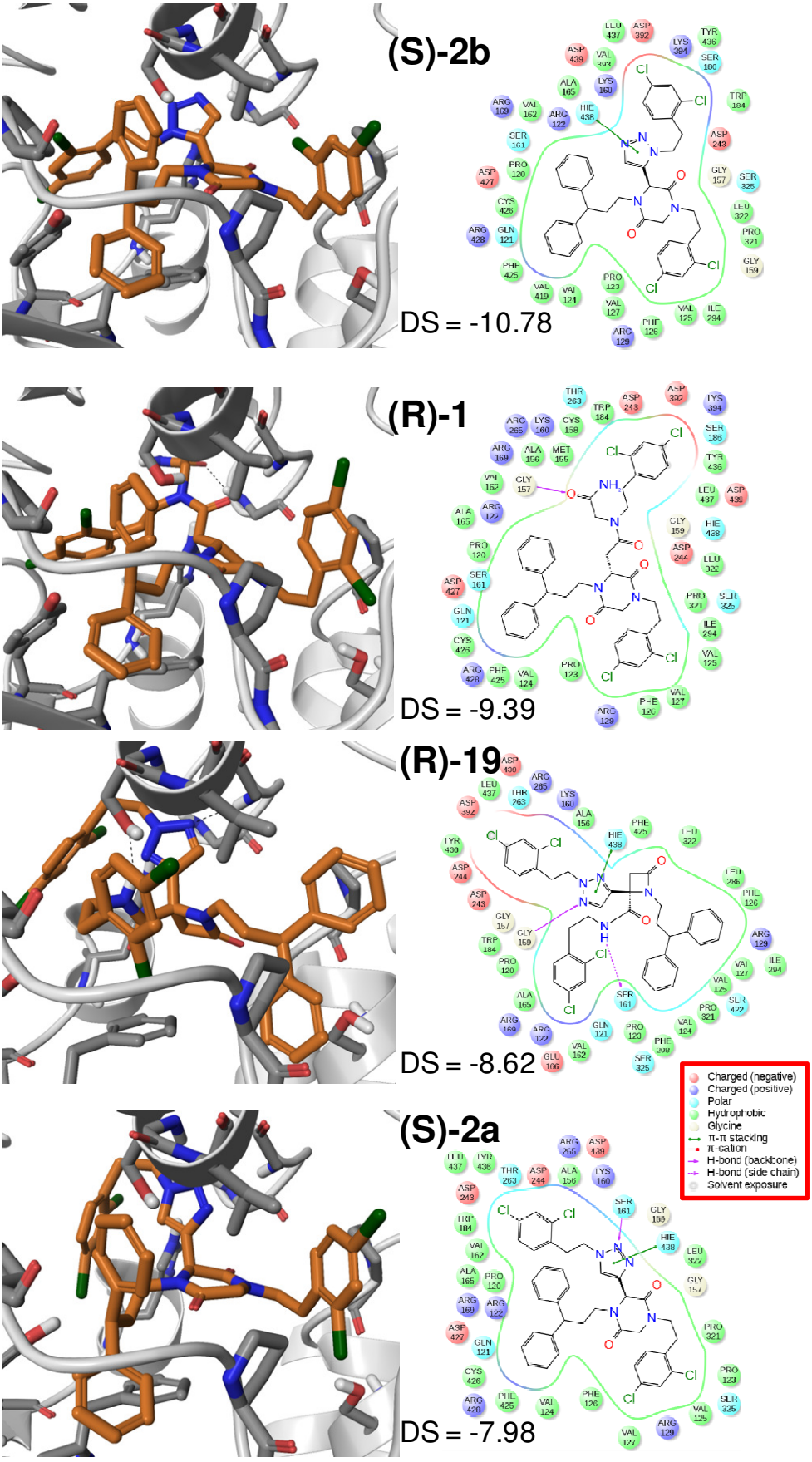


**Figure 1.23:** Best docked poses (left) and interaction diagrams (right) obtained for compounds **1**, **2a**, **2b** and **19** bound ate Site 2.

After analysis of these results, it is worth noting that the relative similarity in bound geometries and binding interactions at each site is in agreement with the comparable biological activities observed for these compounds. It is also remarkable that, considering the best poses obtained for all the compounds (with both enantiomers), the average docking scores for Sites 1 and 2 are 4.9 ± 1.0 and 8.1 ± 1.7 kcal $mol^{-1}$. Although docking scores alone often show little correlation with experimental binding affinities, this difference would suggest that binding at Site 2 is stronger than at Site 1. Therefore it could be speculated that Site 1 could act as a vestibule where the compounds studied could bind with a relatively low affinity before accessing the higher affinity NBS-Site 2 to exert their apoptosome inhibitory activity.

**Induced Fit Docking and Rescoring.**

One of the frequent limitations of the docking methodologies is the fact that although the ligands are usually considered to be flexible, the protein is normally treated as a rigid body. To further asses the docking and scoring of the compounds studied taking into account the flexibility of the protein, a redocking analysis was devised using an Induced Fit Docking protocol. [146-149,150]

This protocol consisted on the following steps:

1. Initial docking of each ligand using a softened potential (van der Waals radii scaling). This has the goal of allowing poses that would “penetrate” into the protein if it was considered as a rigid body, but that would normally be possible if a small conformational change is allowed.
2. Side-chain refinement of residues with atoms within a given distance of any ligand pose. This produces an initial adaptation of the protein to the presence of the ligand.
3. Minimization of the same set of residues and the ligand for each protein/ligand complex pose. The receptor structure in each pose now reflects an induced fit to the ligand structure and conformation.
4. Redocking of each protein/ligand complex structure within a specified energy of the lowest-energy structure. The ligand is now rigorously docked into the induced-fit receptor structures.
5. Estimation of the binding energy (Glide XP and IFD Scoring) for each output pose. The scores generated by this protocol are of two types. On one side, poses are scored with the Glide XP scoring function,[2-4] which tries to correlate binding energies. Secondly, an IFD score is also generated which is obtained by the sum of the Glide XP score plus 5% of the Protein energy, as determined by the software Prime.[148] The IFD score was parameterized to improve the predicted geometry of the bound poses of compounds whose binding involve an induced fit adaptation of the protein, therefore it is not expected that it correlates binding energies, although they contribute somehow to this score.

Analysis of the results from applying this protocol showed, as expected, small changes on the structure of the protein relative to the original structure. Those changes were essentially limited to readjusments of the sidechains of the residues interacting with the ligands. Similarly, small readjustments on the geometries of the best poses were observed. However, comparison of the new Glide XP scores with the previously obtained showed significantly improved, ie. more negative, values (Figure 1.24) which suggest a tighter binding at both sites.

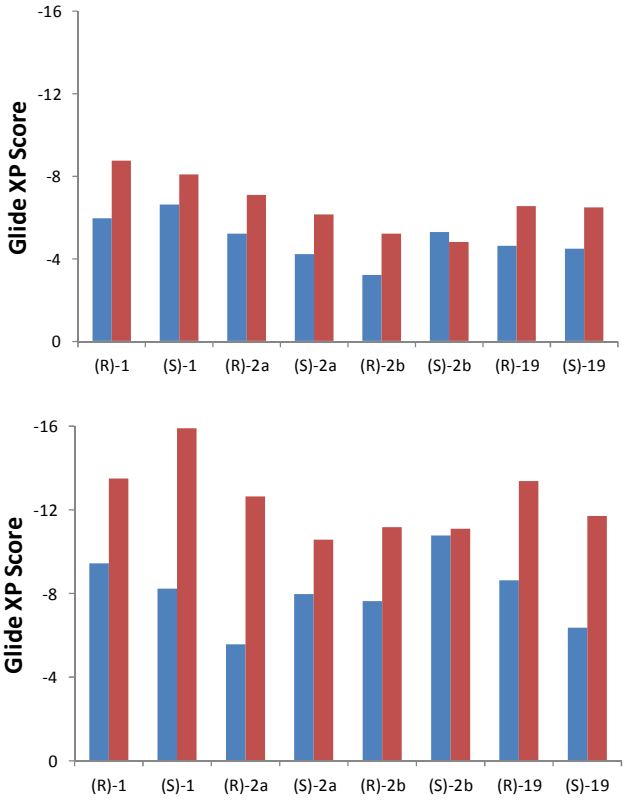


**Figure 1.24:** Glide XP scores obtained for compounds **1**, **2a**, **2b** and **19** at Sites 1 (above) and 2 (below). Scores from docking with the normal Glide XP protocol are shown in blue, and scores from the Induced Fit Docking protocol are shown in red.

The different Glide XP scores among the compounds do not follow the same order of potency as the experimental values, however this was not unexpected since the admitted error of the Glide XP scoring function is ~2.3 kcal/mol[4] although it can be much higher (ie. ~4 kcal/mol; http://www.schrodinger.com/kb/793). However, the differences between the strength of binding at both sites are still significant: average docking score at Site 1: -6.6 ± 1.6 kcal/mol; at Site 2: -12.3 ± 1.8 kcal/mol. Therefore, these results further support the existence of two potential sites of interaction for our compounds on Apaf-1, and the hypothesis that Site 1 could act as a vestibule to access Site 2. Reaching the second site would however require that the protein suffers some conformational change that "opens" the channel so that the ligand can go through and reach the NBD. As it has already been mentioned, this was previously proposed in the paper from Riedl *et al.* to explain how would the ATP/ADP molecule bind into the NBD,[1] however it is not clear by which mechanism would that occur.

## 1.4. Conclusions

- A strategy involving an Ugi multicomponent reaction has been developed to synthesize restricted analogues of the active compound **1**, using 1,4-, 2-4 and 1,5-disubstituted triazoles to mimic the exocyclic tertiary amide bond isomers.

- Unexpectedly, for one of the proposed structures, a new compound bearing a β-lactam structure (**19**) was characterized and showed to be a potent inhibitor of the formation of the apoptosome.

- The improvement of the inhibitory activity of the newly synthesized compounds supports the efficiency of our approach. In this sense, it can be anticipated that the lower the conformational mobility, the lower the risk of unwanted side activities.

- Computational studies with the compounds **1**, **2a**, **2b** and **19** have been carried out to validate the proposed mechanism that would account for their biological effects as apoptosis inhibitors.

# 2.Synthesis and NMR structural study of disubstituted 1,2,3-triazoles

## 2.1. Introduction

### 2.1.1. Isomeric triazoles differentiation

1,2,3-Triazoles are nitrogen heteroarenes that have found a range of important applications in the pharmaceutical and agricultural industries. As we have already mentioned, the 1,3-dipolar cycloaddition of organic azides and alkynes is a direct route to 1,2,3-triazoles, but the reaction course is slow and not regioselective. However, the discovery of the catalytic azide-alkyne cycloadditions (using CuAAC[84,85] or RuAAC[103,90]) provides access to the synthesis of 1,2,3-triazoles under mild conditions and excellent regioselectivity.

The tautomerism and isomerism of triazoles make the structural analysis of these compounds troublesome. The structures of many of these triazoles were elucidated by X-ray crystallography analysis,[91, 103, 151, 152] or by sophisticated NMR methods, including NOE,[84, 91, 153] HMQC, HSQC and HMBC studies.[127, 154]

While the structures of triazoles prepared in the Sharpless/Fokin research and in other studies have been rigorously demonstrated,[155] in many subsequent examples the structures of the isolated triazoles are not proved, but simply assigned using the assumption that Cu (I) catalysis gives 1,4-disubstituted isomers, while Ru (II) catalysis gives the 1,5- distribution. In any case, when a mixture of the two or three possible 1,2,3-triazole isomers is obtained, a method for the verification of the structure is needed.

Creary *et al.*[156] recently reported a simple method combining $^{13}C$ NMR and computational observations for distinguishing between 1,4- and 1,5-disubstituted triazoles. As shown in Figure 2.1, each isomer has a different $^{13}C$ NMR chemical shift. For the 1,4-disubstituted-triazole (**A**), the CH signal appears at ~120 ppm for C5, while C4 in **B** is at ~133 ppm. These $^{13}C$ NMR signals are readily identified by the large $^{1}J_{CH}$ coupling constants in the gated decoupled $^{13}C$ NMR spectrum. These authors also demonstrated that B3LYP/6-31G* GIAO computational studies agree with this trend, although calculated shifts are consistently about 6 ppm upfield from the experimental values.

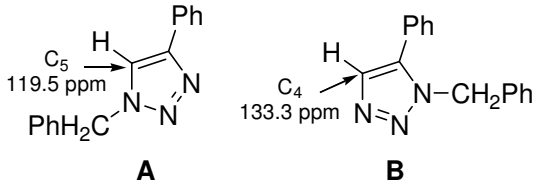


**Figure 2.1:** Characteristic $^{13}C$ signal to distinguish between 1,4- (**A**) and 1,5- (**B**) disubstituted triazoles.[156]

In Chapter 1, we commented the synthesis of 2-hydroxymethyl-2*H* 1,2,3-triazoles[127] (Scheme 1.13, Chapter 1), where a mixture of the 2,4- and the 1,4-disubstiuted triazoles was

obtained. The structure of the 2,4-disubstituted-1,2,3-triazole was confirmed by X-ray structure of the purified product by the original authors. However, to confirm that in all the assayed cases the 2-substituted product was predominant, they used the $^{13}C$ NMR chemical shift of the hydroxymethylene carbon. The identification of the minor product as the 1,4-disubstituted-1,2,3-triazole was carried out by HMQC and HMBC experiments.

In our case, after hydrolyzing the 2-hydroxymethyl-*2H*-1,2,3-triazole to obtain the *NH*-1,2,3 triazole, we performed the $S_N2$ reaction where a mixture of the three possible isomers was formed (Scheme 2.1). With these results, we deemed that an additional method for characterizing 1,2,3-triazole isomers could be very useful to distinguish between all the isomers.

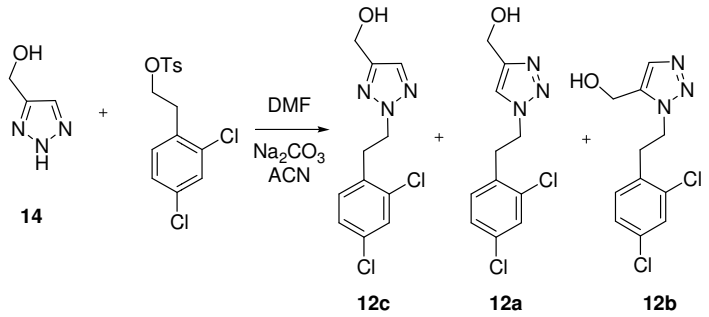


**Scheme 2.1:** Synthesis of triazole **12c** where a mixture of isomers was observed.

## 2.1.2. $^{1}H$-$^{15}N$ HMBC

Long-range heteronuclear chemical shift correlation experiments (HMBC),[157] introduced in 1986 by Summers and Bax, is still the most important NMR experiment for the structure elucidation of natural products. These experiments yield proton connectivities through quaternary carbons or heteronuclei and recently their sensitivity has been improved with the incorporation of pulsed field gradients. The addition of pulsed field gradients to NMR pulse sequences yields spectra with fewer artifacts and reduces the data collection because the selection of the desired coherence pathways occurs without extensive phase cycling.[158] Although the HMBC experiment is widely applied to organic structure determination at $^{13}C$ natural abundance,[159-161] less applications for this experiment at $^{15}N$ natural abundance using pulse field gradients have been reported.[162, 163]

Isomer differentiation has been in many cases troublesome on the basis of spectroscopic data. $^{15}N$ NMR spectroscopy, in particular long-range $^{1}H$-$^{15}N$ heteronuclear multiple-bond correlation ($^{1}H$-$^{15}N$ HMBC) experiments, can constitute a useful alternative to differentiate regioisomers that cannot be distinguished with conventional NMR experiments. Unlike the $^{13}C$ counterparts, these $^{15}N$ experiments have been rarely employed due to the low gyromagnetic ratio $\gamma_N$ of $^{15}N$ and its relatively low natural abundance (0.37%). Despite these shortcomings, $^{15}N$ NMR spectroscopy has the advantage that $^{15}N$ chemical shifts span over large range and

this nuclide still has useful potential as a structural probe even at natural abundance. [164] In addition, since the HMBC experiment is based on the indirect detection pulse sequence, where both the pulse and the acquisition is done through the $^{1}H$ nuclei, the $^{1}H$-$^{15}N$ HMBC experiment is only about three times less sensitive than the $^{1}H$-$^{13}C$ HMBC despite the low gyromagnetic ratio of $^{15}N$. Thus, only the natural abundance of $^{15}N$ to $^{13}C$ is of relevance.[165]

With the recent improved stability of NMR spectrometers and the advent of high-field magnets, cryoprobes and the use of pulsed gradients for coherence selection, the time required to obtain a $^{1}H$-$^{15}N$ HMBC spectrum has been shortened considerably. Moreover, the new electronics of the instruments provides some advantatges. For example, the auto tuning system can automate all routine measurements of the spectrometer. All together, inverse-detected NMR methods with natural isotopic abundance will become more popular in structural determination.[166, 167]

The natural abundance $^{15}N$ gradient-enhanced HMBC experiment is easy to implement, provides high-quality spectra and readily distinguishes nitrogen-containing regioisomers. As already mentioned, because of the availability of pulsed field gradient technology, this experiment should be implemented routinely for structure elucidation. Actually, some regioisomerism problems have been resolved *via* $^{1}H$-$^{15}N$ HMBC.[158,163,165,168,169]

## 2.2. Objectives

Taking the previous information into account, we would like to find a complementary method using $^{1}H$-$^{15}N$ HMBC to characterize and unambiguously assign the different isomers in 1,2,3-triazoles. Moreover, we have planned to study the NMR effects caused by changing the substituents (R1 and R) (Figure 2.2) in the 1,2,3-triazoles.

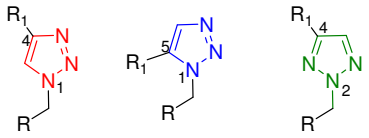


**Figure 2.2**: 1,2,3-triazole isomers (1,4-, 1,5- and 2,4- respectively).

## 2.3. Results and discussion

### 2.3.1. 1,4-Disubstituted 1,2,3-triazoles

In order to study the effects of the substituents on each isomer, a diversity of compounds were synthesized. For the synthesis of the different 1,2,3-triazole isomers, the methods explained in Chapter 1 were used.

First of all, the synthesis of 1,4-disubstituted-1,2,3-triazoles was carried out using the copper (I) catalyzed cycloaddition reaction as follows:

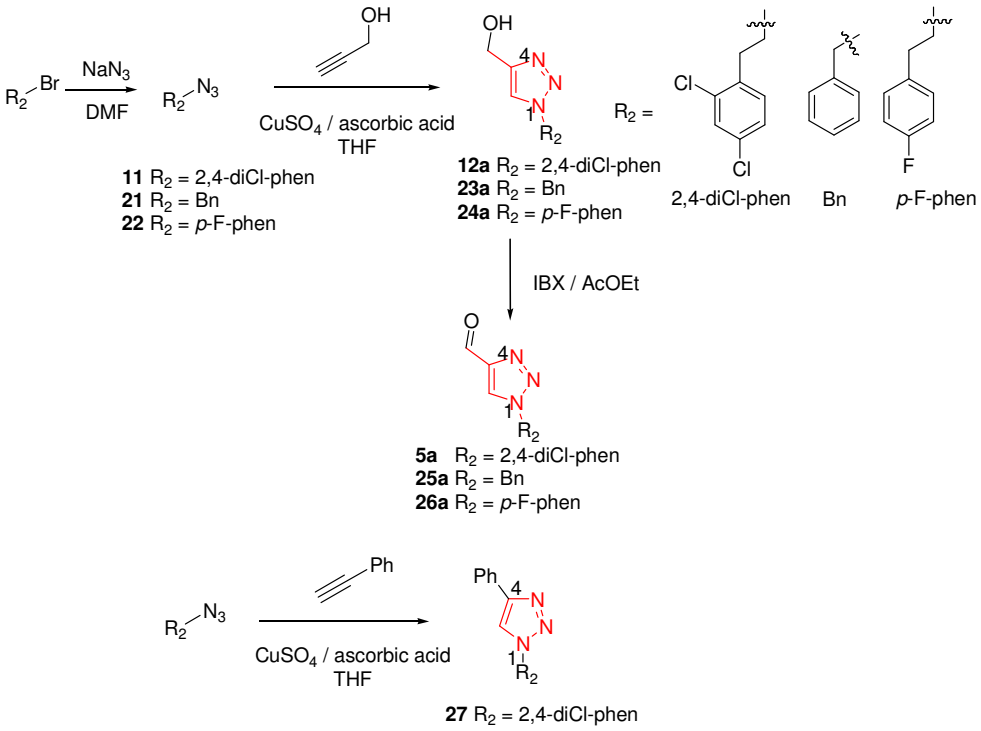


**Scheme 2.2:** Synthesis of 1,4-disubstituted 1,2,3-triazoles bearing different substituents.

Scheme 2.2 shows the different substiuents that were used. As we had already synthesized the 1,4-disubstituted triazole where $R_2$ is a 2,4-dichlorophenethyl group, the hydroxymethyl derivative **12a** and the aldehyde **5a** were added to the NMR study.

Afterwards, the benzyl and *p*-fluorophenethyl azides **21**, **22** were used to obtain both, the derivatives with the hydroxyl group **23a, 24a** and the aldehydes **25a, 26a**. Finally, compound **27** was also prepared from phenylacetylene and 2,4-dichlorophenethyl azide.

The presence of $Cu^{2+}$ traces yields wider signals in the $^{1}H$ NMR and worse $^{1}H$-$^{15}N$ HMBC spectra, due to the paramagnetic character of the metal. Thus, extractions with $NH_3$ (aq) were needed to remove the copper that is complexed with the triazole.

Once all the triazole derivatives described above were available, they were carefully characterized, acquiring $^{1}H$, $^{13}C$, $^{1}H$-$^{13}C$ HSQC, $^{1}H$-$^{13}C$ HMBC and $^{1}H$-$^{15}N$ HMBC NMR experiments. The $^{1}H$ NMR spectrum of the 1,4-disubstituted-1,2,3-triazole with the 2,4-dichlorophenethyl group (**12a**) is shown in Figure 2.3. Only mention that the characteristic proton of the triazole (**b**) appears at 7.36 ppm and that one from the $CH_2$ of the hydroxymethyl group (**a**) at 4.79 ppm. In all other derivatives bearing different $R_2$ groups, the triazole proton appears between 7.34-7.46, while the $CH_2$ (**a**) practically remains unchanged (4.77-4.79 ppm).

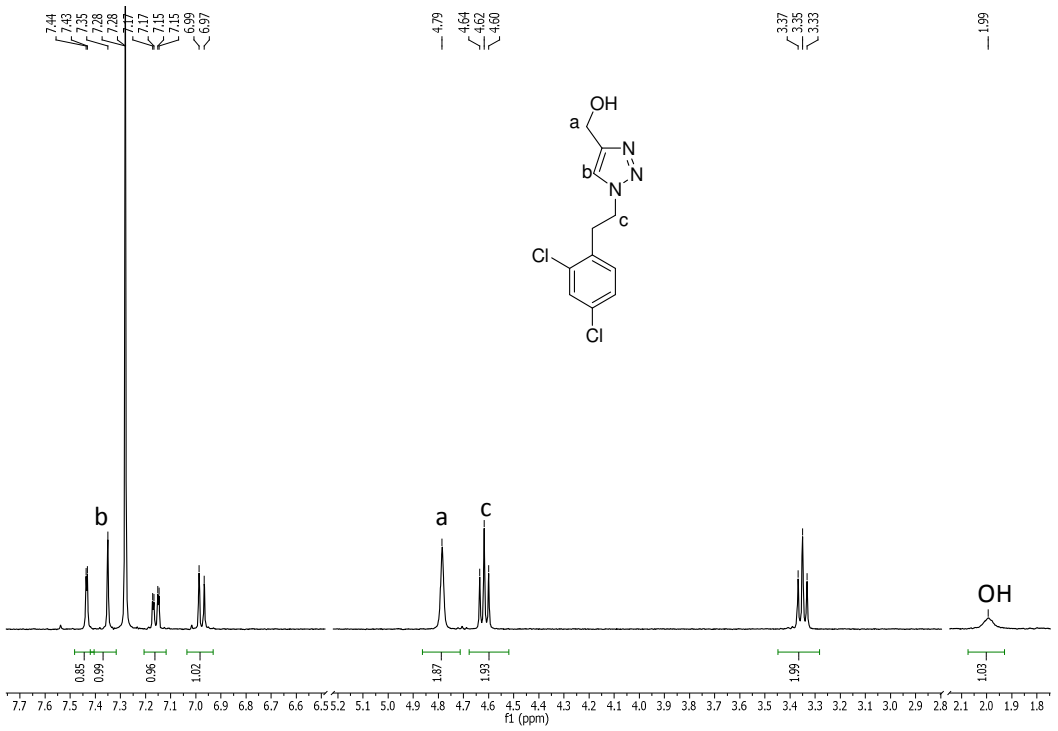


**Figure 2.3:** $^{1}H$ NMR spectrum ($CDCl_3$, 500 MHz, 25ºC) of triazole **12a**.

The presence of different $R_2$ substituents does not have significant effects on the $^{1}H$ NMR spectra. When going from the hydroxymethyl group to the aldehyde or in the presence of the phenyl substituent, the $^{1}H$ chemical shifts are only slightly different. In the aldehyde substituents, the triazole proton (**b**) shows a chemical shift within 7.80-8.0 ppm, which is higher than the previous 7.36 ppm. The phenyl group in **27** produces a decrease in the shielding (7.53 ppm), but not as much as with the aldehyde derivatives. These anisotropic effects are due to a higher conjugation with the triazole nucleus.

To identify all the $^{13}C$ and $^{15}N$ chemical shifts, the $^{1}H$-$^{13}C$ NMR correlation experiments and $^{1}H$-$^{15}N$ HMBC experiment were carried out.

The $^{1}H$-$^{15}N$ HMBC experiment for **12a** is depicted in Figure 2.4. The correlations are critical to assign the nitrogens. This experiment was carried out using a coupling constant of 8 Hz, which is the standard for this type of experiments. As shown, $N_1$ should have a correlation peak with **c**, **d** and **b**. Thus, the N at -134.8 ppm is the alkylated $N_1$, which is in accordance with the fact that is the most shielded. The nitrogen at -31.5 ppm must be $N_3$ because correlates with the $CH_2$ of the hydroxymethyl group (**a**) and because $N_2$ is too far from **a**. Finally, only check that the last nitrogen ($N_2$) correlates with **c** and the chemical shift of $N_2$ appears at -18.3 ppm.

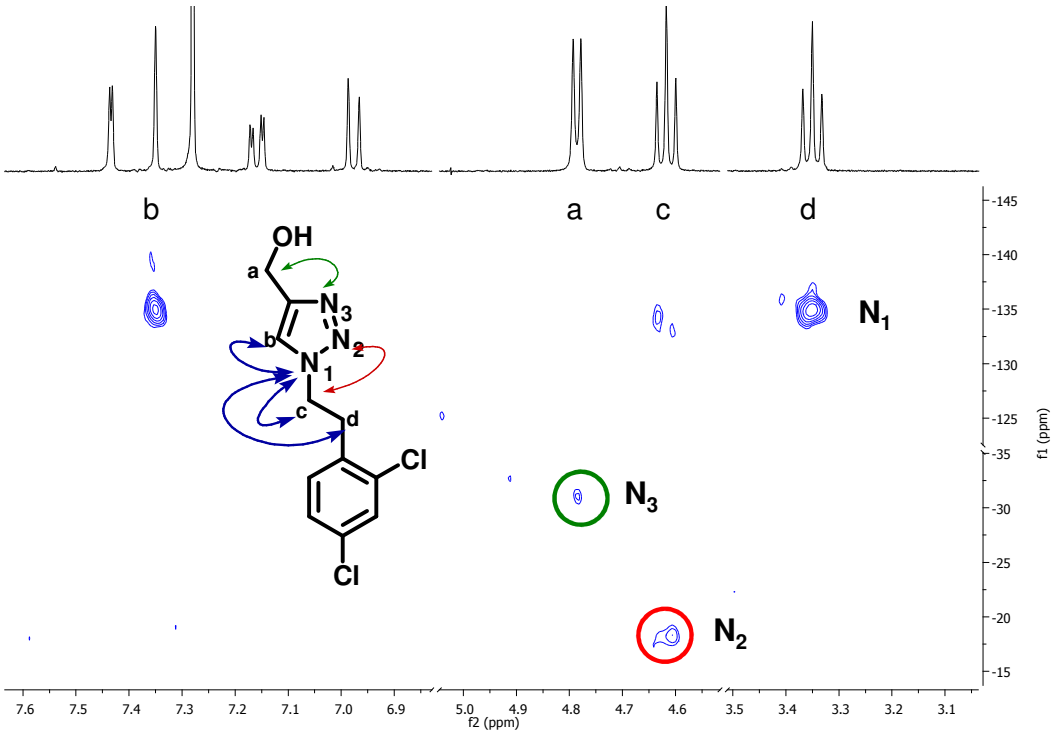


**Figure 2.4:** $^{1}H$-$^{15}N$ HMBC spectrum ($CDCl_3$, 400 MHz, 25ºC referenced to $MeNO_2$) of **12a.**

This experiment was extended to all the other synthesized products. The triazole proton ($H_5$), $^{13}C$ and $^{15}N$ chemical shifts obtained for all products are shown in the Figure 2.5. With this information, the similarities and differences caused by the different substituents are easily found.

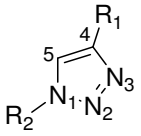


$R_1$ = $CH_2OH$, CHO, Ph

$R_2$ = 2,4-diCl-phen, Bn, *p*F-phen

| $R_1$ | $R_2$ | Cmpd. | $N_1$ | $N_2$ | $N_3$ | $C_4$ | $C_5$ | $H_5$ |
|---|---|---|---|---|---|---|---|---|
| $CH_2OH$ | 2,4-diCl-phen | **12a** | -134.8 | -18.3 | -31.5 | 147.9 | 122.1 | 7.36 |
| | Bn | **23a** | -133.7 | -19.4 | -37.2 | 147.7 | 121.8 | 7.46 |
| | *p*F-phen | **24a** | -134.4 | -19.9 | -36.1 | 147.5 | 122.2 | 7.34 |
| CHO | 2,4-diCl-phen | **5a** | -130.9 | -12.8 | -18.9 | 146.6 | 125.7 | 7.89 |
| | Bn | **25a** | -126.4 | -11.6 | -20.9 | 148 | 125 | 8.0 |
| | *p*F-phen | **26a** | -130.1 | -12.7 | -19.6 | 147.5 | 125.4 | 7.80 |
| Ph | 2,4-diCl-phen | **27** | -134.4 | -18.2 | -34.4 | 147.6 | 119.8 | 7.53 |

**Figure 2.5:** Chemical shifts (ppm) of the 1,4-disubstituted 1,2,3-triazole derivatives.

We have already explained the effects of both substituents in $H_5$, but in the table is easier to see the deshielding effect when replacing the hydroxymethyl group by a carbonyl.

Observing the carbon chemical shifts, there are no big differences between the different compounds. The alkylated carbon ($C_4$) shows a chemical shift between 146.5 and 148 ppm, whereas the chemical shift of $C_5$ depends more on the nature of $R_1$, being for the hydroxymethyl group around 122 ppm and for the aldehyde substituent around 125 ppm. This small deshielding is due to the same conjugation effect that was observed in $H_5$, because the aldehyde produces a **–I** effect in $C_5$. In the case of $R_1$ = Ph, $C_5$ shows a lower chemical shift, which suggests that this carbon atom is more shielded due to the electron cloud produced by the phenyl electrons.

The $^{15}N$ chemical shifts suffer higher changes, although we have to take into account that the nitrogen scale range is wider than for $^{13}C$ or $^{1}H$. In the table is shown that there is nearly no effect when changing $R_2$. However, when oxidizing $R_1$, the sp2 hybridation of the carbon in the aldehyde causes also a deshielding in all nitrogens, being more noticeable in $N_3$ because it is closer to $R_1$.

It was mentioned above that the coupling constant used for these experiments was 8 Hz. When acquiring the $^{1}H$-$^{15}N$ HMBC of the aldehyde compounds, this value was changed from $J$ = 8 Hz to $J$ = 3 Hz. The problem was that with $J$ = 8 Hz, the correlation peak between $H_5$ and $N_3$ was not observed. A CIGAR experiment was assayed, but it did not work. CIGAR is an NMR experiment where the coupling constant is modified during the acquisition to observe correlation peaks with a higher range of atom distances. Afterwards, an intermediate coupling constant value was used ($J$ = 5 Hz).

As already mentioned, it is important to notice that the substituted nitrogen appears always at the lowest chemical shifts (less than -100 ppm), and that $N_3$ is also more shielded than $N_2$, which means that $N_3$ is more basic than $N_2$. This is in accordance with the theorethical calculations (mentioned in Chapter 1) reported by Abboud *et al.*[80] that suggested that the $N_3$ lone pair has a higher basicity than that of the $N_2$ in the gas phase.

### 2.3.2. 1,5-Disubstituted 1,2,3-triazoles

In order to perform an alternative method to unambiguously assign the isomerism of the triazoles, the synthesis of the 1,5-disubstituted triazoles with the same derivatives as with the 1,4-isomer was required. The ruthenium (II) catalyzed reaction explained in Chapter 1 was performed as follows:

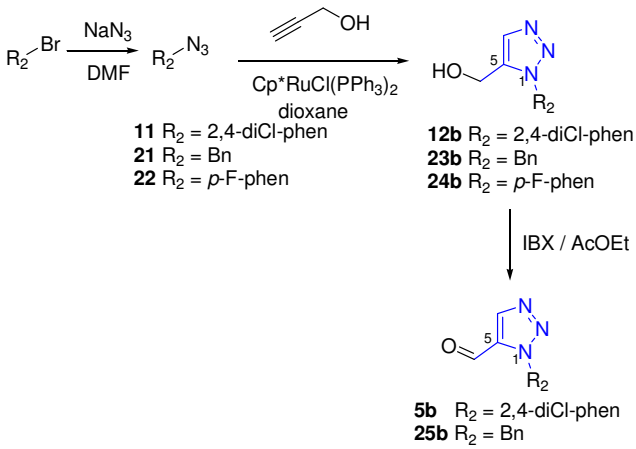


**Scheme 2.3:** Derivatives of the 1,5-disubstituted triazoles bearing different substituents.

After synthesizing the azides **11**, **21** and **22**, the ruthenium catalyst was used to obtain compounds **12b, 23b** and **24b**. As explained in Chapter 1, this catalyst is not as regioselective as the copper one. In addition, we have observed that this reaction depends also on the substituent. With **21** and ***22*,** the conversion was much higher than with the 2,4-dichlorophenethyl azide **11**. There is not an obvious reason to explain this difference, but it can be hypothesized that the *ortho*-substituent hinders the formation of the complex needed for the conversion. In all cases a reverse-phase purification step (semi-preparative HPLC) was needed, and after the characterization, the treatment with IBX/ EtOAC yielded the aldehydes **5b** and **25b.**

The $^1$H NMR spectrum of the 1,5-disubstituted triazole bearing 2,4-dichlorophenethyl as a substituent (**12b**) is shown in Figure 2.6.

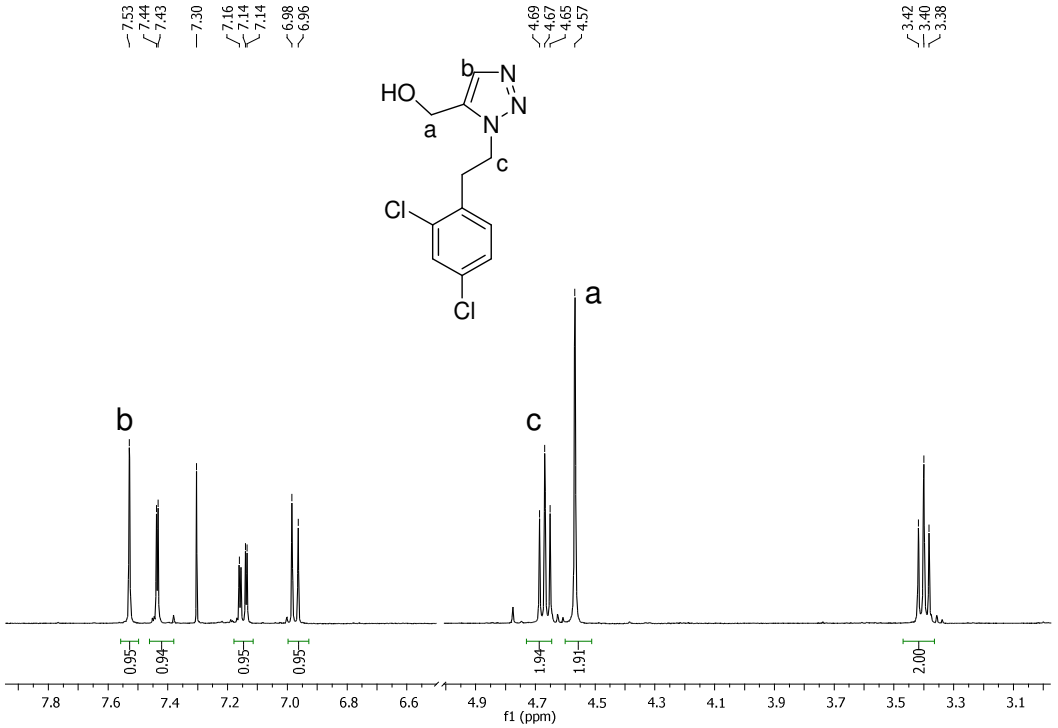


**Figure 2.6:** $^{1}$H NMR spectrum ($CDCl_3$, 500 MHz, 25ºC) of **12b.**

The triazole proton (**b**) appears at 7.52 ppm, whereas with the benzyl group (**23b**) the singlet is at 7.84 ppm and with the *p*-fluorophenethyl **24b** at 7.42. Thus, the chemical shifts are different. When replacing the hydroxymethyl group by the aldehyde, a deshielding effect is observed in all cases, mainly due to the conjugation caused by the aldehyde group. This same effect was observed for the 1,4-disubstituted triazoles.

To characterize the nitrogen chemical shifts, $^{1}$H-$^{15}$N HMBC experiments were also carried out and Figure 2.7 shows the case for **12b**.

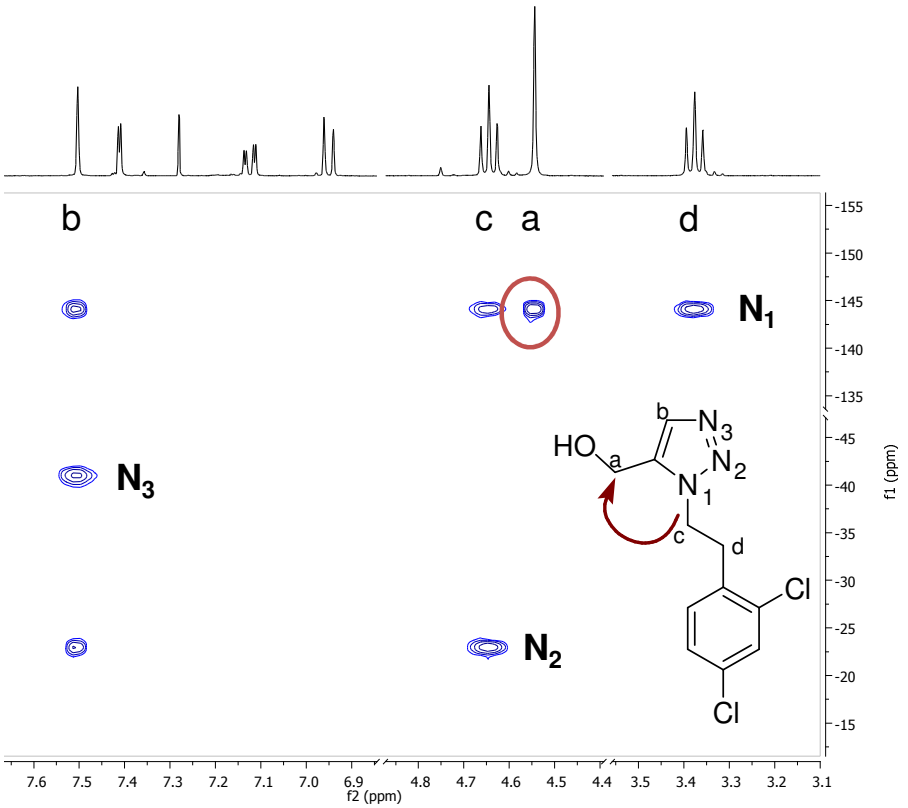


**Figure 2.7:** $^{1}H$ $^{15}N$ HMBC ($CDCl_3$, 400 MHz, 25ºC referenced to $MeNO_2$) of **12b.**

To assign the nitrogen atoms, the same procedure as for **12a** was carried out. In this experiment, there is a nitrogen at -144 ppm that correlates with protons **a**, **b**, **c** and **d**. This nitrogen, which is also the one at the lowest chemical shift, must be $N_1$. Then, to distinguish between $N_2$ and $N_3$, we observe that there is one nitrogen that shows correlation peaks with **b** and **c** and it is difficult that $N_3$ can do that because is too far from **c**. Accordingly, the one at -22.9 ppm is assigned to $N_2$ and the one at -40.9 ppm to $N_3$.

In this case, the other bidimensional NMR experiments were also carried out to assign all the $^{1}H$ and the $^{13}C$, as well as the same $^{1}H$-$^{15}N$ HMBC for the other 1,5-disubstituted triazole derivatives. Figure 2.8, shows a table that summarizes the most important $^{1}H$, $^{13}C$ and $^{15}N$ chemical shifts of these compounds.

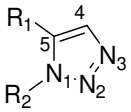


$R_1$ = $CH_2OH$, CHO, Ph

$R_2$ = 2,4-diCl-phen, Bn, *p*F-phen

| $R_1$ | $R_2$ | Cmpd. | $N_1$ | $N_2$ | $N_3$ | $C_4$ | $C_5$ | $H_5$ |
|---|---|---|---|---|---|---|---|---|
| $CH_2OH$ | 2,4-diCl-phen | **12b** | -144.1 | -22.9 | -40.9 | 132.9 | 136.5 | 7.52 |
| | Bn | **23b** | -135.7 | -19.9 | -58.8 | 130.5 | 138.4 | 7.84 |
| | *p*F-phen | **24b** | -136.1 | -16.6 | -35.3 | 132.5 | 136.4 | 7.42 |
| CHO | 2,4-diCl-phen | **5b** | -142.4 | -9.3 | -38.6 | 141.1 | 133.9 | 8.23 |
| | Bn | **25b** | -132.4 | -2.1 | -31.7 | 141.1 | 133.3 | 8.25 |

**Figure 2.8:** Chemical shifts (ppm) of the 1,5-disubstituted triazole derivatives.

Analyzing the carbon chemical shifts, in all cases the chemical shift of $C_5$ is between 133.9 and 138.4 ppm, which is not a big difference. On the other hand, $C_4$ is between 130.5 and 132.9 ppm when $R_1$ is the hydroxymethyl group but it is shifted downfield in the aldehyde cases (141 ppm). This tendency is caused by the deshielding effect in $C_4$ produced by the aldehyde moiety in $R_1$.

It is also observed that the overall chemical shifts in **23b** are slightly different than from **12b** or **24b**. This fact can be explained by the purification method used in this case. Although the three of them were purified using reverse phase chromatography with TFA, in **23b**, the basification and extraction steps required to obtain the product without TFA was not done. The presence of the salt can modify the chemical shifts of the entire molecule.

When oxidizing the hydroxymethyl group (change from **12b** to **5b**), the sp2 hybridization of this carbon atom induces a deshielding effect for all the nitrogens. This effect is higher for $N_2$ due to a more effective conjugation between the triazole and the aldehyde moiety. The same effect is observed with the benzyl derivatives **12b** and **25b**, where $N_2$ shifts from -19.9 ppm to -2.1 ppm. In this isomer this deshielding effect is more evident than in the 1,4-isomer because of the conjugation of the triazole ring with the aldehyde.

It is also noticeably that $R_2$ causes a larger effect in the nitrogen chemical shifts. Particularly in $N_1$, where the difference between **12b** and **23b** or between **5b** and **25b** is about 10 ppm.

### 2.3.3. 2,4-Disubstituted 1,2,3-triazoles

Several 2,4-isomers were also synthesized for comparison porposes. Specifically, the analogous derivatives to those shown before for the 1,4- and 1,5-isomers were prepared. To this aim, the synthetic procedure explained in Chapter 1 was applied and the following

compounds were obtained, both bearing the hydroxymethyl and the aldehyde moieties. (Scheme 2.4)

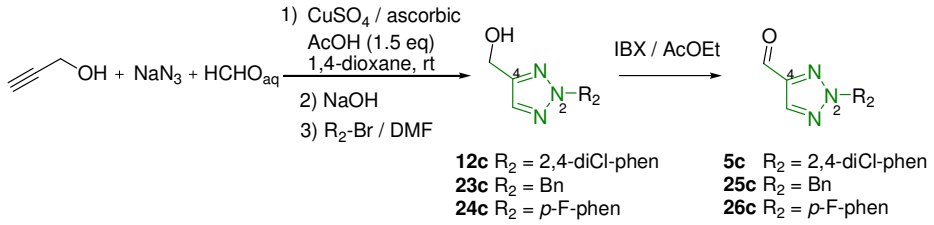


**Scheme 2.4:** Synthesis of 2,4-disubstituted triazole derivatives by means of an $S_N2$ reaction on the *NH*-triazole.

When performing the $S_N2$ reaction, a mixture of the three disubstituted regioisomers was obtained. The separation of the desired triazole from the other compounds was easier than when trying to purify a mixture of the 1,4- and the 1,5-. This is because the 2,4-disubstituted eluted at a different HPLC retention time than the others, as shown in Figure 2.9. Eventhough, different purification techniques were assayed. For **12c** and **24c**, a chromatographic column was used to purify the crude reaction mixture, whereas for **23c** a reverse phase chromatographic method was employed. In all cases, the major product was the desired 2,4-isomer, and the proportion of the other isomers and the formation of by-products (i.e., that from an elimination process), depended on the reaction conditions. The yield of these reactions calculated from the propargylic alcohol was low (10-25%). As explained in Chapter 1, the *NH*-triazole obtained after the two first steps of the Scheme 2.4, was used without purification and its amount was calculated by $^1$H NMR using an internal *tert*-butyl alcohol standard.

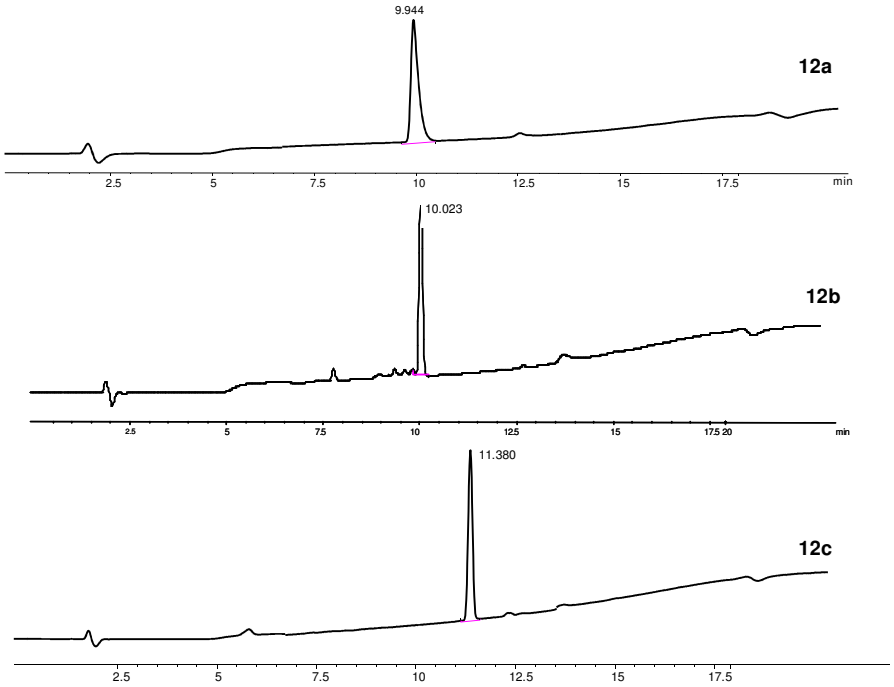


**Figure 2.9:** HPLC profiles for the 1,4- **12a**, the 1,5- **12b** and the 2,4- **12c** triazole derivatives.

With the purified products, the oxidation reactions were carried out to give the expected aldehyde compounds with conversions from 85 to 91%.

The $^{1}$H NMR spectrum of **12c** is depicted in Figure 2.10.

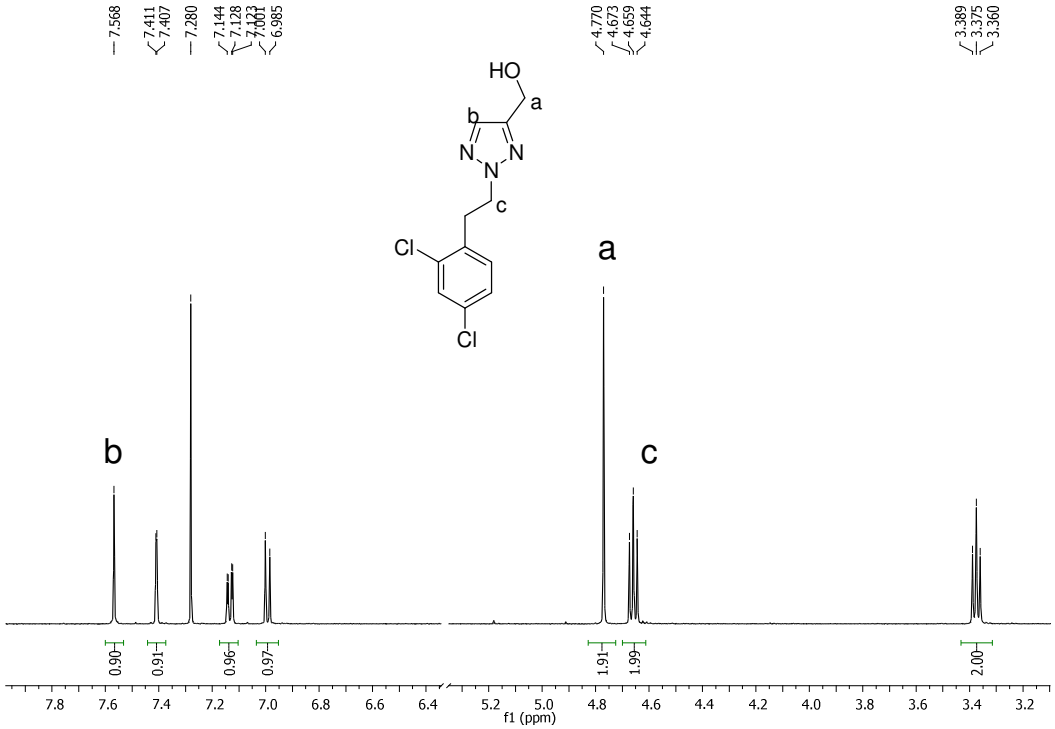


**Figure 2.10:** $^{1}H$ NMR spectrum ($CDCl_3$, 500 MHz, 25ºC) of compound **12c**.

In this case, the triazolic proton shows a singlet at 7.58 ppm and the $CH_2$ of the hydroxymethyl group appears at 4.77 ppm. We also acquired in this case the $^{1}H$-$^{13}C$ and $^{1}H$-$^{15}N$ NMR correlations for this compound and for all the derivatives synthesized. Figure 2.11 shows the $^{1}H$-$^{15}N$ HMBC of **12c,** which was used to characterize the different nitrogen atoms.

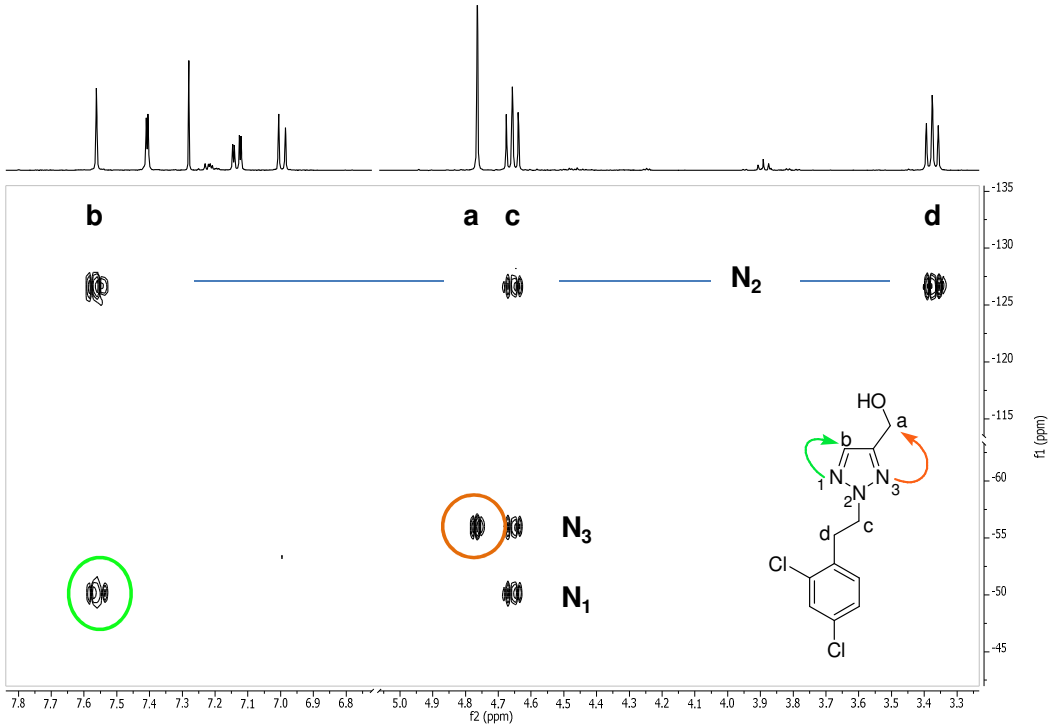


**Figure 2.11:** $^{1}H$-$^{15}N$ HMBC ($CDCl_3$, 400 MHz, 25ºC, referenced to $MeNO_2$) of **12c**.

The nitrogen with the lowest chemical shift should be the substituted one ($N_2$), and this is corroborated with the fact that the nitrogen at -127 ppm correlates with protons **b**, **c** and **d**, but not with the one of the hydroxymethyl group (**a**), which is too far from $N_2$. Then, the nitrogen with a correlation peak with proton **a** must be $N_3$ at -55.9 ppm and that one closer to **b** is $N_1$ at -50.1 ppm. As both nitrogens have more or less the same chemical environment, their chemical shifts are also similar.

Once the proton chemical shifts were assigned, we showed that with the $^{1}H$-$^{15}N$ HMBC experiment it was easy to characterize the nitrogens present in a compound, because the correlations were clear.

Figure 2.12 shows the chemical shifts ($^{1}H$, $^{13}C$ and $^{15}N$) for all the synthesized compounds bearing the 2,4- substitution:

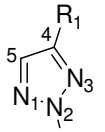


$R_1$ = $CH_2OH$, CHO, Ph

$R_2$ = 2,4-diCl-phen, Bn, *p*F-phen

| $R_1$ | $R_2$ | Cp | $N_1$ | $N_2$ | $N_3$ | $C_4$ | $C_5$ | $H_5$ |
|---|---|---|---|---|---|---|---|---|
| $CH_2OH$ | 2,4-diCl-phen | **12c** | -50.1 | -126.7 | -55.9 | 147.8 | 132.5 | 7.57 |
| | Bn | **23c** | -49.5 | -124.8 | -55.9 | 148.0 | 132.9 | 7.61 |
| | *p*F-phen | **24c** | -51.5 | -127.5 | -57.6 | 147.5 | 132.4 | 7.57 |
| CHO | 2,4-diCl-phen | **5c** | -41.4 | -119.0 | -47.4 | 146.9 | 135.1 | 8.07 |
| | *p*F-phen | **26c** | -41.9 | -119.7 | -48.8 | 147.0 | 134.6 | 8.04 |

**Figure 2.12:** Chemical shifts (ppm) of the 2,4-isomers triazole derivatives.

In these 2,4-isomers, the triazolic proton ($H_5$) has lower chemical shift variations regardless of the $R_2$ substituent, although when $R_1$ is an aldehyde, $H_5$ is more deshielded. The same effect was observed in all the previous cases.

The substituted carbon ($C_4$) appears between 146.4 and 148.0 ppm for all the substituents as well as $C_5$, which is between 132.4 and 134.6 ppm. It is surprising in this case that the aldehyde moiety does not produce changes in the chemical shift. Probably, the lower conjugation of this isomer is the reason because no difference is observed between the alcohols and the aldehydes.

For the call of $^{15}N$, the same effect of the proton is observed: the aldehyde moiety produces a deshielding effect of around 8 ppm to all the nitrogens with all the substituents.

### 2.3.4. Comparison between the triazole isomers

Using NMR techniques we wanted to unambiguously characterize the different possible isomers of the 1,2,3-triazoles and to find the easiest or complementary way to do this characterization. Thus, Figure 2.13 depicts the difference in the $^1H$ NMR of the different isomers bearing the same substituents ($R_1$ = $CH_2OH$ and R = 2,4-dichlorophenethyl alcohol).

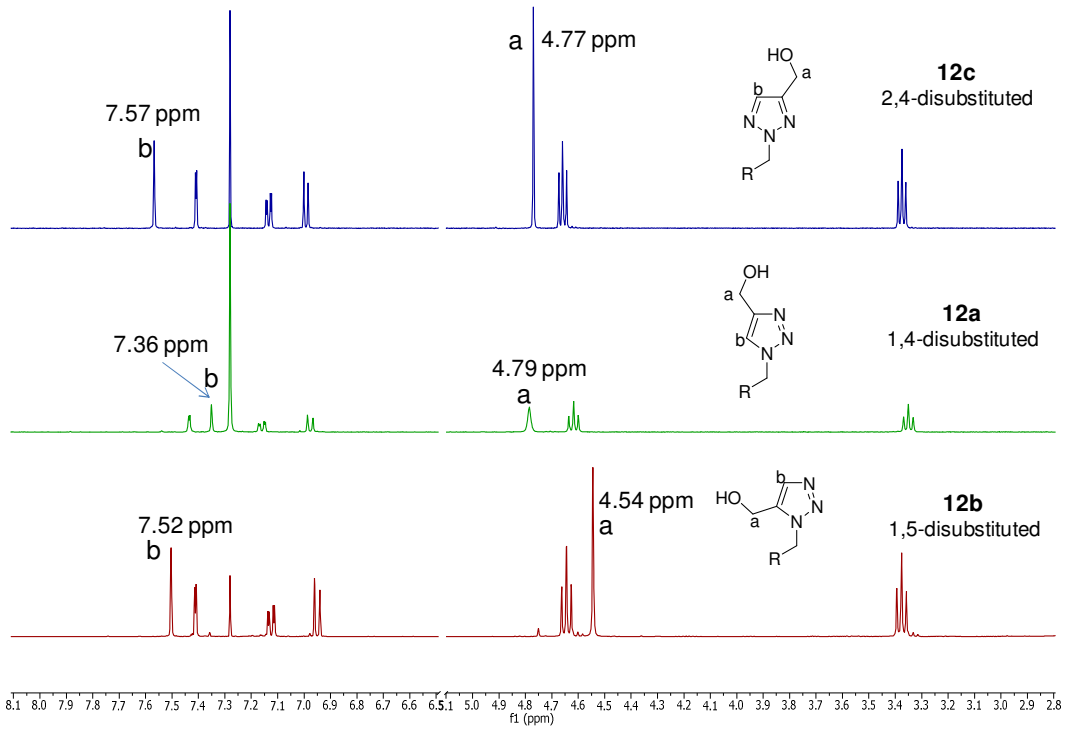


**Figure 2.13:** $^{1}$H NMR spectra of **12c**, **12a** and **12b,** respectively.

The triazolic proton (**b**) is slightly different depending on the isomer, being more shielded in the 1,4-isomer (7.36 ppm) and less for the other isomers (7.52 and 7.57 ppm for 1,5- and 2,4-isomers, respectively). The same tendency was observed when $R_1$ was the aldehyde moiety, appearing at the lowest chemical shift the proton **a** of the 1,4-disubstituted isomer (7.89 ppm) whereas for the other one it appeared over 8 ppm. This tendency was observed with all the substituents assayed.

As with the triazolic proton is easy to distinguish the 1,4-isomer from the other ones, with the $CH_2$ of the hydroxymethyl group is easy to distinguish the 1,5-isomer. In this isomer, proton **a** appears at the lowest chemical shift (4.57 ppm) but at around 4.78 ppm in **12a** and **12c**, which is a notorious difference. The same effect was observed with other $R_2$. For the case of the benzyl group, proton **a** showed a chemical shift of 4.63 ppm in the 1,5-isomer **23b**, whereas in **23a** and **23b** the value was higher (4.79 and 4.77, respectively). In the *p*-fluorophenethyl derivative, the difference is even higher, being the chemical shift 4.41 ppm for **24b** and 4.77 for the 1,4 and 2,4-isomers. (See Supp. Inf.)

We have shown that the identification of the different isomers is possible only with the $^{1}$H NMR data. However, more than one isomer is needed to compare their spectra and assign the appropiate isomer. Thus, an effective method for easily distinguish the isomers is still needed.

On the other hand, as reported in the article of Creary *et. al,.* the CH carbon of the triazole can be used to know which of the two isomers (1,4- or 1,5-disubsituted) is formed.[156] In our case, we also wanted to check whether the derivatives discussed above fulfill that assignation. Figure 2.14 is a summary where an average of the $^{13}C$ chemical shifts of the alkylated carbon and the CH of the triazole for all the substituents has been done.

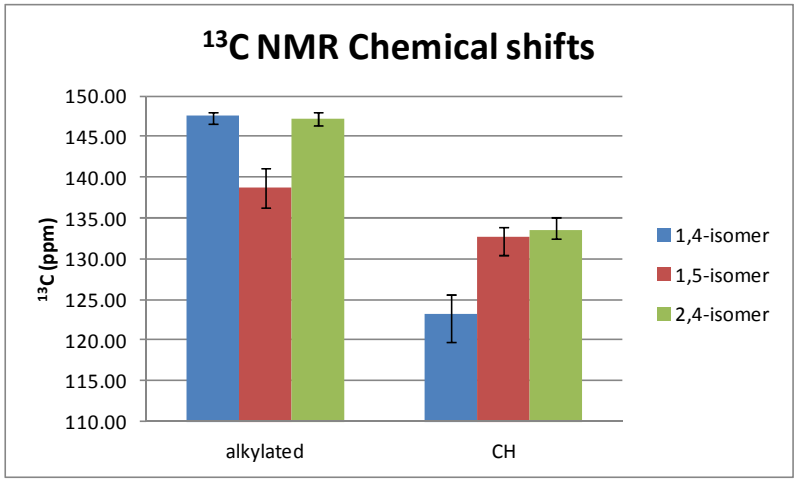


**Figure 2.14:** $^{13}C$ chemical shifts (ppm, $CDCl_3$, 100 MHz) of the alkylated and the CH carbon of the different triazole isomers studied.

It is clear that the $^{13}C$ chemical shift of the CH in the 1,5-isomer (~132 ppm) appears around 10 ppm higher that the same carbon of the 1,4-isomer (~122 ppm). Whereas the alkylated carbon shows the opposite tendency because the chemical shift of the 1,4-isomer is around 147 ppm and the one for the 1,5-isomer at ~137 ppm. Therefore, by using the $^{13}C$ NMR technique it is possible to unambiguously assign the appropriate isomer between 1,4- and 1,5-. This method is not useful for the 2,4-isomer, because the alkylated carbon has a similar chemical shift to that of the 1,4-isomer and the CH carbon is similar to that of the 1,5-isomer. This effect is similarly observed in the $^{1}H$ NMR, where the 2,4-isomer is a kind of combination of the other ones.

Having in mind these difficulties to assign the triazoles isomers, the $^{1}H$-$^{15}N$ HMBC experiments have been compared to see if it is easier the differenentiate characteriation with this method. The $^{1}H$-$^{15}N$ correlations of the three different isomers are shown in Figure 2.15.

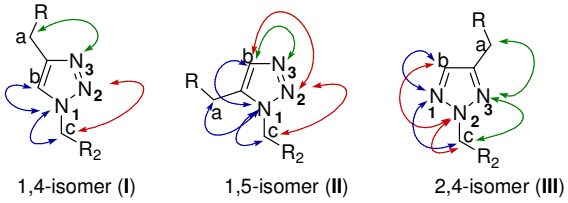


**Figure 2.15:** Peak correlations found in the $^{1}H$-$^{15}N$ HMBC spectra for the disubstituted triazole derivatives.

As it has been individually discussed for each isomer, the nitrogen that appears at the lowest chemical shift (less than -100 ppm) is the alkylated one, being $N_1$ in **I** and **II** and $N_2$ in **III**.

$N_1$ of 1,5-isomer (**II**) shows correlation peaks with protons **a**, **b** and **c** at the same time, which is impossible in both 1,4- and 2,4-isomers because the alkylated nitrogen ($N_1$ and $N_2$ respectively) is too far from the proton **a** in both cases.

In the 2,4-isomer (**III**), $N_3$ has correlation peaks with protons **a** and **c**. This is not possible in the 1,4-isomer (**I**), because $N_3$ in this isomer is too far from the proton **c** to show a correlation peak. Likewise $N_2$ in the 1,4-isomer, which correlates with proton **c,** is too far from **a**. Therefore, the two correlations at the same time are only possible for the 2,4-isomer.

Besides being able to unambiguously characterize all the isomers by their 2D correlations, we also wanted to explain the different $^{15}N$ chemical shifts observed in each isomer. An average of all the $^{15}N$ chemical shifts of the different substituents has been calculated and they are represented in front of the different isomers for comparison purpose. (Figure 2.16)

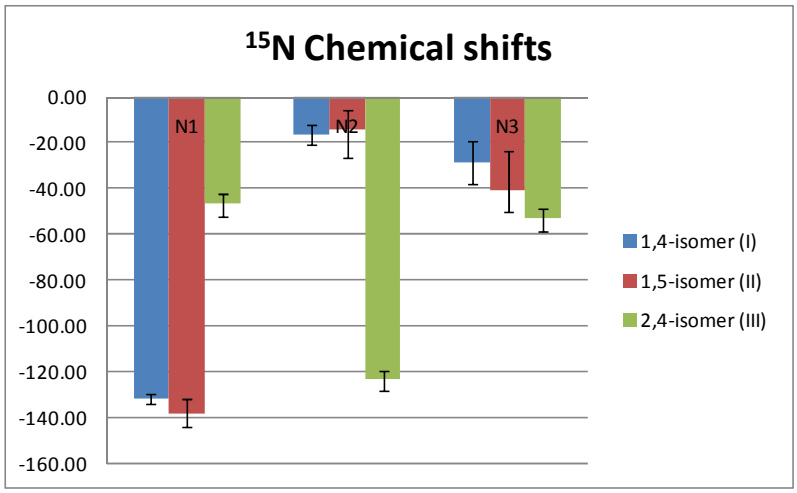


**Figure 2.16:** $^{15}N$ chemical shifts ($CDCl_3$, 400 MHz, referenced to $MeNO_2$) of the isomers for the 1,4-, 1,5- and 2,4-disubstituted triazoles.

As it has already been mentioned, the alkylated nitrogen is the most shielded one, and in the figure it can be observed that the distribution in the 2,4-isomer is different from the other ones and that $N_2$ is the substituted nitrogen in this isomer (**III**). It is also clear that the alkylated nitrogen $N_2$ in **III** shows higher chemical shift compared to the corresponding nitrogen in **I** and **II** ($N_1$). This effect is due to the electronegativities of the nitrogens in *alpha*, causing a **–I** effect.

It can be also observed that the two nitrogens ($N_1$ and $N_3$) in **III** are more similar among them because the electronic environment is nearly the same, whereas in **I** and **II**, the chemical shifts of $N_2$ and $N_3$ are more different among them. Moreover, the substitution in the central $N_2$ (**III**)

causes a **+I** effect of $R_2$ over the two neighboring nitrogens; this is reflected in a shielding in those nitrogens (~ -50 ppm).

$N_1$ is very similar in **I** and **II**, although in **II** appears a little bit more shielded, because it has nearer the other substituent R that produces a **–I** effect. $N_2$ has no remarkable difference between the isomers (**I** and **II**), because the chemical environment around their atoms is similar. On the other hand, the chemical shift of $N_3$ in **I** is higher than in **II,** which means that $N_3$ in **I** is less shielded because the substituent in *alpha* causes a **–I** effect in **I**. $N_3$ in **III** has higher electron density, therefore it is is more basic than in the other isomers.

Finally, in the following picture, a comparison of the $^{1}H$-$^{15}N$ HMBC of the three isomers with the 2,4-dichlorophenethyl substituent is represented and the differences already explained are depicted. (Figure 2.17)

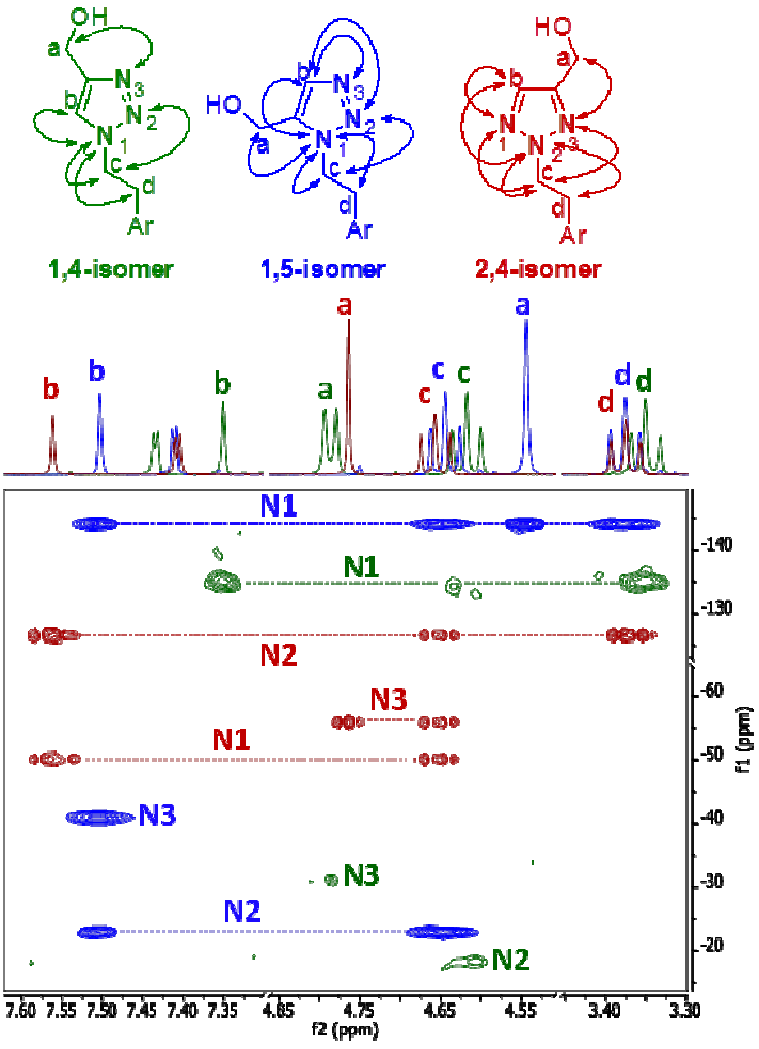


**Figure 2.17:** Comparison of the $^{1}H$-$^{15}N$ HMBC of the 1,4-, 1,5- and 2,4-isomers being Ar = 2,4-diClPh.

## 2.4. Conclusions

- A variety of compounds bearing different substituents on the possible disubstituted 1,2,3-triazole isomers has been synthesized.
- The full NMR analysis (including $^{1}H$-$^{15}N$ correlations at natural abundance) of all compounds has led to the unambiguous characterization of the corresponding substitution patterns.
- The $^{1}H$-$^{15}N$ HMBC experiment has been shown to be an optimal technique to measure and distinguish $^{15}N$ chemical shifts of triazoles as well as unambiguously assign the correct isomer.
- The $^{15}N$ chemical shifts have been correlated with the chemical properties (electronic density, conjugation, inductive effects...) of all synthesized compounds.

-

# 3. Mechanistic studies, synthesis and biological activities of conformationally restricted derivatives bearing a triazole moiety

## 3.1. Introduction

### 3.3.1. β-Lactams

The β-lactams are among the best known and extensively investigated heterocyclic ring systems as a result of both their biological activity[170,171] and their utility as synthetic intermediates.[172-175] The β-lactam ring is part of the core structure of several antibiotic families, the principal ones being the penicillins, cephalosporins, carbapenems, and monobactams, which are, therefore, also called β-lactam antibiotics. Nearly all of these antibiotics work by inhibiting bacterial cell wall biosynthesis. β-Lactams play an important role not only in a major class of antibiotics but also as inhibitors of serine proteases, elastase, cysteine protease and papain.[176]

Commonly, the lactam ring is formed through either ketene-imine cyclizations[177] (the Staudinger reaction) or ester enolateimine condensations[178,179,180] (the Gilman-Speeter reaction). However, other methods are sometimes employed, including photo-induced rearrangements,[181] and radical cyclizations.[182]

Nevertheless, the synthesis of β-lactams using the Ugi reaction has not been extended too much. The Pirrung group found a novel variation of the Ugi reaction where the reaction between acetonedicarboxylic acid, propyl amine, and *tert*-butyl isocyanide yielded the corresponding β-lactam in 15% yield together with the major Passerini-type reaction product. (Scheme 3.1)[183]

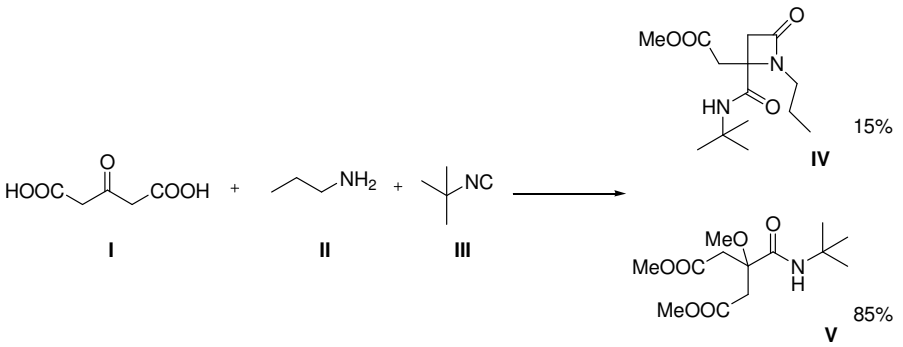


**Scheme 3.1:** Variation of the Ugi reaction where a β-lactam is obtained as a byproduct.

The reaction of β-ketoacids with primary amines and isocyanides in a 1 M glucose solution in water also affords a novel type of β-lactams in MCRs reported by Domling *et al.*[176]

Moreover, the Pepino group also reported a similar synthesis to obtain β-lactams starting from isocyanides in a facile two-step synthesis.[118] (Scheme 3.2). The first step consisted in the reaction between (*E*)-cinnamaldehyde, chloroacetic acid, cyclohexyl isocyanide and primary amines which afforded the expected Ugi adduct. Upon treatment with methanolic KOH under mild conditions, compound **V** underwent a ring-closure reaction to give the β-lactam (**VI**).

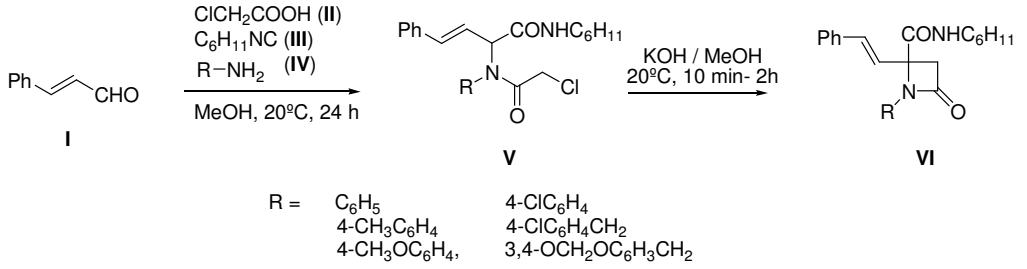


**Scheme 3.2:** Ugi reaction yielding β-lactam products. [118]

More recently, the same group reported that if saturated aldehydes are employed as starting materials in the Ugi reaction, it is reasonable to hypothesize that the enolate anions arising from the corresponding 4-CC adducts are less stable. Thus, a different base-induced cyclization mode, involving the amide nitrogen, to form DKP would also be possible. This is the same reaction employed to synthesize the diketopiperazines commented in Chapter 1.[55]

In our case, in Chapter 1 it was explained that when treating the Ugi adduct (1,4- and 1,5-disubstituted triazole aldehydes) with basic media, the diketopiperazine scaffold was formed, but for the 2,4-disubstituted one, a product containing a β-lactam was obtained. (Figure 3.1)

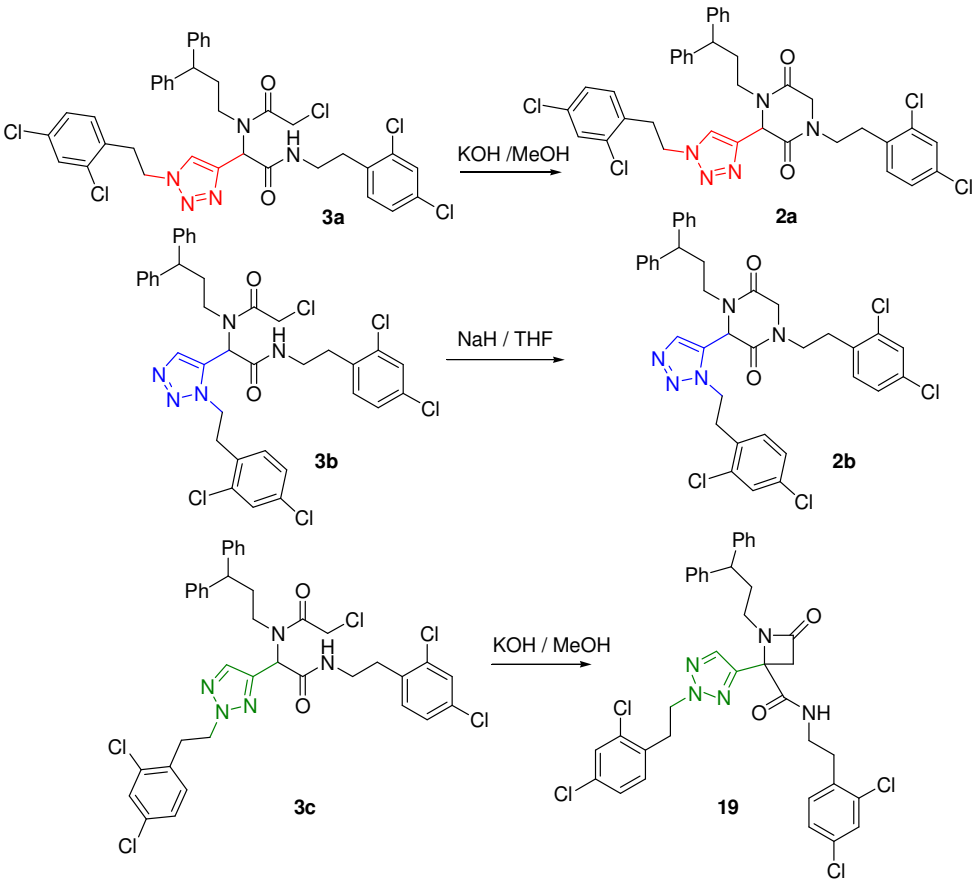


**Figure 3.1:** Cyclization compounds obtained from the different disubstituted triazole derivatives subjected to the Ugi reaction. (cf. Chapter 1)

As the β-lactam product gave the better activity inhibiting the apoptosis pathway, the idea of expanding the chemical diversity and synthesizing a small library of compounds with the same scaffold and different substituents was proposed. By observing the different reactivity when replacing the triazole substituents from 1,4- or 1,5- to the 2,4-disubstituted one, a reactivity study to better understand the cyclization pathway and to predict which compound could be formed was needed before starting the mentioned library.

## 3.2. Objectives

In this chapter a study of the intramolecular cyclization of the Ugi adducts was carried out in order to predict the final product depending on the substituents used. This reactivity study was carried out both experimentally and using computational methods.

Once the sort of substituents that would lead to the β-lactam or the diketopiperazine scaffolds were identified, a small library of compounds was synthesized to test their biological activity as apoptosome formation inhibitors. Moreover, the selection of the substituents was carried out in a rational manner. All compounds in Figure 3.1 have three hydrophobic moieties

that seem to interact with the protein. Then, the removal or change of one of these substituents and the observation of their behavior as apoptotic modulators, can give a better explanation of the mode of interaction of our compounds with the Apaf-1 protein target.

## 3.3. Results and discussion

### 3.3.1. Reactivity study

## Experimental study

Different experiments were designed to further study how the intramolecular cyclization occurs and which is the most favorable product in each case.

Taking into account the following structures (Figure 3.2), where the amide anion (**A**) and the carbanion (**B**) previous to the cycle formation are depicted, it is clear that the acidity of the proton in the NH compared with the one of the CH is important to predict which cycle (**DKP** of **β-Lac**) will be the major one.

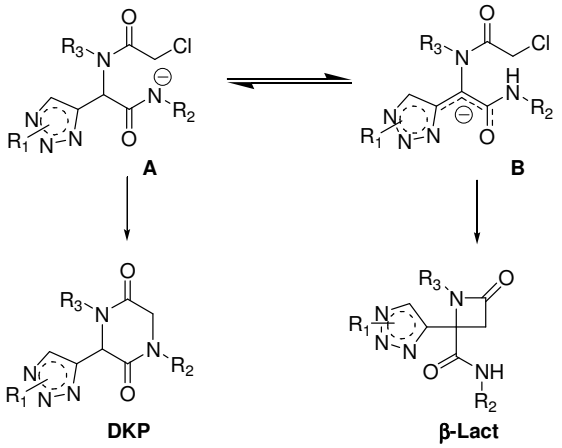


**Figure 3.2:** Reaction with the possible formed anions (A/B) and the final products produced.

The factor that would affect the release of these protons when adding base is their pKa. The pKa of the CH is defined by the triazole and we already know that the result is depending on the substitution pattern. In order to study the effect of the pKa on the NH, different substituents in $R_2$ were tested.

Four compounds were chosen to study these reactivity effects (Figure 3.3). Two of them have the 1,4-disubstituted triazole with a benzyl group (**29**) and with a *p*-methoxyphenyl (**30**) as $R_2$, and the others have the same derivatives in $R_2$ but using the 2,4-disubstituted triazole (**27**, **28**). After the formation of the Ugi adducts, the addition of base to these intermediates would afford the DKP or the β-lactam.

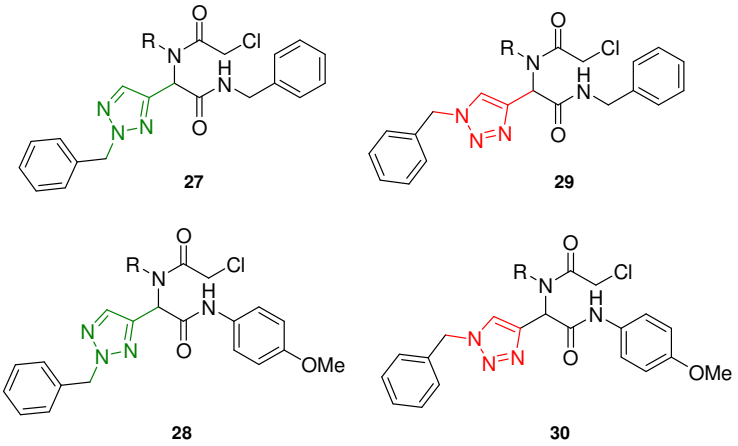


**Figure 3.3:** Compounds selected for the reactivity study where R = *p*-fluorophenethyl.

The synthesis of the open compounds was carried out using the same type of Ugi reactions explained in Chapter 1 (Scheme 3.3):

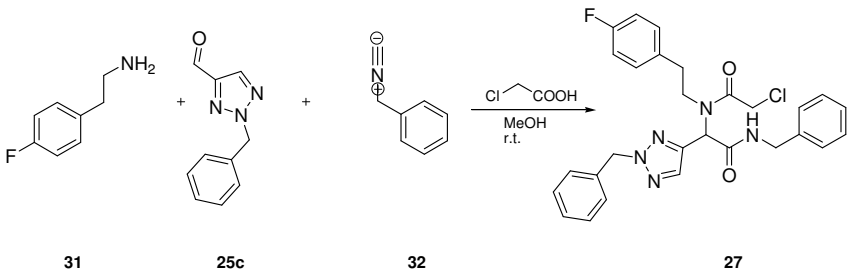


**Scheme 3.3:** Ugi reaction to synthesize adduct **27**.

In this case, the amine and the isocyanide were commercially available, whereas the synthesis of the aldehyde **25c** was explained in Chapter 2 (2.3.3.). Once the Ugi adduct was formed, NaOH in MeOH was added to **27** and Figure 3.4 shows the $^{1}$H-NMR of the crude reaction mixture.

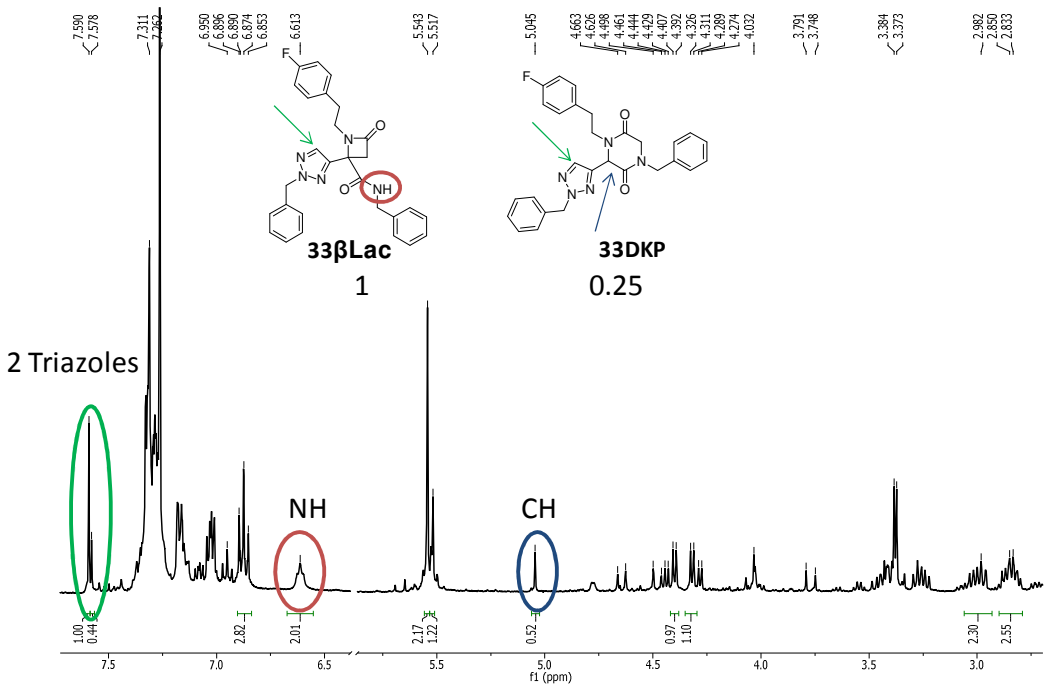


**Figure 3.4:** $^{1}$H-NMR ($CDCl_3$, 500 MHz, 25ºC) of the crude reaction mixture of **27** after the treatment with base.

In the $^{1}$H-NMR, the formation of both heterocyclic products was clear when treating the Ugi adduct **27** with base. Two signals of the triazole moiety appeared in the spectrum (green), and also the NH (red) and the CH (blue) signal, which are incompatible in the same product. The ratio between them is 1 : 0.25 determined by $^{1}$H-NMR, being the major one the β-lactam product (**33βLac**). After checking the ratio, preparative thin layer chromatography allowed us to isolate both products separately: 8% yield of the β-lactam and 13% of the DKP.

In Chapter 1 it was explained that with the 2,4-disubstituted triazole only the β-lactam scaffold was formed. The information that the replacement of the 2,4-dichlorophenethyl group by a benzyl group increased the acidity of the NH in the open compound and allowed the formation of both scaffolds is quite noticeable.

The second change was done using *p*-methoxyphenyl isocyanide (**34**) instead of the benzyl isocyanide (**32**) to give adduct **28**. A chromatographic column and reverse-phase purification was needed to obtain the product **28**. (Scheme 3.4)

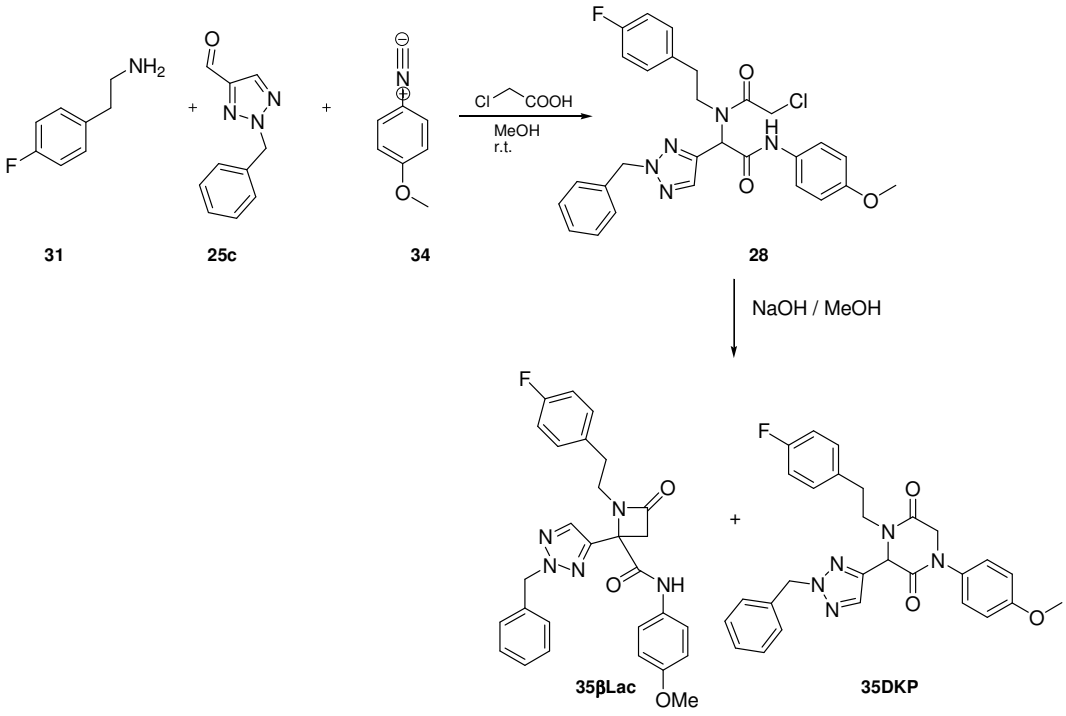


**Scheme 3.4:** Synthesis of **28** using the Ugi reaction with 2,4-disubstituted triazole and isocyanide **34** followed by the addition of NaOH to obtain **35βLac** and **35DKP**.

When treating compound **28** with NaOH, two compounds were also distinguishable by $^1$H-NMR, but in this case the major one was the diketopiperazine **35DKP** and the ratio was 0.13 : 1 (**35βLac : 35DKP**). The separation of both products was not possible due to the small amount of the β-lactam present in the crude reaction mixture; therefore only **35DKP** was characterized.

This increase in the proportion of the DKP compound (**35DKP**) when changing the previously used isocyanide **32** for the *p*-methoxyphenyl (**34**) indicates that when the acidicity of the NH is high enough, the favored cyclization is the formation of the 6-membered diketopiperazine ring because a stabilization of the amide anion is produced.

After the assays of the two 2,4-disubstituted triazoles intermediates **27** and **28**, the 1,4-disubstituted triazoles **29** and **30** were also synthesized. Although with the 2,4-dichlorophenethyl isocyanide as a substituent in **2a** (Chapter 1) the β-lactam scaffold was not formed, the full study of **29** and **30** was carried out using the benzyl and the *p*-methoxyphenyl isocyanides.

The synthesis of compound **29** is depicted in Scheme 3.5. The prepartion of the aldehyde **25a** was explained in Chapter 2. The amine **31** and the isocyanide **32** are the same used to form compound **27**. In all these syntheses, the imine is preformed before adding the isocyanide

and the acid is the last one to be added. After reverse phase chromatographic purification, compound **29** was obtained in 19% yield.

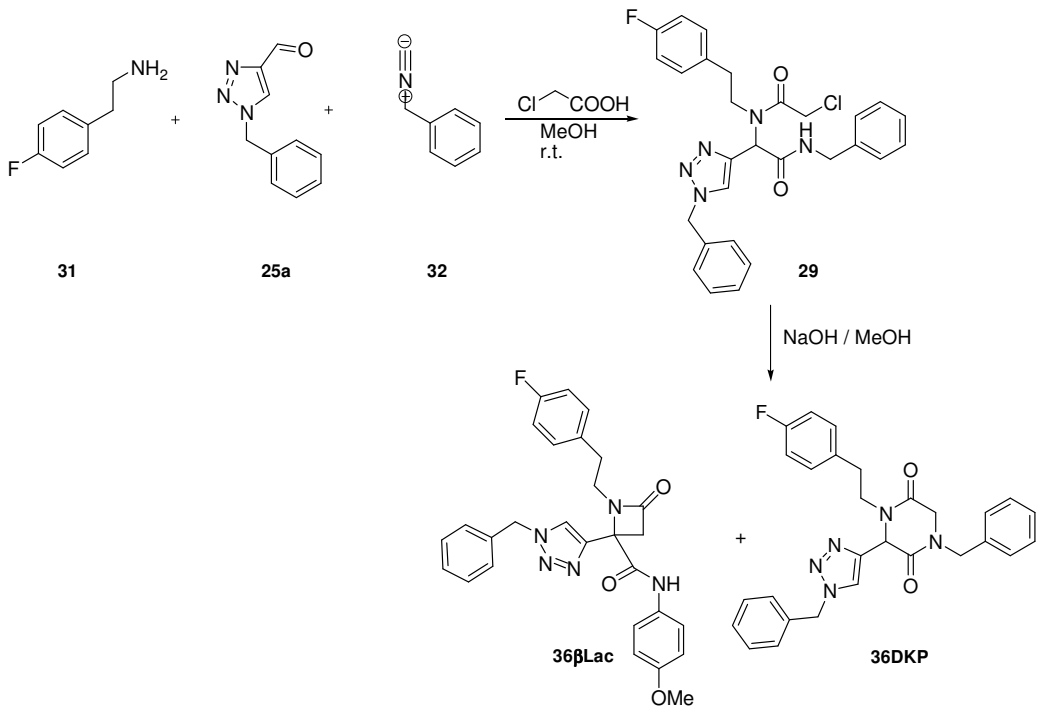


**Scheme 3.5:** Synthesis of **29** and reactivity shown after adding base to obtain **36a** and **36b**.

Surprisingly, after adding NaOH / MeOH to the compound **29**, a mixture of two compounds was formed. In this case, the major product was the β-lactam compound **36βLac** and the ratio between them was 1 : 0.5 as determined by $^{1}$H-NMR. Figure 3.5 shows the $^{1}$H-NMR of the crude reaction mixture, that was not easy to separate. The NH of the β-lactam product (**36βLac**) and the CH from the DKP one (**36DKP**) can be observed, which allows us to ratio the proportion between both products.

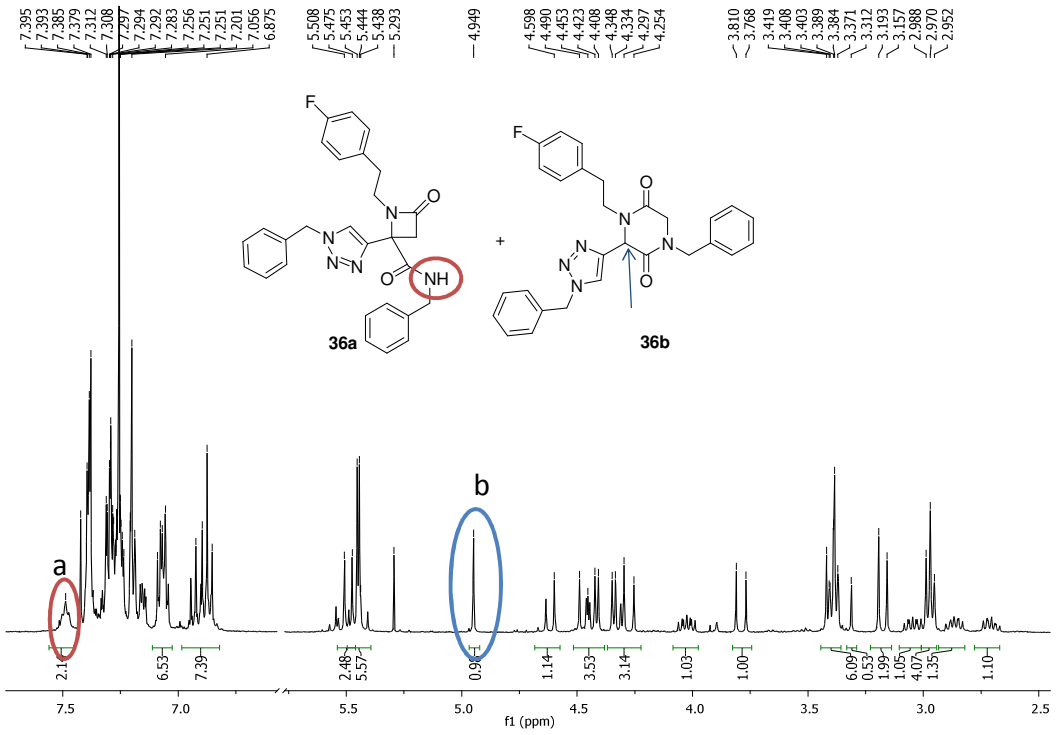


**Figure 3.5:** $^{1}$H-NMR ($CDCl_3$, 500 MHz, 25ºC) of the crude reaction mixture containing **36a** and **36b**.

When instead of NaOH/ MeOH, DBU was used for the cyclization, 100% of the β-lactam product (**36a**) was obtained ($^{1}$H NMR monitoring). The fact that the nature of the base is decisive in the cyclization pathway indicates that a stabilization of the carbanion (**B**, Figure 3.2) facilitates the formation of the β-lactam scaffold.

The fact that in this example the β-lactam was formed was surprising because in Chapter 1, when $R_2$ was 1,4-dichlorophenethyl, only the DKP **2a** was observed. We anticipated that when this substituent was replaced by a benzyl group, only the diketopiperazine would be formed. A reasonable explanation for these observations would be that the $^{1}$H-NMR of the crude reaction mixture of **2a** was complex and after purifying only the diketopyperazine was recovered.

Finally, compound **30** bearing $R_2$ as *p*-methoxyphenyl was synthesized and was obtained pure after a chromatographic purification. (Scheme 3.6).

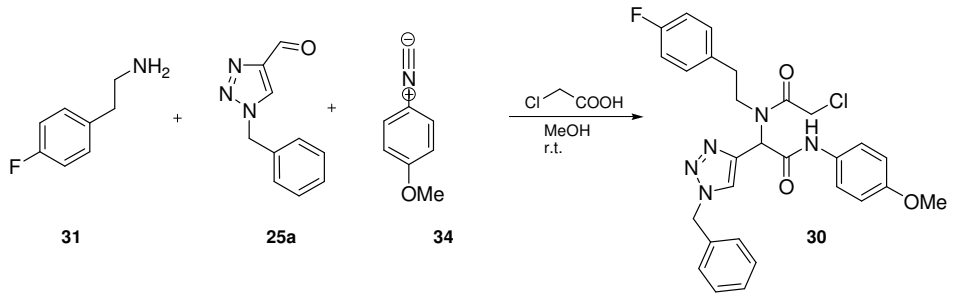


**Scheme 3.6:** Synthesis of the compound **30**.

When a small sample of **30** was treated with NaOH in $CD_3OH$ (assay carried out directly in the NMR tube), only the DKP scaffold was observed. This was the expected result because the acidity of the NH has been increased with the phenyl substituent.

After these experiments, it is clear that compounds bearing the benzyl group in $R_2$ (**27**, **29**), gave higher amoungs of the β-lactam cycle. Moreover, the ratio was higher (1 : 0.25) in **27** which has the 2,4-disubstituted triazole than in **29** (1 : 0.5) with the 1,4-disubstituted triazole. This is in accordance with the results obtained for **28** and **30**, where although in both cases higher amounts of DKP were produced, due to the phenyl substitutent in $R_2$, for **30** (1,4-disubstituted triazole) only this scaffold was formed. It is worth mentioning that in compound **29** where the 1,4-disubstituted triazole favored the DKP scaffold, but the benzyl group in $R_2$ contributes to the formation of both cycles, when changing the base used (NaOH for DBU) only the β-lactam scaffold was observed.

## Computational calculations

As mentioned in the objectives, a computational study was carried out to find a rational explanation of the above experimental results. This study was done by Dr. Jordi Bujons using the program Jaguar (version 7.8, Schrödinger, LCC, N.Y. 2011)

All the examples were done considering methanol in the media and all the substituents were replaced by methyl groups to simplify the calculations. All the possible steps in the cyclization reaction were studied, from the open compounds, through the anions, transition states and finally the cyclic products.

First of all the 1,4-disubsituted triazole (**38**) is explained. Figure 3.6 shows the reaction coordinates with their calculated (B3LYP/6-31G**++) $\Delta G$ values. The possible anions that can be formed when treating **37** with basic media appear in the figure with the corresponding calculated energy. **37**A is the anion formed from releasing the NH proton and it has higher

energy ($\Delta G$ = 5.42) than the other one. However, these energies were calculated without taking into account the cations present in the solution which can affect these energies. Both final products were experimentally observed although the energetic difference between both anions is high.

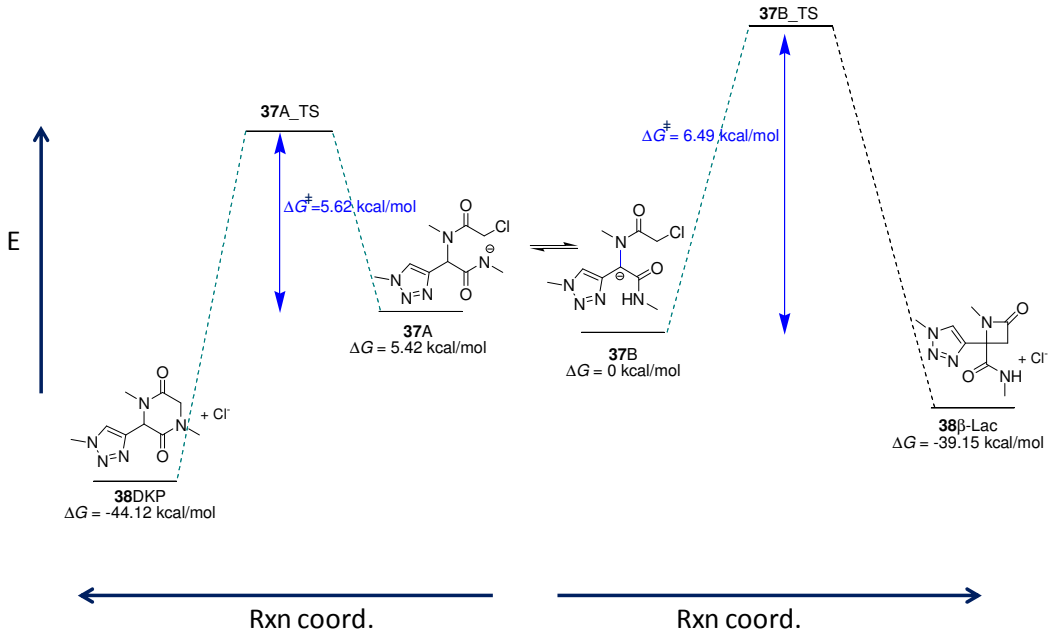


**Figure 3.6:** Reaction coordinates and calculated (B3LYP/6-31*G***++) $\Delta G$ values for the formation of compounds **38** (DKP or β-lactam) from **37**.

The energy required to form the transition state **37**B-TS that would yield the β-lactam compound **38**β-Lac, is 6.49 kcal/mol, whereas the one to form **38**DKP passing through **37**A_TS is 5.62 kcal/mol. The final DKP compound **38**DKP is more stable than the β-lactam (**38**β-Lac). From the canonical structural resonances, a 6-membered-ring compound through the oxigen of the amide bond could also be formed, but in the calculations, the formation of this compound was energetically expensive and the final product was not very stable.

These calculations suggest that both products (β-lactam or DKP) can be formed. The DKP scaffold is kinetically favored by 0.87 kcal/mol, and the reaction to form **38**DKP is faster than to form **38**β-Lac.

This result correlates with the experimental reactivity study explained before, where in most of the cases the formation of DKP is the major product, but for compound **36**, both products were observed and change of the basic media also changed the ratio of both compounds. When the Ugi adduct **29** was treated with DBU, 100% of the β-lactam was formed. In Figure 3.6, this result can be better understood by a stabilization of the transition state **37**B_TS, thus reducing the corresponding energetic barrier.

The same calculations were carried out with the 2,4-disubstituted 1,2,3-triazole and Figure 3.7 shows the main results.

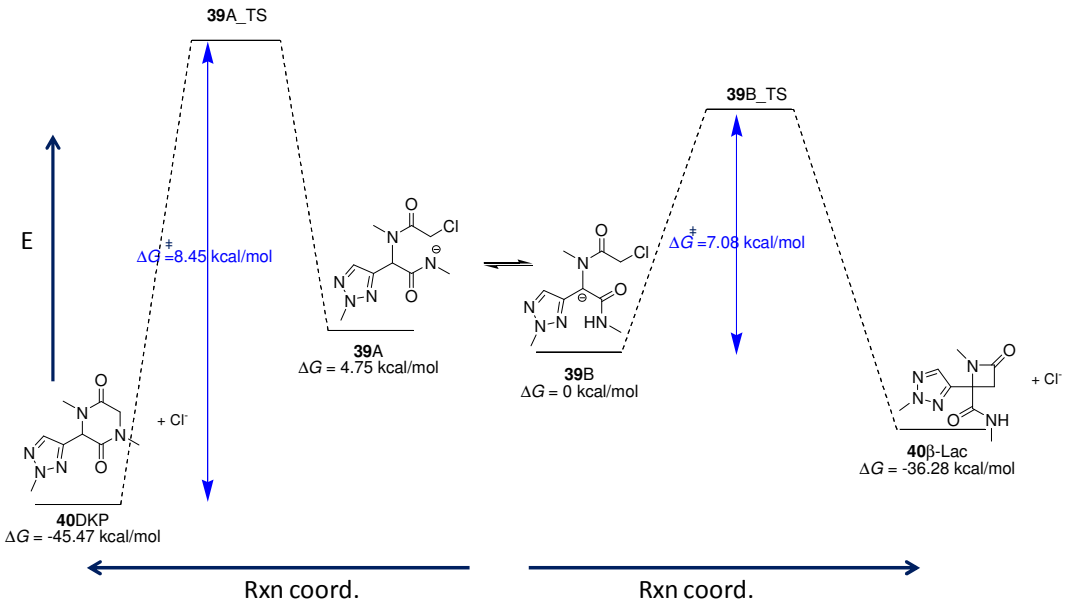


**Figure 3.7:** Reaction coordinates and calculated (B3LYP/6-31G**++) ΔG values for the formation of compounds **40** (DKP or β-lactam) from **39**.

The calculated energies of the anions, transition states and final compounds are similar to those of the 1,4-disubstituted triazole (Figure 3.6). The different reactivity observed in both cases can be explained by the energy needed to form the transition state of the DKP compounds. In the 2,4-disubstituted triazole, the energy required to form **39**A_TS is 8.45 kcal/mol and to form **37**A_TS is 5.62 kcal/mol. In Figure 3.7 it can be seen that the energy needed to obtain the transition state that would yield the β-lactam compound (**40**β-Lac) is 7.08 kcal/mol and in the previous one was 6.49 kcal/mol. In this example, the β-lactam is 1.37 kcal/mol kinetically more favored; thus, the reaction leading to the β-lactam will be faster than the other one. If the energetic barrier ($\Delta G^{\ddagger}$ = 8.45) is reduced stabilizing the transition state, higher amounts of DKP will be formed, whereas if it is increased, the β-lactam will be more favourable.

Finally, the 1,5-disubstituted triazole was also theoretically studied and the energetic barriers are depicted in Figure 3.8.

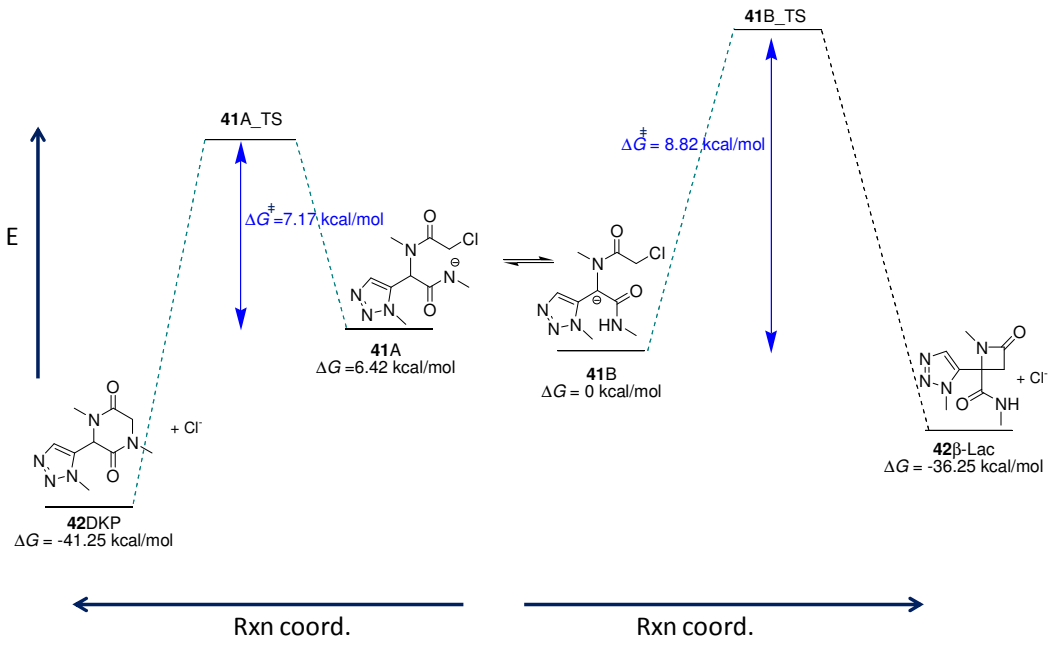


**Figure 3.8:** Reaction coordinates and calculated (B3LYP/6-31G**++) ΔG values for the formation of compounds **42** (DKP of β-lactam) from **41**.

In this case the transition state energy to form the diketopiperazine **42**DKP is 7.17 kcal/mol which is between the energy needed in the 1,4-disubstituted triazoles (5.62 kcal/mol) and in the 2,4-disubstituted triazole (8.45 kcal/mol). However, as the energetic barrier to obtain the β-lactam **42**β-Lac is 8.82 kcal/mol, the diketopyperazine scaffold is 1.66 kcal/mol kinetically favored. This result is in agreement with the experimental assay where this isomer was the less reactive.

Observing all the previously exposed data, we propose that the Curtin-Hammett Principle fulfill the features of our structures. It is a principle in chemical kinetics proposed by David Yarrow Curtin and Louis Plack Hammett, that taking as an example the following reaction:

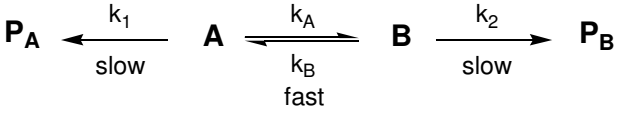


states that *"The Product composition, $P_A$ vs $P_B$ is not solely dependent on relative proportions of the conformational isomers in the substrate; it is controlled by the difference in standard Gibbs energies (ΔΔG*) of the respective transition states."*[184, 185]

The A-B equilibrium (Scheme 3.7) in our case is supposed to be fast. Either because it is an acid-base equilibirium in a protic solvent or because it is a formal 1,3-sigmatropic H-shift. The Curtin-Hammet Principle states then that for a reaction that has a pair of reactive intermediates that interconvert rapidly, each one going irreversibly to a different product (DKP or β-Lac), the

product ratio will depend both on the difference in energy between the two reagants and the free energy of the transition state leading to each product. As a result, the product distribution will not necessarily reflect the equilibrium distribution of the two intermediates.

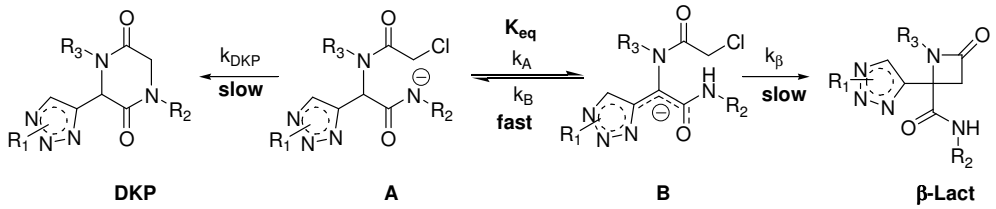


**Scheme 3.7:** Equilibrium reaction of the anions formed and the both expected products.

In Scheme 3.7, the general reaction taking place is depicted and is important to remark that: $k_{DKP}$, $k_\beta$ << $k_A$,$k_B$. Then, if the reaction rates are much slower than the rate of interconversion, ($\Delta G_{AB}^{\ddagger}$ is small relative to $\Delta G_{DKP}^{\ddagger}$ and $\Delta G_{\beta}^{\ddagger}$), then the A/B ratio is constant throughout the course of the reaction. Some kinetic equations can be written and:

$$\frac{d[\beta Lac]}{dt} = k_\beta[B] = k_\beta \cdot K_{eq}[A]$$

$$\frac{d[DKP]}{dt} = k_{DKP}[A]$$

$$\frac{[B]}{[A]} = K_{eq}$$

$$\frac{\frac{d[\beta Lac]}{dt}}{\frac{d[DKP]}{dt}} = \frac{k_\beta . K_{eq}[A]}{k_{DKP}[A]}$$

Considering that the A ⟷ B interconversion is fast, the [A]/[B] relationship remains constant and:

$$\frac{[\beta Lac]}{[DKP]} = \frac{k_\beta}{k_{DKP}} K_{eq}$$

**Equation 3.1**

With these considerations, three scenarios can be envisioned

- If both anions react at the same rate, the product distribution will be the same as the ratio of the reagents at equilibrium.
- If the major anion is also the faster reacting, the product from this one should prevail, and will not reflect the equilibrium distribution.
- If the minor anion is the faster reacting, the product ratio will depend on all three variables of the equation 3.1 and the observed product distribution will not reflect the equilibrium distribution.

As a conclusion from the experimental studies and the calculations, it seems clear that for the 1,4-disubstituted triazole and the 1,5-disubstituted one, the formation of the diketopiperazine is favored compared to the β-lactam, whereas for the 2,4-derivative is the other way around.

Two cases are also explained by the principle. Case 1, where the less stable intermediate leads to the major product and the reaction coordinates would be similar to the graph in Figure 3.9. The less stable anion (**A**) with the higher energy leads to the major product (**DKP**).

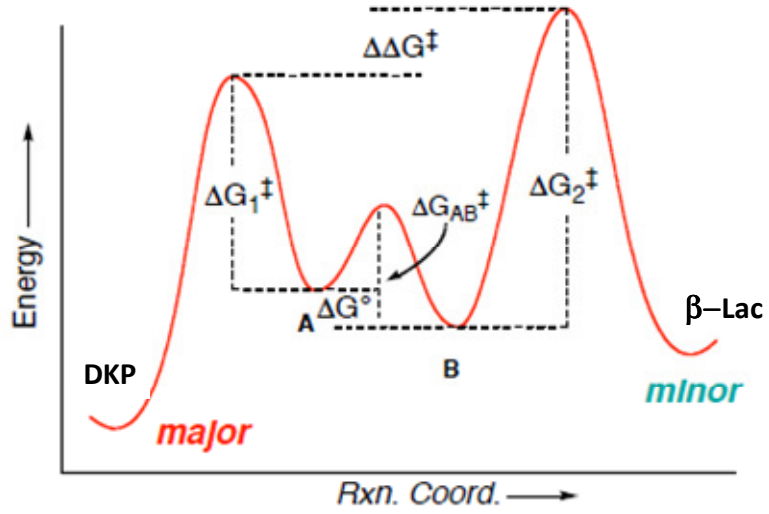


**Figure 3.9:** Reaction evolution where the major product comes from the less stable reagent.

This first case is the same observed with the 1,4- and the 1,5- disubstituted triazoles where the DKP was the major product and the amide anion showed less stability than the carbanion.

The other case (Case2) is explained when the less stable intermediate leads to the minor product, and Figure 3.10 shows how the energetic barriers would be in this case. This example is in agreement with what was observed and calculated for the 2,4-derivative, where the β-lactam product is kinetically more favored than the DKP and is the major product coming from the most stable anion (**B**).

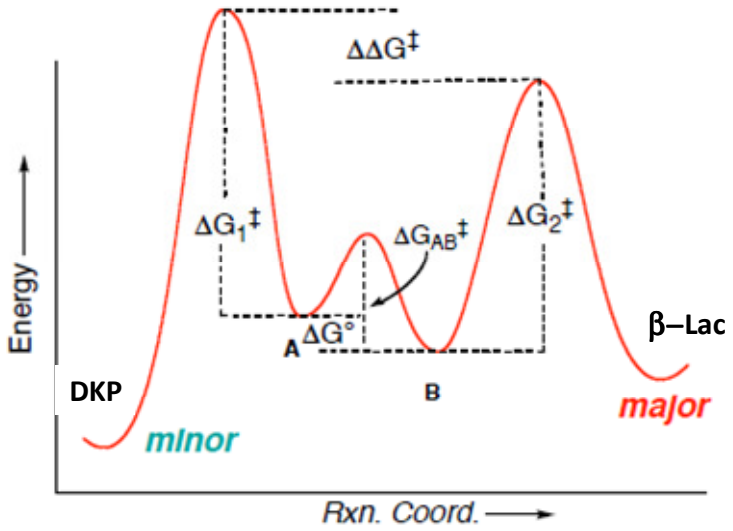


**Figure 3.10:** Reaction evolution where the minor product comes from the less stable reagent.

After all these calculations, it seems clear that in general the DKP scaffold is the most stable, but the energetic barriers passing through the transition states deppends on the substitution of the triazole. In the 1,4- and 1,5-disubstituted triazoles, this barrier is lower to form the diketopiperazine than the β-lactam, whereas in the 2,4-disubstituted triazole is energetically much easier to obtain the β-lactam than the DKP. However, these barriers can be modified by reducing the transition states energies of each case. For example, when stabilizing the anion **A** (Scheme 3.7) with an aromatic group attached to the nitrogen, the energy of the transition state to form the DKP will be reduced and the ratio of DKP/β-Lac will be increased. On the other hand, if the substituent linked to the nitrogen reduces the stabilization of the anion, the transition state barrier would be higher and the amount of DKP will be reduced.

### 3.3.2. Scope and limitations of the cyclization

Another objective in this chapter was the synthesis of a small library of compounds containing the β-lactam scaffold of compound **19** due to its high biological activity.

We know that two products (**βLac** / **DKP** in Scheme 3.8) can be formed when treating the open compounds with base. Fortunately, from the previous reactivity and theorethical studies, we also knew which substituents will shift the reaction to one side or to the other. With this information, the appropriate substituents for the construction of the library were chosen.

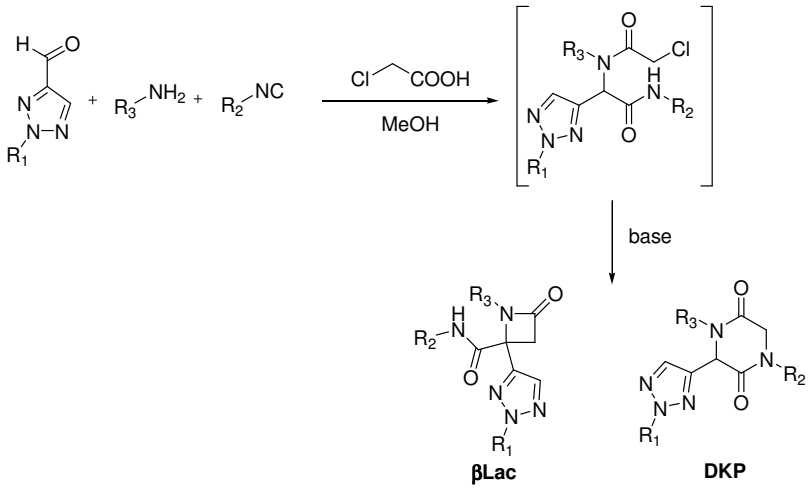


**Scheme 3.8:** Ugi reaction to yield the intermediate that would be cycled to form the **βLac** of the **DKP**.

The Ugi reaction was carried out the same way as already explained and after the obtention of the Ugi adducts, treatment with NaOH / MeOH during 2 hours afforded the cyclic compounds. Table 3.1 shows the ratio measured in the crude reaction mixture by $^{1}$H-NMR between both structures (β-lactam or DKP) after the intramolecular cyclization.

| CMPD | $R_1$ | $R_2$ | $R_3$ | βLac / DKP |
|---|---|---|---|---|
| 43 | 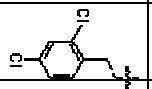 |  |  | 1 / 0 |
| 44 | 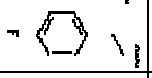 |  |  | 1 / 0 |
| 45 | 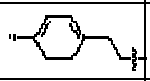 |  |  | 1 / 0 |
| 46 |  |  |  | 1 / 0 |
| 47 |  |  | 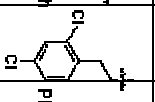 | 1 / 0 |
| 48 |  |  |  | 1 / 0.2 |
| 49 |  |  |  | 1 / 0.2 |
| 50 |  |  | 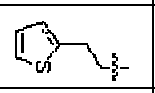 | 1 / 0.25 |
| 33 |  |  | 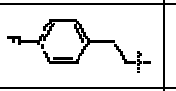 | 1 / 0.4 |
| 35 |  | 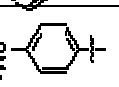 |  | 0.13 / 1 |
| 51 |  | 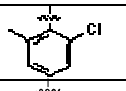 |  | 0 / 1 |
| 52 |  | 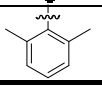 |  | 0.1 / 1 |

**Table 3.3:** Table with the synthesized compounds and their substituents where the proportion of both scaffolds determined by $^1$H-NMR is shown.

The triazole-aldehydes ($R_1$) used are the same described in Chapter 2 for the NMR study of the different triazole substituents.

The isocyanide substituents ($R_2$) were chosen following the previous reactivity study. If our predictions were right, the *tert*-butyl group would yield a major proportion of the β-lactam because the NH acidity has been reduced. Therefore, the amide anion will be less stable and the formation of the DKP slower. As shown in the table, all the products where $R_2$ is *tert*-butyl only yielded the β-lactam. The benzyl group was also used as $R_2$ and a mixture of both products was obtained, being in all cases the β-lactam the major isomer. This is in agreement with the reactivity study using compound **33** and with Case 2 of the Curtin-Hammett Principle.

Finally, to increase the acidity of the NH proton, phenyl groups were used as $R_2$, which would increase the stability of the transition states and should yield DKPs as major compounds.

As seen in the table, the proportion of **DKP** was increased. Overall, the tendency shown in the table is clear: from up to down, changing from the *tert*-butyl to the phenyl substituent, the proportion of **DKP** is increased as the NH acidity is increased too.

Some features of the syntheses of these compounds were interesting. When $R_2$ is *tert*-butyl (**43-47**), nearly in all cases the cyclization was carried out after the Ugi reaction without an intermediate purification and the final compounds were purified by reverse-phase chromatography. Figure 3.11 shows the $^1$H-NMR of the crude reaction mixture before the cyclization step of **43** and the HPLC profile of the mixtures. In the case of compound **47**, reverse-phase purification before the cyclization was needed to obtain a pure adduct, whereas compound **45** was obtained pure enough after both steps.

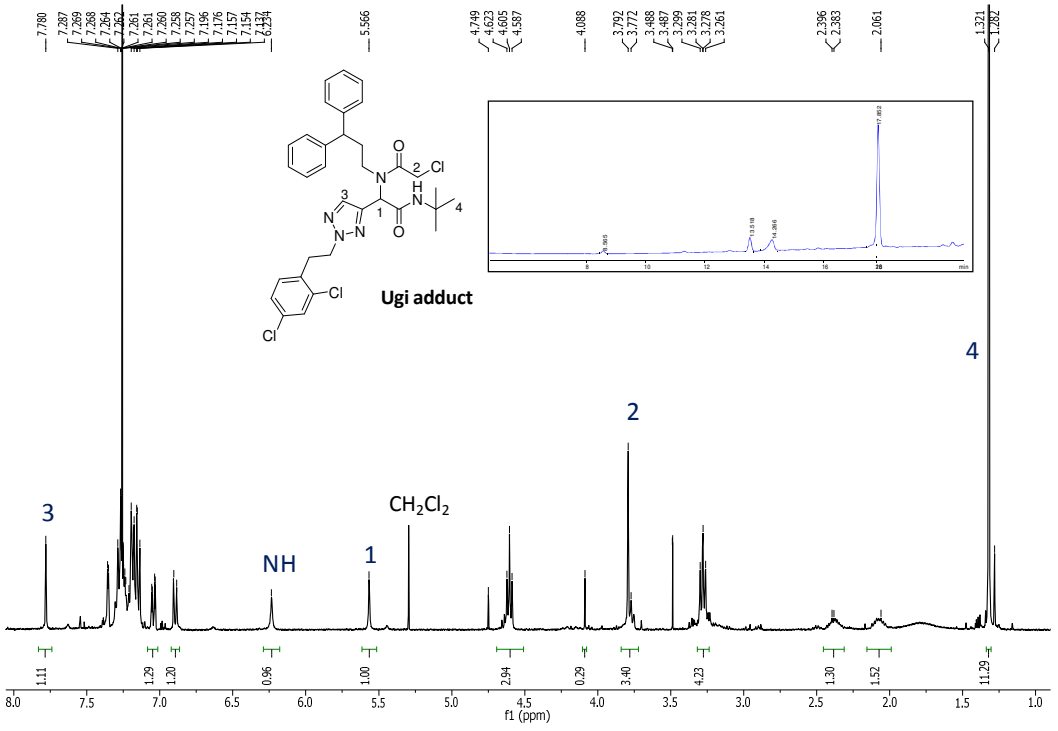


**Figure 3.11:** $^1$H-NMR ($CDCl_3$, 500 MHz, 25ºC) and HPLC profile of the crude reaction mixture of the Ugi adduct before obtaining compound **43**.

When $R_2$ was the benzyl group (**48, 49, 50, 33**), the purification steps were more difficult since mixtures of both structures were formed. After the cyclization step, reverse-phase chromatography was carried out in all cases and a clean mixture of both products was obtained. A further purification by thin layer chromatography was carried out for **48**, **49** and **33** and the two pure compounds were separated and characterized. This separation was not possible for **50**, and both compounds were characterized in the mixture. Figure 3.12 shows the $^1$H-NMR of **50** where the characteristic NH of the β-lactam and the CH of the DKP are present.

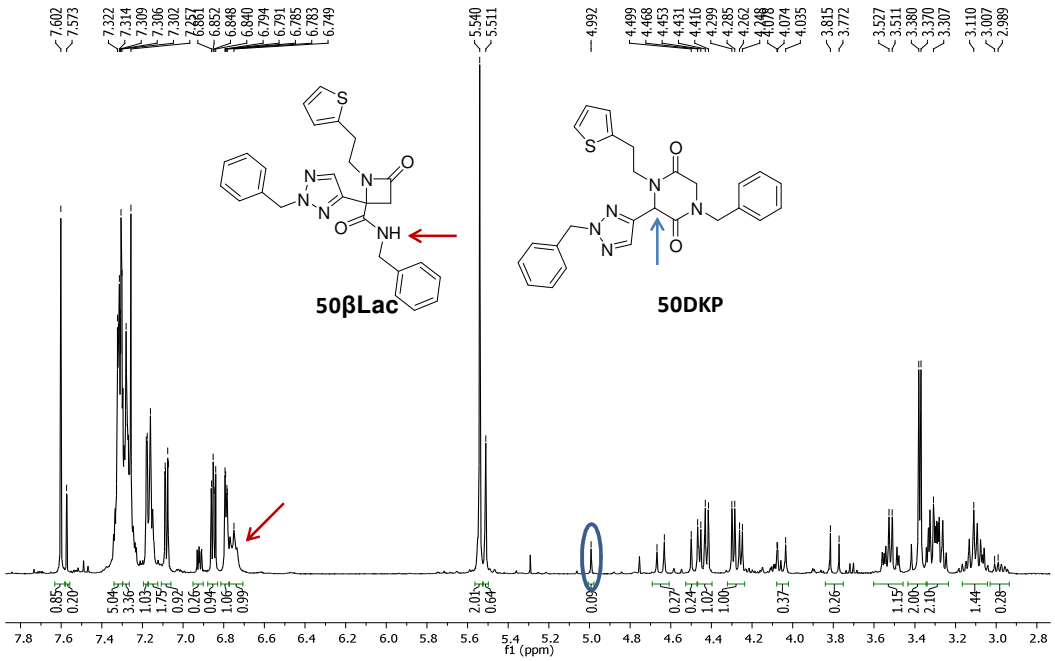


**Figure 3.12:** $^{1}$H-NMR ($CDCl_3$, 400 MHz, 25ºC) of the mixture of compounds **50.**

When the substituent used in $R_2$ is the *p*-methoxyphenyl group (**35**), a chromatographic column was needed to purify the Ugi adduct. Then, as already mentioned in 3.3.1. to a methanol solution of the open product, NaOH was added and a 1 / 0.13 mixture determined by $^{1}$H-NMR of the DKP and the β-lactam compound was obtained. This mixture was characterized as the DKP, due to the low amount of the β-lactam present.

Using 2-chloro-5-methyl-phenylisocyanide, a semi-preparative TLC was needed to obtain the pure cyclic compound **51**. Although only the DKP was formed, the $^{1}$H-NMR spectrum revealed the presence of two conformational isomers of the structure (**A** and **B** in a 1 : 0.8 ratio). Both products are diastereomers and Figure 3.13 shows the $^{1}$H-NMR with the NOE correlations of the *ortho*-methyl group and the $CH_2$ of the DKP. In structure **A**, the methyl has a correlation peak with both $H_2$, whereas in the other one, only one of the $H_2$ correlates with the methyl group, indicating that the rotation around the N-C bond of the phenyl ring is not free.

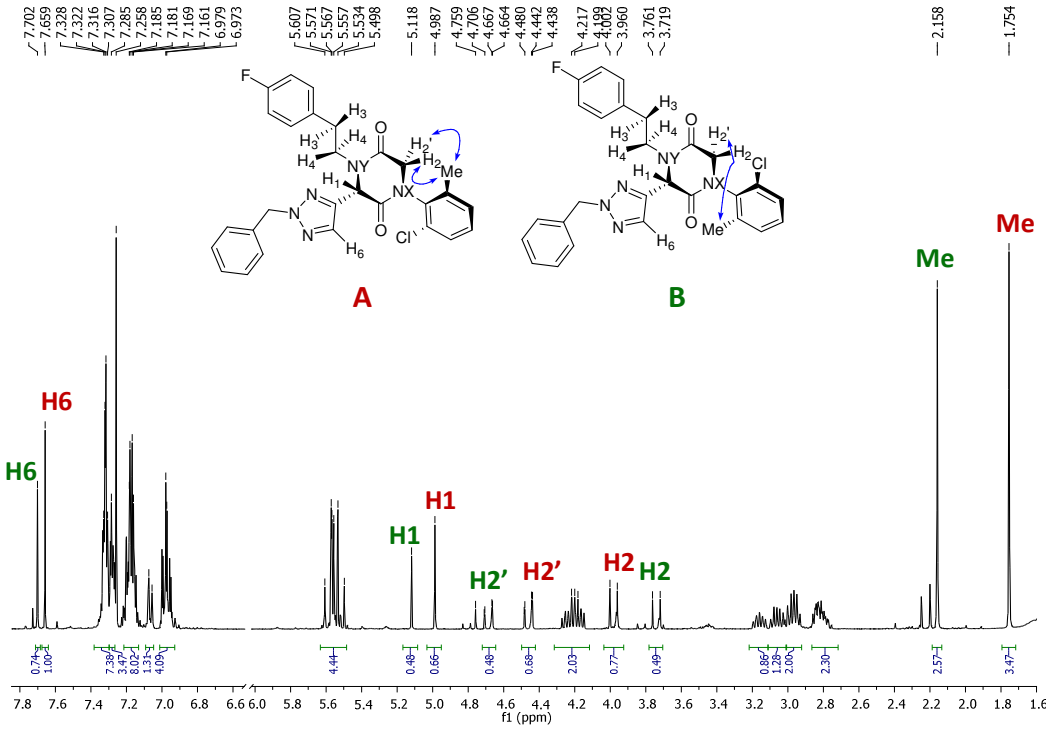


**Figure 3.13:** $^{1}$H-NMR ($CDCl_3$, 500 MHz, 25ºC) of **51** showing the two conformational configurations.

Finally, compound **52** as DKP was obtained pure after the cyclization step followed by a reverse-phase chromatography. Nevertheless, in the crude reaction mixture a 10% of the β-lactam compound was observed by $^{1}$H-NMR.

Taken together, the synthesis of these compounds has proved that by changing the isocyanide used in the Ugi reaction, we can address the cyclization to the DKP scaffold (increasing the acidity of the NH) using a phenyl group or to the β-lactam using a *tert*-butyl as a substituent.

The final library contains different type of compounds, some of them with the same substituents and different scaffolds (such as the ones with benzyl isocyanide), and most of them with different substituents and the same scaffold (β-lactam). We then envisioned that it would be interesting to see if replacing the original 2,4-dichlorophenethyl group in one of the substituents by a shorter *tert*-butyl or a benzylic chain would produce effects in the biological activity of the compounds.

### 3.3.3. Biological activities

In Chapter 1, the biological activities of the initial synthesized compounds were described. The most active one was **19** bearing the β-lactam scaffold (3.94 μM). The biological activities of the library derivatives were carried out in the group of Dr. Enrique Pérez-Payá. Two different assays were performed: *in vitro* and with cellular extracts. In table 3.2, some of the $IC_{50}$ values are reflected. (The inhibitory curves of these compounds are shown in the Supp. Inf.) In some examples the difference between the activities of the same compound in both assays is noticeable.

| CMP | $IC_{50}$_*in vitro* | $IC_{50}$_cell |
|---|---|---|
| **43βLac** | 11 | 26.4 |
| **46βLac** | 100 | 22.8 |
| **47βLac** | 38 | 93.2 |
| **48βLac** | 22 | 25.3 |
| **48DKP** | 100 | 69.3 |
| **33βLac** | 78 | 24.8 |
| **33DKP** | 100 | 14.7 |
| **52DKP** | 24 | 24.2 |

**Table 3.4:** $IC_{50}$ (μM) values for selected compounds as apoptosome formation inhibitors.

Taking into account that the activity of the original β-lactam (**19**) was 3.94 μM *in vitro*, it is clear that none of the new compounds has a better inhibitory activity. Despite this fact, the best result obtained in this batch is for **43** with an $IC_{50}$ of 11 μM in the *in vitro* assay. This compound is very similar to **19** but lacking one of the 2,4-dichlorophenethyl groups. (Figure 3.14).

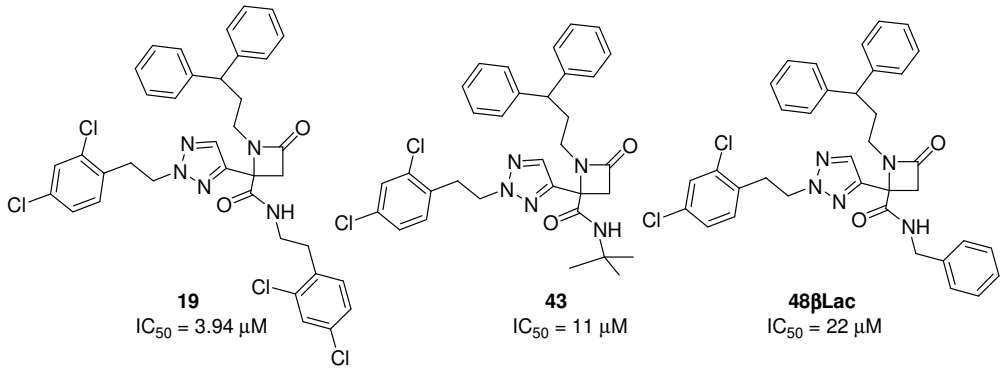


**Figure 3.14:** Compounds **19**, **43** and **48a** and their *in vitro* $IC_{50}$.

The following better *in vitro* activity is for **48βLac** (22 µM) where the 2,4-dichlorophenethyl from **19** was replaced by benzyl group. It is interesting to mention that although the substituent is shorter and without the chloro substituents, the activity has not suffered a large decrease. This fact is relevant because it suggests that maintaining one of the 2,4-dichlorophenethyl groups and the diphenylpropyl substituent, the activity is similar both in presence or absence of the third substituent. If this substituent is not essential for the activity, it can be used as a linking point for further conjugation. This possibility will be discussed in Chapter 4 in more detail.

With the background for all the tested compounds performed at Prof. Pérez-Payá laboratory until the present time, it seems that the diphenylpropyl group and the 2,4-dichlorophenethyl are important for good inhibitory values. The table of activities is also in accordance to this assertion, because the better activities are for compounds that contain these groups (**43βLac**, **48βLac**, **52DKP**).

In some cases the difference of activity between the assays *in vitro* and in cellular extracts is surprising. For example, compound **47βLac** has a good *in vitro* activity, but it worsens when tested in cellular extracts. In addition, the inhibitory curve is not very good, indicating that the value could have a high deviation. The activity of this compound could also decrease due to the absense of the diphenylpropyl group.

It also seems that the presence of the *p*-fluorophenethyl group decreases the activity of the compounds, such as in **46βLac** or **33**. In compound **46βLac**, the difference of activity between the assay *in vitro* and in cellular extracts is also high.

The cellular extract activities for the previously mentioned compounds (Figure 3.14) are 26 µM for **43βLac** and 25 µM for **48βLac**, which are not different between them. On the other hand, comparison of **48βLac** with **48DKP** where the scaffold has changed from the β-lactam to the diketopiperazine, the biological activities in both *in vitro* and cellular extracts fall away. Once again, the inhibitory curve for **48DKP** *in vitro* is not good, so the calculated $IC_{50}$ could be doubtful.

Comparing again the scaffold of the β-lactam with the corresponding DKP such as in **33βLac** and **33DKP**, although both results are quite bad due to the *p*-fluorophenethyl substituent, the best *in vitro* result is for the β-lactam and in cellular extract the best one is for the DKP. This could be because of the different solubility between both scaffolds in different media. Some preliminary solubility studies have shown that in aqueous media β-lactams are more soluble than the corresponding DKPs.

The result of **52DKP** is surprisingly good, because we have seen that with the DKP scaffold, inhibitory activities decrease, but in this case, both *in vitro* and in cellular extracts show good $IC_{50}$ values (24 μM). The activity of this compound also supports the hypothesis that the diphenylpropyl and the dichlorophenethyl groups are relevant for the interaction with the protein target.

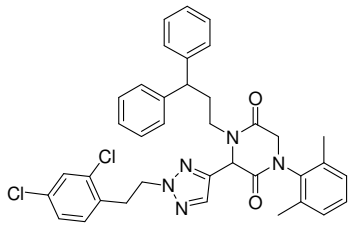


**Figure 3.15:** Compound **52DKP** bearing the DKP scaffold.

## 3.4. Conclusions

- A reactivity study has been carried out to discover what affects the intramolecular cyclization of the Ugi adducts.
- The observed behaviour can be explained considering the Curtin-Hammett Principle.
- The acidity of the NH proceeding from the isocyanide is the key element to set the cyclization to form the diketopiperazine, the β-lactam scaffold or a mixture of both.
- A small library of compounds has been synthesized in order to explore the β-lactam scaffold in the inhibition of apoptosis.
- The three substituents are not essential for obtaining good activities. In general, the 2,4-dichlorophenethyl and the diphenylpropyl groups increase the activity values and the β-lactam scaffold give better results than the DKP.

# 4. Synthesis of modified dendrimers and conjugation with selected apoptotis inhibitors

## 4.1. Introduction

### 4.1.1. Glycodendrimers

Nanomedicine may be regarded as a field of science that employs nanoparticles for the development of new diagnostic and therapeutic agents.[186] Some of the important polymeric structures used in nanomedicine are dendrimers. Dendrimers are synthetic polymers with a highly structured layered architecture, consisting of multiple branched monomers radiating from a central core. Layers of monomers are attached stepwise during synthesis, with the number of branch points defining the dendrimer generation.[187, 188] Since their discovery, there has been a wide and increasing interest in dendrimers and their biological, (bio)medical and pharmaceutical applications[189-191] They may be employed as drug carriers, and bioactive molecules can be either encapsulated inside the dendrimer or attached to its surface.[192]

One advantage of this research field is that dendrimers can be synthesized in a controlled manner to form small or large (macro-)molecules with perfectly branched structures. In most cases, the success of dendrimers as precisely constructed and multifunctional working tools arises from their globular shape and the dendritic effect of surface groups. In particular, the properties of dendrimers in these applications depend strongly on the nature of the surface groups that combine, for example, solubility, interaction and biocompatibility properties.[193]

The most important drawback of these types of dendrimers (cationic dendrimers) is their toxicity, which is due to the presence of a positive charge on their surface. This toxicity may be greatly reduced through the modification of the dendrimers' surface groups. One modification is the attachment of carbohydrate moieties to the surface groups of a dendrimer. In the case of poly(propylene imine) (PPI) dendrimers, it was previously shown that these modifications substantially reduce dendrimers' toxicity both *in vitro* and *in vivo*.[188, 194]. The coupling of mono- and oligosaccharide units to the outer shell has been successfully developed, and these macromolecules have been explored as carrier systems for drugs[195,196] and DNA macromolecules.[197, 198] Novel oligosaccharide architectures on dendritic polymer surfaces for their use as nanosized carrier systems for drugs, bioactive molecules, or (noble)metal nanopaticles have been prepared.[199, 200] Multifunctional carrier systems were set up where the nature of the oligosaccharide shell, ranging from very dense to very open, exhibited different structural, physicochemical and biological features.[201] Thus, the hyperbranched polyethyleneimine (PEI) was selected as dendritic core macromolecule stimulated by the fact that its derivatives has been successfully applied as multifunctional nanocarrier for drugs and dyes, including the first *in vivo* imaging studies with a PEI/dye system on tumor tissues.[202]

Appelhans and co-workers[193] developed an improved method for replacing the cationic charges on amino-terminated dendrimers so that they could be used as efficient antiamyloid agents with low cytotoxicity. The idea was to tune the surface by replacing the cationic charge with hydrogen-bond forming oligosaccharide units. In addition to being possible that the

oligosaccharide units suppress the biological processes involved in neurodegenerative disorders by no covalent hydrogen-bonding interactions with prion and Alzheimer peptides and proteins, this attachment resulted in remarkably low or zero cytotoxicity towards different cell lines.[197]

The concept developed by Appelhans and co-workers was inspired by the following facts: 1) PEGylated dendrimer surfaces are nontoxic and nonimmunogenic and led to the development of unimolecular micelles to encapsulate and release drugs.[203] 2) Glycodendrimers are promising as multivalent ligands for various biointeractions.[204] 3) No other studies have been devoted to study nonspecific hydrogen-bonding interactions with proteins and other biological molecules and systems. 4) Reductive amination is one of the simplest synthetic methods for directly introduce oligosaccharide units without protective groups onto amino-terminated dendrimer surfaces in the aqueous phase.[205,206]

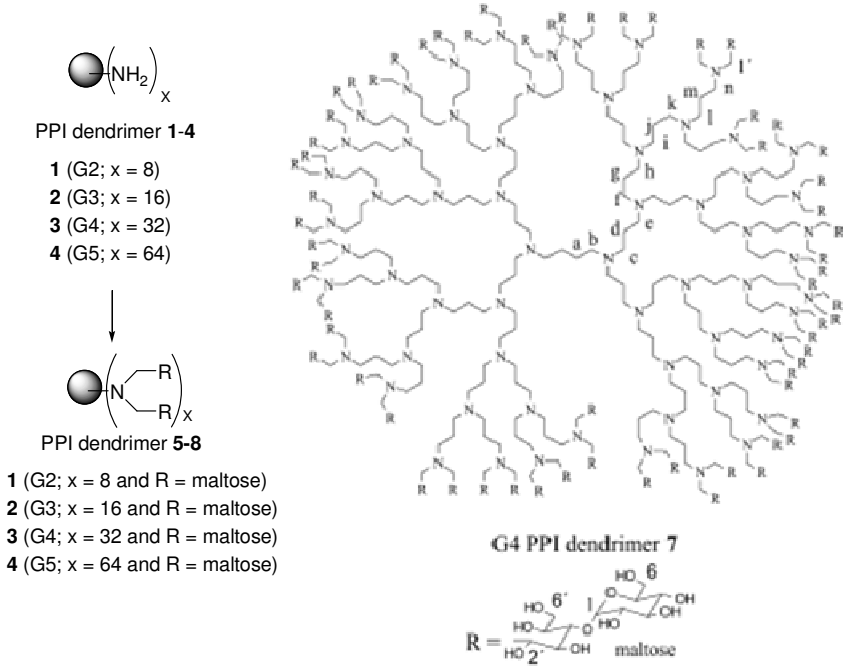


**Figure 4.1:** PPI Dendrimers of 2nd, 3rd, 4th and 5th generations without and with maltose in the surface.[193]

Thus, Appelhans and co-workers reported the synthesis and characterization of higher-generation PPI dendrimers with densely organized oligosaccharide shells in which each peripheral amino group is modified by two chemically coupled oligosaccharide units (maltose) (Figure 4.1.). These dendrimer structures will provide a platform for developing the next generation of dendrimers, combining apparently contradictory properties (e.g., water solubility, nonionic surface groups, neutral charge, non-specific hydrogen-bond-forming surface groups for modifying biological processes, high biocompatibility, and drug encapsulation-release), because having nonionic surface groups is not easily combined with water solubility or with drug

encapsulation-release. Dendrimers are lipophilic molecules with low solubility in water but good membrane permeability. Those oligosacharide-decorated dendrimers increase their solubility resulting in the retainment of the other requiringly biological properties.

In order to couple two maltose units per surface amino group by using a simple one-pot method, the authors adopted the reductive amination of monodendrons and dendrimers using an excess of oligosaccharides[206-209] generating the third-, fourth-, and fifth-generation PPI dendrimers.

With these antecedents, our aim was to design, synthesize and characterize conjugated polymers that enhance the therapeutic possibilities of the active molecules already described in previous chapters of this thesis. The conjugation of the apoptosome inhibitors with a polymer would offer a more specific intracellular transport and release to reach the molecular target. Moreover, it is presumable that the linkage to a hydrophilic polymeric support would increase the solubility of the compounds. In general, the conjugate is internalized by endocytosis and then it goes through the endosome to the lysosome, where the proteolytic enzymes or the acid pH activates the degradation of the polymeric transporter and the drug is released by diffusion to the cytosol.[210]

## 4.2. Objectives

During my PhD I spent three and a half months in the group of Dr. Appelhans at the Leibniz Institute of Polymer Research in Dresden (Germany). All the experiments with dendrimers described in this chapter were carried out there.

The synthesis of some active compounds during this work and the fact that the group of Dr. Appelhans is able to perform high-generation glycodendrimers, offered the possibility to couple the biologically active molecules with a PPI-5G-maltose-glycodendrimer as a nano-carrier. First of all, the synthesis of a small molecule similar to the previously described active ones but bearing an appropriate appendix that allows the coupling with the modified glycodendrimers was required.

Then, the couplings with the dendrimers could be performed in different ways:

- Synthesis of the dense-shell 5$^{th}$ generation glycodendrimer followed by the coupling of the compounds through a spacer.
- Synthesis of the open-shell 5$^{th}$ generation glycodendrimer followed by the coupling of the compounds through a spacer.
- Synthesis of the open-shell 5$^{th}$ generation glycodendrimer where the drug is directly coupled to the dendritic scaffold.

The difference between the dense-shell and open-shell 5th generation glycodendrimers remains in the amount of maltose attached to the PPI scaffold. In Figure 4.2 a schematic picture of each type of dendrimer is depicted. In the dense-shell case, it can be seen that the amount of blue shapes (maltoses) is higher than in the open-shell. Moreover the blue lines represent the linkers with the terminal $NH_2$ group that can be chemically modified with the drugs. In the open-shell without spacer, the drugs are directly attached to the PPI, not through a linker.

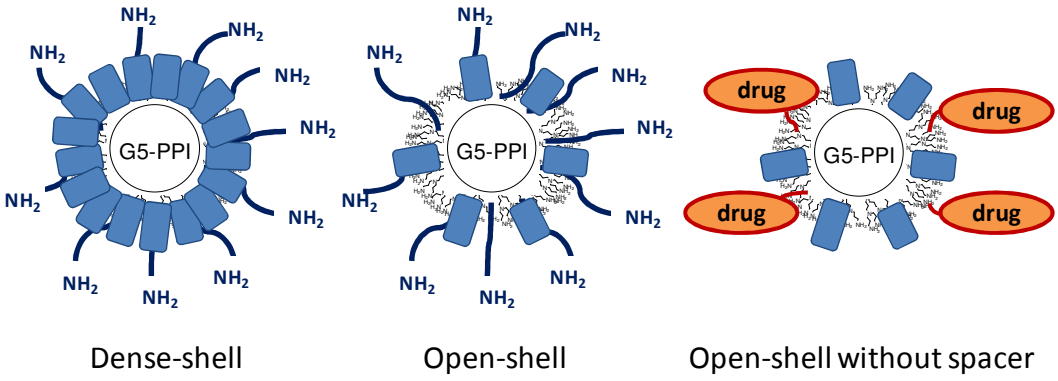


**Figure 4.2:** Representation of the dense-shell and open-shell glycodendrimers with and without spacer 5th generation glycodendrimers.

## 4.3. Results and discussion

### 4.3.1. Synthesis of the lead candidates containing a linker moiety

As shown in Chapter 3, the biological activity of compounds **19**, **43βLac** and **48βLac** did not exhibit big differences. This result suggested that one of the 2,4-dichlorophenethyl substituents at **19** was not determinant for the interaction with the target protein. Therefore, the possibility to remove this substituent and use this part of the molecule as a connector to the dendrimers was contemplated.

Different chemical moieties can be used to attach the compound of interest to a polymer, but in Dr. Appelhans group, they checked the acid-amine binding, the triazole formation by azide-alkyne cycloaddition and the thiol groups. The first option seemed to be the easiest for our case. Thus, the synthesis of the carboxylic acid **55** was devised. (Scheme 4.1):

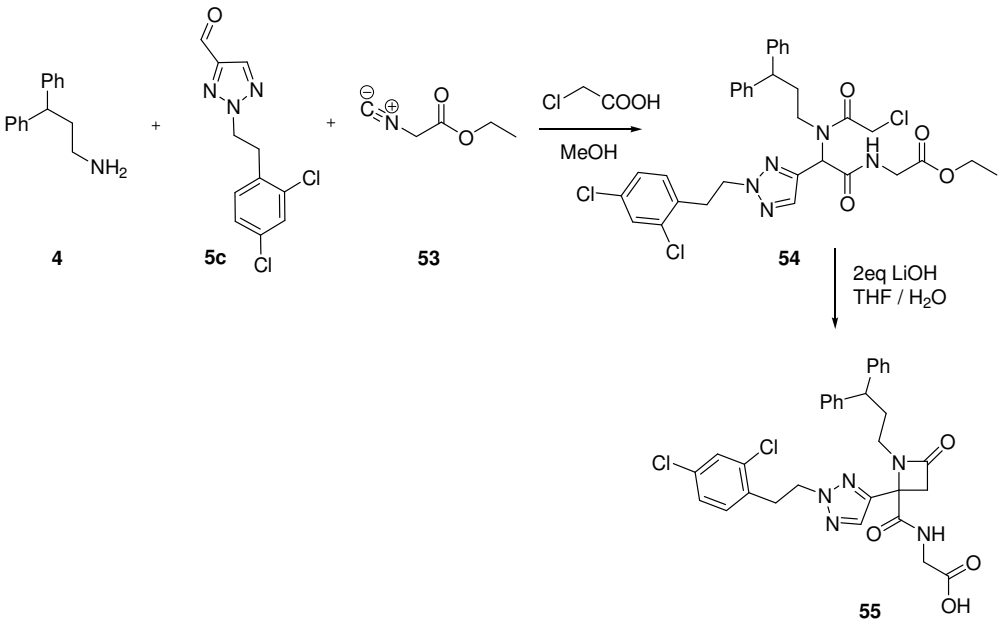


**Scheme 4.1:** Synthesis of β-lactam **55** bearing a carboxylic acid moiety.

The first step was carried out like all the previously Ugi reactions and compound **54** was obtained with 63% yield after chromatographic purification. The fastest method to achieve the cyclization of **54** and the deprotection of the ethyl group in one step was using 2 equivalents of LiOH in a solution of THF : water (1:1). Compound **55** was obtained without any further chromatographic purification in 85% yield from compound **54**. It was fully characterized by NMR ($^{1}H$, $^{13}C$ and $^{15}N$); actually, the disappearance of the CH proton which forms the β-lactam and the absence of the ethyl group was enough to confirm the structure.

Moreover, in order to have a longer chain in the molecule and an alternative linkage moiety, the reaction of **55** with *N*-Boc-ethylendiamine was carried out. To a DCM solution of the reagents, HOBt, DIPEA and EDC were added and the mixture was stirred overnight. After chromatographic purification, the desired product was deprotected with trifluoroacetic acid giving compound **56** in 24% yield. (Scheme 4.2)

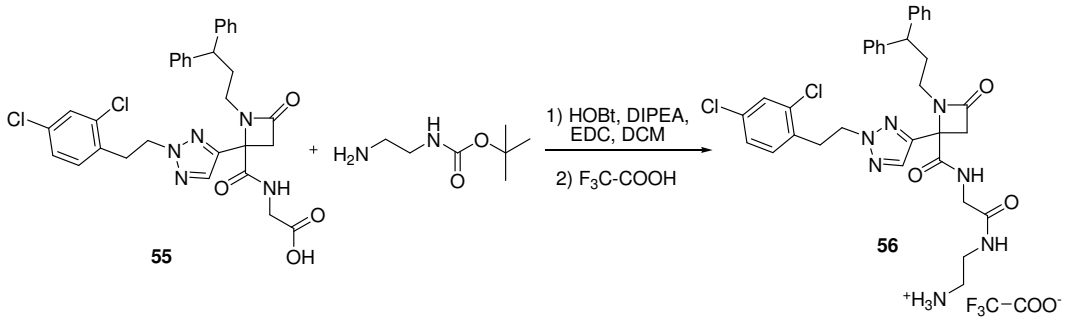


**Scheme 4.2:** Synthesis of the β-lactam **56** bearing an amino terminal group.

The same reaction was performed with the seven-membered ring compound[27], in order to try the couplings also with a different type of molecule. Compound **57** is very similar to QM31 (c.f. Figure 0.9), but with a terminal carboxylic acid instead of the amide present in QM31. This compound was previously synthesized in our group by Dr. A. Moure.[211] The coupling of **57** with *N*-Boc-ethylendiamine was carried out in 90% yield, and the further deprotection in 95%, to give compound **58**. (Scheme 4.3).

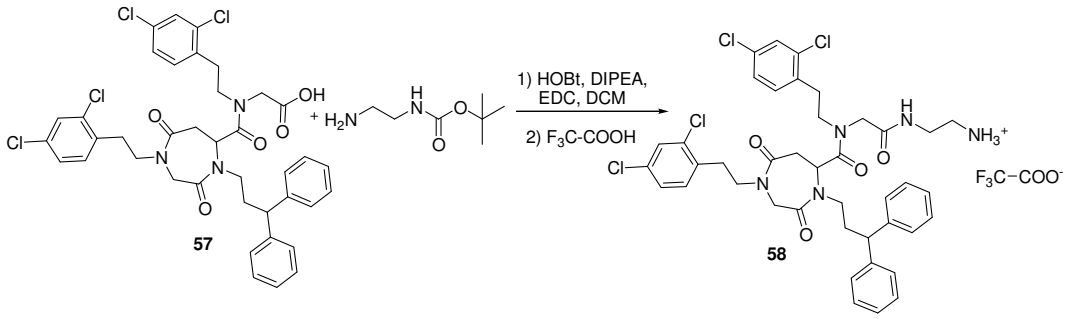


**Scheme 4.3:** Synthesis of a seven-membered ring molecule bearing an amino terminal group (**58**).

### 4.3.2. Synthesis of dense-shell macromolecules

#### 4.3.2.1. Preparation of the small molecules and the dendrimers

The first strategy proposed required a spacer to attach the synthesized molecules to the glycodendrimer units. The spacer used to this aim was a PEG spacer (compound **59**) which was commercially available.

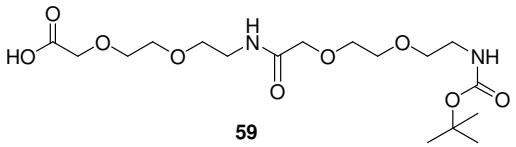


**59**

**Figure 4.3:** Spacer **59** used for coupling the molecules to the glycodendrimers.

Before the synthesis of the maltose-modified PPI dendrimer, the spacer had to be linked to the poly(propylene imine) PPI dendrimer. Scheme 4.2 shows the reaction assayed, where 10 spacers were attached to the dendrimer. If higher amounts of our compounds were linked there, the macromolecules' solubility would decrease. This reaction was performed with spacer **59**.

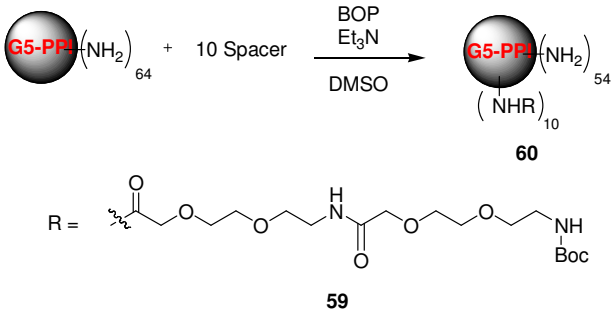


**Scheme 4.5:** Coupling of 10 spacers of **59** and the 5G-PPI giving compound **60**.

Thus, a DMSO solution of compound **59** with BOP was added to a DMSO solution of the 5$^{th}$ generation PPI dendrimer and $Et_3N$. After 24 hours stirring and 24 hours more of dialysis exchanging water regularly, compound **60** was obtained in 100% yield and was fully characterized by $^1H$, $^{13}C$ NMR in $D_2O$ and by IR spectroscopy. In Figure 4.4, the $^1H$ NMR of compound **60** is shown and some of the protons of the spacer are assigned. The other signals correspond to the dendrimer side-chains.

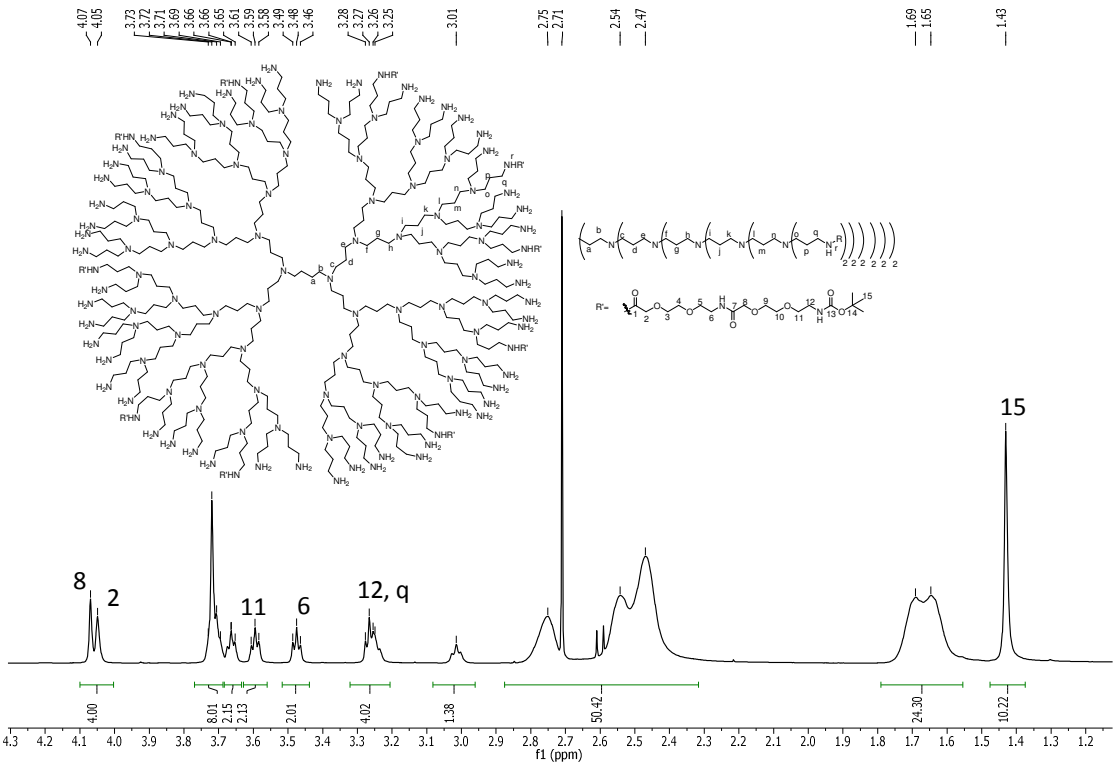


**Figure 4.4:** $^{1}$H NMR spectrum (500 MHz, $D_2O$) of compound **60.**

At this point, the reductive amination method to couple the maltose units to the surface amino group was carried out (Scheme 4.6). The treatment of **60** with a borane-pyridine complex in sodium borate buffer at 50ºC for 7 days led to the desired maltose-modified PPI dendrimer **61**, which was subjected to dialysis in water for 3 days to remove the excess of maltose.

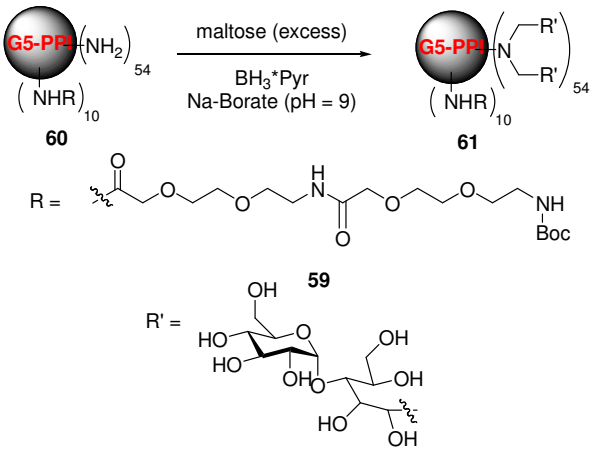


**Scheme 4.6:** Synthesis of the maltose modified PPI dendrimer **61** being R the spacer **59**.

Compound **61** was obtained after freeze drying in 57% yield. Similarly to other compounds already synthesized in Dr. Appelhans group, the proof of the chemical structure of **61** was carried using NMR spectra comparisons. Figure 4.5 shows the $^{13}C$ NMR spectrum of **61** and the presence of maltose groups was confirmed by the signal at 103 ppm assigned to the anomeric carbon (C1'') of the maltose residue.

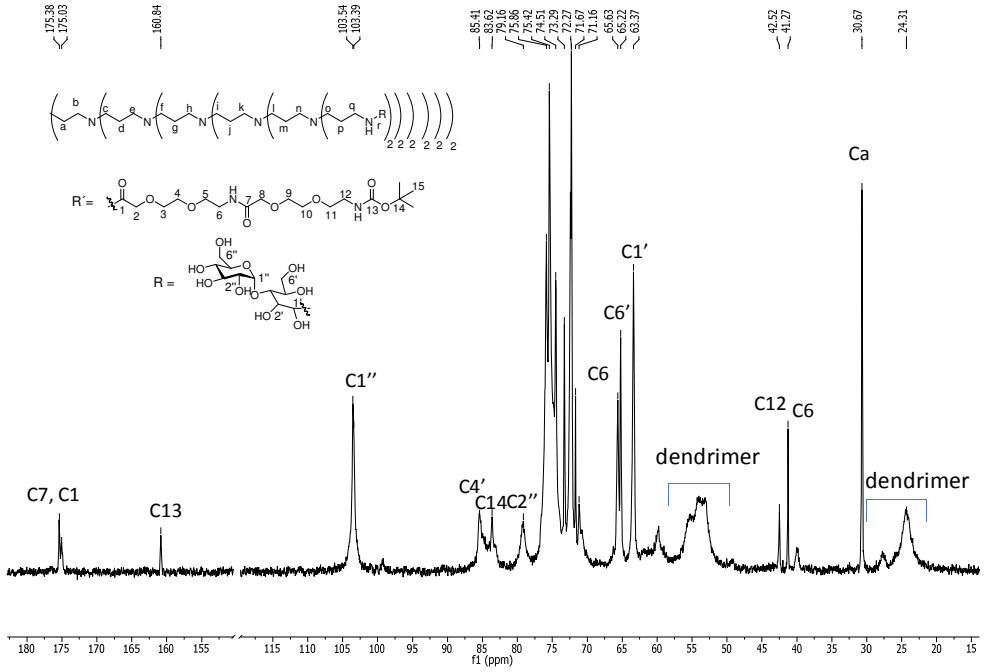


**Figure 4.5:** $^{13}C$ NMR (125 MHz, $D_2O$) of compound **61**.

The amount of maltose units attached to the dendrimer was calculated by $^{1}H$ NMR and by LILBID-MS and they were less than expected. LILBID-MS (Laser Induced Liquid Bead Ion Desorption) is an alternative method developed by Brutschy et. al. to perform mass analysis of biomolecules. In this method, the solvated ions are laser desorbed from the liquid phase by exciting a vibration of the solvent with intense, pulsed IR laser radiation. The idea was to bring the native environment of a biomolecular ion –the solution phase- and the laser desorption detection method together.[212-214]

Figure 4.6 shows the $^{1}H$ NMR of compound **61**. The integration of the $CH_2$ of the PPI (2.00-1.5 ppm), and the anomeric proton of the maltose (5.12 ppm), shows that there are 100 maltose residues instead of 108.

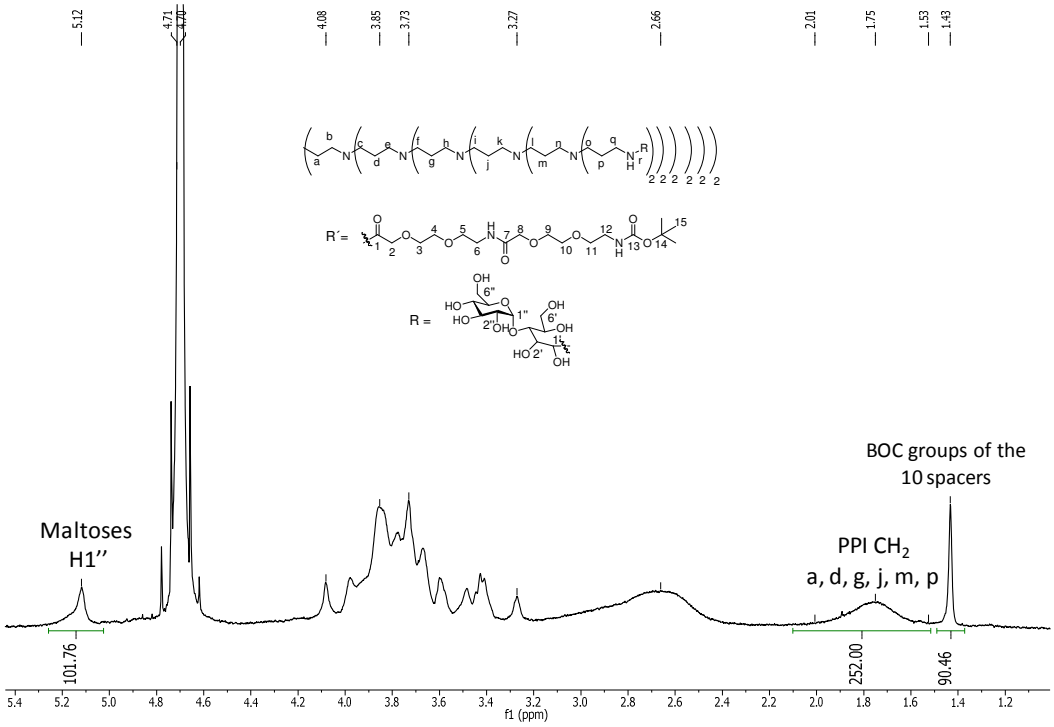


**Figure 4.6:** $^{1}$H NMR spectrum (500 MHz, $D_2O$) of compound **61** showing the integration of the main signals.

Moreover, a detailed structural characterization of the maltose units chemically coupled to the dendrimer surface was achieved using LILBID-MS analysis. (Figure 4.7). The measured molar mass corresponds to the glycodendrimer without 8 maltose units, which is the same value obtained by integrating the $^{1}$H NMR spectrum. This is an interesting result because it means that the $^{1}$H NMR method is reliable to quantify the amount of drug attached to the dendrimer. The difference in the theorical and the calculated maltoses is normal in this type of structures because there are a lot of free $NH_2$ and the steric effect hinders the bond formations.

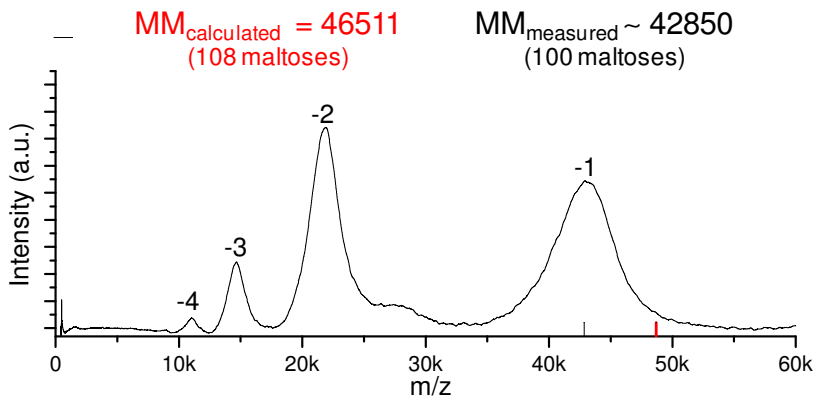


**Figure 4.7:** LILBID-MS spectrum of **61** (M-8).

In order to couple our inhibitors to the spacers, the deprotection of the BOC group was carried out using a 4M HCl solution in dioxane. After overnight stirring, dialysis and freeze drying the compound with the free amine **62** was obtained with complete conversion. The disappearance of the BOC group is easily distinguished in the $^{1}$H NMR spectrum by the absence of the singlet at 1.43 ppm.

### 4.3.2.2. Couplings with the maltose dense-shell PPI dendrimer

#### 1st Coupling

The first coupling assayed was carried out with the glycodendrimer bearing the amine and the small molecule **55** as free acid. (Scheme 4.7).

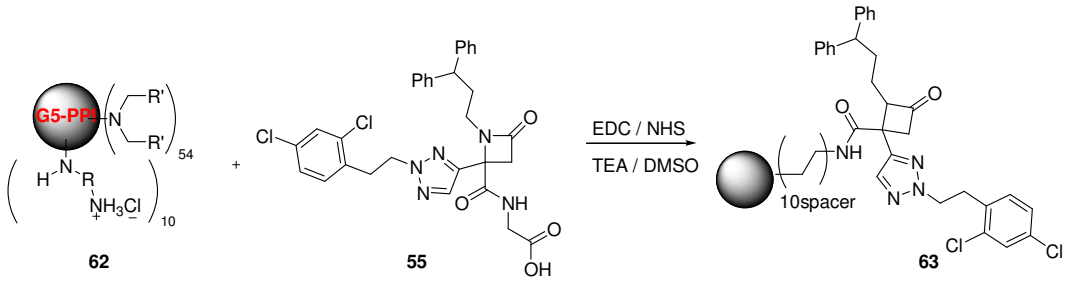


**Scheme 4.7:** Coupling of compound **55** with the dense-shell glycodendrimer bearing the amino-terminal group.

This reaction was performed by dissolving the glycodendrimer **62** in DMSO. It was necessary to heat up at 80ºC to improve the solubility. Then the solution was cooled down again

at 37ºC and TEA was added. Compound **55** (5 eq) was dissolved in DMSO and EDC and NHS (*N*-hydroxysuccinimide) were added to the solution within 1 hour difference. Finally this solution was added to the glycodendrimer solution and stirred overnight. In the $^{1}H$ NMR spectrum in $D_2O$ (Figure 4.8) of compound **63** a broad signal at 7.0 ppm is observed. This signal corresponds to the aromatic protons of the small molecule, which means that the coupling worked. Since compound **55** is not soluble in water, the signals would not be there, if it was not attached to the glycodendrimer.

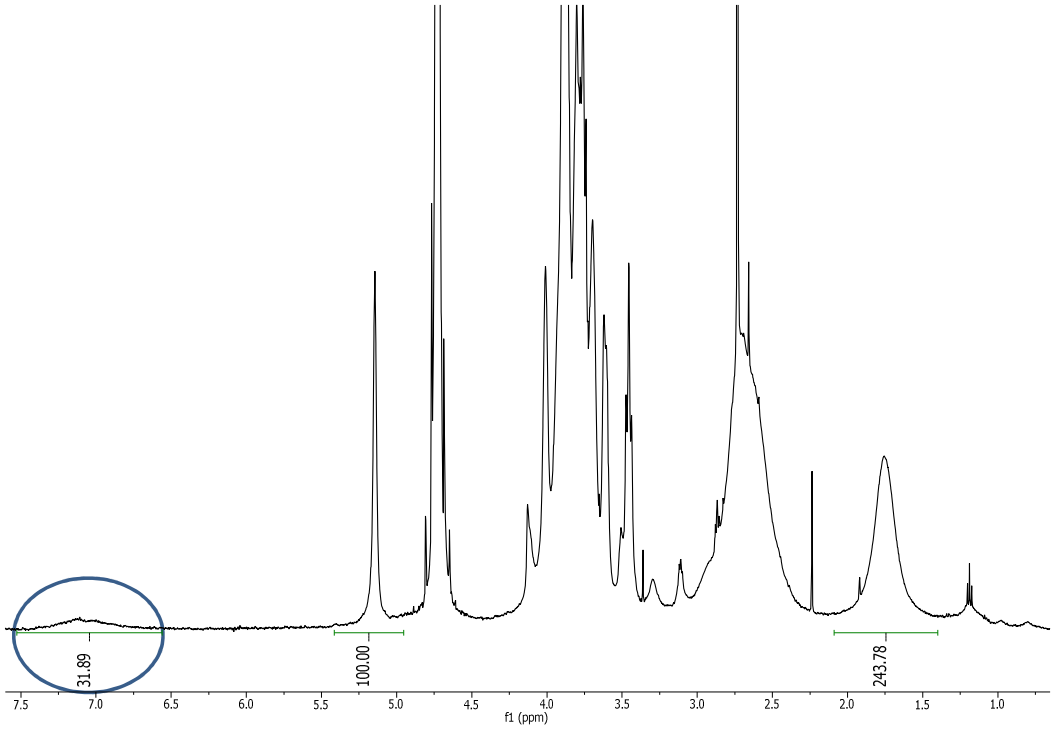


**Figure 4.8:** $^{1}H$ NMR (500 MHz, $D_2O$) of compound **63** where the aromatic signals of **55** can be observed.

Moreover, by integration of the maltose signal (100 maltoses) and the aromatic signals, it could be estimated that the amount of drug coupled was 2 equivalents of drug per polymer.

**2nd Coupling**

Simultaneously, an alternative method using the same dendrimer that was previously developed in the Appelhans group where two amino groups react with *p*-nitrophenyl chloromonocarbonate forming a urea bond was carried out. The reaction assayed is shown in Scheme 4.8. In this reaction all the reagents and the material should be dried, because the humidity could disfavor the conversion.

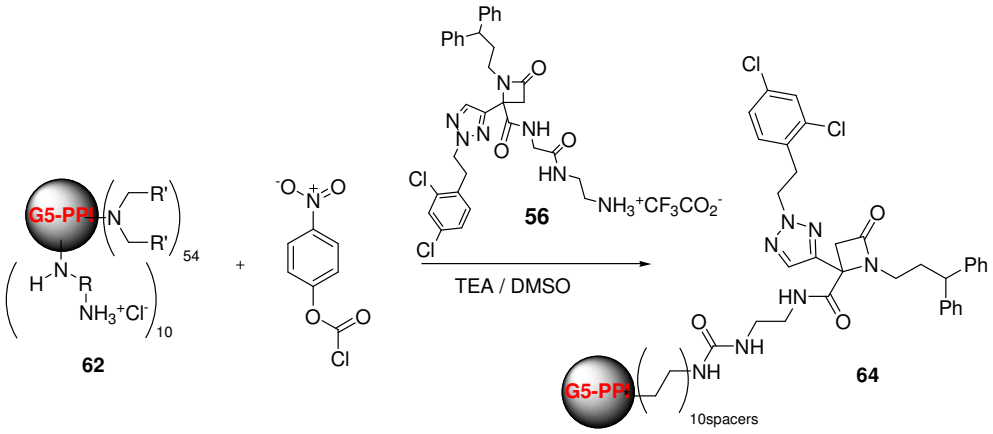


**Scheme 4.8:** Coupling of the glycodendrimer **62** bearing an amino-terminal group with molecule **56** bearing a free amino group.

This reaction was performed several times but in the $^{1}$H NMR spectrum of the crude reaction mixture obtained after dialysis and freeze drying, only the glycodendrimer **62** was observed.

## 3rd Coupling

Another possibility with the dense-shell maltose PPI dendrimer can also be performed with the amino group in the small molecule and the acid moiety in the spacer of the glycodendrimer. For the case of the dendrimer, succinic anhydride was added to compound **62** and an additional C4 chain was included in the spacer. (Scheme 4.9). This reaction was carried out in 68% yield and the $^{1}$H NMR signals of the additional $CH_2$ units confirmed the structure of **65**.

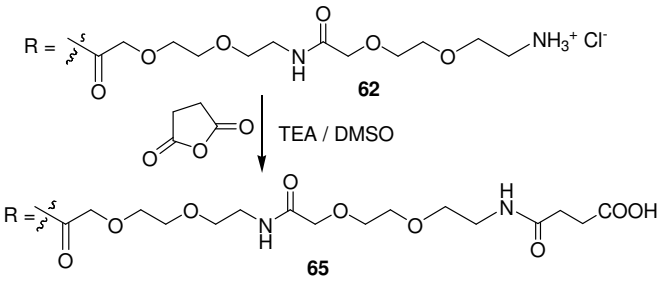


**Scheme 4.20:** Conversion of the amino-terminal glycodendrimer **62** to the acid **65**.

With compound **65**, the coupling with a small molecule bearing an amino terminal group could be possible. To this aim, the seven-member ring molecule **58** was used.

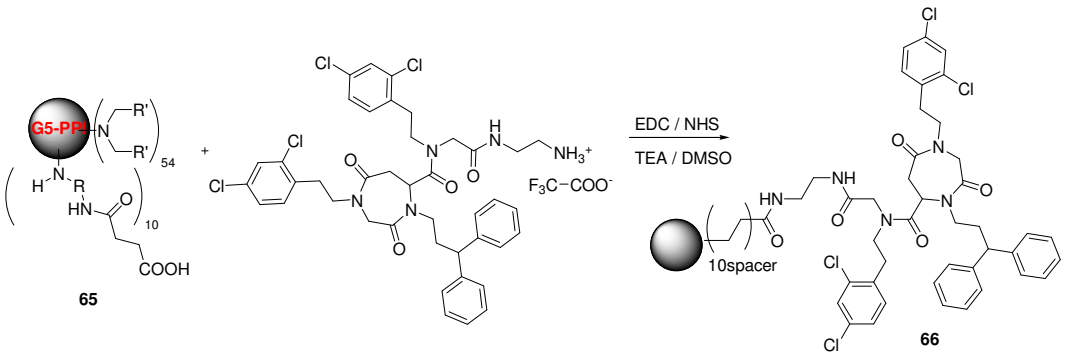


**Scheme 4.10:** Coupling of a seven-membered ring small molecule (**58**) with the glycodendrimer **65** to yield compound **66**.

This reaction was performed several times with no positive results. One possible explanation is that when treating the glycodendrimer **65** with EDC and NHS, the formation of the five-member ring within the terminal acid of each spacer was produced (Figure 4.9) thus avoiding the coupling with compound **58**.

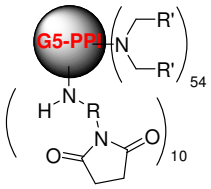


**Figure 4.9:** Possible undesired reaction of compound **65** with NHS /EDC.

After the three described alternatives, the 1st coupling was the most successful. In the other ones, the aromatic signals of the small molecules were not observed in the $^{1}$H NMR spectra. Thus, the coupling with the acid moiety in the drugs and the amino terminal groups in the glycodendrimers seems to be the best option.

### 4.3.3. Synthesis of open-shell glycodendrimers

#### 4.3.3.1. Preparation of the dendrimers

The high amount of maltose groups in the surface of the dendrimers tried in 4.3.2 could hinder the contact of the small molecules with the spacers making more difficult its attachment.

Therefore, to overcome that difficulty, a strategy involving an open-shell dendrimer instead of the dense-shell was assayed using the same methodology as for **61** but with defect of maltose, to give compound **67** (Figure 4.10). For each $NH_2$ present in the molecule 0.5 mol of maltose were added resulting in compound **67** having approximately 10 spacers and 20 maltoses (calculated by $^1$H NMR from the signals of the *tert*-butyl protecting group, see Figure 4.11). On the other hand, the difference of size from the maltose signals in the dense-shell molecule and in the open-shell is clearly observed from the comparision of the spectra.

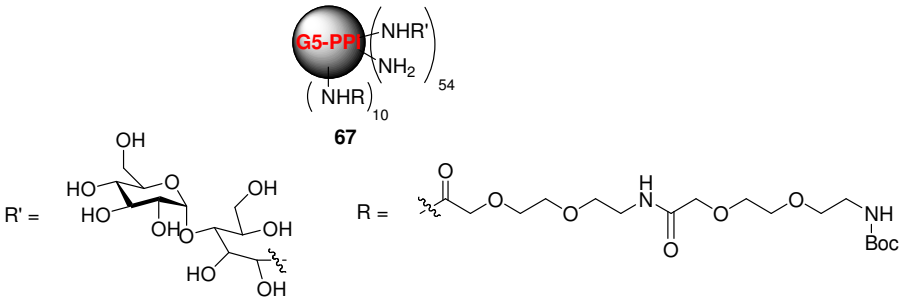


**Figure 4.10:** Compound **67** with open-shell maltose in the 5G PPI dendrimer.

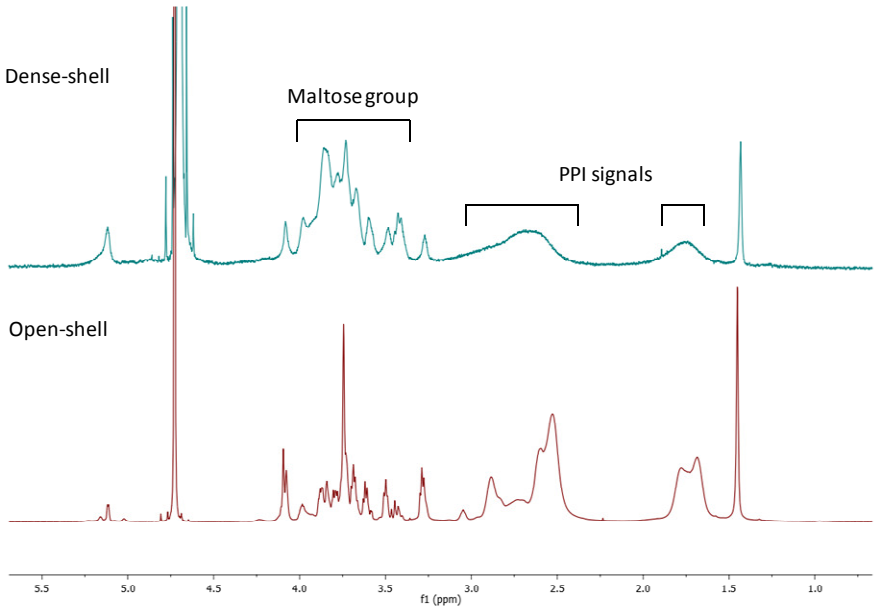


**Figure 4.11:** $^1$H NMR ($D_2O$, 500 MHz) comparison of compound **61** (dense-shell) with **67** (open-shell).

The same deprotective method used above (HCl 4M dioxane / water) was assayed in this case and compound **68** containing the free amine was available for the couplings with the small molecules. This reaction is easily followed by $^1$H NMR due to the disappearance of the *tert*-butyl singlet.

### 4.3.3.2. Couplings with the open-shell macromolecule bearing the spacer

The coupling in this case was carried out between the synthesized deprotected open-shell PPI dendrimer **68** and the seven-membered ring molecule **57** bearing the terminal carboxylic acid moiety. Figure 4.12 shows a schematic picture of the reaction between compound **68,** and the small-molecule **57** leading compound **69**. The blue shapes are the maltose units and the spacers are represented with the $NH_2$ groups at the end. The aromatic signals observed in the $^1$H NMR acquired of compound **69** (blue circle) indicate that the coupling was produced. The amount of drug attached to the dendrimer was quantified by $^1$H NMR and the polymer charge was only 1 equivalent of small molecule per polymer.

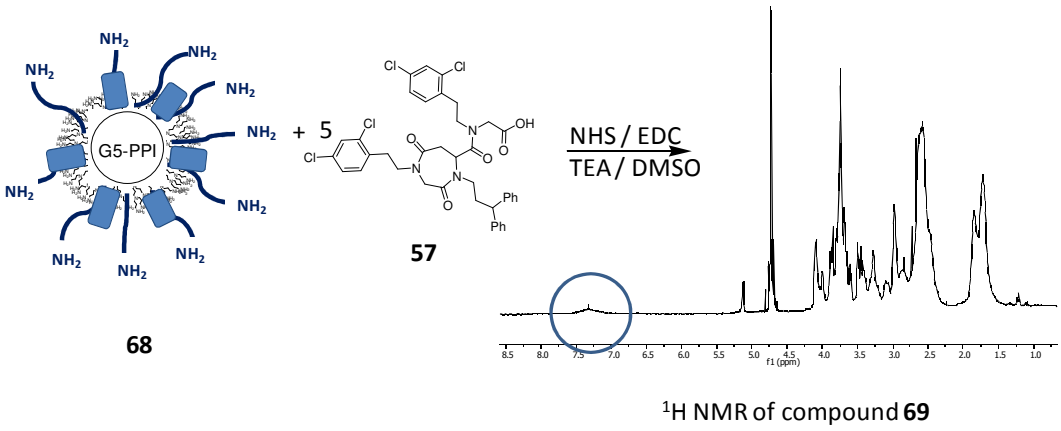


**Figure 4.12:** Reaction between the open-shell glycodendrimer **68** and the molecule **57** leading to compound **69** and its corresponding $^1$H NMR where the aromatic signals are marked with the blue circle.

### 4.3.3.3. Couplings with the open-shell macromolecule without spacer

Simultaneously, a coupling strategy without requiring the spacer was proposed. The small-molecule would be directly linked to the dendrimer surface followed by the reductive amination to form the open-shell maltose dendrimer. The first step of this reaction is shown in Scheme 4.11. A DMSO solution of compound **55** and BOP was stirred for 1 hour. In parallel, a DMSO solution of the dendrimer with TEA was prepared. The first solution was added to the dendrimer and the reaction mixture was stirred for 24 hours. After 1 day dialysis and freeze drying compound **70** was obtained.

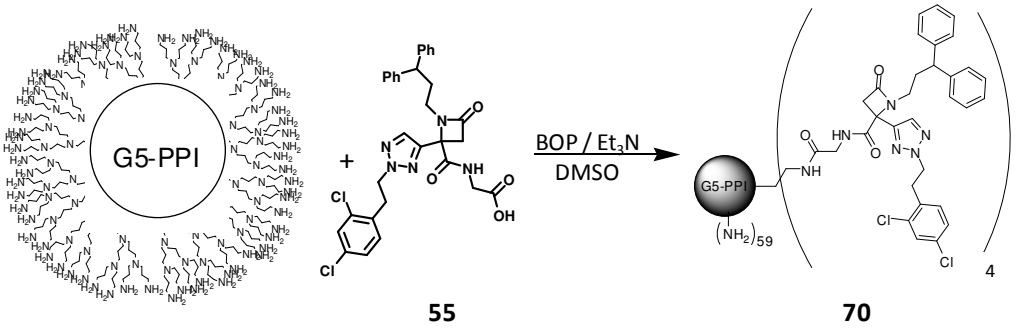


**Scheme 4.11: C**oupling of the 5th generation PPI dendrimer with small molecule **55** exhibiting of about four **55** units in **70**.

In the $^1$H NMR ($D_2O$) spectrum of compound **70** (Figure 4.13), the aromatic signals (~ 7 ppm) corresponding to the aromatic protons and the triazolic proton of the small molecule were observed, thus indicating that the coupling worked well. From the integration of the signals, it was possible to establish that 4 equivalents of drug were attached to the dendrimer.

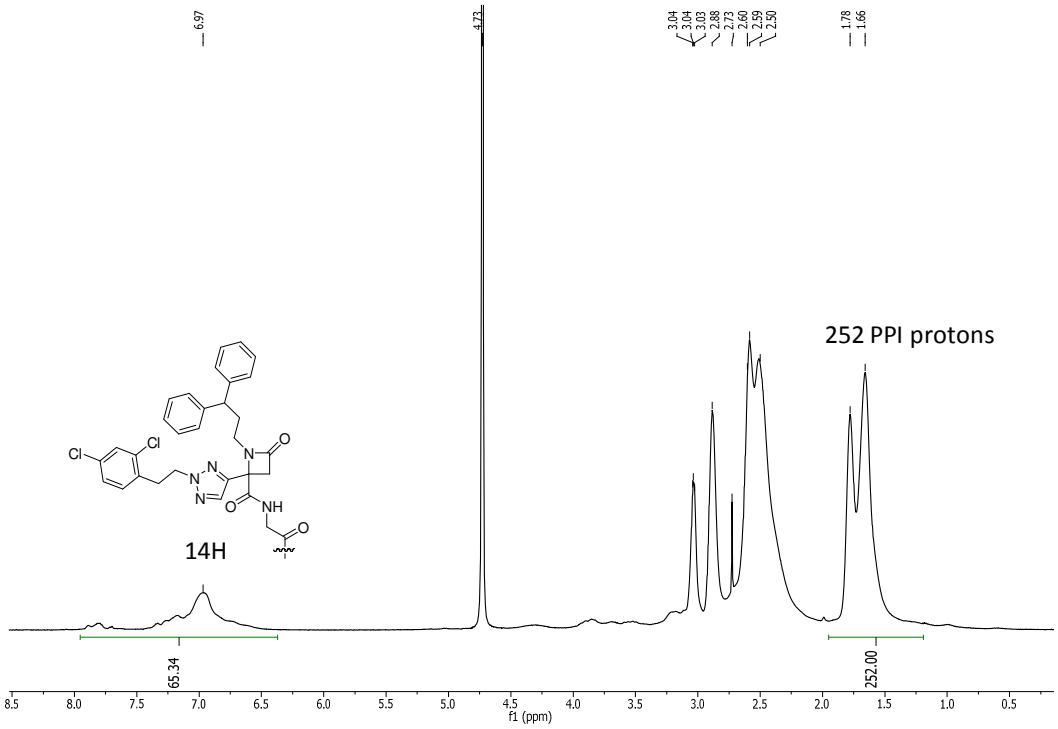


**Figure 4.13:** $^1$H NMR (500 MHz, $D_2O$) of compound **70** where small molecule **55** is attached to the PPI.

The reductive amination of compound **70** with defect of maltose (1:0.5) was carried out and as shown in the $^1$H NMR of Figure 4.14 the aromatic signals of the small-molecule are still there.

The integration of the $CH_2$ of the PPI, the maltose and the aromatic signals, determined that compound **71** has 25 maltoses and 4 equivalents of drug per polymer. Different signals for the anomeric proton of the maltoses (5.1 ppm) are observed in the spectra, this can be due to the various environment in the aqueous phase.

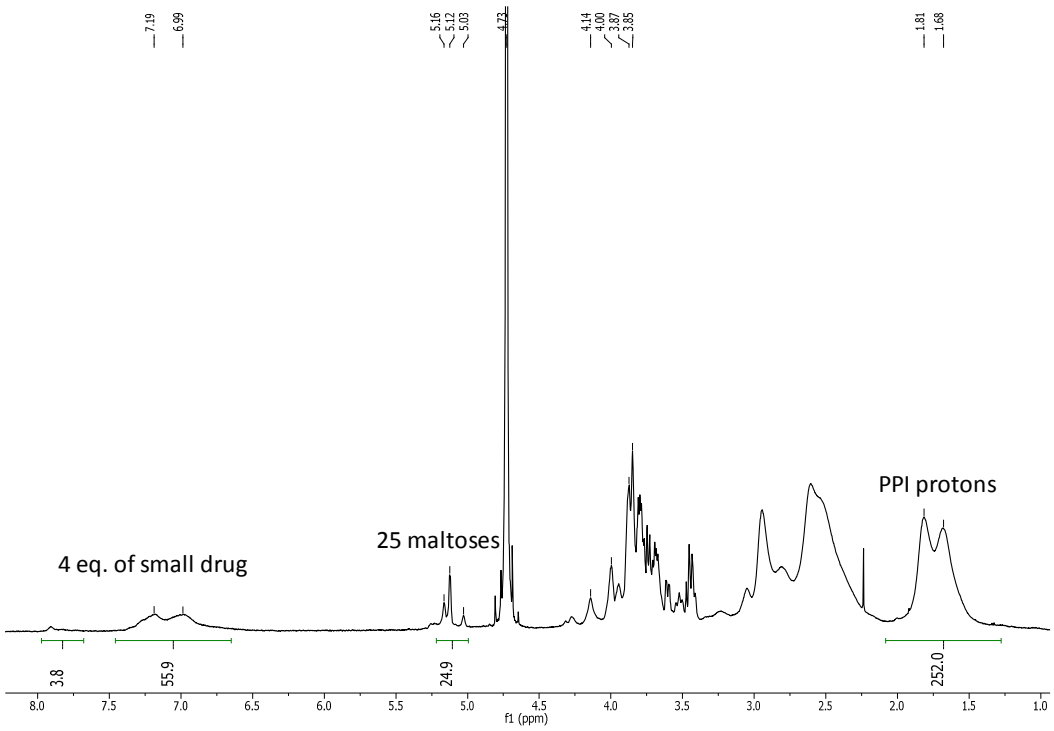


**Figure 4.14:** $^1$H NMR (500 MHz, $D_2O$) of the glycodendrimer **71** coupled with **55**.

### 4.3.4. Biological assays

As one of the reasons to synthesize the polymer-drugs macromolecules was to improve their solubility and availabity as apoptosis inhibitors, an *ex vivo* assay to test the activities of the final compounds **63**, **69** and **71** is in progress in the group of Prof. Enrique Pérez-Payá.

## 4.4. Conclusions

- Several proposed couplings between the active apoptosome inhibitors and the glycodendrimers were carried out. The best couplings were achieved with the amino group in the PPI spacers and a carboxylic terminal moiety in the small molecule, both dense-shell and open-shell as in compounds **63** and **69**.
- Moreover, the attachement directly to the surface of the PPI without spacer worked satisfactory and it was the one with higher amounts of attached drug.
- The β-lactam molecule worked in general better than the seven-membered ring derivative. A future proposal could be the coupling of the open-shell dendrimer **68** with the β-lactam product **55**.
- Results of the biological assays are in due course and they will shed additional light on the best glycodendrimer conjugate system for the apoptosome inhibition.

# 5. General Conclusions

- A strategy involving an Ugi multicomponent reaction has been developed to synthesize restricted analogues of the active compound **1**, using 1,4-, 2-4 and 1,5-disubstituted triazoles to mimic the exocyclic tertiary amide bond isomers. The synthesis of the analogues using 1,4- and 1,5-disubstituted triazoles (**2a** and **2b**) was successful.

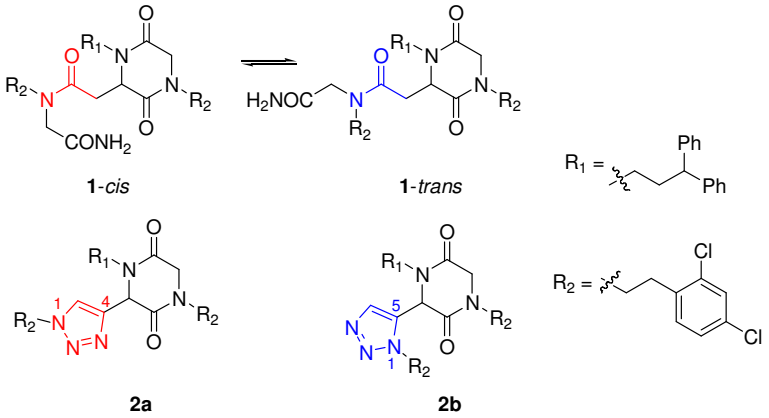


**1**-*cis* **1**-*trans* **2a** **2b**

- Unexpectedly, for the analog with the 2,4-disubstituted triazole, a new compound bearing a β-lactam structure (**19**) was characterized and showed to be the most potent inhibitor of the formation of the apoptosome.

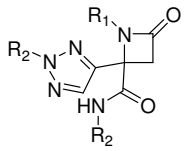

**19** IC50 = 3.93 μM

- Computational studies with compounds **1**, **2a**, **2b** and **19** have been carried out to validate the proposed mechanism that would account for their biological effects as apoptosis inhibitors.

- A variety of compounds bearing different substituents on the possible disubstituted 1,2,3-triazole isomers has been synthesized and the full NMR analysis (including $^{1}H$-$^{15}N$ correlations at natural abundance) of all compounds has led to the unambiguous characterization of the corresponding substitution patterns.

- The $^{1}H$-$^{15}N$ HMBC experiment has been shown to be an optimal technique to measure and distinguish $^{15}N$ chemical shifts of triazoles as well as unambiguously assign the correct isomer. This technique can be used as a routine experiment for isomer differentiation.

- A reactivity study has been carried out to better understand the intramolecular cyclization of the Ugi adducts and the modulation of the cyclization is now available. It has been shown that the acidity of the NH proceeding from the isocyanide is the key element to set the cyclization to form the diketopiperazine, the β-lactam scaffold or a mixture of both.

- A new family of compounds has been designed, synthesized and characterized, and most of them showed good apoptosis inhibitory activities *in vitro* and in cellular extracts. We deem that the reduction of the conformational freedom achieved in this new family of inhibitors could be fundamental to increase the selectivity, which is a highly important condition when regulating the apoptosis process.

- Several proposed couplings between the active apoptosis inhibitors and glycodendrimers were carried out in order to improve the properties of the drug candidates. The best couplings were achieved with the amino group in the PPI spacers and a carboxylic terminal moiety in the small molecule, both with dense- and open-shell compounds. (**63** and **69**). The direct attachement to the surface of the PPI without spacer worked well and it was the one with larger amounts of attached drug.

- A further study of the glycodendrimer-drug conjugates should be carried out exploring other type of couplings. Moreover, a deeper study to increase the solubility of the candidates should be considered.

# 6. Experimental Part

## 6.1. Materials and Methods

All reagents were obtained from commercial sources and used without further purification. The anhydrous solvents were obtained from PureSolv M (Solvent Purification System). Microwave-assisted reactions were performed in a CEM Discover microwave reactor. Analytical RP-HPLC was performed with a Hewlett Packard Series 110 (UV detector 1315A) modular system using a reverse-phase Kromasil 100 C8 (15 x 0.46 cm, 5 μm) column. $CH_3CN$-$H_2O$ Mixtures containing 0.1% TFA at 1 mL/min were used a mobile phase and monitoring wavelength was set at 220 nm. A gradient method from 20% to 100% $CH_3CN$ in 20 min. was used. Semi-preparative RP-HPLC was performed with a Waters (Milford, MA, U.S.A) system using a X-Terra C18 (19 x 259 mm, 5 μm) column and a Biotage Isolera One. High resolution mass spectra were performed with a LCT premier UPLC /MS Q-TOF (Waters) with an electrospray ionization detector. Some of the $^1$H-NMR spectra were recorded with a Varian Unity Inova 500 spectrometer with an indirect detection probe in $CDCl_3$ in δ units referred to TMS. $^1$H NMR, $^{13}$C NMR and $^{15}$N NMR were recorded with a VMRS 400 spectrometer with an OneNMRProbe in $CDCl_3$ with TMS as an internal standard of $^{13}$C and $MeNO_2$ for $^{15}$N.

The HPLC, HRMS and NMR data of all the synthesized compounds from which the characterization has been carried out is available in the Supporting Information.

**Computational Methods**. Molecular simulations were conducted with the package Schrödinger Suites 2011 and 2012[215], through its graphical interface Maestro. [216] The program Macromodel,[217] with its default force field OPLS 2005, a modified version of the OPLS-AA force field, [218] and GB/SA water solvation conditions[2-4,144, 219] were used for all energetic calculations in Chapter 1. The program Jaguar (version 7.8 Schördinger, LCC, N. Y. 2011) was used for the energetic calculations in Chapter 3. The coordinates of WD40-deleted human Apaf-1 (residues 1-591, PDB 1Z6T, chain B) were obtained from the Protein Data Bank[130] at Brookhaven National Laboratory. The structure of the protein was prepared using the Protein Preparation Wizard included in Maestro to remove the unused subunits as well as the solvent molecules and ligands, adding hydrogens, setting protonation states and minimizing the energy using the OPLS force field. SiteMap[143-145] was used to identify and score potential binding sites on the protein. The best scored sites were used as targets for docking with the program Glide XP.[2-4, 147] The structures of the compounds were built within Maestro and then they were prepared with the LigPrep application included in the software[220] to generate ring conformers of the two stereoisomers of each compound. In order to ensure a good conformational sampling during the docking simulations the following settings were used: a maximum of $5 \cdot 10^6$ poses per input structure for the initial phase of docking, the extended sampling protocol, and 50 poses for the post-docking minimization. Glide XP scores were used to rank the resulting docked poses. The interaction diagrams for the best poses were built with the Ligand Interaction Diagram application implemented in Maestro.

Induced Fit dockings were carried out with the workflow with the same name included in Maestro[146-150] This workflow included the following steps:

1 Initial Glide docking of each ligand using a softened potential (van der Waals radii scaling). A maximum of 20 poses per ligand were retained, and by default poses to be retained had a Coulomb-vdW score less than 100 and an H-bond score less than –0.05.
2 Prime side-chain refinement for each protein/ligand complex, on residues within a given distance of any ligand pose (default 5 Å).
3 Prime minimization of the same set of residues and the ligand for each protein/ligand complex pose.
4 Glide redocking of each protein/ligand complex structure within 30 kcal/mol of the lowest-energy structure using the extra-precission (XP) Glide settings.
5 Estimation of the binding energy (Glide XP and IFD scores) for each output pose.

## 6.2. Synthesis and characterization of compounds in Chapter 1

### 6.2.1. N-(2,4-Dichlorophenethyl)formamide (9)

A solution of 2,4-dichlorophenethylamine (2.5 g, 13.2 mmol) and formic acid (1 mL) was heated at 150ºC in a microwave oven for 20 min. After evaporation of the solvent the residue was poured into water and extracted with $CH_2Cl_2$. The combined organic layer was dried over $MgSO_4$ and evaporated in vacuum to give the target compound as pale yellow oil (1.9 g, 8.5 mmol, 65%, 3:1 *trans* / *cis* ratio in the formamide bond, 99% purity calculated by HPLC).

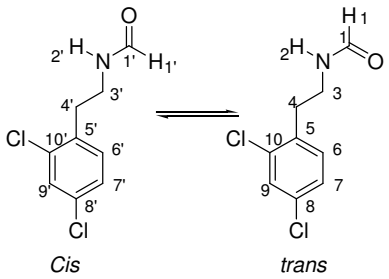


**$^1$H-NMR ($CDCl_3$, 500 MHz):** δ (ppm): 8.18 (s, 1H, H1), 7.92 (d, *J* = 12 Hz, 1H, H1'), 7.43 (d, *J* = 2 Hz, 1H, H9'), 7.41 (d, *J* = 2 Hz, 1H, H9), 7.26-7.11 (m, 4H, H6,6',7,7'), 5.84 (s, 1H, H2'), 5.63 (s, 1H, H2), 3.59 (q, *J* = 7 Hz, 2H, H3), 3.51 (q, *J* = 7 Hz, 2H, H3'), 2.98 (t, *J* = 7 Hz, 2H, H4), 2.95 (t, *J* = 7 Hz, 2H, H4') **$^{13}$C-NMR ($CDCl_3$, 100 MHz):** δ (ppm) 164.7 (C1'), 161.5 (C1), 134.9 (5, 5'), 133.9 (C10'), 133.4 (C10), 132.2 (C8'), 131.9 (C8), 129.9 (C6',9'), 129.7 (C6,9), 127.7 (C7'), 127.5 (C7), 41.4 (C3'), 37.8 (C3), 35.4 (C4'), 33.0 (C4) **HRMS for $C_9H_{10}Cl_2NO$:** Calculated: 218.0139 $(M+H)^+$; found: 218.0251.

### 6.2.2. 2,4-Dichlorophenethyl isocyanide (6)

2,4-Dichlorophenethylformamide **9** (1.21 g, 5.56 mmol) was dissolved in 4 mL of anhydrous $CH_2Cl_2$; then $NEt_3$ (1.97 mL, 14.9 mmol) was added and the solution was cooled at -60ºC. A solution of $POCl_3$ (570 µL, 6.1 mmol) in $CH_2Cl_2$ (2 mL) was added dropwise during 30 minutes under argon atmosphere and the resulting reaction mixture was stirred for 12 hours at room temperature. The mixture was poured into cold water (50 mL) and extracted with $CH_2Cl_2$ (2 x 50 mL). The organic layer was washed with sat. aq. $NaHCO_3$ (3 x 50 mL), dried over $MgSO_4$ and concentrated under reduced pressure to give crude the isocyanide **6** as a brown oil with 85% purity by HPLC. The product was used without further purification due to the observed instability during manipulation. The compound was not stable enough for registering a $^{13}$C NMR spectrum.

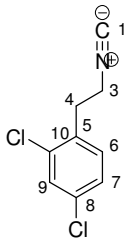

**$^1$H-NMR ($CDCl_3$, 500 MHz):** δ (ppm): 7.44 (s, 1H, H9), 7.27 (m, 2H, H6,7), 3.68 (t, *J* = 7 Hz, 2H, H4), 3.10 (t, *J* = 7 Hz, 2H, H3).

### 6.2.3. 2,4-dichlorophenethylazide (11)

To a solution of 2,4-dichlorophenethylbromide (1 g, 700 µL, 3.96 mmol) in 80 mL of anhydrous DMF, sodium azyde (525 mg, 7.9 mmol) was added and the mixture was stirred at 60ºC for 10h. The crude reaction mixture was diluted with EtOAc (50 mL) and washed with water (3 x 25 mL) and brine (3 x 25 mL). The organic layer was dried with $MgSO_4$ and concentrated under reduced pressure to give a yellow liquid (800 mg, 3.67 mmol, 93%, 97% purity calculated by HPLC).

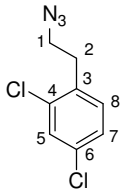


**$^1$H-NMR ($CDCl_3$, 500 MHz):** δ (ppm): 7.40 (d, *J* = 1.4 Hz, 1H, H5), 7.22 (m, 2H, H7,8), 3.52 (t, *J* = 7.1 Hz, 2H, H2), 3.00 (t, *J* = 7.1 Hz, 2H, H1) **$^{13}$CNMR ($CDCl_3$, 100 MHz):** δ (ppm) 134.4 (C3), 134.4 (C4), 133.6 (C6), 132.1 (C8), 129.7 (C5), 127.5 (C7), 50.6 (C1), 32.9 (C2).

### 6.2.4. Synthesis and characterization of 1,4-disubstituted-1,2,3-triazole derivatives

## 1-(2,4-Dichlorophenethyl)-4-hydroxymethyl-*1H*-1,2,3-triazole (12a)

To a solution of 200 mg (0.92 mmol) of 2,4-dichlorophenethyl azide (**11**) and 52 mg (0.92 mmol) of propargyl alcohol in 20 mL of THF, a solution of $CuSO_4$ (165 mg, 0.92 mmol), ascorbic acid (325 mg, 1.89 mmol) in 4 mL of water was added. The reaction was stirred under microwave activation during 2 min. at 100 ºC. The THF was evaporated under reduced pressure, the crude mixture was redissolved in $CH_2Cl_2$ (25 mL), washed with saturated $NaHCO_3$ (3 x 20 mL), dried with $MgSO_4$ and concentrated under reduced pressure to give 150 mg (0.54 mmol, 59%) of the desired product (92% purity by HPLC) as a yellow powder.

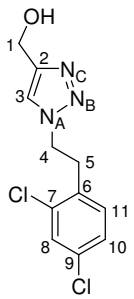


**$^1$H-NMR ($CDCl_3$, 500 MHz):** δ (ppm): 7.43 (d, *J* = 2.1 Hz, 1H, H8), 7.36 (s, 1H, H3) 7.16 (dd, *J* = 8.2, 2.1 Hz, 1H, H10), 6.97 (d, *J* = 8.2 Hz, 1H, H11), 4.79 (s, 2H, H1), 4.62 (t, *J* = 7.0 Hz, 2H, H4), 3.35 (t, *J* = 7.0 Hz, 2H, H5) **$^{13}$C-NMR ($CDCl_3$, 100 MHz):** δ (ppm): 147.9 (C2), 134.9 (C7), 134.1 (C9), 133.3 (C6), 132.14 (C11), 130.0 (C8), 127.9 (C10), 122.1 (C3), 57.1 (C1), 49.5 (C4), 34.4 (C5) **$^{15}$N-NMR ($CDCl_3$, 40.5 MHz):** δ (ppm): -134.8 ($N_A$), -31.5 ($N_C$), -18.3 ($N_B$) **HRMS for $C_{11}H_{11}Cl_2N_3O$:** Calculated: 272.0357 $(M+H)^+$; Found: 272.0368.

## 1-(2,4-Dichlorophenethyl)-4-formyl-*1H*-1,2,3-triazole (5a)

A solution of 1-(2,4-dichlorophenethyl)-4-hydroxymethyl-*1H*-1,2,3-triazole (**12a**) (150 mg, 0.54 mmol) and iodoxybenzoic acid (230 mg, 0.81 mmol) in EtOAc (5.3 mL) was stirred under reflux conditions for 4 hours. The mixture was cooled; the solid was filtered and washed with

EtOAc. The filtrate was washed with 5% $KHCO_3$ (3 x 20 mL) and brine (3 x 15 mL). Finally, the organic layer was dried with $MgSO_4$ and the EtOAc was eliminated under reduced pressure to give a pure pale yellow solid (140 mg, 0.51 mmol, 95% yield and 95% purity by HPLC).

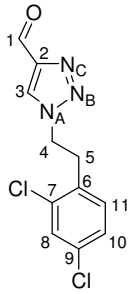

**$^1$H-NMR ($CDCl_3$, 500 MHz):** δ (ppm): 10.14 (s, 1H, H1), 7.89 (s, 1H, H3), 7.44 (d, *J* = 2.0 Hz, 1H, H8), 7.16 (dd, *J* = 8.2, 2.0 Hz, 1H, H10), 6.93 (d, *J* = 8.2 Hz, 1H, H11), 4.72 (t, *J* = 7.0 Hz, 2H, H4), 3.39 (t, *J* = 7.0 Hz, 2H, H5) **$^{13}$C-NMR ($CDCl_3$, 100 MHz):** δ (ppm): 185.2 (C1), 146.6 (C2), 134.8 (C7), 134.5 (C9), 132.6 (C6), 131.9 (C11), 130.0 (C8), 127.8 (C10), 125.7 (C3), 49.9 (C4), 34.17 (C5) **$^{15}$N-NMR ($CDCl_3$, 40.5 MHz):** δ (ppm): -130.9 ($N_A$), -18.9 ($N_C$), -12.8 ($N_B$) **HRMS for $C_{11}H_9Cl_2N_3O$:** Calculated: 270.0201 $(M+H)^+$; Found: 270.0209.

## *N*-(2,4-dichlorophenethyl)-2-[1-(2,4-dichlorophenethyl)-1*H*,1,2,3-triazol-4-yl]-3-(3,3-diphenylpropyl)aza-4-oxo-5-chloropentanoic acid amide (3a)

3,3-Diphenylpropanamine (32 µL, 0.17 mmol) was added to a solution of **5a** (46 mg, 0.17 mmol) in methanol (0.2 mL). The mixture was stirred during 6 hours at room temperature (NMR control for the formation of the corresponding imine); then, a solution of isocyanide **6** (35 mg, 0.17 mmol) in methanol (0.1 mL) and a solution of chloroacetic acid (15 mg, 0.17 mmol) in methanol (0.1 mL) were added and the reaction mixture was stirred during 24 hours at room temperature. Methanol was eliminated under reduced pressure. The crude reaction mixture was treated with a scavenger resin AM-$NH_2$ for 4 hours in DCM to eliminate the residual aldehyde **5a**. Once filtered, 75 mg (0.1 mmol, 58%) of the desired product were obtained with enough purity (92% by HPLC) for its characterization and for the next step.

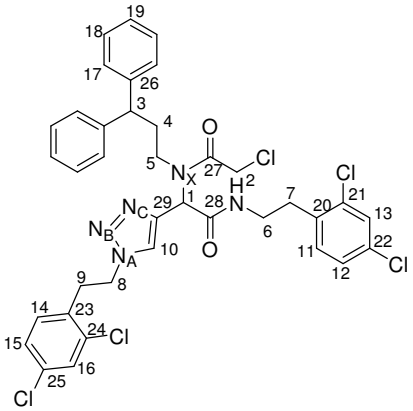

**$^1$H-NMR ($CDCl_3$, 500 MHz):** δ (ppm) 7.52 (s, 1H, H10), 7.36 (d, *J* = 1.8 Hz, 1H, H13), 7.32 (d, *J* = 1.6 Hz, 1H, H16), 7.21 (m, 4H, H18), 7.19 (m, 2H, H19), 7.17 (m, 4H, H17), 7.15 (m, 1H, H14), 7.14 (d, *J* = 1.5 Hz, 1H, H15) 7.03 (dd, *J* = 8.2, 1.8 Hz, 1H, H12), 6.87 (d, *J* = 8.2 Hz, 1H, H11), 6.48 (t, *J* = 5.6 Hz, 1H, NH), 5.41 (s, 1H, H1), 4.55 (t, *J* = 7 Hz, 2H, H8), 3.83 (t, *J* = 8.0 Hz, 1H, H3), 3.76 (q, *J* = 12.7 Hz, 2H, H2), 3.49 (m, 2H, H6), 3.27 (m, 4H, H5, H9), 2.9 (m, 2H, H7), 2.35 (m, 1H, H4), 2.18 (m, 1H, H4') **$^{13}$C-NMR ($CDCl_3$, 100 MHz):** δ (ppm) 167.4 (C28), 166.9 (C27), 143.1 (C26), 142.1 (C29), 134.8 (C20), 134.6 (C25), 134.3 (C23), 134.1 (C21), 132.7 (C24), 132.6 (C22), 131.8 (C11), 131.5 (C14), 129.5 (C13), 129.2 (C16), 127.4 (C12, C17), 127.2 (C15), 124.5 (C10), 57.6 (C1), 49.5 (C8), 48.5 (C3), 47.8 (C5), 40.7 (C2), 39.2 (C6), 34.7 (C4), 33.9 (C9), 32.5 (C7) **$^{15}$N-NMR ($CDCl_3$, 40.5 MHz):** δ (ppm): -274.7 (NH), -260.6 ($N_X$), -140.7 ($N_A$), -36.3 ($N_C$), -25.8 ($N_B$) **HRMS for $C_{37}H_{34}Cl_5N_5O_2$:** Calculated: 756.1233 $(M+H)^+$; Found: 756.1257.

## 1-(2,4-Dichlorophenethyl)-3-[1-(2,4-dichlorophenethyl)-*1H*,1,2,3-triazol-4-yl]-4-(3,3-diphenylpropyl)piperazine-2,5-dione (2a)

A solution of KOH (6 mg, 0.1 mmol) in 0.5 mL of methanol was added to the compound **3a** (75 mg, 0.1 mmol) and the mixture was stirred for 48 hours. Methanol was eliminated and the product was recristallyzed from ethanol to give 30 mg (0.04 mmol, 42%) of a pure pale yellow solid with 100% purity by HPLC.

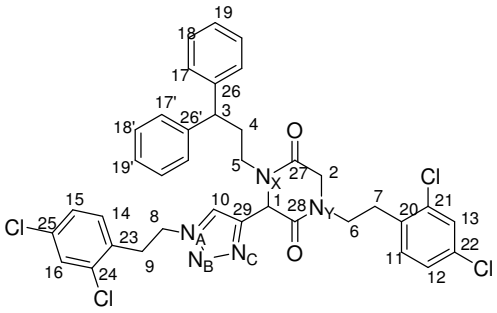

**$^{1}$H-NMR ($CDCl_3$, 500 MHz):** δ (ppm) 7.41 (d, *J* = 2.1 Hz, 1H, H16), 7.36 (s, 1H, H13), 7.33-7.18 (m, 10H, H17,18,19), 7.11 (m, 2H, H11,12), 7.08 (dd, *J* = 8.2, 2.1 Hz, 1H, H15), 6.97 (s, 1H, H10), 6.84 (d, *J* = 8.2 Hz, 1H, H14), 4.82 (s, 1H, H1), 4.54 (m, 2H, H8), 4.36 (d, *J* = 16.8 Hz, 1H, H2'), 3.90 (m, 3H, H3,5',6'), 3.75 (d, *J* = 16.8 Hz, 1H, H2), 3.40 (m, 1H, H6), 3.27 (t, *J* = 7.1 Hz, 2H, H9), 2.95 (m, 2H, H7), 2.57 (m, 1H, H5), 2.32 (m, 2H, H4) **$^{13}$C-NMR ($CDCl_3$, 100 MHz):** δ (ppm) 164.9 (C28), 164.1 (C27), 144.4 (C26), 143.8 (C26'), 143.0 (C29), 134.9 (C22), 134.8 (C25), 134.4 (C21), 134.2 (C24), 133.5 (C20), 133.0 (C23), 132.2 (C11), 132.0 (C14), 129.9 (C13), 129.6 (C16), 128.9 (C18), 127.9 (C17), 127.8 (C17'), 127.7 (C19), 127.5 (C19'), 126.7 (C12), 126.6 (C15), 123.0 (C10), 57.0 (C1), 51.0 (C2), 49.6 (C8), 49.2 (C3), 46.4 (C6), 43.8 (C5), 34.3 (C9), 32.9 (C4), 30.7 (C7) **$^{15}$N-NMR ($CDCl_3$, 40.5 MHz):** δ (ppm): -268.5 ($N_Y$), -258.3 ($N_X$), -133.8 ($N_A$), -30.3 ($N_C$), -14.9 ($N_B$) **HRMS for $C_{37}H_{33}Cl_4N_5O_2$:** Calculated: 720.1467 $(M+H)^+$; Found: 720.1559; Calculated: 742.1286 (M+Na)+; Found: 742.1277.

### 6.2.5. Synthesis and characterization of 1,5-disubstituted-1,2,3-triazoles derivatives

## 1-(2,4-Dichlorophenethyl)-5-hydroxymethyl-1*H*-1,2,3-triazole (12b)

A solution of propargyl alcohol (140 μL, 2.4 mmol) and **11** (260 mg, 1.2 mmol) in 5 mL of dioxane was added to a suspension of $Cp^*RuCl(PPh_3)_2$ (95 mg, 0.12 mmol) in 6 mL of dioxane. The round-bottom flask was purged with nitrogen, sealed, and heated at 60ºC for 12 hours under nitrogen atmosphere. The mixture was concentrated under reduced pressure to obtain a residue of 394 mg, which was purified by semipreparative HPLC (from 20% to 70% of ACN in $H_2O$ + 0.1%TFA in 40 min) to obtain 58 mg as a TFA salt. A solution of 1M NaOH (15 mL) was added to the product and extracted with DCM (2 x 15 mL), the organic layer was dried with $MgSO_4$ and the solvent was eliminated under reduced pressure to give 41 mg of **12b** (0.15 mmol, 13%, 82% purity by HPLC).

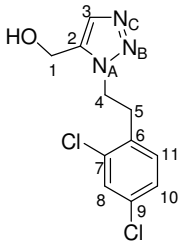

**$^{1}$H-NMR ($CDCl_3$, 500 MHz):** δ (ppm): 7.52 (s, 1H, H3), 7.41 (d, *J* = 2.0 Hz, 1H, H8), 7.12 (dd, *J* = 8.2, 2.0 Hz, 1H, H10), 6.95 (d, *J* = 8.2 Hz, 1H, H11), 4.65 (t, *J* = 7.2 Hz, 2H, H4), 4.54 (s, 2H, H1), 3.38 (t, *J* = 7.2 Hz, 2H, H5), 2.02 (s, 1H, OH) **$^{13}$C-NMR ($CDCl_3$, 100 MHz):** δ (ppm): 136.5 (C2), 134.9 (C9), 133.9 (C7), 133.7 (C6), 132.9 (C3), 132.2 (C11), 129,7 (C8), 127.6 (C10), 53.12 (C1), 47.6 (C4), 34.3 (C5) **$^{15}$N-NMR ($CDCl_3$, 40.5 MHz):** δ (ppm): -144.1 ($N_A$), -40.9 ($N_C$), -22.9 ($N_B$) **HRMS for $C_{11}H_{11}Cl_2N_3O$:** Calculated: 272.0357 $(M+H)^+$; Found: 272.0345.

## 1-(2,4-Dichlorophenethyl)-5-formyl-*1H*-1,2,3-triazole (5b)

Following the same method than for **5a**, 30 mg (0.11 mmol) of **12b** and 46 mg (0.17 mmol) of iodoxybenzoic acid in EtOAc (1.1 mL), afforded the desired aldehyde (37 mg, 0.1 mmol, quantitative, 82% purity).

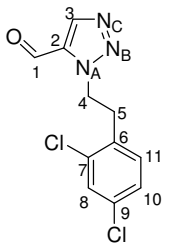

**$^{1}$H-NMR ($CDCl_3$, 500 MHz):** δ (ppm): 9.93 (s, 1H, H1), 8.23 (s, 1H, H3), 7.38 (d, *J* = 2.0 Hz, 1H, H8), 7.13 (dd, *J* = 8.2, 2.0 Hz, 1H, H10), 6.99 (d, *J* = 8.2 Hz, 1H, H11), 4.98 (t, *J* = 7.0 Hz, 2H, H4), 3.32 (t, *J* = 7.0 Hz, 2H, H5) **$^{13}$C-NMR ($CDCl_3$, 100 MHz):** δ (ppm): 178.4 (C1), 141.1 (C2), 135.2 (C7), 134.0 (C9), 133.9 (C3), 133.1 (C6), 131.9 (C11), 129.7 (C8), 127.8 (C10) **$^{15}$N-NMR ($CDCl_3$, 40.5 MHz):** δ (ppm): -142.4 ($N_A$), -38.6 ($N_C$), -9.3 ($N_B$) **HRMS for $C_{11}H_9Cl_2N_3O$:** Calculated: 270.0201 $(M+H)^+$; Found: 270.0270.

## *N*-(2,4-dichlorophenethyl)-2-[1-(2,4-dichlorophenethyl)-*1H*,1,2,3-triazol-5-yl] -3-(3,3-diphenylpropyl)aza-4-oxo-5-chloropentanoic acid amide (3b)

3,3-Diphenylpropanamine (27 μL, 0.14 mmol) was added to a solution of the aldehyde **5b** (40 mg, 0.14 mmol) in methanol (0.1 mL). The mixture was stirred until the completion of the imine formation (12 hours, NMR control). Then, a solution of isocyanide **6** (30 mg, 0.14 mmol) in 0.1 mL methanol and a solution of chloroacetic acid (15 mg, 0.14 mmol) in 0.1 mL methanol were added. The mixture was stirred for 48 hours at room temperature under nitrogen atmosphere. Although the conversion was not complete, methanol was then eliminated under reduced pressure and the mixture was purified by flash chromatography (20-34% EtOAC in hexane) to yield 28 mg (0.04 mmol, 26%) of product **3b** with 75% purity.

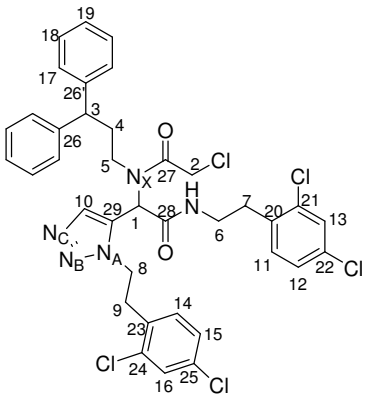

**$^{1}$H-NMR ($CDCl_3$, 500 MHz):** δ (ppm): 7.97 (s, 1H, H10), 7.38 (d, *J* = 2.0 Hz, 1H, H16), 7.35 (d, *J* = 2.0 Hz, 1H, H13), 7.25-7.18 (m, 6H, H18,19), 7.17 (dd, *J* = 8.2, 2.0 Hz, 1H, H12), 7.15-7.09 (m, 4H, H17), 7.11 (d, *J* = 8.2 Hz, 1H, H11), 7.04 (d, *J* = 8.5 Hz, 1H, H15), 6.89 (d, *J* = 8 Hz, 1H, H14), 5.83 (t, *J* = 6 Hz, 1H, NH), 5.68 (s, 1H, H1), 4.55 (m, 1H, H8), 4.22 (m, 1H, H8), 3.79 (s, 2H, H2), 3.64 (t, *J* = 8.0 Hz, 1H, H3), 3.54 (m, 1H, H6), 3.45 (m, 1H, H6), 3.37 (m, 1H, H9), 3.32 (m, 1H, H9), 3.08 (m, 1H, H5), 2.94 (m, 1H, H5), 2.91 (m, 2H, H7), 2.14 (m, 1H, H4), 1.46 (m, 1H, H4) **$^{13}$C-NMR ($CDCl_3$, 100 MHz):** δ (ppm): 168.2 (C27), 166.1 (C28), 142.7 (C26), 142.5 (C26'), 135.9 (C10), 135.0 (C24), 134.8 (C21), 134.4 (C20), 134.2 (C23), 133.9 (C25), 133.4 (C22), 132.3 (C14), 131.8 (C17), 130.4 (C29), 129.5 (C16), 129.5 (C13), 128.9 (C18), 127.6 (C11),127.5 (C15), 127.3 (C12), 127.0 (C19), 126.9 (C19), 50.5 (C1), 48.8 (C5), 47.4 (C8), 44.8 (C3), 40.6 (C2), 39.4 (C6), 35.5 (C4), 33.8 (C9), 32.7 (C7) **$^{15}$N-NMR ($CDCl_3$, 40.5 MHz):** δ (ppm): -265.8 (NH), -253.4 ($N_X$), -136.7 ($N_A$), -31.4 ($N_C$), -14.5 ($N_B$) **HRMS for $C_{37}H_{34}Cl_5N_5O_2$:** Calculated: 756.1233 $(M+H)^+$; Found: 756.1233.

## 1-(2,4-Dichlorophenethyl)-3-[3-(2,4-dichlorophenethyl)-3*H*-1,2,3-triazol-4-y1]-4-(3,3-diphenylpropyl)piperazine-2,5-dione (2b)

NaH (1 mg, 0.03 mmol) was added under nitrogen conditions to a solution of 25 mg (0.03 mmol) of **3b** in THF and the mixture was stirred for 1 hour at room temperature. The reaction mixture was purified by preparative TLC hexane / EtOAC (3 / 2) to yield 4.5 mg (0.006 mmol, 20%) of a white solid that was identified as **2b** with 70% purity. There was not enough sample for acquiring the $^{13}C$ NMR.

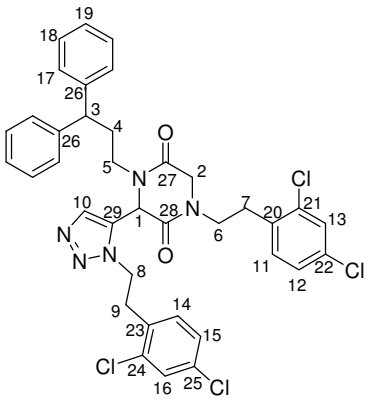

**$^1$H-NMR ($CDCl_3$, 500MHz):** δ (ppm): 7.45 (d, *J* = 2 Hz, 1H, H16), 7.31 (d, *J* = 2 Hz, 1H, H13), 7.30-7.14 (m, 10H, H17,18,19), 6.99 (d, *J* = 8.2 Hz, 1H, H), 6.75 (d, *J* = 8.3 Hz, 1H, H14), 4.63 (m, 1H, H1), 4.86 (m, 1H, H8), 4.49 (m, 1H, H8), 3.85 (d, *J* = 17.5 Hz, 1H, H2), 3.64 (d, *J* = 17.5 Hz, 1H, H2), 3.49 (m, 1H, H6), 3.38 (t, *J* = 7.3 Hz, 1H, H3), 3.26 (m, 2H, H6,5), 3.15 (m, 1H, H9), 2.87 (m, 3H, H7,9), 2.30 (m, 1H, H5), 2.24 (m, 2H, H4) **HRMS for $C_{37}H_{33}Cl_4N_5O_2$:** Calculated: 720.1467 $(M+H)^+$; Found: 720.1474.

### 6.2.6. 4-Hydroxymethyl-1*H*-1,2,3-triazole (14)[127]

A mixture of 37% $HCHO_{aq}$ (735 μL, 9.8 mmol), glacial AcOH (85 μL, 1.47 mmol), and 1,4-dioxane (740 μL) was stirred for 15 min at room temperature. Then $NaN_3$ (95 mg, 1.47 mmol) was added to the reaction mixture, followed by propargyl alcohol (60 μL, 0.98 mmol). At this point the pH of the reaction mixture was 6.5. After an additional 10 min of stirring, sodium ascorbate (35 mg, 0.196 mmol, 20mol %) was added, followed by a $CuSO_4$ solution (10 mg, 0.049 mmol, 5mol %) in 40 μL of $H_2O$. The final mixture was stirred for 18 h at room temperature, then diluted with $H_2O$ (3 mL) and washed using DCM (3 x 10 mL). The aqueous layer was concentrated under vacuum and the residue was treated without further purification with 20 mL of 2M NaOH, and the solution was stirred for 20 hours at room temperature. Then the crude reaction mixture was neutralized with 2M HCl and concentrated under vacuum to give a blue solid residue, which was extracted with methanol. 1.63 g of residue with 12% (202 mg, 2mmol) of the desired triazole were obtained after solvent evaporation used without further purification.

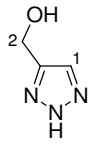

**$^1$H-NMR ($D_2O$, 500 MHz):** δ (ppm): 7.74 (s, 1H, H1), 4.71 (s, 2H, H2).

### 6.2.7. Synthesis and characterization of 2,4-disubstituted-1,2,3-triazoles derivatives

## 2-(2,4-Dichlorophenethyl)-4-hydroxymethyl-1*H*-1,2,3-triazole (12c)

Anhydrous DMF (10 mL) was added to the residue containing the triazole **14** (202 mg prod, 2 mmol, in 1.63 g crude) and the mixture was heated at 60ºC. Then, a solution of *p*-(2,4-dichlorophenethyl) tosylate (865 mg, 2.5 mmol) in anhydrous acetonitrile (10 mL) was added, $Cs_2CO_3$ was also added and the mixture was stirred for 24 hours at 60ºC. The crude reaction mixture was diluted with EtOAc and the solution was washed with water (2 x 15 mL) and brine (2 x 15 mL). The residue obtained after solvent elimination (337 mg) was a mixture of the desired product with the 1,5-disubstituted triazole, the 1,4-disubstituted triazole, the starting tosylate, the product of the elimination and the chloride. This crude was purified by chromatography column eluting with 7:3 hexane:EtOAc to yield 112 mg (0.413 mmol, 21% calculated from the propargyl alcohol) of the desired product **12c** with 97% purity.

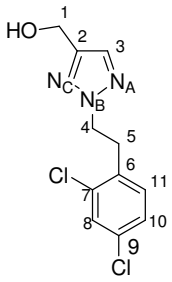


**$^1$H-NMR ($CDCl_3$, 500 MHz):** δ (ppm): 7.56 (s, 1H, H3), 7.40 (d, *J* = 2.0 Hz, 1H, H8), 7.12 (dd, *J* = 8.2, 2.0 Hz, 1H, H10), 6.99 (d, *J* = 8.2 Hz, 1H, H11), 4.75 (s, 2H, H1), 4.65 (t, *J* = 7.3 Hz, 2H, H4), 3.36 (t, *J* = 7.3 Hz, 2H, H5), 2.2 (s, 1H, OH) **$^{13}$C-NMR ($CDCl_3$, 100 MHz)**: δ (ppm): 147.8 (C2), 134.7 (C7), 133.9 (C6), 133.7 (C9), 132.5 (C3), 131.6 (C11), 129.7 (C8), 127.5 (C10), 56.6 (C1), 54.0 (C4), 33.8 (C5) **$^{15}$N-NMR ($CDCl_3$, 40.5 M Hz):** δ (ppm): -50.1 ($N_A$), -126.7 ($N_B$), -55.9 ($N_C$) **HRMS for $C_{11}H_{11}Cl_2N_3O$:** Calculated: 272.0357 $(M+H)^+$; found: 272.0350: Calculated: 295.0255 $(M+NaH)^+$; found: 295.0514.

## 2-(2,4-Dichlorophenethyl)-4-formyl-1*H*-1,2,3-triazole (5c)

Following the same procedure than in **5a** and **5b**, from 2-(2,4-dichlorophenethyl)-4-hydroxymethyl-1*H*-1,2,3-triazole (**12c**) (115 mg, 0.4 mmol) and iodoxybenzoic acid (175 mg, 0.6 mmol) in EtOAc (4 mL) the desired aldehyde as a pale yellow solid (95 mg, 0.35 mmol, 85%) was obtained with 98% purity.

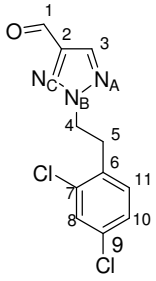


**$^1$H-NMR ($CDCl_3$, 500 MHz):** δ (ppm): 10.09 (s, 1H, H1), 8.07 (s, 1H, H3), 7.43 (d, *J* = 2.0 Hz, 1H, H8), 7.14 (dd, *J* = 8.2, 2.0 Hz, 1H, H10), 6.98 (d, *J* = 8.2 Hz, 1H, H11), 4.78 (t, *J* = 7.2 Hz, 2H, H4), 3.44 (t, *J* = 7.2 Hz, 2H, H5) **$^{13}$C-NMR ($CDCl_3$, 100 MHz):** δ (ppm): 184.3 (C1), 146.9 (C2), 135.1 (C3), 134.6 (C7), 133.6 (C9), 132.8 (C6), 131.4 (C11), 129.7 (C8), 127.4 (C10), 54.88 (C4), 33.58 (C5) **$^{15}$N-NMR ($CDCl_3$, 40.5MHz):** δ (ppm): -41.42 ($N_C$), -47.40 ($N_A$), -118.97 ($N_B$) **HRMS for $C_{11}H_9Cl_2N_3O$:** Calculated: 270.0201 $(M+H)^+$; found: 270.0255.

## *N*-(2,4-dichlorophenethyl)-2-[2-(2,4-dichlorophenethyl)-*1H*,1,2,3-triazol-4-yl]-3-(3,3-diphenylpropyl)aza-4-oxo-5-chloropentanoic acid amide (3c)

3,3-Diphenylpropanamine (65 µL, 0.14 mmol) was added to a solution of 2-(2,4-dichlorophenethyl)-4-formyl-1H-1,2,3-triazole (**5c**) (95 mg, 0.35 mmol) in methanol (0.1 mL). The mixture was stirred for 6 hours at room temperature (NMR monitoring for the imine

formation). Then, a solution of 2,4-dichlorophenethyl isocyanide (**6**) (70 mg, 0.35 mmol) in 0.1 mL methanol and a solution of chloroacetic acid (35 mg, 0.35 mmol) in 0.1 mL of methanol were added and the mixture was stirred for 48 hours at room temperature under nitrogen atmosphere. The solvent was eliminated under reduced pressure and the crude product **3c** (87% purity by HPLC) was used without further purification.

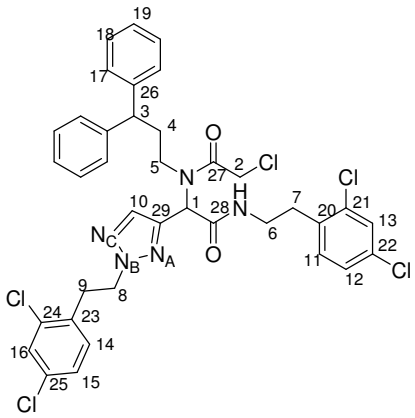

**$^{1}$H-NMR ($CDCl_3$, 500 MHz):** δ (ppm): 7.72 (s, 1H, H10), 7.39 (d, *J* = 2 Hz, 1H, H13), 7.35 (d, *J* = 2 Hz, H16), 7.32 (m, 1H, H11), 7.29 (m, 2H, H19), 7.22-7.18 (m, 5H, H18, H12), 7.18-7.14 (m, 4H, H17), 7.03 (dd, *J* = 8.2, 2.0 Hz, 1H, H15), 6.86 (d, *J* = 8.2 Hz, 1H, H14), 6.34 (t, *J* = 5.7 Hz, 1H, NH), 5.39 (s, 1H, H1), 4.58 (t, *J* = 7.2 Hz, 2H, H8), 3.8 (m, 1H, H3), 3.77 (q, *J* = 12.8 Hz, 2H, H2), 3.48 (m, 2H, H6), 3.29 (m, 2H, H5), 3.26 (t, *J* =7.2 Hz, 2H, H9), 2.89 (m, 2H, H7), 2.35 (m, 1H, H4), 2.11 (m, 1H, H4) **$^{13}$C-NMR ($CDCl_3$, 100 MHz):** δ (ppm) 167.2 (C27), 165.1 (C28), 143.1 (C26), 142.4 (C29), 134.8 (C25), 134.7 (C10), 133.5 (C24), 133.4 (C20), 131.8 (C21), 131.7 (C11), 131.4 (C14), 131.5 (C23), 129.5 (C13), 129.3 (C16), 128.8 (C22), 128.5-126.4 (C12,17,18,19), 127.14 (C15), 57.1 (C1), 53.8 (C8), 48.3 (C3), 47.3 (C5), 40.8 (C2), 34.7 (C4), 33.2 (C9), 32.6 (C7) **$^{15}$N-NMR ($CDCl_3$, 40.5 MHz):** δ (ppm): -261.9 (NH), -125.3 ($N_B$), -52.4 ($N_A$), -48.9 ($N_C$) **HRMS for $C_{37}H_{35}Cl_5N_5O_2$:** Calculated: 756.1233 $(M+H)^+$; found: 756.1238; Calculated: 778.1053 $(M+Na)^+$; found: 778.1058.

### 6.2.8. *N*-(2,4-Dichlorophenethyl)-2-(2-(2,4-dichlorophenethyl)-2*H*-1,2,3-triazol-4-yl)-1-(3,3-diphenylpropyl)-4-oxoazetidine-2-carboxamide (19)

A solution of KOH (20 mg, 0.35 mmol) in 2 mL of methanol was added to the Ugi product **3c** and the mixture was stirred for 12 hours at room temperature. After the elimination of solvent, the new residue was purified by column chromatography eluting with EtOAc:hexane to give 50 mg (0.07 mmol, 19% calculated from **5c**) of a white powder with 99% purity.

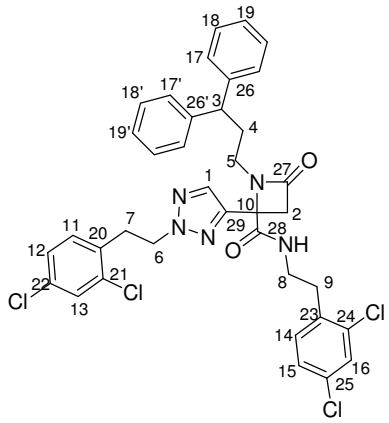

**$^{1}$H-NMR ($CDCl_3$, 500 MHz):** δ (ppm) 7.54 (s, 1H, H1), 7.38 ( d, *J* = 2.1 Hz, 1H, H13), 7.36 (d, *J* = 2.1 Hz, 1H, H16), 7.29-7.26 (m, 4H, H18,18'), 7.20-7.16 (m, 6H, H17,17',19,19'), 7.13 (dd, *J* = 8.2, 2.1 Hz, 1H, H15), 7.08 (dd, *J* = 8.2, 2.1 Hz, 1H, H12), 7.06 (d, *J* = 8.4 Hz, 1H, H14), 6.89 (d, *J* = 8.2 Hz, 1H, H11), 6.51 (t, *J* = 5.9 Hz, 1H, NH), 4.59 (t, *J* = 7.1 Hz, 2H, H6), 3.90 (t, *J* = 7.7 Hz, 1H, H3), 3.54 (m, 2H, H8), 3.34 (d, *J* = 14.4 Hz, 1H, H2), 3.27 (t, *J* = 7.1 Hz, 2H, H7), 3.27 (d, *J* = 14.4 Hz, 1H, H2), 3.07 (m, 2H, H5), 2.90 (m, 2H, H9), 2.42 (m, 1H, H4), 2.29 (m, 1H, H4) **$^{13}$C-NMR ($CDCl_3$, 100 MHz):** δ (ppm) 169.1 (C28), 166.8 (C27), 145 (C29), 143.9 (C26,C26'), 135.0 (C23), 134.9 (C20), 133.9 (C21 i 22 ), 133.6 (C1), 133.54 (C24), 133.47 (C25), 131.9 (C14), 131.7 (C11), 129.74 (C13), 129.66 (C16), 128.9 (C18), 128.8 (C18), 127.9 (C17), 127.9 (C17'), 127.5 (C15), 127.47 (C12), 126.72 (C19), 126.68 (C19'), 58.9 (C10), 54.4 (C6), 50.7 (C2), 49.1 (C3), 41.9 (C5), 39.6 (C8), 33.6 (C7), 33.4 (C4 ), 32.7 (C9) **$^{15}$N-NMR ($CDCl_3$, 40.5 MHz):** δ (ppm): -269.2 (NH), -229.4 ($N_X$), -124.2 ($N_B$), -55.9 ($N_A$), -48.6 ($N_C$) **HRMS for $C_{37}H_{34}Cl_4N_5O_2$:** Calculated: 720.1467 $(M+H)^+$; found: 720.1453.

## 6.3. Computational Methods: Docking results of 1, 2a, 2b, 19

**Figure 6.1**. Best docked poses (left) and interaction diagrams (right) obtained for compounds (***R***)-**1**, (***S***)-**1**, (***R***)-**2a**, (***S***)-**2a**, (***R***)-**2b**, (***S***)-**2b**, (***R***)-**19** and (***S***)-**19** bound at the CARD (green ribbons) – NOD (light grey ribbons) interface (Site 1). The interaction diagrams show the Apaf-1 residues with atoms which are at less than 4 Å from the ligands.

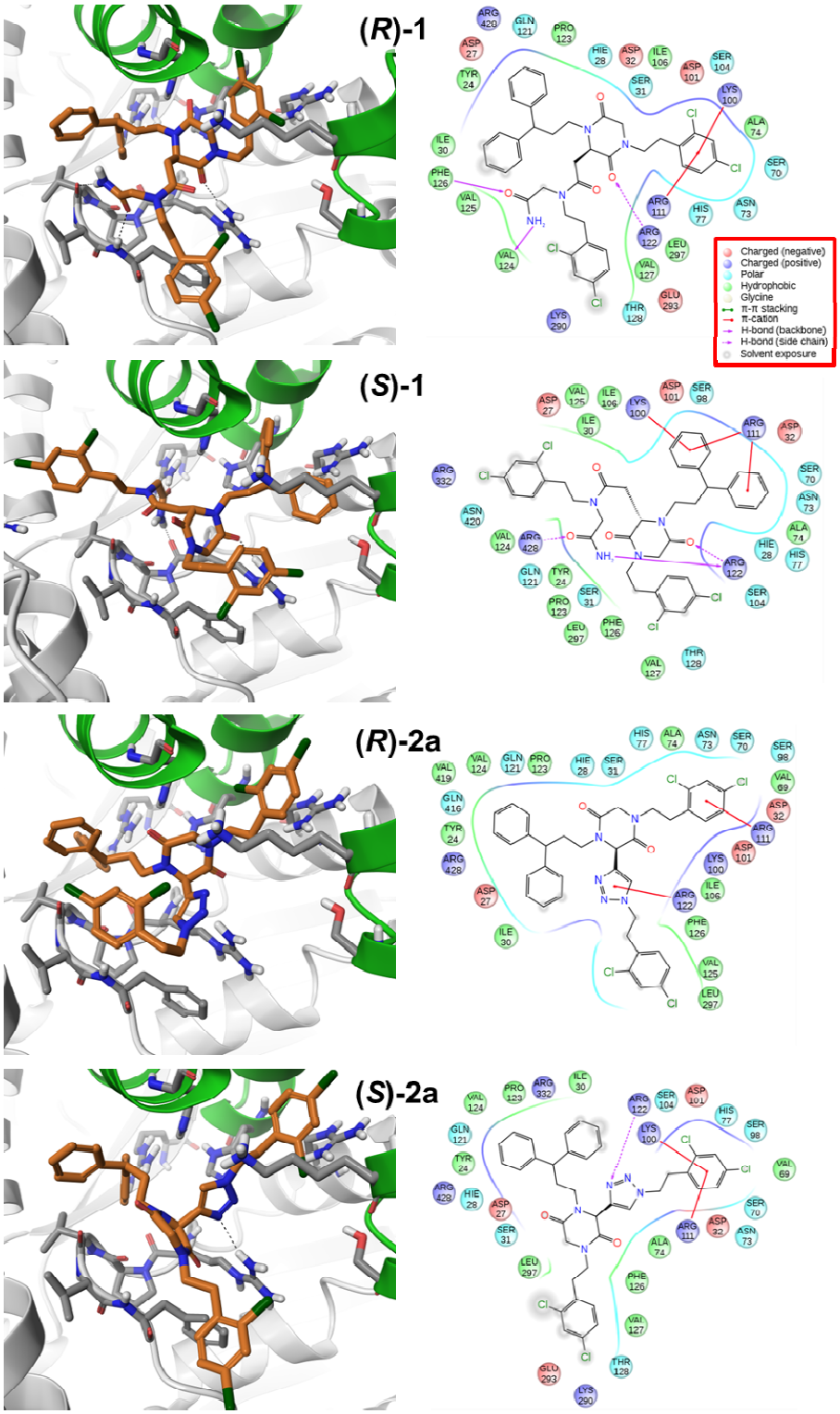

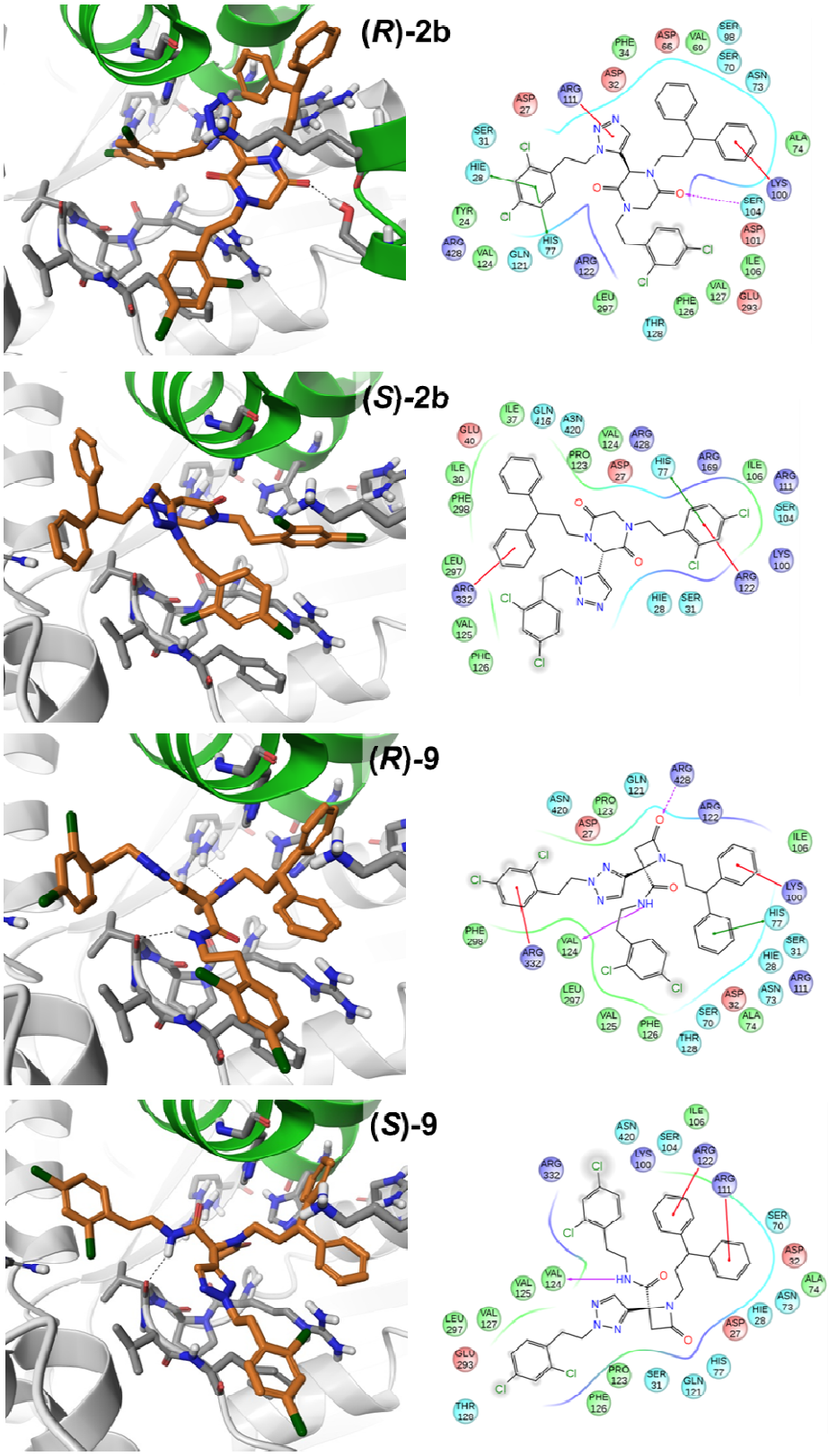
(R)-2b
(S)-2b
(R)-9
(S)-9

**Figure 6.2**. Best docked poses (left) and interaction diagrams (right) obtained for compounds (***R***)-**1**, (***S***)-**1**, (***R***)-**2a**, (***S***)-**2a**, (***R***)-**2b**, (***S***)-**2b**, (***R***)-**19** and (***S***)-**19** bound into the ADP binding site (Site 2). The interaction diagrams show the Apaf-1 residues with atoms which are at less than 4 Å from the ligands.

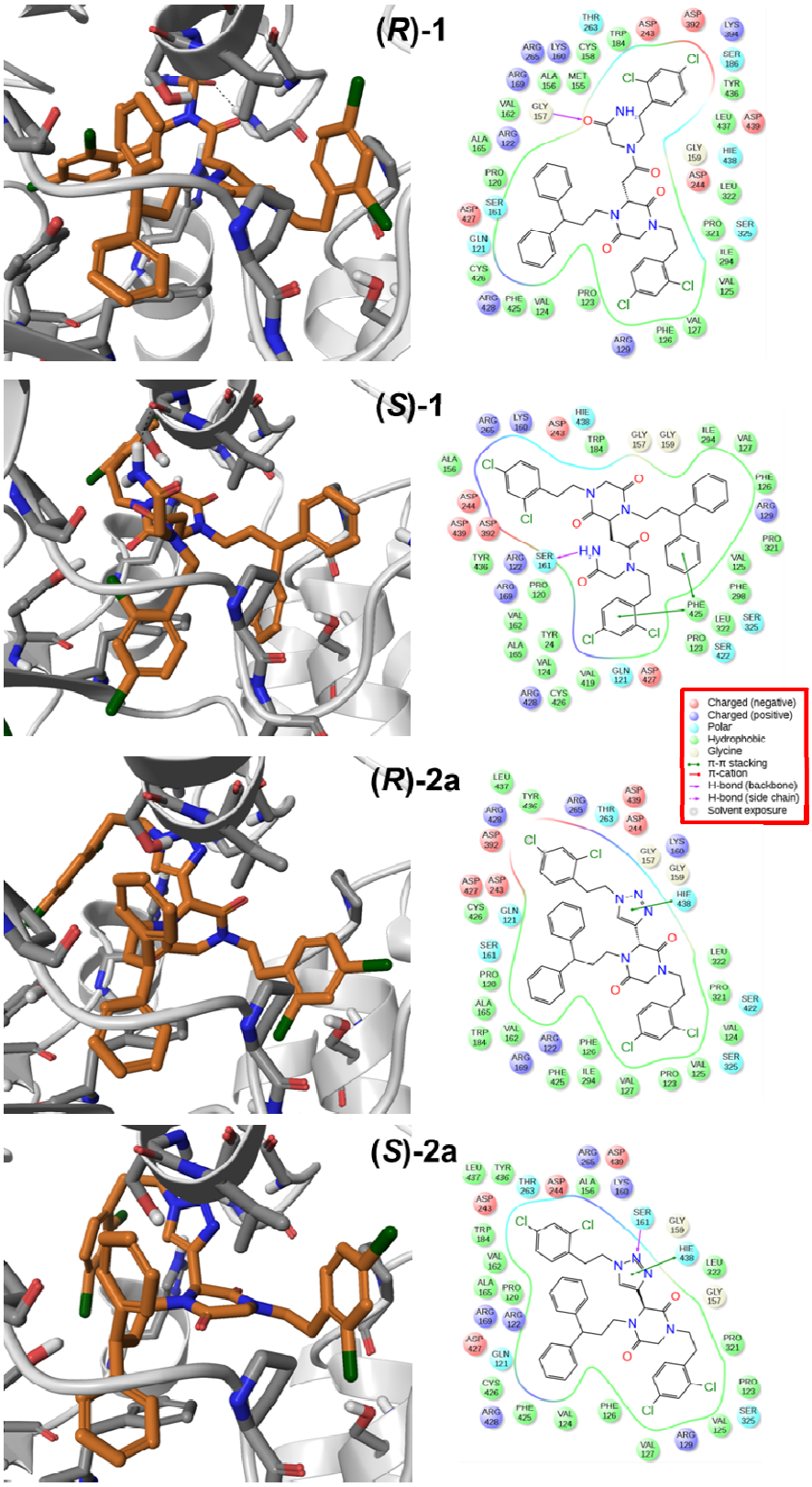

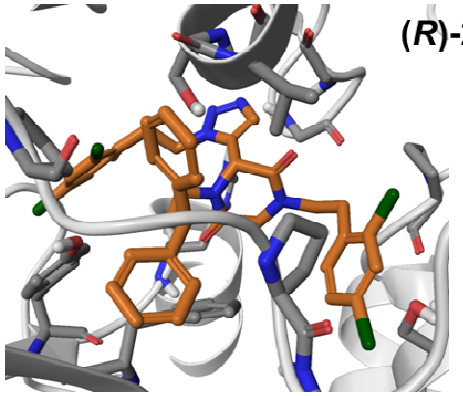

(*R*)-2b

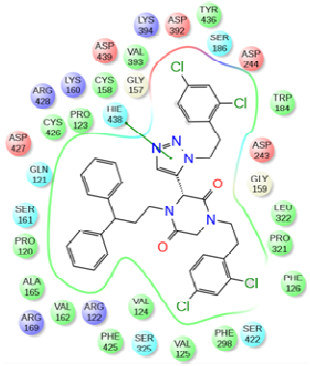

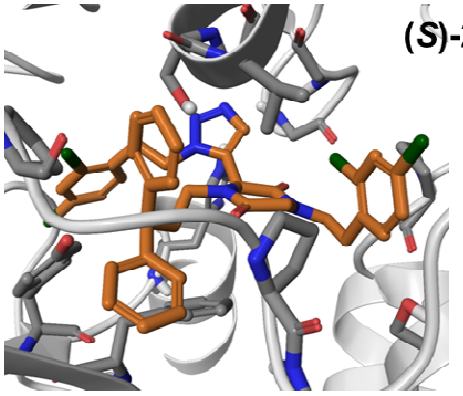

(*S*)-2b

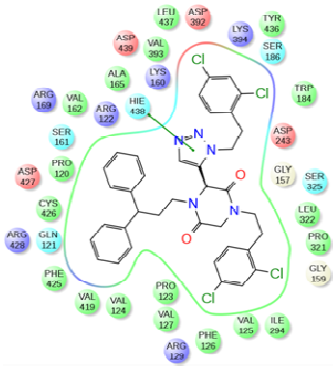

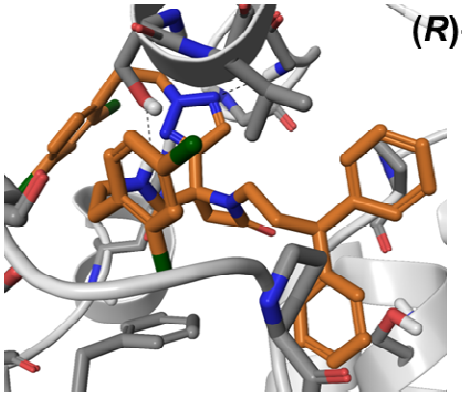

(*R*)-9

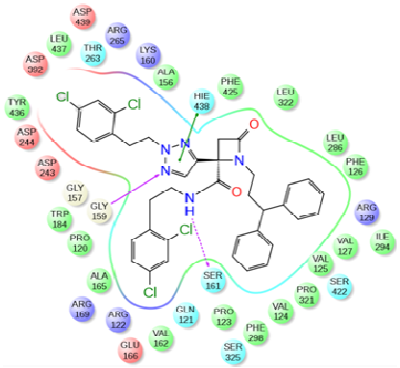

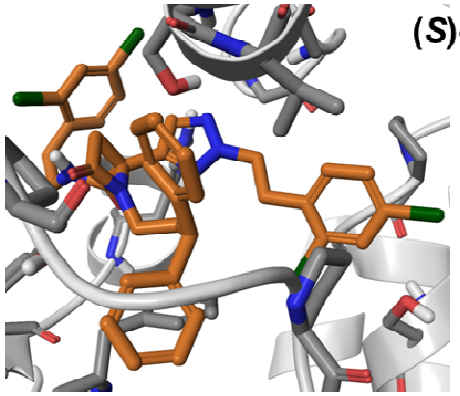

(*S*)-9

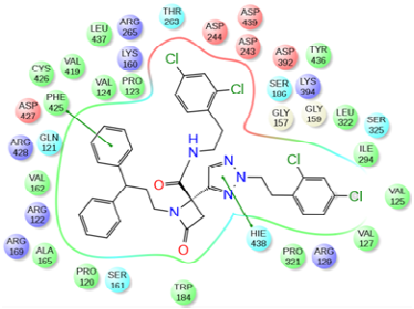

## 6.4. Biological assays of compounds 1, 2a, 2b, 19

**Apoptosome reconstitution assay**

Recombinant Apaf-1 (rApaf-1) produced in insect cells (100 nM) was incubated in the presence or absence of test compounds in assay buffer (20 mM Hepes-KOH pH 7.5, 10 mM KCl, 1.5 mM $MgCl_2$, 1 mM EDTA, 1 mM EGTA, 1 mM DTT, 0.1 mM PMSF) for 15 min at 30 oC. Then dATP/Mg (100 µM) and purified horse cytochrome *c* (100 nM) were added. The mixture was incubated for 60 min at 30 ºC and then E. coli produced recombinant procaspase-9 (100 nM) was added. Incubation was prolonged for 10 min at the same temperature before the addition of the caspase-9 fluorogenic substrate Ac-LEDH-afc (50 µM). The caspase activity was measured continuosly by the release of afc in a Wallac 1420 Workstation ($\lambda_{exc}$ = 390 nm; $\lambda_{em}$ = 510 nm).

**HEK293 cell-free caspase activation assay**

Apoptosome reconstitution in cellular extracts was carried out using cytosolic extracts (S100) of HEK 293 cells depleted of Apaf-1. To this aim, cytosolic extracts from 2 x 108 cells were fractionated by ionic exchange chromatography in a MonoQ FPLC column (Amersham Pharmacia Biotech). Flow through fraction (FT) contained caspase-3, caspase-9 and cytochrome c; thus, the addition of rApaf-1 and dATP makes possible the apoptosome reconstitution. Test compounds were preincubated in 100 µL for 30 min at 30 ºC in the presence of rApaf-1 (100 nM). The cytosolic extract (0.1 mg/ml) and dATP (100 µM) were then added. The mixture was incubated for 30 min at 37 ºC, and caspase activity was measured continuosly by the release of afc from the caspase-3 fluorogenic substrate (afc-DEVD; 20 µM). in a Wallac 1420 Workstation ($\lambda_{exc}$ = 390 nm;$\lambda_{em}$ = 510 nm).

| Compound | IC50 /µM | SD |
|---|---|---|
| **In vitro assays** | | |
| **1** | 12.41 | 1.06 |
| **2a** | 9.72 | 1.11 |
| **2b** | 6.13 | 1.18 |
| **19** | 3.94 | 1.20 |
| **Cellular extracts** | | |
| **1** | 3.49 | 1.36 |
| **2a** | 0.98 | 1.49 |
| **2b** | 0.34 | 2.24 |
| **19** | 0.22 | 4.32 |

## 6.5. Synthesis and characterization of compounds in Chapter 2

### 6.5.1. Synthesis and characterization of azides

### Benzyl azide (21)[221]

To a solution of benzylbromide (210 µL, 1.8 mmol) in 35 mL of anhydrous DMF, sodium azyde (230 mg, 3.5 mmol) was added and the mixture was stirred at 60ºC for 10 h. The crude reaction mixture was diluted with EtOAc (50 mL) and washed with water (3 x 25 mL) and brine (3 x 25 mL). The organic layer was dried over $MgSO_4$ and concentrated under reduced pressure to give a yellow liquid (170 mg, 1.3 mmol, 73%).

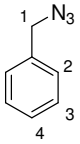


**$^1$H-NMR ($CDCl_3$, 500 MHz):** δ (ppm): 7.40-7.25 (m, 5H, H2,3,4), 4.37 (s, 2H, H1).

### *P*-Fluorophenethyl azide (22)

Following the above procedure, from a solution of *p*-fluorophenethyl bromide (1 g, 690 µL, 4.9 mmol) in 98 mL of anhydrous DMF and sodium azyde (650 mg, 9.8 mmol) the desired product was achieved as a yellow liquid (651 mg, 3.9 mmol, 80%, 99% purity).

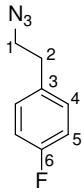


**$^1$H-NMR ($CDCl_3$, 500 MHz):** δ (ppm): 7.18 (dd, *J* = 8.7, 5.4 Hz, 2H, H4), 7.01 (t, 2H, H5), 3.49 (t, *J* = 7.1 Hz, 2H, H2), 2.86 (t, *J* = 7.1 Hz, 2H, H1) **$^{13}$C-NMR ($CDCl_3$, 100 MHz):** δ (ppm) 163.0 (C6), 133.6 (C3), 130.2 (C4), 115.6 (C5), 52.5 (C1), 34.5 (C2).

### 6.5.2. Synthesis and characterization of 1,4-disubstituted-1,2,3-triazole derivatives

### 1-Benzyl-4-hydroxymethyl-1*H*-1,2,3-triazole (23a)

To a solution of 65 mg (0.50 mmol) of azide **21** and 30 µL (0.50 mmol) of propargyl alcohol in 11 mL of THF, a solution of CuSO4 (95 mg, 0.5 mmol), ascorbic acid (175 mg, 1 mmol) in 2 mL of water was added. The reaction was stirred under microwave activation during 2 min. at 100ºC. The THF was evaporated under reduced pressure, the crude mixture was redisolved in DCM (10 mL), washed with saturated $NaHCO_3$ (3 x 10 mL), dried with $MgSO_4$ and concentrated under reduced pressure to give 48 mg (0.23 mmol, 50%) of **23a** with 93% purity by HPLC.

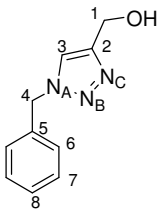

**$^1$H-NMR: ($CDCl_3$, 500 MHz):** δ (ppm): 7.46 (s, 1H, H3), 7.39-7.37 (m, 3H, H7, H8), 7.29-7.27 (m, 2H, H6), 5.53 (s, 2H, H4), 4.79 (s, 2H, H1) **$^{13}$C-NMR: ($CDCl_3$, 100 MHz):** δ (ppm):147.7 (C2), 134.2 (C5), 129.2 (C7), 128.9 (C8), 128.2 (C6), 121.8 (C3), 56.6 (C1), 54.4 (C4) **$^{15}$N-NMR ($CDCl_3$, 40.5 MHz):** δ (ppm) -133.7 ($N_A$), -37.2 ($N_C$), -19.4 ($N_B$) **HRMS for $C_{10}H_{11}N_3O$:** Calculated: 190.098 $(M+H)^+$; Found: 190.099.

## 1-*p*-Fluorophenethyl-4-hydroxymethyl-1*H*-1,2,3-triazole (24a)

Following the above procedure, from 200 mg (1.2 mmol) of azide **22**, 70 µL (1.2 mmol) of propargyl alcohol, $CuSO_4$ (215 mg, 1.2 mmol), ascorbic acid (425 mg, 2.4 mmol) in water (5 mL) and THF (20 mL). The solvent was evaporated and 30 mL of DCM were added and washed with $NaHCO_3$ (3 x 25 mL) and $NH_3$ aqueous sol. 30% (3 x 25 mL). After evaporating the organic phase, 60 mg (0.27 mmol, 25%) of **24a** with 100% purity were obtained.

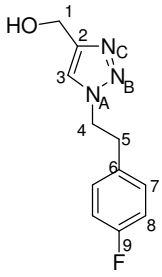

**$^1$H-NMR : ($CDCl_3$, 500 MHz):** δ (ppm): 7.34 (s, 1H, H3), 7.06 (dd, *J* = 8.7, 5.4 Hz, 2H, H7), 6.98 (t, *J* = 8.7 Hz, 2H, H8), 4.77 (s, 2H, H1), 4.57 (t, *J* = 7.2 Hz, 2H, H4), 3.2 (t, *J* = 7.2 Hz, 2H, H5) **$^{13}$C-NMR: ($CDCl_3$, 100 MHz):** δ (ppm): 161.9 (d, *J* = 244 Hz, C9), 147.5 (C2), 132.5 (C6), 130.1 (C7), 122.2 (C3), 115.6 (d, *J* = 21 Hz, C8), 56.6 (C1), 51.7 (C4), 35.8 (C5) ) **$^{15}$N-NMR ($CDCl_3$, 40.5 MHz):** δ (ppm): -134.4 ($N_A$), -36.1 ($N_C$), -19.9 ($N_B$) **HRMS for $C_{11}H_{12}N_3OF$:** Calculated: 221.1043 $(M+H)^+$; Found: 221.1030.

## 1-(*2,4*-Dichlorophenethyl)-4-phenyl-1*H*-1,2,3-triazole (27)

Following the above procedure, from 150 mg (0.7 mmol) of azide **11**, 75 µL (0.7 mmol) of phenylacetylene, $CuSO_4$ (125 mg, 0.7 mmol), ascorbic acid (245 mg, 1.4 mmol) in water (3 mL) and THF (15 mL). The reaction afforded, after reverse phase chromatographic purification, 137 mg (0.31 mmol, 45%) of **27** as TFA salt with 100% purity.

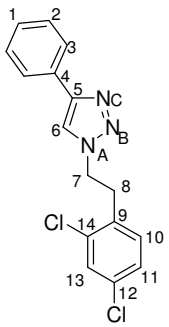

**$^1$H-NMR: ($CDCl_3$, 500 MHz):** δ (ppm): 7.78 (dd, *J* = 8.3, 1.3 Hz, 1H, H3), 7.53 (s, 1H, H6), 7.42 (m, 3H, H2, H13), 7.33 (m, 1H, H1), 7.13 (dd, *J* = 8.2, 2.1 Hz, 1H, H11), 6.97 (d, *J* = 8.2 Hz, 1H, H10), 4.65 (t, *J* = 7.1 Hz, 2H, H7), 3.38 (t, *J* = 7.1 Hz, 2H, H8) **$^{13}$C-NMR: ($CDCl_3$, 100 MHz):** δ (ppm): 147.6 (C5), 134.5 (C14), 133.1 (C9), 131.9 (C10), , 130.3 (C4), 129.5 (C13), 128.7 (C11), 128.1 (C1), 125.7 (C3), 119.8 (C6), 49.2 (C7), 34.1 (C8) **$^{15}$N-NMR ($CDCl_3$, 40.5 MHz):** δ (ppm): -134.4 ($N_A$), -34.4 ($N_C$), -18.16 ($N_B$) **HRMS for $C_{16}H_{13}N_3Cl_2$:** Calculated: 318.0565 $(M+H)^+$; Found: 318.0570.

## 1-Benzyl-4-formyl-*1H*-1,2,3-triazole (25a)

A solution of **23a** (25 mg, 0.13 mmol) and iodoxybenzoic acid (55 mg, 0.19 mmol) in EtOAc (5 mL) was stirred for 4 hours under reflux conditions. The mixture was cooled; the solid was

filtered and extracted with EtOAc. The filtrate was washed with 5% $KHCO_3$ (3 x 20 mL) and brine (3 x 15 mL). Finally, the organic layer was dried with $MgSO_4$ and the EtOAc was eliminated under reduced pressure to give **25a** as a pure pale (100% purity) yellow solid (22 mg, 0.11 mmol, 85%).

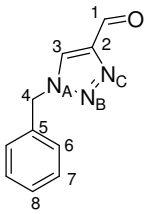

**$^1$H-NMR : ($CDCl_3$, 500 MHz):** δ (ppm): 10.1 (s, 1H, H1), 8.0 (s, 1H, H3), 7.42-7.40 (m, 3H, H7, H8), 7.33-7.31 (m, 2H, H6), 5.6 (s, 2H, H4) **$^{13}$C-NMR: ($CDCl_3$, 100 MHz):** δ (ppm): 185.0 (C1), 148.0 (C2), 133.3 (C5), 129.4 (C6), 129.3 (C8), 128.4 (C7), 125.0 (C3), 54.6 (C4) **HRMS for $C_{10}H_9N_3O$:** Calculated: 188.0824 $(M+H)^+$; Found: 188.0827.

## 1-(*p*-Fluorophenethyl)-4-formyl-1*H*-1,2,3-triazole (26a)

Following the above procedure, from 30 mg (0.13 mmol) of **24a** and 55 mg (0.2 mmol) of 2-iodoxybenzoic acid, 28 mg (0.12 mmol, 94%) of **26a** were obtained with 80% purity.

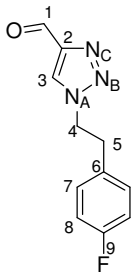

**$^1$H-NMR: ($CDCl_3$, 500 MHz):** δ (ppm): 10.1 (s, 1H, H1), 7.8 (s, 1H, H3), 7.00 (m, 4H, H7, H8), 4.64 (t, *J* = 7 Hz, 2H, H4), 3.24 (t, *J* = 7 Hz, H5) **$^{13}$C-NMR: ($CDCl_3$, 100 MHz):** δ (ppm): 184.9 (C1), 162.0 (d, *J* = 246 Hz, C9), 147.5 (C2), 131.8 (C6), 130.1 (d, *J* = 8 Hz, C7), 125.4 (C3), 115.9 (d, *J* = 21 Hz, C8), 52.1 (C4), 35.6 (C5) **$^{15}$N-NMR ($CDCl_3$, 40.5 MHz):** δ (ppm): -130.1 ($N_A$), -19.6 ($N_C$), -12.7 ($N_B$) **HRMS for $C_{11}H_{10}FN_3O$:** Calculated: 220.0886 $(M+H)^+$; Found: 220.0873.

### 6.5.3. Synthesis and characterization of 1,5-disubstituted-1,2,3-triazole derivatives

## 1-Benzyl-5-hydroxymethyl-1*H*-1,2,3-triazole (23b)

A solution of propargyl alcohol (90 μL, 1.4 mmol) and 100 mg (0.75 mmol) benzyl azide (**21**) in 5 mL of dioxane was added to a solution of Cp*RuCl$(PPh_3)_2$ (60 mg, 0.08 mmol) in 7 mL of the same solvent. The round-bottom flask was purged with nitrogen, sealed, and heated for 12 h at 60ºC under nitrogen atmosphere. The mixture was concentrated under reduced pressure to obtain a residue that after a reverse phase chromatographic purification afforded 25 mg (0.12 mmol, 16%) of a pale yellow solid identified as **23b** with 99% purity.

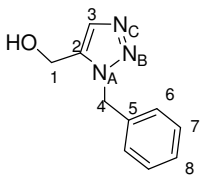

**$^1$H-NMR ($CDCl_3$, 500 MHz):** δ (ppm): 8,1 (s, 1H, OH), 7.84 (s, 1H, H3), 7.35 (m, 3H, H7, H8), 7.24 (m, 2H, H6), 5.66 (s, 2H, H4), 4.63 (s, 2H, H1) **$^{13}$C-NMR ($CDCl_3$, 100 MHz):** δ (ppm): 138.4 (C2), 132.7 (C5), 130.5 (C3), 129.2 (C6), 129.1 (C8), 127.8 (C7), 53.6 (C1), 52.8 (C4) **$^{15}$N-NMR ($CDCl_3$, 40.5 MHz):** δ (ppm): -135.7 ($N_A$), -58.8 ($N_C$), -19.9 ($N_B$) **HRMS for $C_{10}H_{11}N_3O$:** Calculated: 190.098 $(M+H)^+$; Found: 190.097.

## 1-(*p*-Fluorophenethyl)-5-hydroxymethyl-*1H*-1,2,3-triazole (24b)

Following the above procedure, from 150 mg (0.90 mmol) of *p*-fluorophenethylazide (**22**), 105 μL, (1.8 mmol) of propargyl alcohol and a solution of $Cp^*RuCl(PPh_3)_2$ (70 mg, 0.09 mmol) in 9 mL of dioxane, the reaction afforded, after a reverse phase chromatographic purification, 60 mg (0.27 mmol, 30%) of **24b** as a yellow pale solid with 83% purity.

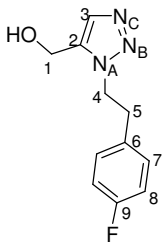

**$^1$H-NMR ($CDCl_3$, 500 MHz):** δ (ppm): 7,42 (s, 1H, H3), 7.02 (dd, *J* = 8.7 Hz, 5.4 Hz, 2H, H7), 6.93 (t, *J* = 8.7 Hz, 2H, H8), 4.56 (t, *J* = 7.2 Hz, 2H, H4), 4.41 (s, 2H, H1), 3.21 (t, *J* = 7.2 Hz, 2H, H5) **$^{13}$C-NMR ($CDCl_3$, 100 MHz):** δ (ppm): 161.8 (d, *J* = 260 Hz, C9), 136.4 (C2), 132.5 (C3), 130.4 (C7), 130.1 (C6), 115.6 (C8, 52.6 (C1), 49.7 (C4), 35.7 (C5) **$^{15}$N-NMR ($CDCl_3$, 40.5 MHz):** δ (ppm): -136.1 ($N_A$), -35.3 ($N_C$), -16.6 ($N_B$) **HRMS for $C_{11}H_{12}FN_3O$:** Calculated: 222.1043 $(M+H)^+$; Found: 222.1037.

## 1-Benzyl-5-formyl-*1H*-1,2,3-triazole (25b)

Following the same procedure described above for **25a**, from **23b** (25 mg, 0.12 mmol) and iodoxybenzoic acid (50 mg, 0.18 mmol) in EtOAc (1.2 mL), the reaction afforded the aldehyde **25b** (16 mg, 0.09 mmol, 70%) with 78% purity.

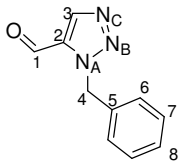

**$^1$H-NMR ($CDCl_3$, 500 MHz):** δ (ppm): 9.95 (s, 1H, H1), 8.25 (s, 1H, H3), 7.33 (m, 5H, H6,7,8), 5.88 (s, 2H, H4) **$^{13}$C-NMR ($CDCl_3$, 100 MHz):** δ (ppm): 178.1 (C1), 141.1 (C2), 134.3 (C5), 133.3 (C3), 128.8 (C6), 128.7 (C8), 128.2 (C7), 53.8 (C4) **$^{15}$N-NMR ($CDCl_3$, 40.5 MHz):** δ (ppm): -132.4 ($N_A$), -31.7 ($N_C$), -2.1 ($N_B$) **HRMS for $C_{10}H_9N_3O$:** Calculated: 188.0824 $(M+H)^+$; Found: 188.0847.

### 6.5.4. Synthesis and characterization of 2,4-disubstituted-1,2,3-triazoles derivatives

## 2-Benzyl-4-hydroxymethyl-1*H*-1,2,3-triazole (23c)

Anhydrous DMF (10 mL) was added to the residue containing triazole **14** (690 mg, 6.8 mmol) and the mixture was heated at 60ºC. A solution of benzyl bromide (830 μL, 6.9 mmol) in acetonitrile (10 mL) and excess of $Cs_2CO_3$ were added and the mixture was stirred for 24 hours at 60ºC. The crude reaction mixture was diluted with EtOAc (25 mL) and washed with water (2 x 15 mL) and brine (2 x 15 mL). The elimination of solvents afforded a residue (445 mg) that was purified by a reverse phase chromatography (from 10% to 40% of ACN in water (0.1% TFA) in 30 min) to give 77 mg (0.41 mmol, 10%) of yellow oil identified as **23c** with 99% purity.

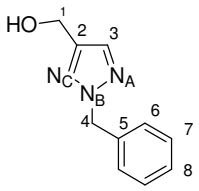

**$^{1}$H-NMR ($CDCl_3$, 500 MHz):** δ (ppm): 7.61 (s, 1H, H3), 7.36 (m, 5H, H6,7,8), 5.57 (s, 2H, H4), 4.77 (H1) **$^{13}$C-NMR ($CDCl_3$, 100 MHz):** δ (ppm): 148.0 (C2), 135.1 (C5), 132.9 (C3), 128.8 (C7), 128.3 (C8), 128.0 (C6), 58.6 (C4), 56.7 (C1) **$^{15}$N-NMR ($CDCl_3$, 40.5 MHz):** δ (ppm): -124.8 ($N_B$), -55.9 ($N_C$), -49.5 ($N_A$) **HRMS for $C_{10}H_{12}N_3O$:** Calculated: 190.098 $(M+H)^+$; found: 190.0989.

## 2-(*p*-Fluorophenethyl)-4-hydroxymethyl-1*H*-1,2,3-triazole (24c)

This compound was prepared as described before for **23c**, but using 800 mg (8.1 mmol) of **14**, 960 µL (8.1 mmol) of *p*-fluorophenethyl bromide and 5 eq of $Cs_2CO_3$. The crude reaction mixture was purified by column chromatography EtOAC / hexane (1 / 9) to give 282 mg (1.27 mmol, 16%) of **24c** with 98% purity.

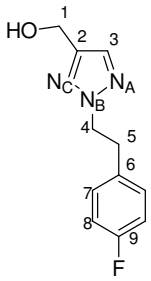

**$^{1}$H-NMR ($CDCl_3$, 500 MHz):** δ (ppm): 7.57 (s, 1H, H3), 7.12 (m, 2H, H7), 6.98 (m, 2H, H8), 4.77 (s, 2H, H1), 4.61 (t, *J* = 7.6 Hz, 2H, H4), 3.25 (t, *J* = 7.6 Hz, 2H, H5) **$^{13}$C-NMR ($CDCl_3$, 100 MHz):** δ (ppm): 161.8 (d, *J* = 245 Hz, C9), 147.5 (C2), 133.0 (C6), 132.4 (C3), 130.1 (C7), 115.6 (C8), 115.4 (C8), 56.6 (C1), 55.9 (C4), 35.3 (C5) **$^{15}$N-NMR ($CDCl_3$, 40.5 MHz):** δ (ppm) -127.5 ($N_B$), -57.6 ($N_C$), -51.5 ($N_A$) **HRMS for $C_{11}H_{13}FN_3O$:** Calculated: 222.1043 $(M+H)^+$; Found: 222.1038; Calculated: 245.094 (M+Na); Found: 245.1201.

## 2-Benzyl-4-formyl-1*H*-1,2,3-triazole (25c)

A solution of **23c** (80 mg, 0.4 mmol) and iodoxybenzoic acid (175 mg, 0.6 mmol) in EtOAc (4 mL) was stirred for 4 hours under reflux conditions. The mixture was cooled down; the solid was filtered and washed with EtOAc. The filtrate was washed with 5% $KHCO_3$ (3 x 20 mL) and brine (3 x 15 mL). Finally, the organic layer was dried with $MgSO_4$ and the EtOAc was eliminated under reduced pressure to give **25c**, a pure pale yellow solid (78 mg, 0.4 mmol, 95%) with 100% purity.

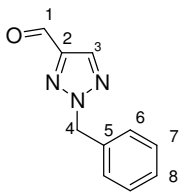

**$^{1}$H-NMR ($CDCl_3$, 500 MHz):** δ (ppm): 10.12 (s, 1H, H1), 8.11 (s, 1H, H3), 7.39 (m, 5H, H6,7,8), 5.67 (s, 2H, H4) **$^{13}$C-NMR ($CDCl_3$, 100 MHz):** δ (ppm): 184.1 (C1), 147.4 (C2), 134.9 (C3), 133.9 (C5), 129.0 (C7), 128.9 (C8), 128.3 (C6), 59.5 (C4) **HRMS for $C_{10}H_{10}N_3O$**: Calculated: 188.0824 $(M+H)^+$; found: 188.0816.

## 2-(*p*-Fluorophenethyl)-4-formyl-1*H*-1,2,3-triazole (26c)

This compound was prepared as described above for **25c**, but using 280 mg (1.3 mmol) of **24c** and 535 mg (1.91 mmol) of iodoxybenzoic acid, to give 255 mg (1.16 mmol, 91%) of a white powder.

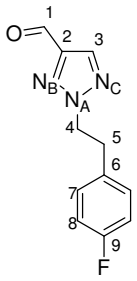


**$^{1}$H-NMR (CDCl$_3$, 500 MHz)**: δ (ppm): 10.06 (s, 1H, H1), 8.04 (s, 1H, H3), 7.1-7.08 (m, 2H, H7), 6.98-6.95 (m, 2H, H8), 4.71 (t, *J* = 7.4 Hz, 2H, H4), 3.29 (t, *J* = 7.4 Hz, 2H, H5) **$^{13}$C-NMR (CDCl$_3$, 100 MHz):** δ (ppm): 183.9 (C1), 161.9 (d, *J* = 245 Hz, C9), 147.0 (C2), 134.6 (C3), 132.3 (C6), 130.1 (C7), 115.6 (C8), 56.8 (C4), 34.9 (C6) ) **$^{15}$N-NMR (CDCl$_3$, 40.5 MHz):** δ (ppm) -119.7 ($N_A$), -48.8 ($N_C$), -41.9 ($N_B$) **HRMS for $C_{11}H_{11}FN_3O$:** Calculated: 220.0886 $(M+H)^+$; found:220.0899.

## 6.6. Synthesis and characterization of compounds in Chapter 3

### 6.6.1. Compounds from the reactivity study

### *N*-benzyl-2-(2-benzyl-2*H*-1,2,3-triazol-4-yl)-1-(4-fluorophenethyl)-4-oxoazetidine-2-carboxamide (33βLac) and 1-(2',4'-dichlorophenethyl)-3-[2'-(benzyl)-2*H*-1,2,3-triazol-4'-yl]-4-(*p*-fluorophenethyl) piperazine-2,5-dione (33DKP)

Following the same Ugi reaction used in compounds **3**, *p*-fluorophenethylamine (25 μL, 0.19 mmol) was added to a solution of **25c** (35 mg, 0.19 mmol) in methanol (0.1 mL). The mixture was stirred for 6 hours at room temperature. Then, a solution of benzyl isocyanide (20 mg, 0.19 mmol) in 0.1 mL of methanol and a solution of chloroacetic acid (20 mg, 0.19 mmol) in 0.1 mL methanol were added and the mixture was stirred for 48 hours at room temperature under nitrogen atmosphere. Straightaway, a solution of KOH (15 mg, 0.2 mmol) in 2 mL of MeOH was added into the Ugi adduct and afforded a crude reaction mixture containing a 1: 0.3 mixture of the β-lactam derivative (**33βLac**) and the DKP (**33DKP**), that was separated by preparative thin layer chromatography (hexane: EtOAc) to give 6 mg (0.014 mmol, 8%) of **33βLac** and 12 mg (0.024 mmol, 13%) of **33DKP**.

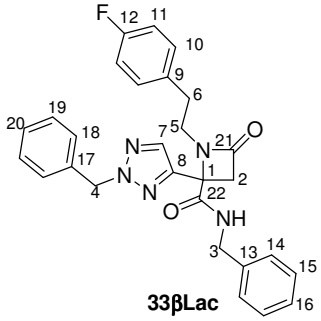

**33βLac**

**$^1$H-NMR: ($CDCl_3$, 500 MHz):** δ (ppm): 7.59 (s, 1H, H7), 7.33-7.28 (m, 8H, H15, 19, 14,18), 7.17 (m, 2H, H20,16), 7.02 (dd, *J* = 8.5, 5.4 Hz, 2H, H10), 6.87 (t, *J* = 8.7 Hz, 2H, H11), 6.61 (s, 1H, NH), 5.54 (s, 2H, H4), 4.42 (dd, *J* = 14.8, 6.0 Hz, 1H, H3), 4.30 (dd, *J* = 14.8, 6 Hz, 1H, H3), 3.42 (m, 1H, H5), 3.0 (m, 1H, H6), 2.85 (m, 1H, H6) **$^{13}$C-NMR: ($CDCl_3$, 100 MHz):** δ (ppm): 168.9 (C22), 167.4 (C21), 161.8 (C12), 145.0 (C8), 137.4 (C13), 134.5 (C17), 134.2 (C9), 133.7 (C7), 130.1 (C10), 128.9 (C19), 128.8 (C18), 128.6 (C20), 127.7, 128.1 (C15), 127.7 (C14), 115.4 (C11), 59.1 (C4), 58.9 (C1), 50.6 (C2), 44.9 (C5), 43.9 (C3), 32.9 (C6) **HRMS for $C_{28}H_{27}FN_5O_2$:** Calculated: 484.2149 $(M+H)^+$; Found:484.2122.

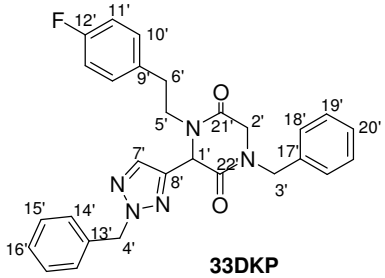

**33DKP**

**$^1$H-NMR: ($CDCl_3$, 500 MHz):** δ (ppm): 7.58 (s, 1H, H7'), 7.33-7.28 (m, 8H, H15', 19', 14',18'), 7.17 (m, 2H, H20',16'), 7.08 (dd, *J* = 8.6, 5.5 Hz, 2H, H10'), 6.95 (t, *J* = 8.7 Hz, 2H, H11'), 5.52 (s, 1H, H4'), 5.0 (s, 1H, H1'), 4.56 (dd, *J* = 66, 15 Hz, 2H, H3'), 4.02 (m, 1H, H5'), 3.91 (dd, *J* = 112, 16 Hz, 2H, H2'), 3.42 (m, 1H, H5'), 2 (m, 1H, H6'), 2.71 (m, 1H, H6') **$^{13}$C-NMR: ($CDCl_3$, 100 MHz):** δ (ppm): 164.9 (C22'), 163.9 (C21'), 161.8 (C12'), 143.9 (C8'), 134.8 (C17'), 134.5 (C13'), 133.6 (C9'), 130.0 (C10'), 128.9 (C15'), 128.8 (C14'), 128.5 (C16'), 128.1 (C20'), 128.1 (C19'), 128.0 (C18'), 115.5 (C11'), 59.0 (C4'), 57.8 (C1'), 49.6 (C3'), 49.3 (C2'), 46.7 (C5'), 32.7 (C6') **HRMS for $C_{28}H_{27}FN_5O_2$:** Calculated: 484.2149 $(M+H)^+$; Found:484.2195.

## *N*-(*p*-methoxyphenyl)-2-[2-benzyl-*1H*,1,2,3-triazol-4-yl]-3-(*p*-fluorophenethyl)aza-4-oxo-5-chloropentanoic acid amide (28)

Following the above procedure, from *p*-fluorophenethylamine (25 μL, 0.20 mmol), **25c** (35 mg, 0.2 mmol), *p*-methoxyphenyl isocyanide (25 mg, 0.2 mmol) and chloroacetic acid (20 mg, 0.2 mmol), the Ugi reaction afforded after a chromatographic column purification 45 mg (0.069 mmol, 35%) of the desired compound **28** with 98% of purity by HPLC.

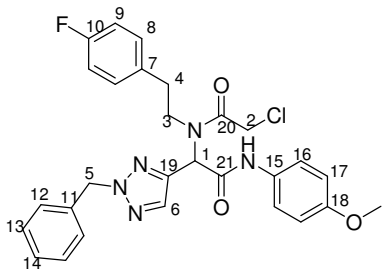

**$^{1}$H-NMR: ($CDCl_3$, 500 MHz):** δ (ppm): 8.4 (s, 1H, NH), 7.9 (s, 1H, H6), 7.36-7.30 (m, 7H, H12,13,14,17), 6.97-6.91 (m, 4H, H8,9), 6.83 (d, *J* = 8.9 Hz, 2H, H16), 5.92 (s, 1H, H1), 5.61 (s, 2H, H5), 3.88 (s, 2H, H2), 3.78 (s, 3H, H3), 3.59 (m, 2H, H3), 2.74 (m, 1H, H4), 2.61 (m, 1H, H4) **$^{13}$C-NMR: ($CDCl_3$, 100 MHz):** δ (ppm): 167.7 (C20), 165.2 (C21), 161.8 (d, *J* = 245 Hz, C10), 156.7 (C18), 142.5 (C19), 135.4 (C6), 134.7 (C11), 133.2 (C7), 130.4 (C15) 130.2 (C), 130.1 (C8), 128.9 (C13), 128.6 (C14), 128.2 (C12), 121.9 (C17), 115.8 (C9), 115.6 (C9), 114.1 (C16), 59.1 (C5), 57.3 (C1), 55.5 (CMe), 49.9 (C3), 40.9 (C2), 34.7 (C4) **HRMS for $C_{28}H_{28}ClFN_5O_3$:** Calculated: 536.1865 $(M+H)^+$; Found: 536.1863.

## 1-(*p*-methoxyphenyl)-3-[2'-(benzyl)-1,2,3-triazol-4'-yl]-4-(*p*-fluorophenethyl) piperazine-2,5-dione (35DKP)

To a methanol solution of **28** (5 mg, 0.009 mmol), NaOH (0.5 mg / 0.01 mmol) was added and a mixture 1: 0.1 of the DKP (**35DKP**) and the β-lactam (**35βLac**) was obtained. This mixture was characterized as product **35DKP** due to the low amount of **35βLac**.

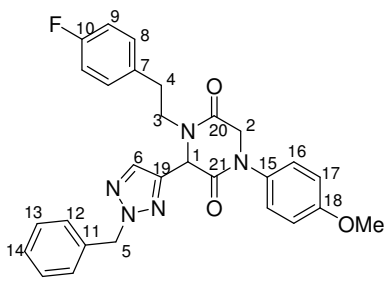

**$^{1}$H-NMR: ($CDCl_3$, 500 MHz):** δ (ppm): 7.64 (s, 1H, H6), 7.36-7.30 (m, 5H, H12, 13, 14), 7.13 (dd, *J* = 8.5, 5.5 Hz, 2H, H8), 7.08 (d, *J* = 9 Hz, H17), 6.98 (t, *J* = 8.5 Hz, H9), 6.91 (d, *J* = 9 Hz, H16), 5.56 (d, *J* = 2 Hz, H5), 5.11 (s, 1H, H1), 4.58 (d, *J* = 17 Hz, 1H, H2), 4.12 (d, *J* = 17 Hz, 1H, H2), 4.05 (m, 1H, H3), 3.81 (s, 3H, HMe), 3.19 (m, 1H, H3), 2.90 (m, 1H, H4), 2.80 (m, 1H, H4) **$^{13}$C-NMR: ($CDCl_3$, 100 MHz):** δ (ppm): 165.1 (C20), 163.8 (C21), 161.6 (d, *J* = 260 Hz, C10), 158.7 (C18), 143.9 (C19), 134.5 (C11), 133.5 (C7), 133.2 (C6), 132.3 (C15), 130.1 (C8), 128.8 (C14), 128.6 (C13), 128.2 (C12), 126.4 (C17), 115.5 (d, *J* = 21.2 Hz, C9), 114.6 (C16), 59.1 (C5), 58.5 (C1), 55.5 (CMe), 53.4 (C2), 47.1 (C3), 32.9 (C4) **HRMS for $C_{28}H_{26}FN_5O_3$:** Calculated: 500.2098 $(M+H)^+$; Found: 500.2128.

## *N*-benzyl-2-[1-benzyl-1*H*,1,2,3-triazol-4-yl]-3-(*p*-fluorophenethyl)aza-4-oxo-5-chloropentanoic acid amide (29)

Following the above procedure, from *p*-fluorophenethylamine (20 μL, 0.14 mmol), **25a** (25 mg, 0.14 mmol), benzyl isocyanide (15 μL, 0.14 mmol) and chloroacetic acid (15 mg, 0.14 mmol), the Ugi reaction afforded after a reverse phase purification 17 mg (0.03 mmol, 19%) of **29** with 98% purity by HPLC.

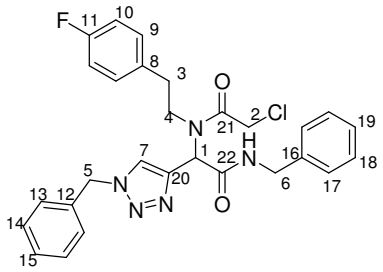

**$^1$H-NMR: ($CDCl_3$, 500 MHz):** δ (ppm): 7.95 (s, 1H, H7), 7.39-7.30 (m, 6H, H14, 15, 18, 19), 7.26-7.25 (m, 4H, H13, H17), 6.94 (dd, *J* = 8, 5.8 Hz, 2H, H9), 6.9 (m, 1H, NH), 6.89 (t, *J* = 8 Hz, 2H, H10), 5.81 (s, 1H, H1), 5.59 (d, *J* = 14.5 Hz, 1H, H5), 5.49 (d, *J* = 14.5 Hz, 1H, H5), 4.47 (m, 2H, H6), 3.87 (dd, *J* = 15, 13 Hz, 2H, H2), 3.6 (m, 2H, H4), 2.8 (m, 1H, H3), 2.67 (m, 1H, H3) **$^{13}$C-NMR: ($CDCl_3$, 100 MHz):** δ (ppm): 167.4 (C22), 167.2 (C21), 161.7 (d, *J* = 246 Hz, C11), 142.5 (C20), 137.5 (C16), 133.9 (C12), 133.3 (C8), 130.1 (C9), 129.2 (C14), 128.9 (C15), 128.7 (C18), 128.1 (C13, 19), 127.5 (C17), 124.8 (C7), 115.7 (C10), 57.5 (C1), 54.5 (C5), 50.5 (C4), 43.8 (C6), 40.9 (C2), 34.3 (C3) **HRMS for $C_{28}H_{27}ClFN_5O_2$:** Calculated: 520.1916 $(M+H)^+$; Found: 520.1898.

## *N*-benzyl-2-(1-benzyl-2*H*-1,2,3-triazol-4-yl)-1-(4-fluorophenethyl)-4-oxoazetidine-2-carboxamide (36βLac) and 1-(2',4'-dichlorophenethyl)-3-[1'-(benzyl)-2*H*-1,2,3-triazol-4'-yl]-4-(*p*-fluorophenethyl) piperazine-2,5-dione (36DKP)

To 5 mg (0.009 mmol) of **29**, 0.5 mg of NaOD in 50 μL of MeOD were added and a 1 / 2 mixture of the DKP (**36DKP**) and the β-lactam (**36βLac**) compound was obtained.

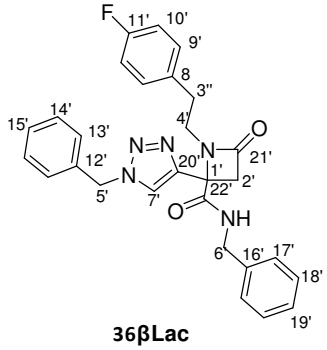

**36βLac**

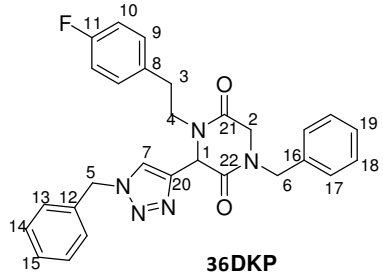

**36DKP**

**$^1$H-NMR: ($CDCl_3$, 500 MHz):** δ (ppm): 7.48 (t, *J* = 5.7 Hz, NH), 7.42 (s, 1H, H7), 7.39-7.14 (m, 20H, H13, 13', 14, 14', 15, 15', 17, 17', 18, 18', 19, 19'), 7.19 (s, 1H, H7'), 7.07 (m, 4H, H9,9'), 6.92 (m, 2H, H10), 6.87 (m, 2H, H10'), 5.49 (dd, *J* = 28, 15 Hz, 2H, H5), 5.45 (dd, *J* = 18.3, 14.8 Hz, 2H, H5'), 4.95 (s, 1H, H1), 4.62 (d, *J* = 14.7 Hz, 1H, H6), 4.47 (d, *J* = 14.7 Hz, 1H, H6), 4.43 (dd, *J* = 14.8, 6 Hz, 1H, H6'), 4.32 (dd, *J* = 14.8, 6 Hz, 1H, H6'), 4.28 (d, *J* = 17 Hz, 1H, H2), 4.02 (m, 1H, H4), 3.79 (d, *J* = 17 Hz, 1H, H2), 3.39 (t, *J* = 7.2 Hz, 2H, H4'), 3.38 (d, *J* = 14.5 Hz, 1H, H2'), 3.18 (d, *J* = 14.5 Hz, 1H, H2'), 3.05 (m, 1H, H4), 2.97 (t, *J* = 7.2 Hz, 2H, H3'), 2.86 (m, 1H, H3), 2.70 (m, 1H, H3) **$^{13}$C-NMR: ($CDCl_3$, 100 MHz):** 168.9 (C22'), 167.5 (C21'), 164.8 (C21), 164.1 (C22), 161 (C11), 145.1 (C20'), 143.2 (C20), 137.5 (C16'), 134.9 (C16), 134.5 (C8'), 133.9 (C8), 130.3 (C9'), 130.0 (C9), 129.3-127.3 (Ar), 122.7 (C7'), 121.9 (C7), 115 (C10, 10'), 58.7 (C1'), 57.6 (C1), 54.4 (C2'), 51.3 (2'), 49.5 (C6), 49.4 (C2), 46.8 (C4), 45.2 (C4'), 43.8 (C6'), 32.7 C3), 32.6 (C3').

When instead of NaOH/ MeOH, DBU is used for the cyclization, a 100% of the β-lactam product (**36βLac**) was obtained.

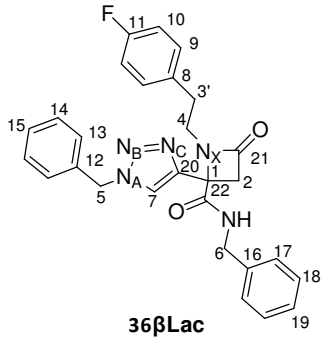

**36βLac**

**$^1$H-NMR: ($CDCl_3$, 500 MHz):** δ (ppm): 7.49 (1H, NH), 7.39-7.37 (m, Ar), 7.31-7.29 (m, Ar), 7.20 (s, 1H, H7), 7.07 (dd, *J* = 8.6, 5.4 Hz, 2H, H9), 6.88 (t, *J* = 8.6 Hz, 2H, H10), 5.45 (d, *J* = 3.5 Hz, 2H, H5), 4.44 (dd, *J* = 14.8, 6 Hz, 1H, H6), 4.32 (dd, *J* = 14.8, 6 Hz, 1H, H6), 3.41-3.39 (m, 3H, H2, H4), 3.19 (d, *J* = 14.5 Hz, 1H, H2), 2.97 (t, *J* = 7.2 Hz, 2H, H3) **$^{15}$N-NMR ($CDCl_3$, 40 MHz): δ (ppm):** -263.7 (NH), -231.3 ($N_X$), -130.4 ($N_A$) -35.1 ($N_C$), -16.0 ($N_B$).

### 6.6.2. Compounds of the section 3.3.2.

## *N-tert*-Butyl-2-(2-(2,4-dichlorophenethyl)-2*H*-1,2,3-triazol-4-yl)1-(3,3-diphenylpropyl)-4-oxoazetidine-2-carboxamide (43)

Following the above procedure, from 3,3-diphenylpropanamine (35 μL, 0.20 mmol), aldehyde **5c** (55 mg, 0.2 mmol), *tert*-butyl isocyanide (15 mg, 0.2 mmol) and chloroacetic acid (20 mg, 0.2 mmol), the Ugi reaction followed by the cyclization in basic media (1 mg, 0.2 mmol of KOH) afforded after a reverse phase purification 38 mg (0.06 mmol, 21%) of the β-lactam **43** as a yellow oil.

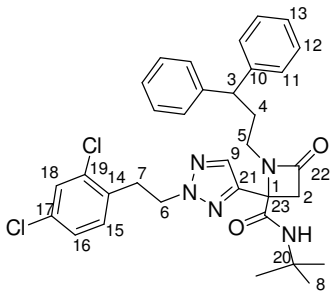

**$^1$H-NMR: ($CDCl_3$, 500 MHz):** δ (ppm): 7.56 (s, 1H, H9), 7.36 (d, *J* = 2.1 Hz, 1H, H18), 7.29-7.22 (m, 4H, H12), 7.21-7.10 (m, 6H, H11, 13), 7.06 (dd, *J* = 8.2, 2.1 Hz, 1H, H16), 6.89 (d, *J* = 8.2 Hz, 1H, H15), 6.43 (s, 1H, NH), 4.60 (t, *J* = 7.0 Hz, 2H, H6), 3.88 (t, *J* = 7.8 Hz, 1H, H3), 3.38 (d, *J* = 14.3 Hz, 1H, H2), 3.28 (t, *J* = 7.0 Hz, 2H, H7), 3.25 (d, *J* = 14.3 Hz, 1H, H2), 3.17 (m, 1H, H5), 3.05 (m, 1H, H5), 2.36 (m, 2H, H4), 1.32 (s, 9H, H8) **$^{13}$C-NMR: ($CDCl_3$, 100 MHz):** δ (ppm): 167.7 (C23), 166.9 (C22), 147.1 (C19), 145.5 (C17), 145.0 (C21), 143.6 (C10), 134.6 (C14), 133.4 (C9), 129.6 (C18), 128.6 (C12), 127.7 (C11), 127.3 (C15), 127.2 (C16), 126.4 (C13), 59.0 (C1), 54.1 (C6), 51.6 (C20), 50.3 (C2), 48.9 (C3), 41.4 (C5), 33.3 (C7), 33.2 (C4), 28.4 (C8) **HRMS for $C_{33}H_{36}Cl_2N_5O_2$:** Calculated: 604.2246 $(M+H)^+$; Found: 604.2273.

## *N-tert*-Butyl-2-(2-(4-fluorophenetyl)-*2H*-1,2,3-triazol-4-yl)-1-(4-methoxy phenethyl)-4-oxoazetidine-2-carboxamide (44)

Following the above procedure, from *p*-methoxyphenethylamine (35 μL, 0.24 mmol), 2-(p-fluorophenethyl)-4-formyl-1*H*-1,2,3-triazole (**26c**) (55 mg, 0.24 mmol), *tert*-butyl isocyanide (20 mg, 0.24 mmol) and chloroacetic acid (25 mg, 0.24 mmol), the Ugi reaction followed by the cyclization in basic media (15 mg, 0.24 mmol of KOH) afforded after a reverse phase purification 35 mg (0.07 mmol, 29%) of product **44**.

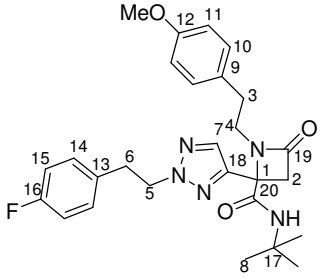

**$^1$H-NMR: ($CDCl_3$, 500 MHz):** δ (ppm): 7.55 (s, 1H, H7), 7.05 (m, 4H, H10, H14), 6.91 (t, *J* = 8.6 Hz, 2H, H15), 6.81 (d, *J* = 8.6 Hz, 2H, H11), 6.29 (s, 1H, NH), 4.62 (t, *J* = 7.3 Hz, 2H, H5), 3.77 (s, 3H, Me), 3.38 (m, 1H, H4), 3.34 (q, *J* = 14.5 Hz, 2H, H2), 3.23 (m, 1H, H4), 3.23 (t, *J* = 7.3 Hz, 2H, H6), 2.86 (m, 2H, H3) **$^{13}$C-NMR: ($CDCl_3$, 100 MHz):** δ (ppm): 181.2 (C20), 167.4 (C19), 161.6 (C16), 158.1 (C12), 144.6 (C18), 133.4 (C7), 132.5 (C13), 130.2 (C9), 129.5 (C10, C14), 115.5 (C15), 113.9 (C11), 58.8 (C1), 56.0 (C5), 54.9 (CMe), 51.4 (C17), 50.3 (C2), 44.3 (C4), 34.8 (C6), 32.6 (C3), 28.1 (C8) **$^{19}$F-NMR: ($CDCl_3$, 500 MHz):** δ (ppm): -115.6 (m, 1F) **HRMS for $C_{27}H_{33}FN_5O_3$:** Calculated: 494.2567 $(M+H)^+$; Found: 494.2458.

## *N-tert*-Butyl-2-(2-(4-fluorophenethyl)-2H-1,2,3-triazol-4-yl)-oxo-1-(4-(trifluoromethoxy)benzyl)azetidine-2-carboxamide (45)

Following the above procedure, from 4-trifluoromethoxybenzylamine (35 μL, 0.24 mmol), **26c** (55 mg, 0.24 mmol), *tert*-butyl isocyanide (20 mg, 0.24 mmol) and chloroacetic acid (25 mg, 0.24 mmol), the Ugi reaction followed by the cyclization in basic media (15 mg, 0.24 mmol of KOH) afforded 95 mg (0.18 mmol, 75%) of a yellow oil, product **45**.

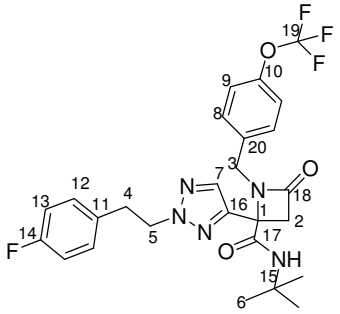

**$^1$H-NMR: ($CDCl_3$, 500 MHz):** δ (ppm): 7.60 (s, 1H, H7), 7.27 (d, *J* = 8 Hz, 2H, H8), 7.17 (d, *J* = 8 Hz, 2H, H9), 7.08 (dd, *J* = 8.5, 5.4 Hz, 2H, H12), 6.94 (t, *J* = 8.6 Hz, 2H, H13), 5.8 (s, 1H, NH), 4.63 (t, *J* = 7.3 Hz, 2H, H5), 4.58 (d, *J* = 15.5 Hz, 1H, H3), 3.88 (d, *J* = 15.5 Hz, 1H, H3), 3.43 (d, *J* = 14.8 Hz, 1H, H2), 3.39 (d, *J* = 14.8 Hz, 1H, H2), 3.23 (t, *J* = 7.3 Hz, 2H, H4), 1.08 (s, 9H, H6) **$^{13}$C-NMR: ($CDCl_3$, 100 MHz):** δ (ppm): 167.8 (C17), 167.6 (C18), 161.8 (d, *J* = 245 Hz, C14), 148.9 (C10), 144.1 (C16), 134.9 (C20), 134.1 (C7), 132.8 (C11), 130.4 (C8), 130.2 (C12), 121.5 (C9), 120.3 (q, *J* = 257.5 Hz, C19), 115.6 (C13), 60.04 (C1), 56.2 (C5), 51.5 (C2), 51.4 (C15), 44.7 (C3), 35.1 (C4), 27.9 (C6) **$^{19}$F-NMR: ($CDCl_3$, 500 MHz):** δ (ppm): -115.7 (m, 1F), -47.9 (s, 3F) **HRMS for $C_{26}H_{28}F_4N_5O_3$:** Calculated: 534.2128 $(M+H)^+$; Found: 534.2111.

## *N-tert*-Butyl-1-(3,3-diphenylpropyl)-2-(2-(4-fluorophenetyl)-2H-1,2,3-triazol-4-yl)-4-oxoazetidine-2-carboxamide (46)

Following the above procedure, from 3,3-diphenylpropanamine (55 μL, 0.24 mmol), **26c** (55 mg, 0.24 mmol), *tert*-butyl isocyanide (20 mg, 0.24 mmol) and chloroacetic acid (25 mg, 0.24 mmol), the Ugi reaction followed by the cyclization in basic media (15 mg, 0.24 mmol of KOH) afforded after a reverse phase purification 60 mg (0.011 mmol, 46%) of product **46**.

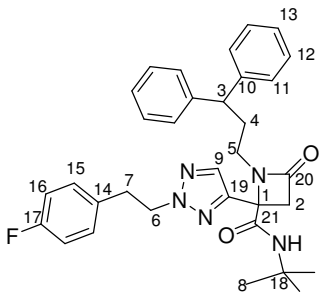

**$^1$H-NMR: ($CDCl_3$, 500 MHz):** δ (ppm): 7.57 (s, 1H, H9), 7.29-7.22 (m, 4H, H12), 7.21-7.10 (m, 6H, H11, 13), 7.02 (dd, *J* = 8.5, 5.4 Hz, 2H, H15), 6.92 (t, *J* = 8.5 Hz, H16), 6.37 (s, 1H, NH), 4.55 (t, *J* = 7.4 Hz, 2H, H6), 3.87 (t, *J* = 7.8 Hz, 1H, H3), 3.38 (d, J = 14.4 Hz, 1H, H2), 3.28 (d, *J* = 14.4 Hz, 1H, H2), 3.19 (m, 1H, H5), 3.16 (t, *J* = 7.4 Hz, 2H, H7), 3.05 (m, 1H, H5), 2.36 (m, 2H, H4), 1.32 (s, 9H, H8) **$^{13}$C-NMR: ($CDCl_3$, 100 MHz):** δ (ppm): 166.9 (C20), 161.7 (d, *J* = 243 Hz, C17), 161.2 (C21), 144.8 (C9), 143.5 (C10), 133.24 (C9),132.6 (C14), 129.9 (C15), 127.6 (C11), 115.4 (C16), 56.2 (C6), 51.7 (C18), 50.3 (C2), 48.8 (C3), 41.3 (C5), 34.9 (C7), 33.3 (C4), 28.3 (C8) **HRMS for $C_{33}H_{37}FN_5O_2$:** Calculated: 554.2931 $(M+H)^+$; Found: 554.2902.

## 2-(2-Benzyl-*2H*-1,2,3-triazol-4-yl)-*N-tert*-butyl-1-(2,4-dichlorophenethyl)-4-oxoazetidine-2-carboxamide (47)

Following the above procedure, from 2,4-dichlorophenethylamine (25 μL, 0.15 mmol), aldehyde **25c** (30 mg, 0.15 mmol), *tert*-butyl isocyanide (20 μL, 0.15 mmol) and chloroacetic acid (15 mg, 0.15 mmol), the Ugi reaction afforded a crude that was purified with reverse phase chromatographic column and 40 mg (0.076 mmol, 51%) of a white powder was obtained. A

solution of KOH (5 mg, 0.076 mmol) in MeOH (1mL) was added to the product and stirred during 3 hours. The crude reaction mixture was purified by reverse phase chromatography to give 15 mg (34%) of the expected final product **47**.

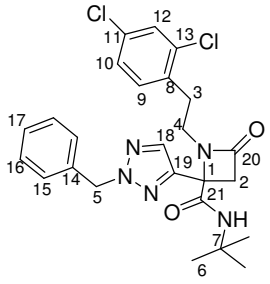

**$^1$H-NMR: ($CDCl_3$, 500 MHz):** δ (ppm): 7.55 (s, 1H, H18), 7.33-7.31 (m, 5H, H15, 16, 17), 7.12 (d, *J* = 1.2 Hz, 2H, H9,10), 6.33 (s, 1H, NH), 5.55 (s, 1H, H5), 3.42 (d, *J* = 14.2 Hz, 1H, H2), 3.40 (m, 2H, H4), 3.30 (d, *J* =14.2 Hz, 1H, H2), 3.01 (m, 2H, H3), 1.28 (s, 9H, H6) **$^{13}$C-NMR: ($CDCl_3$, 100 MHz):** δ (ppm): 167.6 (C21), 167.0 (C20), 145.5 (C19), 134.6 (C13), 134.5 (C8), 134.5 (C14), 133.3 (C18), 133.1 (C11), 133.6 (C9), 129.2 (C17), 128.9 (C16), 128.7 (C12), 128.2 (C15), 127.2 (C10), 59.2 (C5), 59.1 (C1), 51.9 (C7), 49.8 (C2), 41.9 (C4), 31.4 (C3), 28.4 (C6) **HRMS for $C_{25}H_{28}Cl_2N_5O_2$:** Calculated: 500.162 $(M+H)^+$; Found: 500.1599.

## *N*-Benzyl-2-(2-(2,4-dichlorophenthyl)-*2H*-1,2,3-triazol-4-yl)-1-(3,3-diphenylpropyl)-4-oxoazetidine-2-carboxamide (48βLac) and 1-benzyl-3-[2'-(2'',3''-dichlorophenethyl)-1,2,3-triazol-4'-yl]-4-(3',3'-diphenylpropyl) piperazine-2,5-dione (48DKP))

Following the above procedure, from 3,3-diphenylpropanamine (45 μL, 0.24 mmol), **5c** (65 mg, 0.24 mmol), benzyl isocyanide (30 mg, 0.24 mmol) and chloroacetic acid (25 mg, 0.24 mmol), the Ugi reaction followed by the cyclization in basic media (15 mg, 0.24 mmol of KOH) afforded after a reverse phase purification 70 mg of a mixture containing a 1: 0.2 proportion of the β-lactam derivative (**48βLac**) and the DKP (**48DKP**). This mixture was purified by preparative thin layer chromatography (hexane:EtOAc 3: 2) to give 50 mg (0.08 mmol, 34%) of **48βLac** and 8 mg (0.01 mmol, 5%) of **48DKP**.

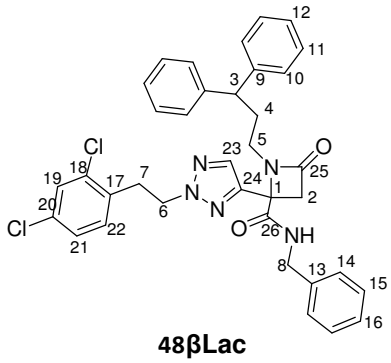

**48βLac**

**$^1$H-NMR: ($CDCl_3$, 500 MHz):** δ (ppm): 7.57 (s, 1H, H23), 7.31 (d, *J* = 2.2 Hz, 1H, H19), 7.3 (m, 4H, H11), 7.28-7.19 (m, 5H, H10, H16), 7.17-7.13 (m, 6H, H12, 14, 15), 7.01 (dd, *J* = 8.2 Hz, 2.1 Hz, 1H, H21), 6.83 (d, *J* = 8.2 Hz, 1H, H22), 6.78 (t, *J* = 5.6 Hz, 1H, NH), 4.58 (t, *J* = 7.1 Hz, 2H, H6), 4.44 (dd, *J* = 5.7, 2.3 Hz, 2H, H8), 3.86 (t, *J* = 7.8 Hz, 1H, H3), 3.44 (d, *J* = 14.4 Hz, 1H, H2), 3.30 (d, *J* =14.4 Hz, 1H, H2), 3.24 (t, *J* = 7.1 Hz, 2H, H7), 3.16 (m, 1H, H5), 3.04 (m, 1H, H5), 2.33 (m, 2H, H4) **$^{13}$C-NMR: ($CDCl_3$, 100 MHz):** δ (ppm): 168.8 (C26), 166.7 (C25), 144.8 (C24), 143.7 (C9), 143.6 (C9), 137.4 (C13), 134.7 (C17), 133.6 (C23), 133.4 (C18), 133.3 (C20), 131.5 (C22), 129.5 (C19), 128.9 (C15), 128.6 (C11), 128.5 (C11), 127.8 (C10), 127.7 (C10), 127.7 (C16), 127.6 (C21), 127.2 (C14), 126.4 (C12), 126.4 (C12), 58.8 (C1), 54.2 (C6), 50.5 (C2), 48.9 (C3), 44.0 (C8), 41.6 (C5), 33.4 (C7), 33.3 (C4) **HRMS for $C_{36}H_{34}Cl_2N_5O_2$:** Calculated: 638.209 $(M+H)^+$; Found: 638.2076.

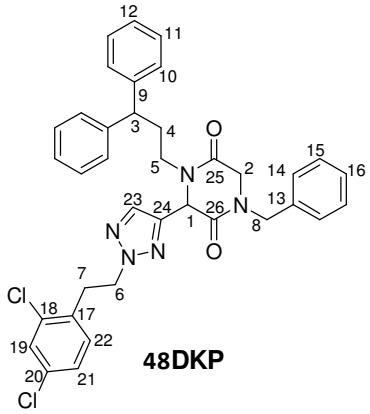

**48DKP**

**$^1$H-NMR: ($CDCl_3$, 500 MHz):** δ (ppm): 7.34 (s, 1H, H23), 7.33 (d, *J* = 2.2 Hz, H19), 7.31-7.26 (m, 5H, H12, 14, 16), 7.25-7.16 (m, 10H, H10, 11, 15), 6.98 (dd, *J* = 8.2, 2.2 Hz, 1H, H21), 6,78 (d, *J* = 8.2 Hz, 1H, H22), 5.00 (s, 1H, H1), 4.75 (d, *J* = 14.6 Hz, 1H, H8), 4.57 (td, *J* = 7, 1.9 Hz, 2H, H6), 4.31 (d, *J* = 14.6 Hz, 1H, H8), 3.93 (d, *J* = 17.1 Hz, 1H, H2), 3.91 (t, *J* = 10 Hz, 1H, H3), 3.83 (m, 1H, H5), 3.69 (d, *J* = 17.2 Hz, 1H, H2), 3.23 (t, *J* = 7 Hz, 2H, H7), 2.7 (m, 1H, H5), 2.32 (m, 2H, H4) **$^{13}$C-NMR: ($CDCl_3$, 100 MHz):** δ (ppm): 164.6 (C26), 163.7 (C25), 143.9 (C9), 143.8 (C9), 143.6 (C24), 134.9 (C20), 134.7 (C18), 133.5 (C17), 133.4 (C13), 132.9 (C22), 131.5 (C19), 129.5 (C21), 128.9 (C15), 128.7 (C11), 128.2 (C14), 128.1 (C12), 127.5 (C10), 127.2 (C12), 126.5 (C16), 57.3 (C1), 54.2 (C6), 49.7 (C3), 49.4 (C8), 49.1 (C2), 44.1 (C5), 33.4 (C7), 32.7 (C4) **HRMS for $C_{36}H_{34}Cl_2N_5O_2$:** Calculated: 660.1909 $(M+Na)^+$; Found: 660.1934, Calculated $(M+K)^+$; 676.1648; Found: 676.1672.

## *N*-benzyl-2-(2-(4-fluorophenethyl)-2*H*-1,2,3-triazol-4-yl)-1-(4-methoxy phenethyl)-4-oxoazetidine-2-carboxamide (49βLac) and 1-(benzyl)-3-[2'-(*p*-fluorophenethyl)-2*H*-1,2,3-triazol-4'-yl]-4-(*p*-methoxyphenethyl) piperazine-2,5-dione (49DKP)

Following the above procedure, from *p*-methoxyphenethylamine (35 µL, 0.24 mmol), aldehyde **26c** (50 mg, 0.24 mmol), benzyl isocyanide (30 mg, 0.24 mmol) and chloroacetic acid (25 mg, 0.24 mmol), the Ugi reaction followed by the cyclization in basic media (15 mg, 0.24 mmol of KOH) afforded after a reverse phase purification 55 mg of a mixture containing 1: 0.25 of the β-lactam derivative (**49βLac**) and the DKP (**49DKP**). This mixture was purified by preparative thin layer chromatography (hexane:EtOAc) to give 35 mg (0.06 mmol, 27%) of **49βLac** and 7 mg (0.01 mmol, 5%) of **49DKP**.

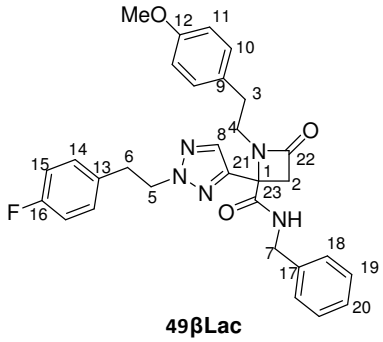

**49βLac**

**$^1$H-NMR: ($CDCl_3$, 500 MHz):** δ (ppm): 7.62 (s, 1H, H8), 7.31 (m, 2H, H19), 7.29 (m, 1H, H20), 7.14 (m, 2H, H18), 7.08 (d, *J* = 8.6 Hz, 2H, H10), 7.03 (m, 2H, H14), 6.9 (m, 2H, H15), 6.76 (d, *J* = 8.6 Hz, 2H, H11), 6.34 (m, 1H, NH), 4.61 (t, *J* = 7.3 Hz, 2H, H5), 4.36 (dd, *J* = 14.9, 6.4 Hz, 1H, H7), 4.13 (dd, *J* = 14.9, 5.7 Hz, 1H, H7), 3.71 (s, 3H, OMe), 3.41 (m, 1H, H4), 3.32 (s, 2H, H2), 3.20 (t, 2H, H6), 3.06 (m, 1H, H4), 2.99 (m, 1H, H3), 2.79 (m, 1H, H3) **$^{13}$C-NMR: ($CDCl_3$, 100 MHz):** δ (ppm): 168.8 (C23), 167.6 (C22), 160.3 (C16), 158.4 (C12), 144.0 (C21), 137.2 (C17), 133.6 (C8), 132.5 (C13), 130.2 (C9), 129.9 (C14), 129.6 (C10), 128.7 (C19), 127.5 (C20), 127.1 (C18), 115.2 (C15), 114.2 (C11), 58.8 (C1), 56.1 (C5), 55.2 (CMe), 50.5 (C2), 45.1 (C4), 43.5 (C7), 34.8 (C6), 32.4 (C3) **$^{19}$F-NMR: ($CDCl_3$, 500 MHz):** δ (ppm): -115.7 (m, 1F) **HRMS for $C_{30}H_{31}FN_5O_3$:** Calculated: 528.2411 $(M+H)^+$; Found: 528.2410.

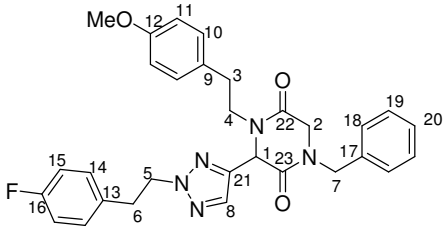

**49DKP**

**$^1$H-NMR: ($CDCl_3$, 500 MHz):** δ (ppm): 7.52 (s, 1H, H8), 7.30-7.27 (m, 3H, H19, 20), 7.17 (m, 2H, H18), 7.08 (d, *J* = 8.6 Hz, 2H, H10), 7.03 (m, 2H, H14), 6.9 (m, 2H, H15), 6.82 (d, *J* = 8.7 Hz, 2H, H11), 4.99 (s, 1H, H1), 4.57 (t, *J* = 7.3 Hz, 2H, H5), 4.55 (s, 2H, H7), 4.03 (m, 1H, H4), 3.97 (d, *J* = 17.1 Hz, 1H, H2), 3.78 (s, 3H, OMe), 3.76 (d, *J* = 17.1 Hz, 1H, H2), 3.16 (t, *J* = 7.4 Hz, 2H, H6), 2.91 (m, 1H,

H4), 2.82 (m, 1H, H3), 2.71 (m, 1H, H3) **$^{13}$C-NMR: ($CDCl_3$, 100 MHz):** δ (ppm): 164.7 (C22), 163.9 (C23), 162.9 (C16), 158.4 (C12), 134.9 (C17), 132.7 (C8), 130.1 (C13), 130.0 (C9), 129.9 (C14), 129.5 (C10), 128.9 (C19), 128.2 (C18), 128.1 (C20), 115.6 (C15), 115.3 (C15), 114.1 (C11), 57.7 (C1), 56.3 (C5), 55.2 (Cme), 49.5 (C2), 49.2 (C7), 46.8 (C4), 35.1 (C6), 32.6 (C3).

## *N*-benzl-2-(2-benzyl-2*H*-1,2,3-triazol-4-yl)-4-oxo-1-(2-(thiophen-2-yl)ethyl)azetidine 2-carboxamide (50βLac) and 1-(benzyl)-3-[2'-(benzyl)-1,2,3-triazol-4'-yl]-4-(*2*-thiophen -2-yl)piperazine-2,5-dione (50DKP)

Following the above procedure, from 2-(thiphen-2-yl)ethanamine (15 μL, 0.13 mmol), aldehyde **25c** (25 mg, 0.13 mmol), benzyl isocyanide (15 μL, 0.13 mmol) and cloroacetic acid (10 mg, 0.13 mmol), the Ugi reaction was performed. The cyclization was done with KOH (7 mg, 0.13 mmmol) in MeOH. After reverse phase purification, a mixture of two products was obtained 18 mg (0.04 mol, 29%, **50βLac**) and a 20% of the DKP **50DKP**.

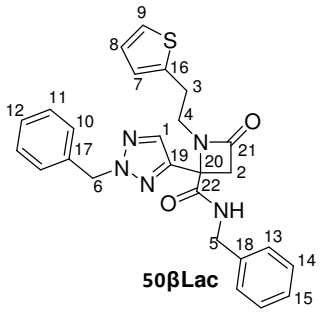


**$^{1}$H-NMR: ($CDCl_3$, 500 MHz):** δ (ppm): 7.60 (s, 1H, H1), 7.32-7.30 (m, 4H, H11, 14), 7.28 (m, 3H, H13, 15), 7.18-7.15 (m, 3H, H10, 12), 7.08 (dd, *J* = 5.1 Hz, 1H, H9), 6.8 (dd, *J* = 5, 3.4 Hz, 1H, H8), 6.79 (dd, *J* = 3.4, 1 Hz, 1H, H7), 6.75 (t, *J* = 6 Hz, 1H, NH), 5.54 (s, 2H, H6), 4.44 (dd, *J* = 14.8, 6 Hz, 1H, H5), 4.27 (dd, *J* = 14.8, 6 Hz, 1H, H5), 3.52 (m, 1H, H4), 3.37 (m, 2H, H2), 3.32 (m, 1H, H4), 3.27 (m, 1H, H3), 3.11 (m, 1H, H3) **$^{13}$C-NMR: ($CDCl_3$, 100 MHz):** δ (ppm): 168.8 (C22), 167.3 (C21), 144.8 (C19), 140.5 (C16), 137.4 (C17), 134.4 (C18), 133.7 (C1), 128.4 (C14, 15), 127.9 (C13), 127.5 (C11), 127.4 (C10), 127.0 (C8), 125.6 (C7), 124.3 (C12), 124.1 (C9), 58.8 (C6), 58.7 (C20), 50.6 (C2), 44.7 (C4), 43.7 (C5), 27.5 (C3) **HRMS for $C_{26}H_{26}N_5O_2S$:** Calculated: 472.1807 $(M+H)^+$; Found: 472.1794.

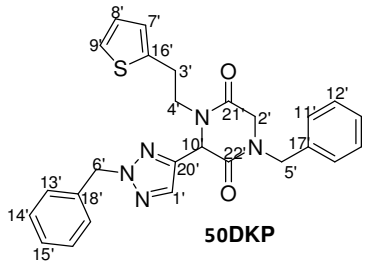


**$^{1}$H-NMR: ($CDCl_3$, 500 MHz):** δ (ppm): 7.57 (s, 1H, H1'), 7.32-7.15 (m, 10H, Ar), 7.09 (m, 1H, H9'), 6.92 (dd, *J* = 5, 3.5 Hz, 1H, H8'), 6.75 (m, 1H, H7'), 5.5 (s, 2H, H6'), 4.99 (s, 1H, H10), 4.57 (dd, *J* = 67, 14 Hz, 2H, H5'), 4.07 (m, 1H, H4'), 3.92 (dd, *J* = 104, 16 Hz, 2H, H2'), 3.15 (m, 1H, H3'), 3.09 (m, 1H, H4'), 2.98 (m, 1H, H3') **$^{13}$C-NMR: ($CDCl_3$, 100 MHz):** δ (ppm): 164.9 (C21'), 163.8 (C22'), 143.6 (C20'), 140.1 (C16'), 134.7 (C17'), 133.2 (C1'), 127.9 (C11'), 127.1 (C8'), 125.4 (C7'), 58.9 (C6'), 58.2 (C10'), 49.5 (C5'), 49.2 (C2'), 47.0 (C4'), 27.5 (C3').

## 1-(2'-chloro-5'-methyl-phenyl)-3-[2'-(benzyl)-1,2,3-triazol-4'-yl]-4-(*p*-fluoro phenethyl) piperazine-2,5-dione (51)

Following the above procedure, from *p*-fluorophenethylamine (20 μL, 0.15 mmol), **25c** (28 mg, 0.15 mmol), 2-chloro-5-methyl-isocyanide (25 mg, 0.14 mmol) and chloroacetic acid (15 mg, 0.15 mmol), the Ugi reaction followed by the cyclization in basic media (8 mg, 0.15 mmol of KOH) afforded after a TLC semipreparative purification 15 mg (0.03 mmol, 19%) of product **51**.

After the analysis of the product, two conformational isomers were observed by NMR; **A** and **B** with a ratio of 1: 0.8.

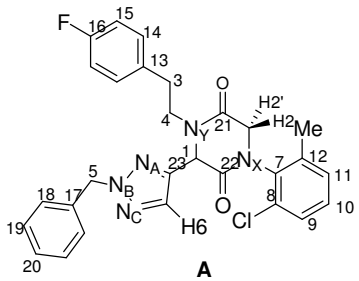

**A**

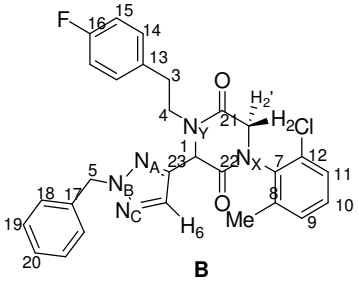

**B**

**$^1$H-NMR (500 MHz, $CDCl_3$):** δ (ppm) 7.73 (s, 1H, H6B), 7.69 (s, 1H, H6A), 7.42-7.33 (m, Ar), 7.33-7.30 (m, Ar), 7.26-7.15 (m, Ar), 7.09 (d, *J* = 7.0 Hz, 2H, H11A), 7.01 (t, *J* = 8.5 Hz, 1H, H15A), 7.00 (t, *J* = 8.5 Hz, 1H, H15B), 5.59 (dd, *J* = 19.5, 13.5 Hz, 1H, H5B), 5.58 (dd, *J* = 35.5, 14.5 Hz, 1H, H5A), 5.14 (s, 1H, H1B), 5.01 (s, 1H, H1A), 4.71 (dd, *J* = 17.0, 1.8 Hz, 1H, H2'B), 4.49 (dd, *J* = 16.8, 1.8 Hz, 1H, H2'A), 4.24 (m, 2H, H4A,B), 4.01 (d, *J* = 16.8 Hz, 1H, H2A), 3.77 (d, *J* = 16.9 Hz, 1H, H2B), 3.18 (m, 1H, H4B), 3.09 (m, 1H, H4A), 2.99 (m, 2H, H3AiB), 2.84 (m, 2H, H3A,B), 2.18 (s, 3H, MeB), 1.78 (s, 3H, MeA) **$^{13}$C-NMR (100 MHz, $CDCl_3$):** δ (ppm) 164.81 (C21A), 162.89 (C22B), 162.61 (C22A), 161.64 (C16), 143.79 (C23A), 143.02 (C23B), 138.55 (C12A), 137.55 (C12B), 135.1 (C7B), 134.99 (C7A), 134.57 (C17), 133.5 (C13), 133.35 (C6A), 133.17 (C6B), 132.72 (C8A), 132.03 (C8B), 129.36 (C11A), 128.77 (C9A), 127.89 (C18), 115.59 (C15A), 115.36 (C15B), 58.95 (C5), 58.16 (C1A), 58.09 (C1B), 46.87 (C4A), 46.46 (C4B), 32.80 (C3), 17.62 (CMeB), 17.05 (CMeA) **$^{15}$N-NMR ($CDCl_3$, 40.5 MHz):** δ (ppm): -264.7(NY), -259.2 (NX), -121.7 ($NB_{(B)}$), -120.8 ($NB_{(A)}$), -54.6 ($NA_{(A)}$), -53.6 ($NA_{(B)}$), -46.9 (NC)
**HRMS for $C_{28}H_{25}ClFN_5O_2$:** Calculated: 518.1759 $(M+H)^+$; Found: 518.1774.

## 1-(2,6-Dimethylphenyl)-3-[2'-(2,4-dichlorophenehyl)-1,2,3-triazol-4'-yl]-4-(3,3-diphenylpropyl) piperazine-2,5-dione (52)

Following the above procedure, from 3,3-diphenylpropylamine (45 μL, 0.24 mmol), aldehyde **5c** (65 mg, 0.24 mmol), 2,6-dimethylphenylisocyanide (30 mg, 0.24 mmol) and chloroacetic acid (25 mg, 0.24 mmol), the Ugi reaction was performed followed by the cyclization in basic media (15 mg, 0.24 mmol of KOH in 3 mL of MeOH) and although the major compound was the DKP scaffold (**52DKP**), 10% of the β-lactam (**52**) was observed in the $^1$H NMR before purification. After a reverse-phase chromatography 35 mg (0.05 mmol, 21%) of product **52βLac** were obtained.

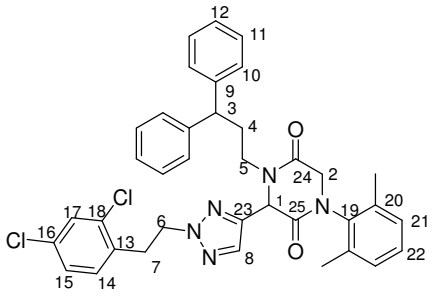

**$^1$H-NMR: ($CDCl_3$, 500 MHz):** δ (ppm): 7.41 (s, 1H, H8), 7.36 (d, *J* = 2.1 Hz, 1H, H17), 7.31-7.27 (m, 6H, H11, 12), 7.24-7.17 (m, 4H, H10), 7.14 (d, *J* = 6 Hz, 2H, H21), 7.07 (m, 1H, H22), 7.04 (dd, *J* = 8.2, 2.1 Hz, 1H, H15), 6.89 (d, *J* = 8.2 Hz, 1H, H14), 5.09 (s, 1H, H1), 4.62 (m, 2H, H6), 4.53 (d, *J* = 17.2 Hz, 1H, H2), 3.96 (t, *J* = 7.8 Hz, 1H, H3), 3.85 (d, *J* = 17.2 Hz, 1H, H2), 3.83 (m, 1H, H5), 3.29 (m, 2H, H7), 2.82 (m, 1H, H5), 2.42 (m, 1H, H4), 2.34 (m, 1H, H4), 2.25 (s, 3H, Me), 1.98 (s, 3H, Me)
**HRMS for $C_{37}H_{35}Cl_2N_5O_2$:** Calculated: 652.2246 $(M+H)^+$; Found: 652.2231.

## 6.7. Synthesis and characterization of compounds in Chapter 4

### 6.7.1. Synthesis of small molecules

### *N*-(Ethyl-2-acetate)-2-[2-(2,4-dichlorophenethyl-1*H*,1,2,3-triazol-4-yl]-3-(3,3-diphenylpropyl)aza-4-oxo-5-chloropentanoic acid amide (54)

Following the procedures of the Ugi reaction described in 6.2, from 3,3-diphenylpropylamine (120 mg, 0.58 mmol), aldehyde **5c** (155 mg, 0.58 mmol), ethyl-2-isocyanoacetate (65 µL, 0.57 mmol) and chloroacetic acid (55 mg, 0.58 mmol), the reaction afforded after a chromatographic column purification, 242 mg (0.36 mmol, 63%) of compound **54**.

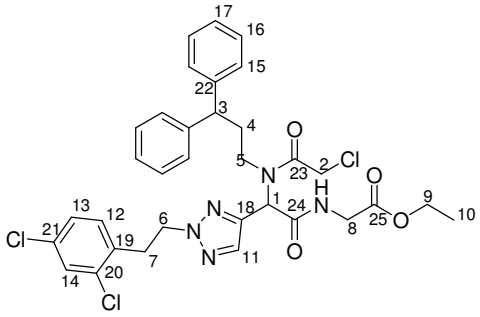

**$^{1}$H-NMR ($CDCl_3$, 500 MHz):** δ (ppm): 7.76 (s, 1H, H11), 7.35 (d, *J* = 2 Hz, 1H, H14), 7.30-7.27 (m, 4H, H16), 7.21-7.16 (m, 6H, H15, 17), 7.05 (dd, *J* = 8.2, 2 Hz, 1H, H13), 6.9 (m, 1H, NH), 6.89 (d, *J* = 8.2 Hz, 1H, H12), 5.54 (s, 1H, H1), 4.63 (t, *J* = 7.1 Hz, 2H, H6), 4.19 (q, *J* = 7.1 Hz, H9), 4.09 (dd, *J* = 18, 5 Hz, 1H, H8), 3.97 (dd, *J* = 18, 5 Hz, 1H, H8), 3.83 (t, *J* = 8 Hz, 1H, H3), 3.77 (s, 2H, H2), 3.3 (m, 4H, H7, H5), 2.3 (m, 1H, H4), 2.2 (m, 1H, H4), 1.27 (t, *J* = 7.1 Hz, 3H, H10) **$^{13}$C-NMR ($CDCl_3$, 100 MHz):** δ (ppm) 169.3 (C25), 167.3 (C24), 167.2 (C23), 143.3 (C22), 143.2 (C22), 142.4 (C18), 134.9 (C11), 134.8 (C20), 133.5 (2C, C19,21), 131.6 (C12), 129.5 (C14), 128.8 (2C, C16), 128.7 (2C, C16), 127.6 (2C, C15), 127.5 (2C, C15), 127.2 (C13), 126.8 (C17), 126.7 (C17), 61.5 (C9), 56.9 (C1), 54.0 (C6), 48.4 (C3), 47.4 (C7), 41.6 (C8), 40.9 (C2), 34.8 (C4), 33.5 (C5), 14.1 (C10) **HRMS for $C_{33}H_{35}Cl_3N_5O_4$:** Calculated: 670.1755 $(M+H)^+$; found: 670.1794; Calculated: 693.1652 (M+Na)+; found: 693.1608.

### *N*-Carboxymethyl-2[2-(2,4-dichlorophenethyl)-2*H*-1,2,3-triazol-4-yl]-1-(3,3-diphenyl propyl)-4-oxoazetidine-2-carboxamide (55)

To a 190 mg (0.28 mmol) of **54** solved in 10 mL THF: $H_2O$ (1:1), 15 mg (2 eq) of LiOH were added and stirred for 6 hours at room temperature. The solvent was evaporated and the mixture was treated with 10 mL of HCl and extracted with EtOAC (3 x 20 mL), dried with $MgSO_4$ and evaporated, obtaining 144 mg (0.24 mmol, 85%) of the acid **55** with 95% purity.

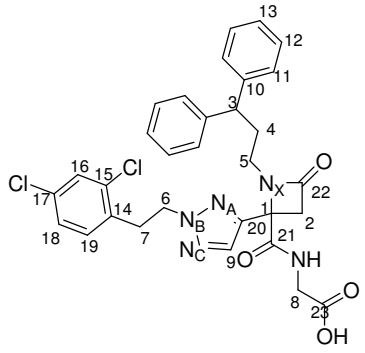

**$^{1}$H-NMR ($CDCl_3$, 500 MHz):** δ (ppm): 7.61 (s, 1H, H9), 7.36 (d, *J* = 2.1 Hz, 1H, H16), 7.24-7.21 (m, 4H, H12), 7.18-7.14 (m, 6H, H11, H13), 7.09 (t, *J* = 5.2 Hz, 1H, NH), 7.05 (dd, *J* = 2.1, 8.2 Hz, 1H, H18), 6.89 (d, *J* = 8.2 Hz, 1H, H19), 4.60 (t, *J* = 7.1 Hz, 2H, H6), 4.05 (dd, *J* = 5.3, 1.6 Hz, 2H, H8), 3.88 (t, *J* = 7.8 Hz, 1H, H3), 3.46 (d, *J* = 14.5 Hz, 1H, H2), 3.35 (d, *J* = 14.5 Hz, 1H, H2), 3.28 (t, *J* = 7.1 Hz, 2H, H7), 3.14 (m, 1H, H5), 3.09 (m, 1H, H5), 2.35 (m, 2H, H4) **$^{13}$C-NMR ($CDCl_3$, 100 MHz):** δ (ppm): 171.1 (C23), 169.3 (C21), 167.2 (C22), 144.1 (C20), 143.5 (C10), 134.7 (C15), 133.5 (C17), 133.3 (C14), 131.4 (C19), 129.3 (C16), 127.6 (C18), 127.5 (C11), 128.4 (CAr), 126.3 (CAr), 58.5 (C1), 53.8 (C6), 48.6 (C3), 41.3 (C5), 33.0 (C7), 32.7 (C4) **$^{15}$N-NMR ($CDCl_3$, 41.5 MHz)**: δ (ppm): -277.7

(NH), -227.6 ($N_X$), -123.9 ($N_B$), -55.3 ($N_A$), -48.9 ($N_C$) **HRMS for $C_{31}H_{29}Cl_2N_5O_4$:** Calculated: 606.1675 $(M+H)^+$; found: 606.1711.

## *N*-((2-Aminoethylcarbamoyl)methyl)-2-(2,4-dichlorophenethyl)-2*H*-1,2,3-triazol-4-yl)-1-(3,3-diphenylpropyl)-4-oxoazetidine-2-carboxamide (56)

70 mg (0.12 mmol) of compound **55**, 20 µL (0.12 mmol) of *N*-Boc-ethylenediamine and 15 mg (1.1 eq) of HOBt were dissolved in DCM and treated with *N,N*-diisopropylethylamine (40 µL, 2 eq) and then with EDC (25 mg, 1.1 eq) and stirred overnight at room temperature. Then DCM was added and the solution was washed with water (3 x 10 mL) and brine (3 x 10 mL), dried over MgSO4 and the solvent was evaporated under reduced pressure to give 95 mg that were purified by column chromatography EtOAC/ hexane (1/4) to obtain 40 mg (0.06 mmol, 49%) of the desired compound with the Boc-Nprotected group. Then, to 40 mg (0.06 mmol) of the previous compound dissolved in DCM (5 mL), excess of trifluoroacetic acid was added and stirred 2 hours at room temperature. The reaction was washed with water (3 x 10 mL) and dried over MgSO4 to obtain 20 mg (0.02 mmol, 24%) of compound **56**.

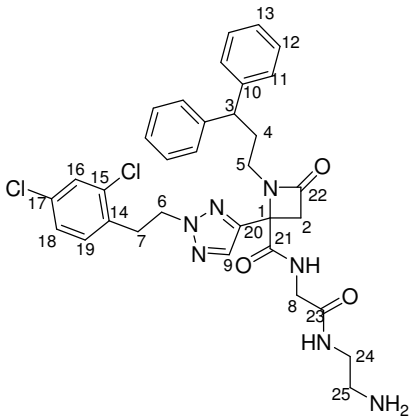


**$^1$H-NMR ($CDCl_3$, 500 MHz):** δ (ppm): 7.63 (s, 1H, H9), 7.35 (d, *J* = 2.1 Hz, 1H, H16), 7.24-7.21 (m, 4H, H12), 7.18-7.14 (m, 6H, H11, H13), 7.04 (dd, *J* = 2.1, 8.2 Hz, 1H, H18), 6.89 (d, *J* = 8.2 Hz, 1H, H19), 4.54 (t, *J* = 7.1 Hz, 2H, H6), 3.94 (m, 2H, H8), 3.84 (t, *J* = 7.8 Hz, 1H, H3), 3.56 (d, *J* = 14.5 Hz, 1H, H2), 3.39 (d, *J* = 14.5 Hz, 1H, H2), 3.8 (m, 2H, H24), 3.23 (t, *J* = 7.1 Hz, 2H, H7), 3.14 (m, 2H, H5), 2.95 (m, 2H, H25), 2.3 (m, 2H, H4) **HRMS for $C_{33}H_{35}Cl_2N_7O_3$:** Calculated: 648.2257 $(M+H)^+$; found: 648.2258.

## 1-(3',3'-Diphenylpropyl)-4-[2'-(2'',4''-dichlorophenyl)ethyl]-7-[*N*-(*N*-(2-aminoethyl)carbamoyl)-*N*-[2'-(2'',4''-dichlorophenyl)ethyl]aminocarbonyl] perhydro-1,4-diazepin-2,4-dione (58)

Following the previous procedure, 74 mg (0.096 mmol) of compound **57**,15 µL (0.09 mmol) of *N*-Boc-ethylendiamine, 14 mg (1.1 eq) of HOBt were dissolved in DCM and treated with 33 µL (2 eq) of *N,N*-diisopropylethylamine and then with 20 mg (1.1 eq) of EDC and stirred overnight at room temperature. After washing and drying, 80 mg (0.09 mmol, 90%) of the compound with the *N*-Boc-ethylenediamine were obtained. The deprotection step was carried out by treatment with TFA. A solution of this compound in DCM was stirred for 2 hours at room temperature, followed by washes with water (3 x 10 mL) and drying over $MgSO_4$, to finally yield 75 mg (0.09 mmol, 95%) of compound **58**.

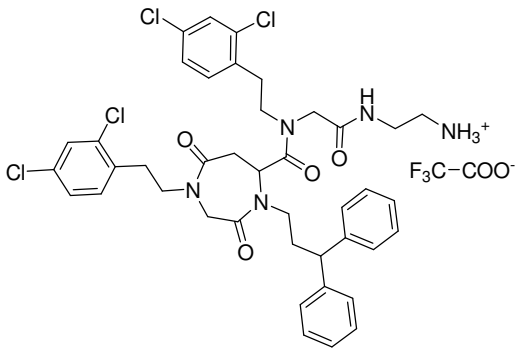

**$^1$H-NMR ($CDCl_3$, 500 MHz):** δ (ppm): 7.45-7.06 (16H, $CH_{Ar}$), 4.52 (dd, *J* = 9.2 y 6.6 Hz, 1H, NCH), 4.45 (d, *J* = 16.8 Hz, 1H, $COCH_2$), 4.41 (t, *J* = 8.4 Hz, 1H, NCH), 4.35 (d, *J* = 17.1 Hz, 1H, $COCH_2$), 4.18 (d, *J* = 17.1 Hz, 1H, $COCH_2$), 3.90-3.56 (1H x CH + 2H x $COCH_2$ + 4 H x $N\underline{CH_2}CH_2$), 3.8 (m, 2H, CO-NH-$\underline{CH_2}CH_2$), 3.37-2.40 (8H, 2H x $N\underline{CH_2}CH_2$ + 4H x $NCH_2\underline{CH_2}$ + 2H x $CO\underline{CH_2}CH$), 2.9 (m, 2H, $\underline{CH_2}$-$NH_2$), 2.31-2.20 (2H, $NCH_2\underline{CH_2}CH$).

### 6.7.2. Preparation of dense-shell glycodendrimers

## Coupling of the spacer with the 5$^{th}$ Generation PPI (60)

Boc-O2Oc-O2Oc-OH spacer (0.465 g, 1.14 mmol) was dissolved in 20 mL of DMSO, BOP (504 mg, 1.14 mmol) was added to the solution and the mixture was stirred for 1 hour at room temperature. 5$^{th}$ Generation PPI dendrimer (DAB/Am64) (815 mg, 0.114 mmol) and $Et_3N$ (0.6 mL) were dissolved in 20 mL DMSO and the spacer solution was added over this one. The reaction was stirred for 24 hours. Then, the crude mixture product was purified by dialysis with deionised water for 1 day, exchanging water regularly. Compound **60** with 10 spacers was obtained from freeze drying as a white solid. (1.35 g, 0.12 mmol, 100%).

**$^1$H-NMR ($D_2O$, 500 MHz):** δ (ppm): 4.07 (s, H8), 4.05 (s, H2), 3.72 (m, H3, 4, 9, 10), 3.66 (t, *J* = 5.1 Hz, H5), 3.60 (t, *J* = 5.3 Hz, H11), 3.48 (t, *J* = 5.5 Hz, H6), 3.27 (m, H12), 3.25 (m, Hq), 2.75 (-$CH_2$-$NH_2$), 2.55-2.47 (b,c,e,f,h,i,k,l,n,o), 1.69-1.65 (a,d,g,j,m,p), 1.43 (s, H15). **$^{13}$C-NMR ($D_2O$, 125 MHz):** δ (ppm): 175.3 (C7), 174.9 (C1), 160.7 (C13), 83.5 (C14), 73.3 (C3), 73.2 (C9), 72.4 (C2,8), 72.2 (C4,10,11), 71.7 (C5), 55-53 (Cb,c,e,f,h,I,k,l,n,o), 42.5 (C12), 41.7 ($CH_2$-$NH_2$), 4.13 (C6), 40.2 (Ca), 30.7 (C15), 29.4-24.9 (Cd, g, j, m, p).

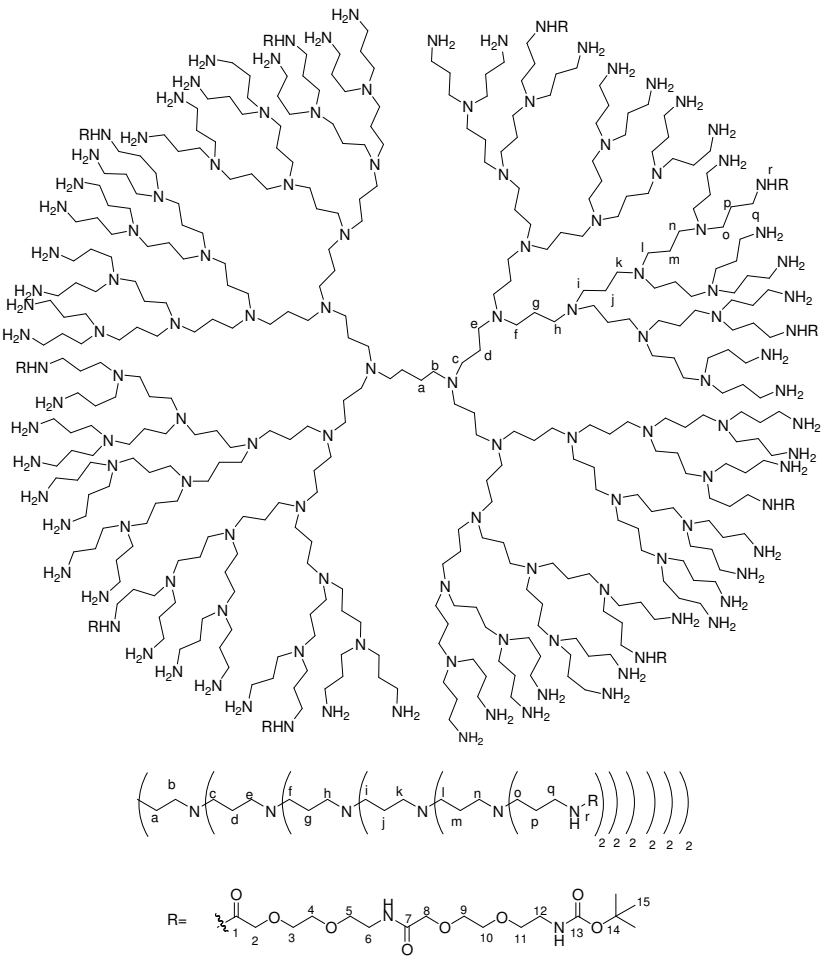

## Dense-shell glycodendrimer containing the spacer (61)

The previous dendrimer **60**, (0.3 g, 0,027 mmol), maltose (14.6 g, 40 mmol) and borane-pyridine complex (10 mL, 81 mmol, 8M solution) were taken up in a sodium borate buffer (50 mL, 0.1 M, pH = 9). The reaction mixture was stirred at 50°C for 7 days. Then, the crude mixture product was purified by dialysis with deionised water for 4 days and after freeze drying, 744 mg (0,015mmol, 57%) of the glycodendrimer **61** were obtained.

**$^{1}$H-NMR ($D_2O$, 500 MHz):** δ (ppm): 5.12 (H1''), 4.08 (H2), 3.98 (s, H8), 3.85-3.78 (H3,4,5), 3.73 (H9,10), 3.60 (H11), 3.48 (H6), 3.43-3.90 (2',2'',3',3'',4',4'',5',5'',6',6''), 3.27 (H12,q), 2.86 (H1'), 2.52-2.95 (b,c,e,f,h,i,k,l,n,o), 1.75 (a,d,g,j,m,p), 1.43 (H15) **$^{13}$C-NMR ($D_2O$, 125 MHz):** δ (ppm): 175.4 (C7), 175.5 (C1), 160.8 (C13), 103.5 (C1''), 85.4 (C4'), 83.6 (C14), 79.2 (C2''), 73.3 (C3, 9), 72.4-72.2 (C2,4,8,10,11,2',3'',4'',5',5''), 71.7 (C5), 70.9 (C2''), 65.6 (C6'), 65.2 (C6''), 59.9 (C1'), 52-56 (Cb,c,e,f,h,i,k,l,n,o), 42.5 (C12), 41.3 (C6), 40.0 (Ca), 30.7 (C15), 27,7-24.4 (Cd,g,j,m,p). **LILBID-MS: m/z** calcd for $C_{1842}H_{3743}N_{146}O_{1160}$: 46511 (relating to 108 maltose units connected to the surface of 5$^{th}$ generation PPI; found 42850 [M-8maltose]$^{-}$.

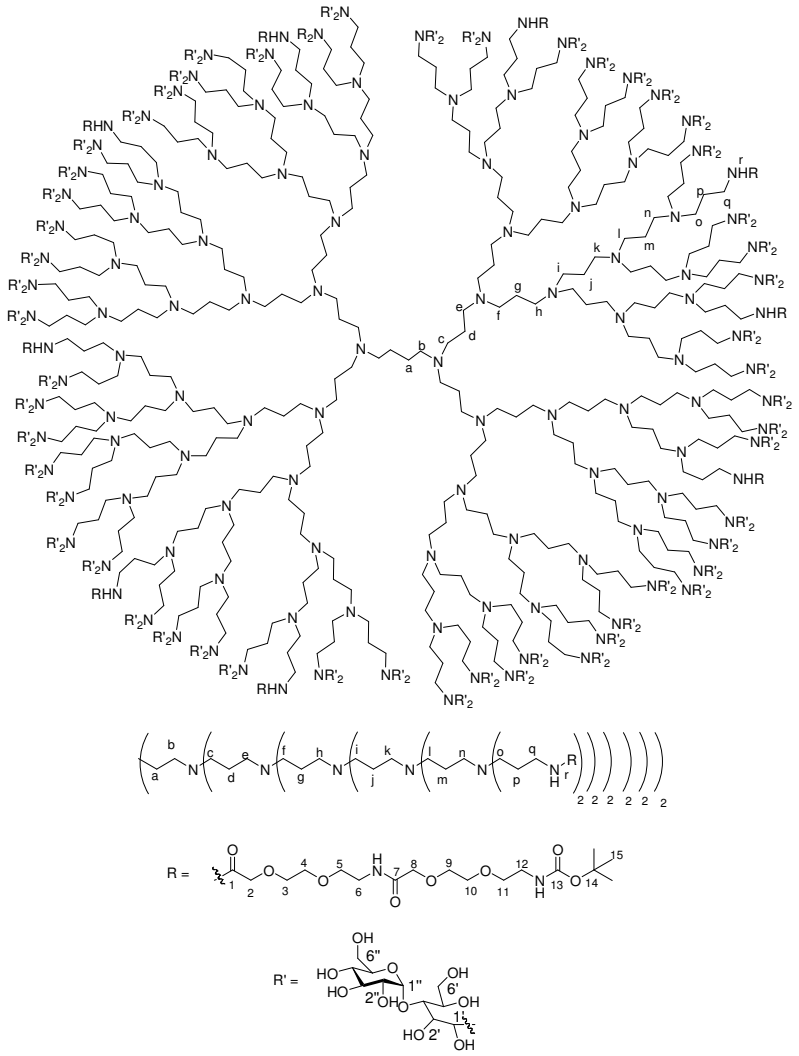

## Dense-shell glycodendrimer containing the deprotected spacer (62)

A solution of the previous glycodendrimer **61** (600 mg, 0.012 mmol) in 15 mL of water was treated with 30 mL of HCl (4M in dioxane). The mixture was stirred overnight and purified by dialysis with deionised water for 6 hours exchanging water frequently. After freeze drying, 202 mg (0.004 mmol, 100%) of the deprotected product **62** were obtained.

**$^1$H-NMR ($D_2O$, 500 MHz):** δ (ppm): 5.12 (H1''), 4.11 (H2,8), 3.87-3.78 (H3,4,5), 3,75 (H9,10), 3.60 (H11), 3.48 (H6), 3.43-3.90 (2',2'',3',3'', 4',4'',5',5'',6',6''), 3.30 (Hq), 3.20 (H12), 2.86 (H1'), 2.60-3.0 (b,c,e,f,h,i,k,l,n), 1.90-1.75 (a,d,g,j,mp) **$^{13}$C-NMR ($D_2O$, 125 MHz):** δ (ppm): 175.3 (C1,7), 163.0 (C13), 103.5 (C1''), 85.2 (C4'), 75.8 (C2''), 75.4 (C5',5''), 74.5 (C2',3''), 73.2 (C3,9), 72.3 (C2,8, 4'), 71.6 (C5), 70.8 (C2''), 65.2 (C6'), 63.4 (C6''), 59.7 (C1'), 52.7-55.1 (Cb,c,e,f,h,i,k,l,n,o), 41.9 (C6), 41.2 (C12), 39.4 (Cq), 23.5 (Cd,g,j,m,p). **IR:** ν = 3300 (OH), 2900 (CH, $CH_2$), 1660 (C=O amide st), 1560 (NH δ), 1440 ($CH_2$ δ), 1015 (C-N amine st).

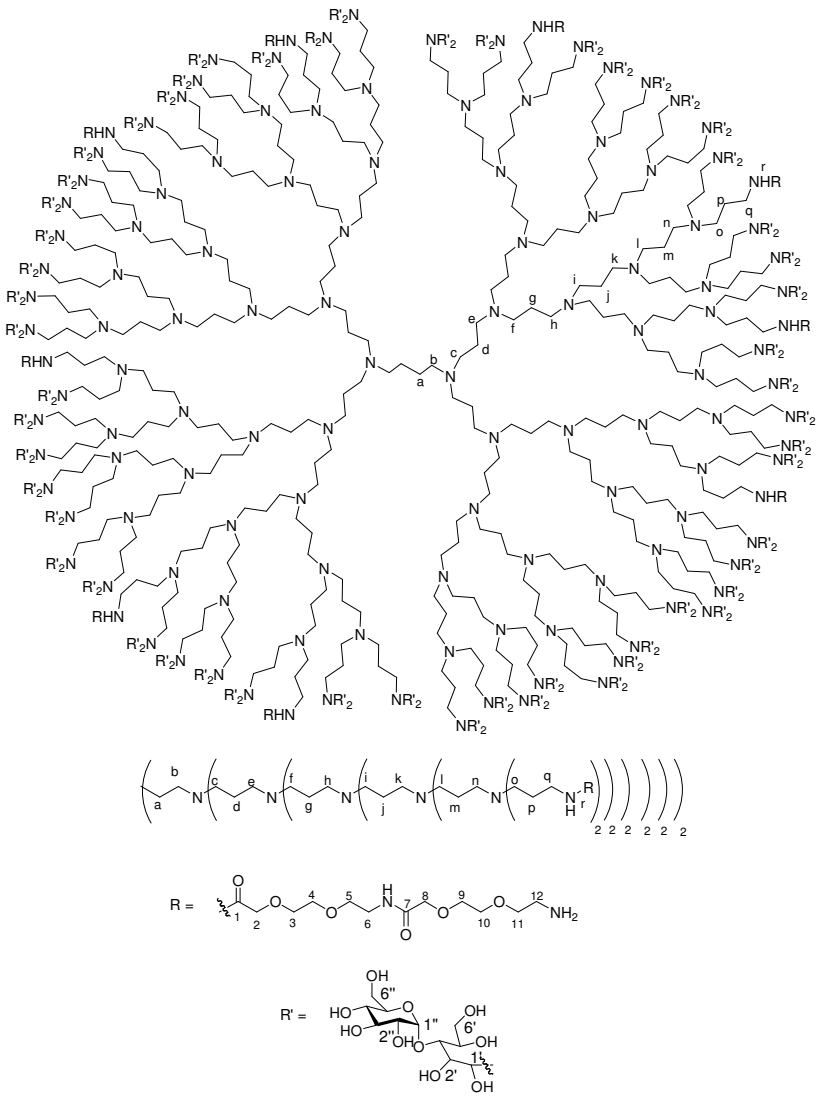

### 6.7.3. Couplings with the maltose dense-shell PPI glycodendrimers

## 1st Coupling: Compound 63

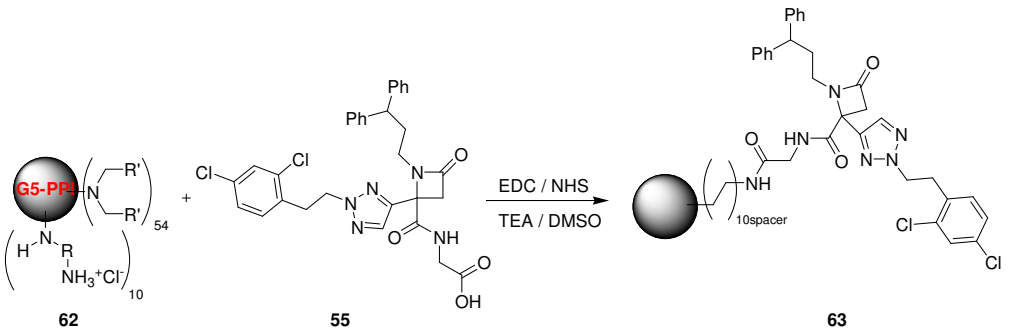


**62** **55** **63**

A mixture of 100 mg (0.002 mmol) of glycodendrimer **62** and 10 mL of DMSO was heated at 80°C until a solution was formed and then it was cooled down at 37°C. At his point, 0.2 mL of

$Et_3N$ was added. Simultaneously, 5 eq. (6.5 mg, 0.01 mmol) of the small molecule (cf. 6.7.1) were dissolved in 10 mL DMSO, EDC (0.8 mg, 0.004 mmol) was added to this solution and stirred for 1 hour. Then NHS (0.9 mg, 0.004 mmol) was added and the new mixture was stirred for more 2 hours. Finally this solution was added to the glycodendrimer solution and stirred overnight. The crude reaction mixture was purified by dyalisis exchanging water, water/THF and water again regularly. This solution was washed with $CHCl_3$ (3 x 20 mL) and after freeze drying, 90 mg (0.002 mmol, 95%) of product were obtained.

The aromatic signals present in the $^1H$ NMR ($D_2O$) allowed us to know that the desired coupling took place. By integration it was estimated an average of 2 equivalents of **55** per polymer unit.

**$^1$H-NMR ($D_2O$, 500 MHz):** δ (ppm): 7.30-6.90 (Ar), 5.12 (H1''), 4.10 (H2,8), 3.89-3.80 (H3,4,5), 3.75 (H9,10), 3.60 (H11), 3.48 (H6), 3.43-3.90 (2',2'',3',3'',4',4'',5',5'',6',6''), 3.30 (Hq), 3.20 (H12), 2.86 (H1'), 2.60-3.0 (b,c,e,f,h,i,k,l,n), 1.90-1.75 (a,d,g,j,m,p). **IR:** ν = 3340 (OH), 2950 (CH, $CH_2$), 1660 (C=O amide st), 1570 (NH δ), 1450 ($CH_2$ δ), 1030 (C-N amine st).

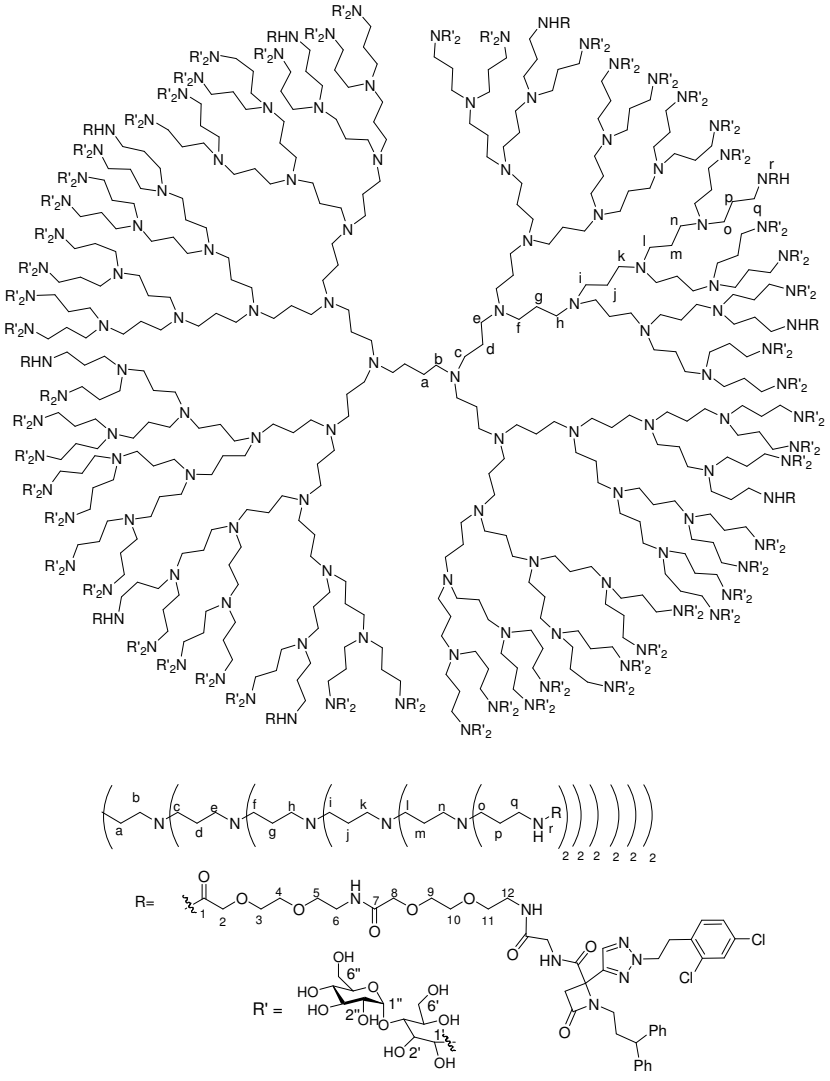

## 2nd Coupling: Compound 64

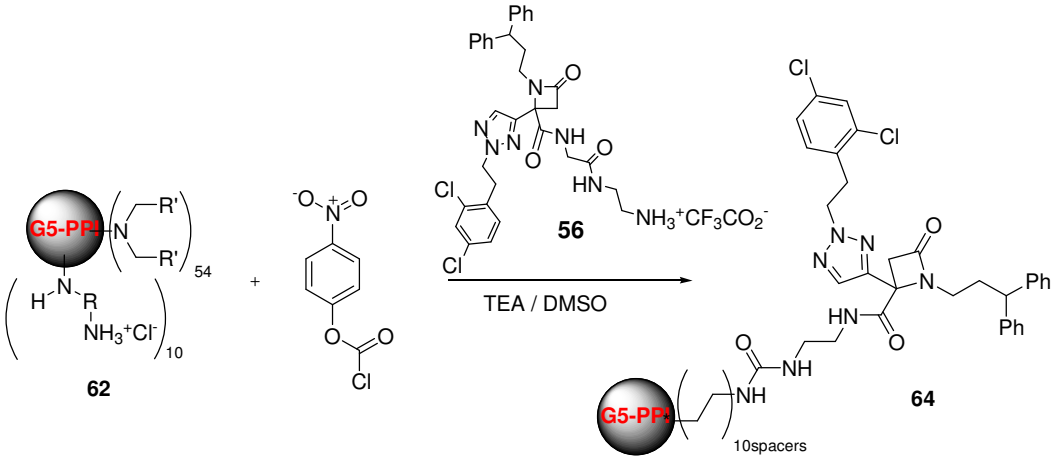


Modified PPI dendrimer **62** (100 mg, 0.002 mmol) was dissolved in dried DMSO, $Et_3N$ (3 eq, 0.45 mL) was added and the mixture was stirred for 30 min. On the other hand, a solution of the small molecule **56** (of section 5.7.1) (5 eq, 0.01 mmol, 6.5 mg) in dry DMSO was treated with $E_3N$ (1.5 eq, 1.1 mL) and *p*-nitrophenyl chloroformate (1.2 eq, 2.42 mg) and stirred for 30 min at room temperature. Then this solution was added to the glycodendrimer solution and the mixture was stirred overnight at the same temperature. After 24h dyalisis and freeze drying, the analysis of the crude reaction mixture revealed that the reaction did not work as expected, the coupling had not been produced.

## 3rd Coupling:

### - Preparation of compound 65

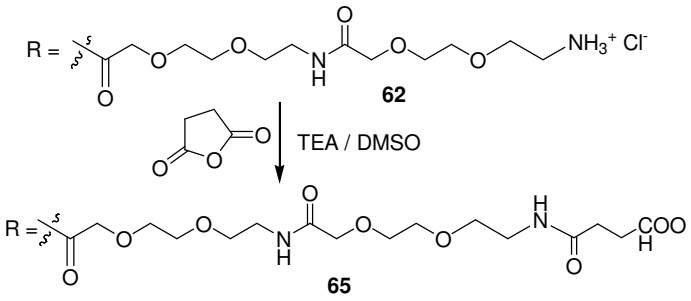


A solution of the maltose-modificed dendrimer **62** (100 mg, 0.002 mmol) in 15 mL of DMSO was heated at 35°C under argon atmosphere. Then, this solution was treated with 0.05 mL of $Et_3N$ and succinic anhydride (13 mg, 0.128 mmol) and the mixture was stirred overnight at room temperature. The crude reaction mixture was subjected to dyalisis for 2 days and freeze drying, to give 65 mg (0.00135 mmol, 68%) of the desired product.

**$^1$H-NMR ($D_2O$, 500 MHz):** δ (ppm): 5.12 (H1''), 4.11 (H2,8), 3.87-3.78 (H3,4,5), 3.75 (H9), 3.60 (H11), 3.45 (H10), 3.42 (H6), 3.43-4.00 (2',2'',3',3'', 4',4'',5',5'',6',6''), 3.33 (Hq), 3.50 (H12), 2.86 (H1'), 2.60-3.0 (b,c,e,f,h,i,k,l,n), 2.54-2.44 (H14,H15),1.90-1.75 (a,d,g,j,mp) **$^{13}$C-NMR ($D_2O$, 125 MHz):** δ (ppm): 178.7 (C16), 178.3 (C13), 175.4 (C1), 175.3 (C7), 103.5 (C1''), 85.2 (C4'), 75.8 (C2''), 75.2 (C5',5''), 74.5 (C2',3''), 73.5 (C3,11), 72,5 (C9), 72.2 (C2,8), 71.7 (C5), 71.6 (C10), 70.8 (C2''), 65.2 (C6', 6''), 63.4 (C4), 59.7 (C1'), 52.3-55.7 (Cb,c,e,f,h,i,k,l,n,o), 41.8 (C6), 41.2 (C12), 39.3 (Cq), 35.9, 35.2 (C15, C14), 23.5 (Ca,d,g,j,m,p). **IR:** ν = 3400 (OH), 2960 (CH, $CH_2$), 1740 (C=O, acid st),1660 (C=O amide st), 1570 (NH δ), 1420 ($CH_2$ δ),1030 (C-N amine st).

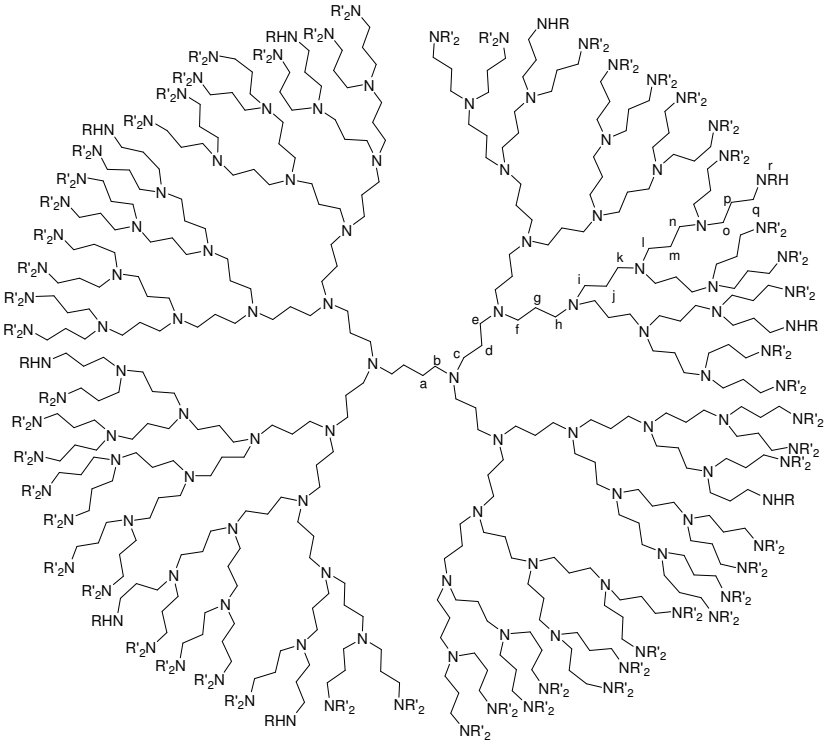


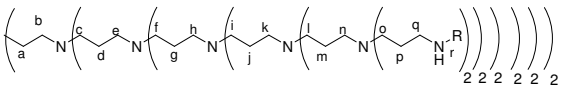

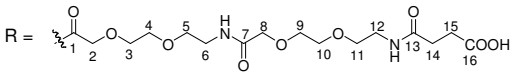


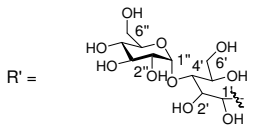

- **Compound 66**

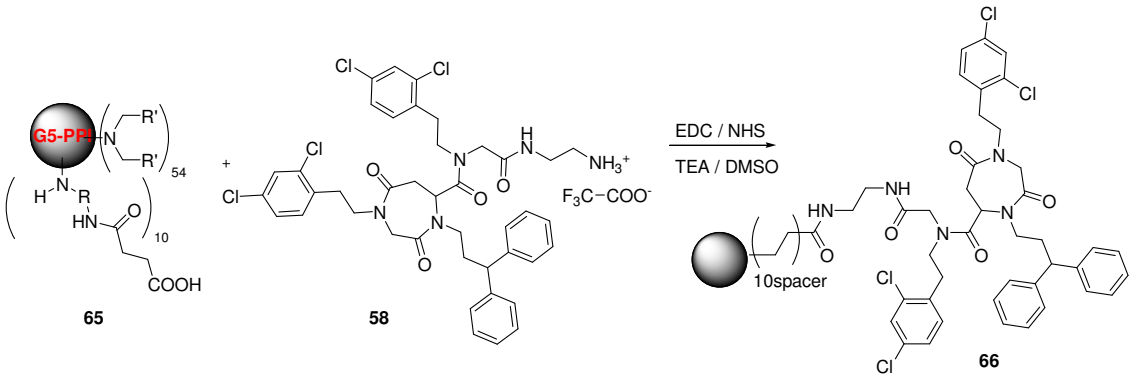


A mixture of the glycodendrimer **65** (100 mg, 0.002 mmol) and 5 mL of DMSO was heated at 80ºC and then cooled down. This solution was treated with EDC (0.79 mg, 0.004 mmol) and stirred for 1 hour at room temperature. Then *N*-hydroxysulfosuccinimide sodium salt (0.9 mg, 0.004 mmol) was added and the new mixture was stirred for 2 hours at the same temperature. Separately, compound **58** (8.5 mg, 0.01 mmol) was dissolved in 5 mL DMSO and $Et_3N$ (0.2 mL) and this solution was mixed with the glycodendrimer solution and stirred for 24 hours at the same temperature. The crude reaction mixture was subjected to a dialysis process exchanging water every 30 minuts with water, water / THF and water again. Finally, the solution was washed with $CHCl_3$ (3 x 20 mL) and after freeze drying, 67 mg were obtained. The analysis of the residue by $^1H$ NMR ($D_2O$) did not show the aromatic rings of the small molecule. Then, evaporation of the organic phase from the extractions showed the signals corresponding to compound **58**.

### 6.7.4. Preparation of open-shell glycodendrimers

## Open-shell maltose-PPI-5G-PEG spacer (67)

5$^{th}$ Generation PPI dendrimer **60** (250 mg, 0.022 mmol), D-(+)-maltose monohydrate (190 mg, 0.56 mmol) and the borane-pyridine complex (10 mL, 81 mmol, 8M solution) were dissolved in a sodium borate buffer (50 mL, 0.1 M, pH = 9) solution. The solution was stirred at 50ºC for 7 days. The crude product was then purified by dialysis towards deionized water for 3 days. Dendrimer **67** was obtained (286 mg, 0.016 mmol, 73%) from freeze-drying.

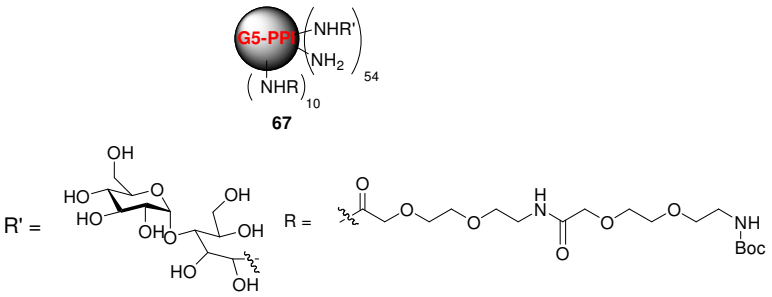

**$^1$H-NMR ($D_2O$, 500 MHz):** δ (ppm): 5.12 (H1''), 4.09 (H2), 4.08 (H8), 3.88-3.80 (H3,4,5), 3.74-3.70 (H9,10), 3.62 (H11), 3.50 (H6), 3.43-3.99 (2',2'',3',3'',4',4'',5',5'',6',6''), 3.27 (H12), 3.05 (Hq), 2.88 (H1'), 2.52-2.88 (b,c,e,f,h,i,k,l,n,o), 1.78-1.68 (a,d,g,j,m,p), 1.45 (H15). **IR:** ν = 3300 (OH), 2900 (CH, $CH_2$), 1660 (C=O amide st), 1550 (NH δ), 1470 ($CH_2$ δ), 1370 ($CH_3$ δ sim, 1050 (C-N amine st).

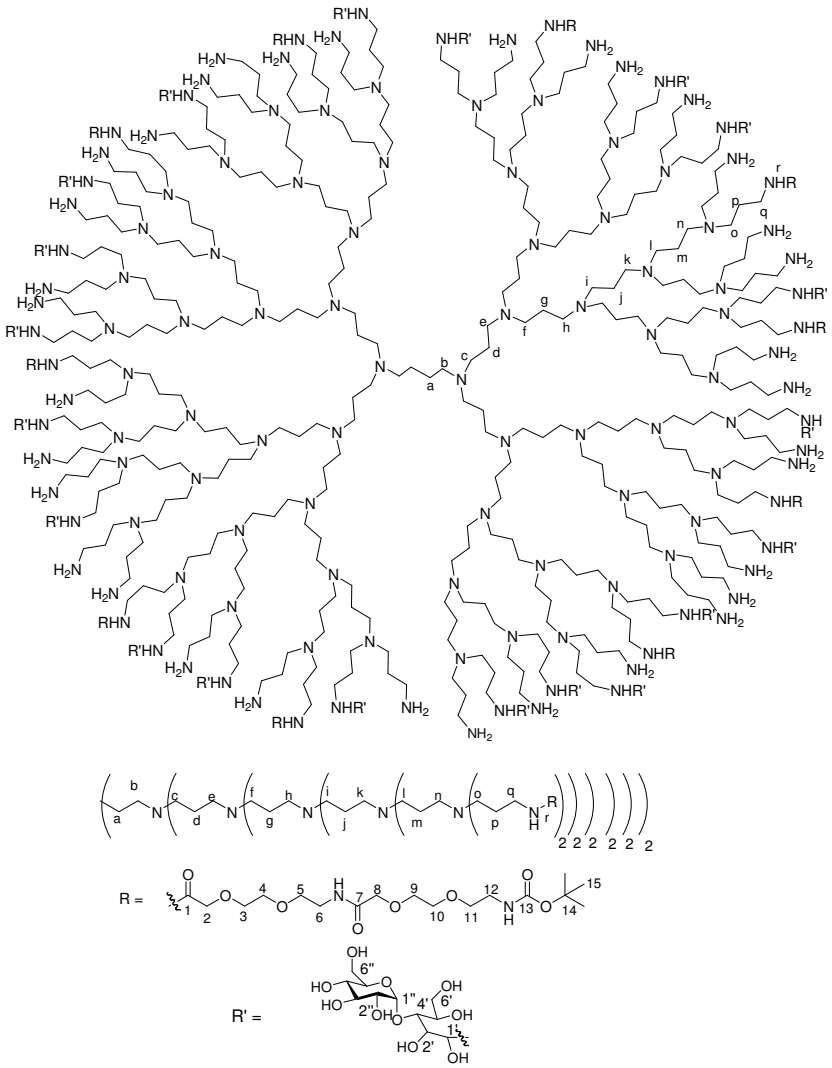

## Open-shell glycodendrimer containing the deprotected spacers (68)

A solution of the previous glycodendrimer **67** (200 mg, 0.01 mmol) in 15 mL of water was treated with 30 mL of HCl (4M in dioxane). The mixture was stirred overnight and purified by dialysis exchanging water regularly and freeze drying to give 77 mg (0.005 mmol, 50%) of product.

**$^1$H-NMR ($D_2O$, 500 MHz):** δ (ppm): 5.12 (H1''), 4.12 (H2), 4.09 (H8), 3.88-3.78 (H3,4,5), 3.77 (H9), 3.75 (H10), 3.68 (H11), 3.49 (H6), 3.43-3.90 (2',2'',3',3'',4',4'',5',5'',6',6''), 3.29 (H12,q), 3.02 (H1'), 2.55-2.80 (b,c,e,f,h,i,k,l,n,o), 1.91.71 (a, d, g, j, m, p)

In the $^1$H NMR, an impurity from the HCl in dioxane can be seen at 7.52 and 7.29 ppm.

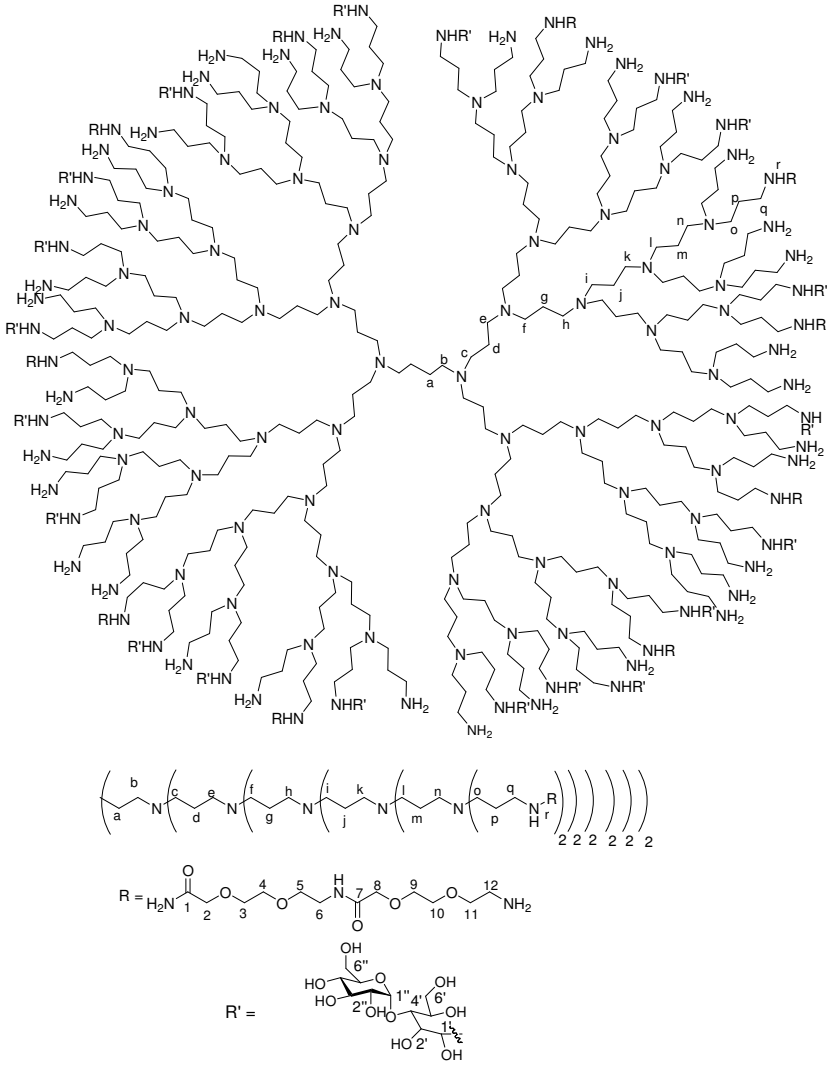

### 6.7.5. Couplings with the maltose open-shell PPI glycodendrimers (69)

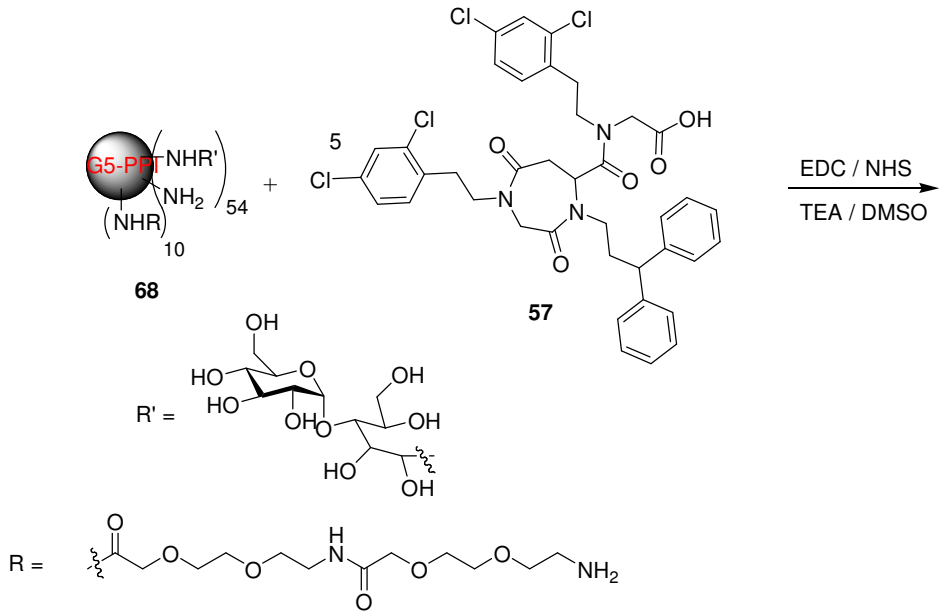


A mixture of 70 mg (0.0045 mmol) of glycodendrimer **68** and 10 mL of DMSO was heated at 80°C until a solution was formed and then in was cooled down at 40°C. At this point, 0.2 mL of $Et_3N$ were added. Simultanoeulsy, 5 eq. of compound **57** (c.f. 5.7.1) (17.5 mg, 0.023 mmol) were dissolved in DMSO, EDC (0.8 mg, 0.013 mmol) was added and the solution was stirred for 1 hour. Then, NHS (3 mg, 0.013 mmol) was added and the new mixture was stirred for 2 more hours. Finally this solution was added to the glycodendrimer solution and stirred for 24 hours at room temperature. After dialysis with combinations of water /THF and freeze drying, 74 mg (100%) of compound **69** was obtained.

The aromatic signals observed in the $^1H$ NMR spectrum revealed that the coupling goal worked out satisfactorily. The amount of drug attached was quantified and the average was 1 equivalent of molecule per polymer unit.

**$^1$H-NMR ($D_2O$, 500 MHz):** δ (ppm): 7.44-7.16 (Ar), 5.12 (H1''), 4.12-4.08 (H2,H8), (3.88-3.76 (H3,4,5), 3.75 (H9, H10), 3.60 (H11), 3.49 (H6), 3.43-4.00 (2',2'',3',3'',4',4'',5',5'',6',6''), 3.27 (H12,q), 3.10 (H1'), 2.36-3.00 (b,c,e,f,h,i,k,l,n,o), 1.91.60 (a, d, g, j, m, p)

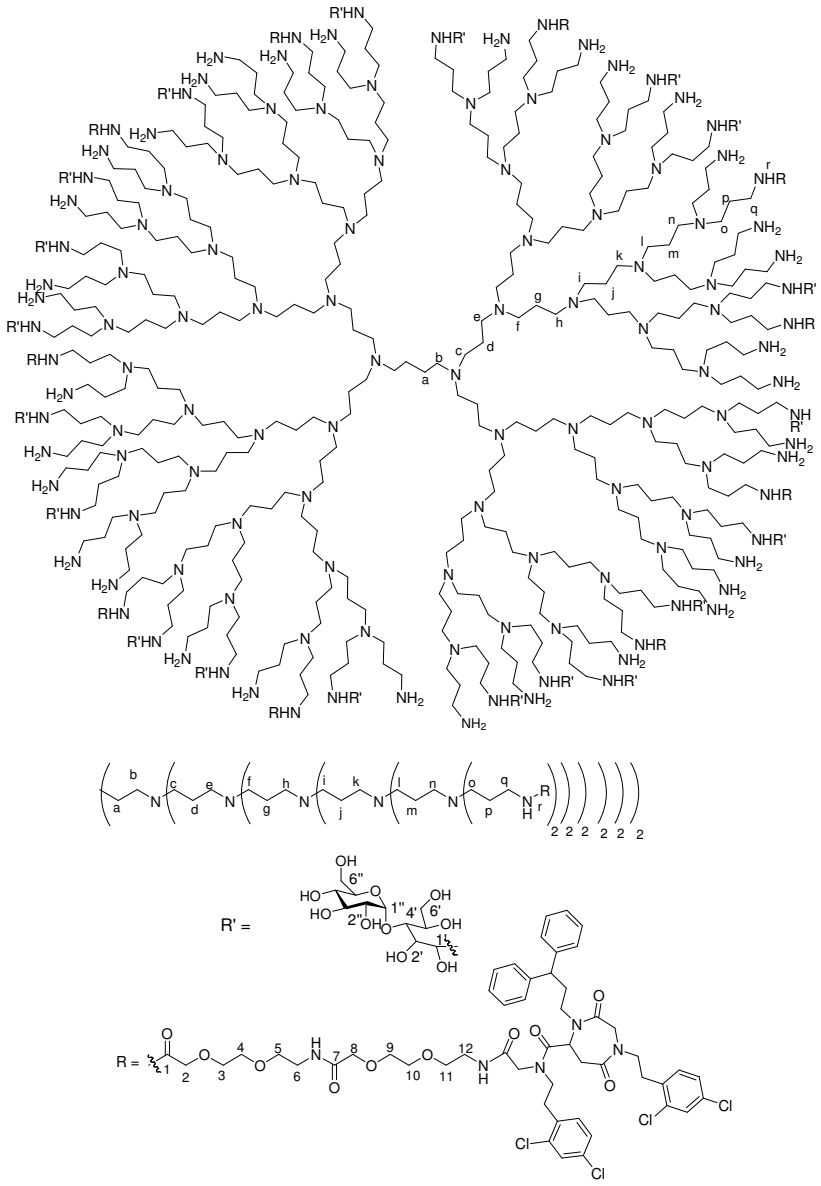

### 6.7.6. Coupling with the open-shell PPI without spacer

## Coupling of small molecule with 5$^{th}$ generation PPI (70)

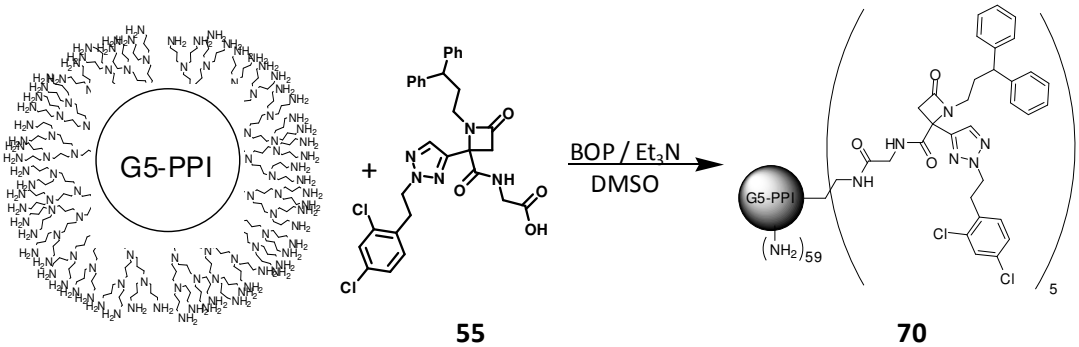


**55** **70**

A mixture of compound **55** (30 mg, 0.05 mmol) and BOP (22 mg, 0.05 mmol) in 2 mL of DMSO was stirred for 1 hour. This mixture was added over a solution of the 5$^{th}$ generation PPI dendrimer (DAB /Am64) (72 mg, 0.01 mmol) and $Et_3N$ (0.06 mL) in 2 mL. The reaction was stirred for 24 hours at room temperature. Then, the crude mixture product was purified by dialysis with deionized water for 1 day exchanging water regularly and after freeze drying 86 mg (0.009 mmol, 86%) of product were obtained. By integration it was estimated an average of 4 equivalents of small drug per polymer unit.

**$^1$H-NMR ($D_2O$, 500 MHz):** δ (ppm): 7.81 (m, triazole), 6.97 (m, Ar), 3.04 (Hq), 2.91-2.35 ((b, c, e, f, h, i, k, l, n), 1.82-1.61 (a,d, g, j, m, p).

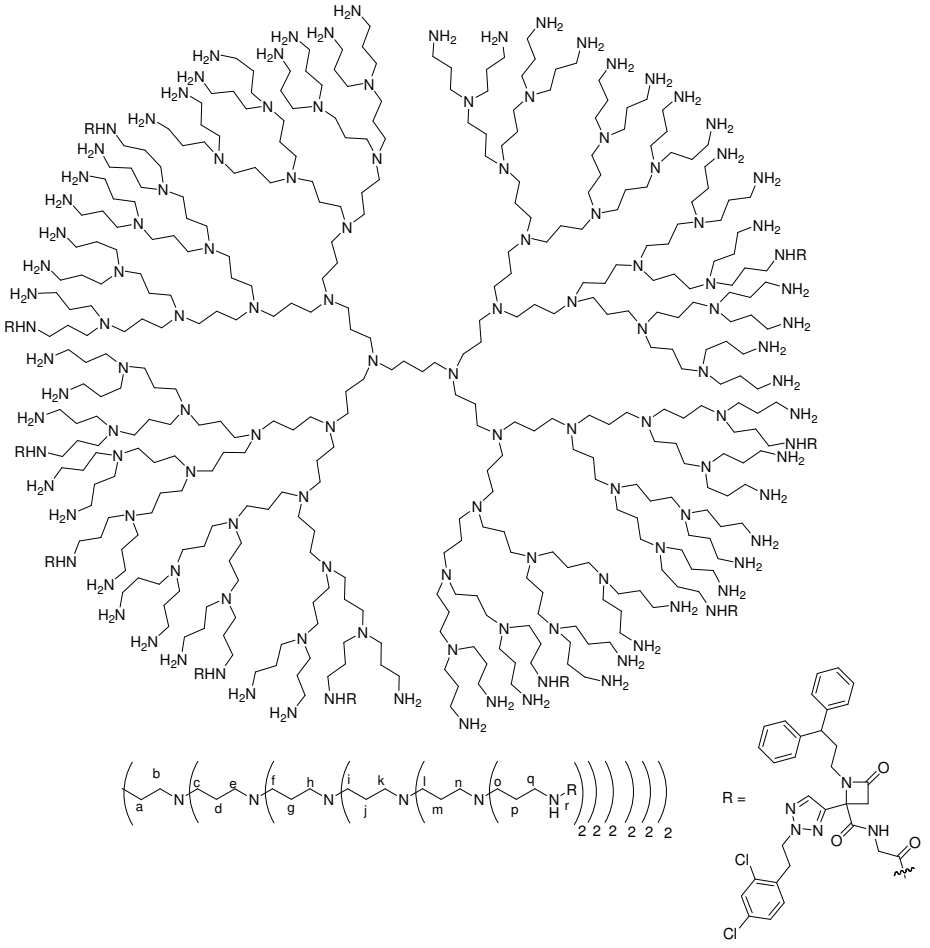

## Open-shell glycodendrimer without spacer (71)

Dendrimer **70** (60 mg, 0.005 mmol), D-(+)-maltose monohydrate (51 mg, 0.125 mmol, 25 maltoses) and borane-pyridine complex (31 µL, 0.25 mmol, 8M solution,) were taken up in a sodium borate buffer (8.3 mL, 0.1M, pH = 9) solution. The reaction solution was stirred at 50°C for 7 days. The crude mixture was then purified by dialysis towards deionized water for 3 days. Glycodendrimer **71** was obtained (90 mg, 85%) from freeze drying.

The signals at ~7 ppm on the $^1$H NMR spectrum were assigned to the aromatic protons of the small molecule. By integration of the $CH_2$ of the PPI and the maltoses, it can be determined that the compound **71** has 25 maltoses and 4 equivalents of drug per polymer unit.

**$^1$H-NMR ($D_2O$, 500 MHz):** δ (ppm): 7.30-6.90 (Ar), 5.16-5.12 (H1''), 3.40-4.00 (2',2'',3',3'',4',4'',5',5'',6',6''), 3.05 (Hq), 2.94 (H1'), 2.30-2.88 (b,c,e,f,h,i,k,l,n,o), 1.82-1.61 (a, d, g, j, m, p).

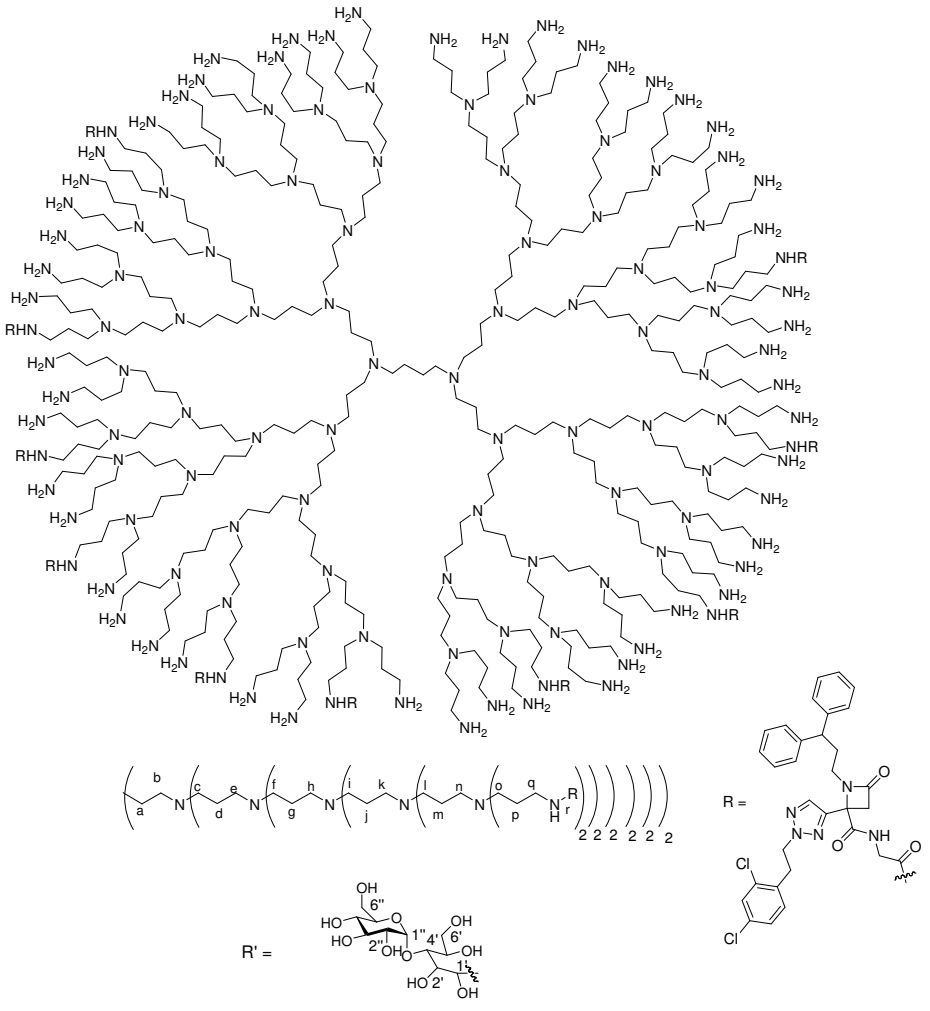

# 7. References

1. Riedl, S. J.; Li, W.; Chao, Y.; Schwarzenbacher, R.; Shi, Y., Structure of the apoptotic protease-activating factor 1 bound to ADP. *Nature* **2005,** 434, (7035), 926-933.

2. Halgren, T. A.; Murphy, R. B.; Friesner, R. A.; Beard, H. S.; Frye, L. L.; Pollard, W. T.; Banks, J. L., Glide: a new approach for rapid, accurate docking and scoring. 2. Enrichment factors in database screening. *J Med Chem* **2004,** 47, (7), 1750-1759.

3. Friesner, R. A.; Banks, J. L.; Murphy, R. B.; Halgren, T. A.; Klicic, J. J.; Mainz, D. T.; Repasky, M. P.; Knoll, E. H.; Shelley, M.; Perry, J. K.; Shaw, D. E.; Francis, P.; Shenkin, P. S., Glide: a new approach for rapid, accurate docking and scoring. 1. Method and assessment of docking accuracy. *J Med Chem* **2004,** 47, (7), 1739-49.

4. Friesner, R. A.; Murphy, R. B.; Repasky, M. P.; Frye, L. L.; Greenwood, J. R.; Halgren, T. A.; Sanschagrin, P. C.; Mainz, D. T., Extra precision glide: docking and scoring incorporating a model of hydrophobic enclosure for protein-ligand complexes. *J Med Chem* **2006,** 49, (21), 6177-96.

5. Mondragón, L.; Orzáez, M.; Sanclimens, G.; Moure, A.; Armiñán, A.; Sepúlveda, P.; Messeguer, A.; Vicent, M.J.; Pérez-Payá, E. , Modulation of cellular apoptosis with Apaf-1 inhibitors. *J. Med. Chem* **2008,** 51, 521-529.

6. Fesik, S. W., Promoting apoptosis as a strategy for cancer drug discovery. *Nat. Rev. Cancer* **2005,** 5, 876-885.

7. Nencioni, A.; Grunebach, F.; Patrone, F.; BAllestrero, A.; Brossart, P., The proteasome and its inhibitors in immune regulation and immune disorders. *Critical Rev. Immunol.* **2006,** 26, 487-497.

8. Fischer, U.; Schulze-Osthoff., K., New approaches and therapeutics targeting apoptosis in disease. *Pharmacol. Rev.* **2005,** 57, 187-215.

9. Takemura, G.; Fuijwara, H., Morphological aspects of apoptosis in heart diseases. *J. Cel. Mol. Med.* **2006,** 10, 56-75.

10. Mattson, M. P.; Kroemer, G., Mitochondria in cell death: novel targets for neuroprotection and cardioprotection. *Trends. Mol. Med.* **2003,** 9, 196-205.

11. Strasser, A.; O'Connor,L.; Dixit, V. M. , Apoptosis signaling. *Annu. Rev. Biochem.* **2000,** 69, 217-245.

12. Siegel, R. M., Caspases at the crossroads of immune-cell life and death. *Nat. Rev. Immunol.* **2006,** 6, 308-317.

13. Mahrus, S.; Trinidad,, J. C.; Barkan, D.T.; Sali, A.; Burlingame, A. L.; Wells, J. A., Global sequencing of proteolytic cleavage sites in apoptosis by specific labeling of protein N termini. *Cell* **2008,** 134, 866-876.

14. Chai, J. J.; Du, C. Y.; Wu, J. W.; Kyin, S.; Wang, X. D., Structural and biochemical basis of apoptotic activation by Smac/Diablo. *Nature* **2000,** 406, 855-862.

15. Li, P.; Nijhawan, D.; Budihardjo, I.; Srinivasula, S. M.; Ahmad, M.; Alnemri, E. S.; Wang, X., Cytochrome c and dATP-dependent formation of Apaf-1/caspase-9 complex initiates an apoptotic protease cascade. *Cell* **1997**, (91), 459-489.

16. Pérez-Payá, E.; Orzáez, M.; Mondragón, L. Wolan, D.; Well,s J. Messeguer, A.; Vicent, M.J., Molecules that modulate Apaf-1 activity. *Med. Res. Rev.* **2011,** 31, 3-19.

17. Martin, A. G.; Nguyen, J.; Wells, J. A.; Fearnhead, H. O. , Apo cytochrome c inhibits caspases by preventing apoptosome formation. *Biochem. Biophys. Res. Comm.* **2004,** 319, 944-950.

18. Zou, H.; Li, Y.; Liu, X.; Wang, X., An APAF-1 cytochrome c mutlimeric complex is a functional apoptosome that activates procaspase-9. *J. Biol. Chem.* **1999**, (274), 11549-11556.

19. Acehan, D.; Jiang, X. J.; Morgan, D. G.; Heuser, J. E.; Wang, X. D.; Akey, C. W., Three-dimensional structure of the apoptosome: Implications for assembly, procaspase-9 binding and activation. *Mol. Cell.* **2002,** 9, 423-432.

20. Kim, H. E. Du, F.; Fang, M.; Wang, X., Formation of apoptosome is initiated by cytochrome c-induced dATP hydrolysis and subsequent nucleotide exchange on Apaf-1. *Proc. Natl. Acad. Sci USA* **2005**, (102), 17545-17550.

21. Ledgerwood, E. C.; Morison, I., Targeting the apoptosome for cancer therapy. *Clin. Cancer. Res.* **2009,** 15, 420-424.

22. Corvaro, M.; Cecconi, F., Atlas of Genetics and Cytogenetics in Oncology and Haematology. In 2004.

23. Benedict, M. A.; Hu, Y.; Inohara, N.; Nunez, G. , Expression and functional analysis of Apaf-1 isoforms. Extra Wd-40 repeat is required for cytochrome c binding and regulated activation of procaspase-9. *J. Biol. Chem.* **2000,** 275, 8461-8468.

24. Srinivasula, S. M.; Ahmad, M.; Fernandes-Alnemri, T.; Alnemri, E. S., Autoactivation of procaspase-9 by Apaf-1 mediated oligomerization. *Mol. Cell.* **1998,** 1, (7), 949-957.

25. Green, D. R.; Kroemer, G., The pathophysiology of mitochondrial cell death. *Science* **2004**, (305), 626-629.

26. Reed, J. C., Apoptosis-based therapies. *Nat. Rev. Drug Discov.* **2002,** 1, 111-121.

27. Malet, G.; Martin, A.G.; Orzáez, M.; Vicent, M.J.; Masip, I.; Sanclimens, G.; Ferrer-Montiel, A.; Mingarro, I.; Messeguer, A.; Fearnhead, H.O.; Pérez-Payá, E. , Small molecule inhibitors of Apaf-1-related caspase-3/-9 activation that control mitochondrial-dependent apoptosis. *Cell. Death Differ.* **2006,** 13, 1523-1532.

28. Scott, C. W. Sobotka.-Briner, C.; Wilkins, D.E.; Jacobs, R.T.; Folmer, J.J.; Frazee, W.J.; Bhat, R.V.; Ghanekar, S.V.; Aharony, D. , Novel small molecule inhibitors of caspase-3 block cellular and bio-chemical features of apoptosis *J. Pharmacol. Exp. Ther.* **2003,** 304, 433-440.

29. O'Brien, T.; Lee, D., Prospects for caspase inhibitors. *Mini-rev. Med. Chem.* **2004,** 4, 153-165.

30. Zhu, S.; Stavrovskaya, I. G.; Drozda, M.; Kim, B. Y.; Ona, V.; Li, M.; Sarang, S.; Liu, A. S.; Hartley, D. M.; Wu du C.; Gullans, S.; Ferrante, R. J.; Prezdoborski, S.; Kristal, B. S.; Friedlander, R. M., Minocycline inhibits cytochrome c release and delays progression of amyotrophic lateral sclerosis in mice. *Nature* **2002**, (417), 74-78.

31. Wang, X.; Zhu, S.; Drozda, M.; Zhang, W.; Stavrovskaya, I. G.; Cattaneo, E.; Ferrante, R. J.; Kristal, B. S.; Friedlander, R. M.; Kim, B. Y.; Ona, V.; Li, M.; Sarang, S.; Liu, A. S.; Hartley,

D. M.; Wu du C.; Gullans, S.; Przedborski, S., Minocycline inhibits caspase-independent and-dependent mitochondrial cell death pathways in models o fHuntington's disease. *Proc. Natl. Acad. Sci USA* **2003**, (100), 10483-10487.

32. Mochizuki, H.; Hayakawa, H.; Migita, M.; Shibata, M.; Tanaka, R.; Suzuki, A.; Shimo-Nakanishi, Y.; Urabe, T.; Yamada, M.; Tamayose, K.; Shimada, T.; Miura, M.; Mizuno, Y., An AAV-derived Apaf-1 dominant negative inhibitor prevents MPTP toxicity as antiapoptotic gene therapy for Parkinson's disease. *Proc. Natl. Acad. Sci USA* **2001**, (98), 10918-10923.

33. Lessene, G.; Czabotar, P. E.; Colman, P. M., BCL-2 family antagonists for cancer therapy. *Nat. Rev. Drug Discov.* **2008,** 7, 989-1000.

34. Lettre, G.; Hengartner, M. O., Developmental apoptosis in C. elegans: A complex CEDnario. *Nat. Rev. Mol. Cell. Biol.* **2006,** 7, 97-108.

35. Meier, P.; Vousden, K. H., Lucifer's labyrinth - Ten years of path finding in cell death. *Mol. Cell.* **2007,** 28, 746-754.

36. Simon, R. J.; Kania, R. S.; Zuckermann, R. N.; Huebner, V. D.; Jewell, D. A., Banville, S.; Ng S.; Wang, L.; Rosenberg, S.; Marlowe, C. K.; Spellmeyer, D. C.; Tan, R.; Frankel, A. D.; Santi, D. V.; Cohen, F. E.; Bartlett, P. A., Peptoids: a modular approach to drug discovery. *Proc. Natl. Acad. Sci USA* **1992,** 89, 9367-9371.

37. Burkoth, T. S.; Beausoleil, E.; Kaur, S.; Tang, D.; Cohen, F. E.; Zuckermann, R. N., Toward the synthesis of artificial protiens: the discovery of an amphiphilic helical peptoid assembly. *Chem. Biol.* **2002,** 9, 647-654.

38. Miller, S. M.; Simon, R. J.; Ng, S.; Zuckermann, R. N.; Kerr, J. M.; Moos, W. H. , Proteolytic studies of homologous peptide and N-substituted glycine peptoid oligomers. *Bioorg. Med. Chem. Lett.* **1994,** 4, 2657-2662.

39. Kirschenbaum, K.; Barron, A. E.; Goldsmith, R. A.; Armand, P.; Bradley, E. K.; Truong, K. T. V.; Dill, K. A.; Cohen, F. E.; Zuckermann, R. N., Sequence-specific polypeptoids: A diverse family of heteropolymers with stable secondary structure. *Proc. Natl. Acad. Sci USA* **1998,** 95, 4303-4308.

40. Fowler, S. A.; Blackwell, H. E., Structure–function relationships in peptoids: Recent advances toward deciphering the structural requirements for biological function. *Org. Biomol. Chem.* **2009,** 7, 1508-1524.

41. Kuemin, M.; Nagel Y. A.; Schweizer, S.; Monnard, F. W.; Ochsenfeld, C.; Wennemer,s H., Tuning the cis:trans Conformer Ratio of Xaa-Pro Amide Bonds by Intramolecular Hydrogen Bonds - Effect on the Stability of the PPII Helix. *Angew. Chem. Int. Ed.* **2010,** 49, 6324-6327.

42. Wedemeyer, W. J.; Welker, E.; Scheraga, H. A., Proline cis-trans isomerization and protein folding. *Biochemistry* **2002,** 41, (50), 14637-14644.

43. Sui, Q.; Borchardt, D.; Rabenstein, D. L., Kinetics and equilibria of cis/trans isomerization of backbone amide bonds in peptoids. *J. Am. Chem. Soc.* **2007,** 129, 12042-12048.

44. Bryant, S. D. Balboni, G.; Guerrini, R.; Salvadori, S.; Tomatis, R.; Lazarus, L. H., Opioid Diketopiperazines: Refinement of the sigma opioid antagonist pharmacophore. *Biol. Chem.* **1997,** 378, 107-114.

45. Barrow, C. J.; Musza, L. L.; Cooper, R., Structure-activity studies of the natural product substance P antagonist win 64821. *Bioorg. Med. Chem. Lett.* **1995,** 5, 377-380.

46. Szardenings, A. K.; Harris, D.; Lam, S.; Shi, L.; Tien, D.; Wang, Y.; Patel, D. V.; Navre, M.; Campbell, D. A., Rational Design and Combinatorial Evaluation of Enzyme Inhibitor Scaffolds: Identification of Novel Inhibitors of Matrix Metalloproteinases. *J. Med. Chem* **1998,** 41, 2194-2200.

47. Szardenings, A. K.; Antonenko, V.; Campbell, D. A.; DeFrancisco, N.; Ida, S.; Shi, L.; Sharkov, N.; Tien, D.; Wang, Y.; Navre, M,, Identification of Highly Selective Inhibitors of Collagenase-1 from Combinatorial Libraries of Diketopiperazines. *J. Med. Chem* **1999,** 42, 1348-1357.

48. Goodfellow, V.; Laudeman, C.; Gerrity, JI.; Burkard, M.; Strobel, E.; Zuzack, JS.; McLeod, DA., Rationally designed non-peptides: Variously substituted piperazine libraries for the discovery of bradykinin antagonists and other G-protein-coupled receptor ligands. *Mol. Divers.* **1996,** 2, 97-102.

49. Guo, T.; Adang, A. E. P.; Dolle, R. E.; Dong, G.; Fitzpatrick, D.; Geng, P.; Ho, K.-K.; Kultgen, S. G.; Liu, R.; McDonald, E.; McGuinness, B. F.; Saionz, K. W.; Valenzano, K. J.; van Straten, N. C. R.; Xie, D.; Webb, M. L., Small molecule biaryl FSH receptor agonists. Part 1: Lead discovery via encoded combinatorial synthesis. *Bioorg. Med. Chem. Lett.* **2004,** 14, 1713-1716.

50. Borthwick, A. D.; Davies, D. E.; Exall, A. M.; Hatley, R. J. D.; Hughes, J. A.; Irving, W. R.; Livermore, D. G.; Sollis, S. L.; Nerozzi, F.; Valko, K. L.; Allen, M. J.; Perren, M.; Shabbir, S. S.; Woolard, P. M.; Price, M. A., 2,5-Diketopiperazines as Potent, Selective, and Orally Bioavailable Oxytocin Antagonists. 3. Synthesis, Pharmacokinetics, and in Vivo Potency. *J. Med. Chem* **2006,** 49, (4159-4170).

51. Wyatt, P. G.; Allen,M. J.; Borthwick, A. D.; Davies, D. E.; Exall, A. M.; Hatley, R. J. D.; Irving, W. R.; Livermore, D. G.; Miller, N. D.; Nerozzi, F.; Sollis, S. L.; Szardenings, A. K., 2,5-Diketopiperazines as potent and selective oxytocin antagonists 1: identification, stereochemistry and initial SAR. *Bioorg. Med. Chem. Lett.* **2005,** 15, 2579-2582.

52. Capasso, S.; Vergara, A.; Mazzarella, L., Mechanism of 2,5-Dioxopiperazine formation. *J. Am. Chem. Soc.* **1998,** 120, 1990-1995.

53. Van Langen, L. M.; van Rantwijk, F.; Svedas, V. K.; Sheldon, R. A., Penicillin acylase-catalyzed peptide synthesis: a chemo-enzymatic route to stereoisomers of 3,6-diphenylpiperazine-2,5-dione *Tetrahedron: Asymm.* **2000,** 11, 1077-1083.

54. Hulme, C.; Morrissete, M. M.; Volz, F. A.; Burns, C. J., The solution phase synthesis of diketopiperazine libraries via the Ugi reaction: Novel application of Armstrong's convertible isonitrile. *Tetrahedron Lett.* **1998,** 39, 1113-1116.

55. Marcaccini, S.; Pepino, R.; Pozo, M.C. , A facile synthesis of 2,5-diketopiperazines based on the isocyanide chemistry. *Tetrahedron Lett.* **2001,** 42, 2727-2728.

56. Scott, B. O.; Siegmund, A. C.; Marlowe, C. K.; Pei, Y.; Spear, K. L., Solid phase organic synthesis (SPOS): a novel route to diketopiperazines and diketomorpholines. *Mol. Divers.* **1996,** 1, 125-134.

57. Carbonell, T.; Masip, I.; Sánchez-Baeza, F.; Delgado, M.; Araya, E.; Llorens, O.; Corcho, F.; Pérez, J.; Pérez-Payá, E.; Messeguer, A., Identification of selective inhibitors of

acetylcholinesterase from a combinatorial library of 2,5-piperazinediones. *Mol. Divers.* **2000,** 5, 131-143.

58. Masip, I.; Cortés, N.; Abad, M. J.; Guardiola, M.; Perez-Paya, E.; Ferragut, J.; Ferrer-Montiel, A.; Messeguer, A, Design and synthesis of an optimized positional scanning library of peptoids: identification of novel multidrug resistance reversal agents. *Bioorg. Med. Chem.* **2005,** 13, 1923-1929.

59. Moure, A.; Sanclimens, G.; Bujons, J.; Masip, I.; Alvarez-Larena, A.; Pérez-Payá, E.; Alfonso, I.; Messeguer, A, Chemical modulation of peptoids : synthesis and conformational studies on partially constrained derivatives. *Chem. Eur. J.* **2011,** 17, 7927-7939.

60. Lebleu, B.; Moulton, H. M.; Abes, R.; Ivanova, G. D.; Abes, S.; Stein, D. A.; Iversen, P. L.; Arzumanov, A. A.; Gait, M., Cell penetrating peptide conjugates of steric block oligonucleotides. *J. Adv. Drug. Deliv. Rev.* **2008,** 60, 517-529.

61. Lewin, M.; Carlesso, N.; Tung, C.-H.; Tang, X.-W.; Cory, D.; Scadden, D. T.; Weissleder, R., Tat peptide-derivatized magnetic nanoparticles allow in vivo tracking and recovery of progenitor cells. *Nat. Biotech* **2000,** 18, 410-414.

62. Torchilin, V. P.; Rammohan, R.; Weissig, V.; Levchenko, T. S., TAT peptide on the surface of liposomes affords their efficient intracellular delivery even at low temperature and in the presence of metabolic inhibitors. *Proc. Natl. Acad. Sci USA* **2001,** 98, 8786-8791.

63. Orzáez, M., Mondragón. L., Marzo, I., Sanclimens. G., Messeguer, A., Pérez-Payá, E., Vicent, M.J., Conjugation of a novel Apaf-1 inhibitor to peptide-based cell-membrane transporters. Effective methods to improve inhibition of mitochondria-mediated apoptosis. *Peptides* **2007,** 28, 958-968.

64. Holub, J. M., Jang, H., Kirshenbaum, K., Fit To Be Tied: Conformation-Directed Macrocyclization of Peptoid Foldamers. *Org. Lett.* **2007,** 9, 3275-3278.

65. Shin, S.-B. Y.; Yoo, B.; Todaro, L.; Kirshenbaum, K., Cyclic Peptoids. . *J. Am. Chem. Soc.* **2007,** 129, 3218-3225.

66. Vercillo, O. E.; Kleber, C.; Andrade, Z.; Wessjohan, L. A., Design and synthesis of cyclic RGD pentapeptoids by consecutive Ugi reactions. *Org. Lett.* **2007,** 10, 205-208.

67. Pedersen, D. J.; Abell, A., 1,2,3-Triazoles in organic chemistry. . *J. Org. Chem.* **2011,** 13, 2399-2411.

68. Brik, A.; Alexandratos, A., J.; Lin, Y.C.; Elder, J.H.; Olson, A.J.; Wlodawer, A.; Goodsell, D.S.; Wong, C.H, 1,2,3-Triazole as a peptide surrogate in the rapid synthesis of HIV-1 protease inhibitors. *Chem. Bio. Chem.* **2005,** 6, 1167-1169.

69. Chierici, S.; Jourdan,M.; Figuet, M.; Dumy, P. , A case study of 2,2-dimethylthiazolidine as locked cis proline amide bond: synthesis, NMR and molecular modeling studies of a [small delta]-conotoxin EVIA peptide analog. *Org. Biomol. Chem.* **2004,** 2, 2437-2441.

70. Che, Y.; Marshall, G.R., Impact of Cis-Proline analogs on peptide conformation. *Biopolymers* **2006,** 81, 392-406.

71. Zabrocki, J.; Smith, G.D.; Dunbar, J.B.; Iijima, H.; Marshall, G.R., Conformational mimicry. 1,5-disubstituted tetrazole ring as a surrogate for the cis amide bond. *J. Am. Chem. Soc.* **1988,** 110, 5875-5880.

72. Horne, W. S.; Olsen, C.A.; Beierle, J.M.; Montero, A.; Ghadiri, M.R., Probing the bioactive conformation of an archetypal natural product HDAC inhibitor with conformationally homogeneous triazole-modified cyclic tetrapeptides. *Angew. Chem.* **2009,** 121, 4812-4818.

73. Tietze, D.; Tischler, M.; Voigt, S.; Imhof, D.; Ohlenschläger, O.; Görlach, M.; Buntkowsky, G., Development of a functional cis-Prolyl bond biomimetic and mechanistic implications for nickel superoxide dismutase. *Chem. Eur. J.* **2010,** 16, 7572-7578.

74. Tam, A.; Arnold, U.; Soellner, M.B.; Raines, R.T., Protein prosthesis: 1,5-disubstituted[1,2,3]triazoles as cis-Peptide bond surrogates. *J. Am. Chem. Soc.* **2007,** 129, (42), 12670-12671.

75. Tischler, M.; Nasu,D.; Empting, M.; Schmelz, S.; Heinz, D.W.; Rottmann, P.; Kolmar, H.; Buntkowsky, G.; Tietze, D.; Avrutina, O. , Braces for the Peptide Backbone: Insights into Structure-Activity Relationships of Protease Inhibitor Mimics with Locked Amide Conformations *Angew. Chem. Int. Ed.* **2012,** 51, 3708-3712.

76. Agalave, S. G.; Maujan, S.R.; Pore, V.S., Click Chemistry: 1,2,3-Triazoles as Pharmacophores. *Chem. Asian J.* **2011,** 6, 2696-2718.

77. Chow, H. F.; Lau, K.N.; Ke, Z.; Liang, Y.; Lo, C.M., Conformational and supramolecular properties of main chain and cyclic click oligotriazoles and polytriazoles. *Chem. Commun.* **2010,** 46, 3437-3453.

78. Horne, W. S.; Yadav, M. K.; Stout, C.D.; Ghadiri, M.R. , Heterocyclic peptide backbone modifications in an α-helical coiled coil. *J. Am. Chem. Soc.* **2004,** 126, 15366-15367.

79. Kolb, H. C.; Sharpless, K.B., The growing impact of click chemistry on drug discovery. *Drug Discovery Today* **2003,** 8, (24), 1128-1137.

80. Abboud, J. L. M.; Foces-Foces, C.; Notario, R.; Trifonov, R.E.; Volovodenko, A.P.; Ostrovskii, V.A.; Alkorta, I.; Elguero, J., Basicity of N-H- and N-Methyl-1,2,3-triazoles in the gas phase, in solution, and in the solid state - An experimental and theoretical study. *Eur. J. Org. Chem.* **2001**, (16), 3013-3024.

81. McClellan, A. L., Tables of Experimental Dipole Moments. In Enterprises, R., Ed. El Cerrito, 1974; Vol. 2.

82. Ahn, J. M.; Boyle; N.A.; MacDonald, M. T. J., K.D., Peptidomimetics and peptide backbone modifications. *Mini-rev. Med. Chem.* **2002,** 2, 463-473.

83. Wu, P.; Fokin, V.V., Click Chemistry for biotechonology and material science. . *Aldrichimica Acta* **2007,** 40, 7-17.

84. Tornoe, C. W.; Christensen, C.; Meldal, M. , [1,2,3]-triazoles by regiospecific copper(I)-catalyzed 1,3-dipolar cycloadditions of terminal alkynes to azides. . *J. Org. Chem.* **2002,** 67, 3057-3064.

85. Kolb, H. C.; Finn, M.G.; Sharpless, K.B., Click Chemistry: Diverse Chemical Function from a Few Good Reactions. *Angew. Chem. Int. Ed.* **2001,** 40, 2004-2021.

86. Banert, K., Reactions of unsaturated azides. Synhtesis of 1,2,3-triazoles from propargyl azides by rearrengement of the azido group. *Chem. Ber.* **1989,** 122, 911-918.

87. Huisgen, R., Kinetics and Mechanism of 1,3-Dipolar Cycloadditions. *Angewandte Chemie International Edition in English* **1963,** 2, (11), 633-645.

88. Damodiran, M.; Muralidharan, D.; Perumal, P.T., Regioselective synthesis and biological evaluation of bis(indolyl)methane derivatized 1,4-disubstituted 1,2,3-bistriazoles as anti-infective agents. *Bioorg. Med. Chem. Lett.* **2009,** 19, 3611-3614.

89. Himo, F.; Lovell, T.; Hilgraf, R.; Rostovtsev, V.V.; Noodleman, L.; Sharpless, K.B.; Fokin, V.V., Copper(I)-catalyzed synthesis of azoles. DFT study predicts unprecedented reactivity and intermediates. *J. Am. Chem. Soc.* **2005,** 127, (1), 210-216.

90. Boren, B. C.; Narayan, S.; Rasmussen, L.K.; Zhang, L.; Zhao, H.; Lin, Z.; Jia, G.; Fokin, V.V., Ruthenium-catalyzed azide-alkyne cycloaddition: Scope and Mechanism. *J. Am. Chem. Soc.* **2008,** 130, 8923-8930.

91. Rostovtsev, V. V., Green, L.G.; Fokin, V.V.; Sharpless, K.B., A stepwise Huisgen cycloaddition process: Copper(I)-catalyzed regioselective "ligation" of azides and terminal alkynes. *Angew. Chem. Int. Ed.* **2002,** 41, 2596-2599.

92. Link, A. J.; Tirrell, D.A., Cell surface labeling of Escherichia coli via Copper(I)-catalyzed [3+2] cycloaddition. *J. Am. Chem. Soc.* **2003,** 125, (37), 11164-11165.

93. Wang, Q.; Chan, T.R.; Hilgraf, R.; Fokin, V.V.; Sharpless, K.B.; Finn, M.G., Bioconjugation by copper (I)-catalyzed azide-alkyne [3+2] cycloaddition. *J. Am. Chem. Soc.* **2003,** 125, (11), 3192-3193.

94. Hawker, C. J.; Fokin,V.V.; Finn, M.G.; Sharpless, K.B., Bringing efficiency to materials synthesis: The philosophy of Click chemistry. *Aust. J. Chem.* **2007,** 60, 381-383.

95. Evans, R. A., The Rise of azide-alkyne 1,3-dipolar "Click" cycloaddition and its application to polymer science and surface modification. *Aust. J. Chem.* **2007,** 60, 384-395.

96. Zhou, Z.; Fahrni, C.J., A fluorogenic probe for the copper(I)-catalyzed azide-alkyne ligation reaction. *J. Am. Chem. Soc.* **2004,** 126, (29), 8862-8863.

97. Lewis, W. G.; Magallon, F.G.; Fokin, V.V.; Finn, M.G., Discovery and characterization of catalysts for azide-alkyne cycloaddition by fluorescence quenching. *J. Am. Chem. Soc.* **2004,** 126, (30), 9152-9153.

98. Aucagne, V.; Hänni, K.D.; Leigh, D.A.; Lusby, P.J.; Walker, D.B., Catalytic "Click" rotaxanes: A substoichiometric metal-template pathway to mechanically interlocked architectures. *J. Am. Chem. Soc.* **2006,** 128, (7), 2186-2187.

99. O'Reilly, R. K.; Joralemon, M.J.; Hawker, C.J. Wooley, K.L., Facile syntheses of surface-functionalized micelles and shell cross-linked nanoparticles. *Polym. Sci. Polym. Chem.* **2006,** 44, 5203-5217.

100. Zhang, W. B.; Yingfeng, T.; Ranjan, R.; Van Horn, R.M.; Leng, S.; Wang, J.; Polce, M.J.; Wesdemiotis, C.; Quirk, R.P.; Newkome, G.R.; Cheng, S.Z.D., "Clicking" Fullerene with polymers: Synthesis of [60] fullerene end-capped polystyrene. *Macromolecules* **2008,** 41, 515-517.

101. Krasinski, A.; Fokin, V.V.; Sharpless, K.B., Direct synthesis of 1,5-disubstituted-4-magnesio-1,2,3-triazoles. *Org. Lett.* **2004,** 6, 1237-1240.

102. Imperio, D.; Pilari, T.; Galli, U.; Pagliai, F.; Cafici, L.; Canonico, P.L.; Sorba, G.; Genazzani, A.A.; Tron, G.C., Replacement of the lactone moiety on podophyllotoxin and steganacin analogues with a 1,5-disubstituted 1,2,3-triazole via ruthenium-catalyzed click chemistry. *Bioorg. Med. Chem.* **2007,** 15, 6748-6757.

103. Zhang, L.; Chen, X.; Xue, P.; Sun, H.H.Y.; Williams, I.D.; Sharpless, K.B.; Fokin, V.V.; Jia, G., Ruthenium-catalyzed cycloaddition of alkynes and organic azides. *J. Am. Chem. Soc.* **2005,** 127, (46), 15998-15999.

104. Moumné, R.; Larue, V.; Seijo, B.; Lecourt, T.; Micouin, L.; Tisné. C, Tether influence on the binding properties of $tRNA^{Lys3}$ ligands designed by a fragment-based approach. *Org. Biomol. Chem.* **2010,** 8, 1154-1159.

105. Majireck, M. M.; Weinreb, S.M., A study of the scope and regioselectivity of the ruthenium-catalyzed [3+2]-cycloaddition of azides with internal alkynes. *J. Org. Chem.* **2006,** 71, 8680-8683.

106. Ugi, I., The a-addition of immonium ions and anions to isoniriles accompanied by secondary reactions. *Angew. Chem. Int. Ed.* **1962,** 1, 8-21.

107. Dömling, A.; Ugi, I., Multicomponent reactions with isocyanides. *Angew. Chem. Int. Ed.* **2000,** 39, (18), 3168-3210.

108. Marcaccini, S.; Torroba, T., The use of the Ugi four-component condensation. *Nat. Protoc.* **2007,** 2, 632-639.

109. Ugi, I., Dömling, A.; Hörl, W, Multicomponent reactions in organic chemistry. *Endeavour* **1994,** 18, (3), 115-122.

110. Thompson, M. J.; Chen, B.N., Ugi reactions with ammonia offer rapid access to a wide range of 5-aminothiazole and oxazole derivatives. *J. Org. Chem.* **2009,** 74, 7084-7093.

111. Lehnhoff, S.; Goebel, M.; Karl, R.M.; Klösel, R.; Ugi, I., Stereoselective syntheses of peptide derivatives with 2-acetamido-3,4,6-tri-*O*-acetyl-1-amino-2-deoxy-b-D-glucopyranose by Four-component condensation. *Angew. Chem. Int. Ed.* **1995,** 34, (10), 1104-1107.

112. Ugi, I.; Offermann, K., Asymmetric 1,3-induction during the a-addition of immonium ions and carboxylate anions onto isonitriles. *Angew. Chem. Int. Ed.* **1963,** 2, (10), 624.

113. Ugi, I.; Heck,S., The Multicomponent Reactions and their Libraries for Natural and Preparative Chemistry. *Comb. Chem. High Through. Screen.* **2001,** 4, (1), 1-34.

114. Kusebauch, U.; Beck, B.; Messer, K.; Herdtweck, E.; Dömling, A., Massive parallel catalyst screening: toward asymmetric MCRs. *Org. Lett.* **2003,** 5, 4021-4024.

115. Keating, T. A.; Armstrong, R. W., Molecular diversity via a convertible isocyanide in the Ugi Four-component condensation. *J. Am. Chem. Soc.* **1995,** 117, (29), 7842-7843.

116. Hulme, C.; George-Morton, J. P.; Salvino, J. M.; Herpin, T.; Labaudiniere, R., Novel Safety-Catch Linker and its Application with a Ugi/De-BOC/Cyclization (UDC) Strategy to access Carboxylic acids, 1,4-Benzodiazepines, Diketopiperazines, Ketopiperazines and Dihydroquinoxalinones. *Tetrahedron Lett.* **1998,** 39, 7227-7230.

117. Szardenings, A. K.; Burkoth, T. S.; Lu, H. H.; Tien, D.; Campbell, D. A., A simple procedure for the solid phase synthesis of diketopiperazine and diketomorpholine derivatives. *Tetrahedron* **1997,** 53, 6573-6593.

118. Bossio, R.; Marcos, C.F.; Marcaccini, S.; Pepino, R. , A facile synthesis of -lactams based on the isocyanide. *Tetrahedron Lett.* **1997,** 38, 2519-2520.

119. Mroczkiewicz, M.; Ostaszewski, R., A new and general method for the synthesis of tripeptide aldehydes based on the multicomponent Ugi reaction. *Tetrahedron* **2009,** 65, 4025-4034.

120. Minozzi, M.; Nanni, D.; Walton, J.C., Alkenylthioimidoyl Radicals: Competition between beta-scission and cyclization to dihydrothiophen-2-ylidene-amines. *Org. Chem.* **2003,** 5, (6), 901-904.

121. Rivera, D. G.; Wessjohann, L.A., Supramolecular compounds from multiple Ugi multicomponent macrocyclizations: Peptoid-based cryptands, cages and cryptophanes. *J. Am. Chem. Soc.* **2006,** 128, (22), 7122-7123.

122. Millich, F., Polymerization of isocyanides. *Chem. Rev.* **1972,** 72, (2), 101-104.

123. Visser, H. G. J.; Nolte, R. J. M.; Zwikker, J. W.; Drenth, W., Synthesis of copolymers of isocyanides derived from alanylserine and alanylhistidine. *J. Org. Chem.* **1985,** 50, 3133-3137.

124. El Kaim, L.; Grimaud, L.; Schiltz, A,, "Isocyanide-free" Ugi reactions. *Org. Biomol. Chem.* **2009,** 7, 3024-3026.

125. Krivopalov, V. P.; Shkurko, O.P., 1,2,3-Triazole and its derivatives. Development of methods for the formation of the triazole ring. *Russ. Chem. Rev.* **2005,** 74, (4), 339-379.

126. Kamijo, S.; Jin, T.; Huo, Z.; Yamamoto, Y., Synthesis of triazoles from nonactivated terminal alkynes via the Three-Component coupling reaction using a Pd(0)-Cu(I) bimetallic catalyst. **2003**.

127. Kalisiak, J.; Sharpless, K.B.; Fokin, V.V., Efficient synthesis of 2-substituted-1,2,3-triazoles. *Org. Lett.* **2008,** 15, 3171-3174.

128. Coates, J., Interpretation of Infrared Spectra, A Practical Approach. In *Encyclopedia of Analytical Chemistry*, Meyers, R. A., Ed. John Wiley & Sons Ltd.: Chichester, 2000; pp 10815-10837.

129. Wang, X., The expanding role of mitochondria in apoptosis. *Genes Dev.* **2001,** 15, 2922-2933.

130. Berman, H. M.; Westbrook, J.; Feng, Z.; Gilliland, G.; Bhat, T. N.; Weissig, H.; Shindyalov, I. N.; Bourne, P. E., The Protein Data Bank. *Nucleic.Acids.Res.* **2000,** 28, (1), 235-242.

131. Hou, T.; Xu, X., Recent development and application of virtual screening in drug discovery: an overview. *Curr. Pharm. Des.* **2004,** 10, (9), 1011-1033.

132. Shoichet, B. K., Virtual screening of chemical libraries. *Nature* **2004,** 432, (7019), 862-865.

133. Alvarez, J. C., High-throughput docking as a source of novel drug leads. *Curr. Opinion Chem. Biol.* **2004,** 8, 365-370.

134. Cross, J. B.; Thompson, D. C.; Rai, B. K.; Baber, J. C.; Fan, K. Y.; Hu, Y.; Humblet, C., Comparison of Several Molecular Docking Programs: Pose Prediction and Virtual Screening Accuracy. *J. Chem. Inf. Model* **2009,** 49, 1455-1474.

135. Englebienne, P.; Fiaux, H.; Kuntz, D. A.; Corbeil, C. R.; Gerber-Lemaire, S.; Rose, D. R.; Moitessier, N., Evaluation of docking programs for predicting binding of Golgi a-mannosidase II inhibitors: A comparison with crystallography. *Proteins* **2007,** 69, 160-176.

136. Wei, B. Q.; Baase,W. A.; Weaver, L. H.; Matthews, B. W.; Shoichet, B. K., A Model Binding Site for Testing Scoring Functions in Molecular Docking. *J. Mol. Biol.* **2002,** 322, 339-355.

137. Warren, G. L.; Andrews, C. W.; Capelli, A.M.; Clarke, B.; LaLonde, J.; Lambert, M.H.; Lindvall, M.; Nevins, N.; Semus, S. F.; Senger, S.; Tedesco, G.; Wall, I. D.; Woolven, J. M.; Peishoff, E.; Head, M. S., A critical assessment of docking programs and scoring functions. *J. Med. Chem* **2006,** 49, (20), 5912-5931.

138. Kollman, P. A.; Massova, I.; Reyes, C.; Kuhn, B.; Huo, S.; Chong, L.; Lee, M.; Lee, T.; Duan, Y.; Wang, W.; Donini, O.; Cieplak, P.; Srinivasan, J.; Case, D.A.; Cheatham, T.E., Calculating structures and free energies of complex molecules: combining molecular mechanics and continuum models. *Acc. Chem. Res.* **2000,** 33, (12), 889-897.

139. Wang, J. M.; Hou, T. J.; Xu, X. J., Recent Advances in Free Energy Calculations with a Combination of Molecular Mechanics and Continuum Models. *Curr. Computer-Aided Drug Design* **2006,** 2, (3), 287-306.

140. Wang, W.; Donini, O.; Reyes, C. M.; Kollman, P. A., BIOMOLECULAR SIMULATIONS: Recent Developments in Force Fields, Simulations of Enzyme Catalysis, Protein-Ligand, Protein-Protein, and Protein-Nucleic Acid Noncovalent Interactions. *Annu. Rev. Biophys and Biomol Struct.* **2001,** 30, 211-243.

141. Hou, T.; Wang, J.; Li, Y.; Wang, W., Assessing the performance of the MM/PBSA and MM/GBSA methods: II. The accuracy of ranking poses generated from docking. *J. Comput. Chem.* **2012,** 32, (5), 866-877.

142. Pérez-Payá, E. e. a., *In preparation*.

143. SiteMap, version 2.5, Schrödinger, *LLC*, New York, NY, 2011.

144. Halgren, T., New method for fast and accurate binding-site identification and analysis. *Chem Biol Drug Des* **2007,** 69, (2), 146-8.

145. Halgren, T., Identifying and characterizing binding sites and assessing druggability. *J Chem Inf Model* **2009,** 49, (2), 377-89.

146. Schrödinger Suite, *Induced Fit Docking protocol*, LLC, New York, NY, 2012.

147. Glide, version 5.8, *Schrödinger, LLC*, New York, NY, 2012.

148. Prime, version 3.1, *Schrödinger*, LLC, New York, NY, 2012.

149. Sherman, W.; Beard, H. S.; Farid, R., Use of an induced fit receptor structure in virtual screening. *Chem Biol Drug Des* **2006,** 67, (1), 83-4.

150. Sherman, W.; Day, T.; Jacobson, M. P.; Friesner, R. A.; Farid, R., Novel procedure for modeling ligand/receptor induced fit effects. *J Med Chem* **2006,** 49, (2), 534-53.

151. Rasmussen, L. K.; Boren, B.C.; Fokin, V.V, Ruthenium-catalyzed cycloaddition of aryl azides and alkynes. *Org. Lett.* **2007,** 9, (26), 5337-5339.

152. Johansson, J. R.; Lincoln,P.; Nordén, B.; Kann, N., Sequential one-pot ruthenium-catalyzed azide-alkyne cycloaddition from primary alkyl halides and sodium azide. *J. Org. Chem.* **2011,** 76, 2355-2359.

153. Holzer, W., On the application of NOE difference spectroscopy for spectran ald structural assignments with substituted 1,2,3-triazoles. *Tetrahedron* **1991,** 47, (47), 9783-9792.

154. Cohrt, A. E.; Jense, J.F.; Nielsen, T.E., Traceless azido linker for the solid-phase synthesis of NH-1,2,3-triazoles via Cu-catalyzed azide-alkyne cycloaddition reactions. *Org. Lett.* **2010,** 12, (23), 5414-5417.

155. Nulwala, H.; Takizawa, K.; Odukale, A.; Khan, A.; Thibault, R.J.; Taft, B.R.; Lipshutz, B.H.; Hawker, C.J., Synthesis and characterization of isomeric vinyl-1,2,3-triazole materials by azide-alkyne click chemistry. *Macromolecules* **2009,** 42, (16), 6068-6074.

156. Creary, X.; Anderson, A.; Brophy, C.; Crowell, F.; Funk, Z., Method for assigning structure of 1,2,3-triazoles. *J. Org. Chem.* **2012**.

157. Bax. A.; Summer, M. F., Proton and carbon-13 assignment from sensitivity-enhanced detection of heteronuclear multiple-bond connectivity by 2D multiple quantum NMR. *J. Am. Chem. Soc.* **1986,** 108, 2093-2094.

158. McDonnell, P. A.; Gauthier, A.D.; Ferro, M.P, Differentiation of regioisomers at $^{15}N$ natural abundance using gradient-enhances $^{1}H/^{15}N$ HMBC NMR spectroscopy. *Magn. Reson. Chem.* **1998,** 36, 35-38.

159. Castle, L. W.; Tominaga,Y.; Castle, R.N., Total 1H and 13C Chemical shift assignment of indolizino [3,4,5-a,b]idoindole and 2-methylthiobenz[f]imidazo[5,1,2-c-d]indolizine. *J. Heterocycl. Chem.* **1995,** 32, 1033-1038.

160. Cherkaoui, O.; Nebois,P.; Fillion, H.; Domard, M.; Fenet. B., Regiospecific hetero Diels-Alder synthesis of furo[2,3-g] and furo [3,2-g]quinoline-4,9-diones. *Tetrahedron* **1996,** 52, 9499-9508.

161. David, A. L.; Cai, Y.; Davies, A.P.; Lewis, J.R., 1H and 13C NMR assignments of some green tea polyphenols. *Magn. Reson. Chem.* **1996,** 34, 887-890.

162. Crouch, R. C.; Martin, G.E., Long-range 1H-15N correlation at natural abundance using gradient-enhanced inverse-detection. *J. Heterocycl. Chem.* **1995,** 32, 1665-1669.

163. Fukuzawa, S.; Matsunaga, S.; Fusetani, N., Use of 15N-HMBC NMR techniques to detemine the orientation of the steroidal units in Ritterazine $A^{1}$. *Tetrahedron Lett.* **1996,** 37, (9), 1447-1448.

164. Salgado, A.; Varela, C.; García-Collazo, A.M.; Pevarello, P., Differentiation between [1,2,4]triazolo[1,5-a]pyrimidine and [1,2,4]triazolo[4,3-a]-pyrimidine regioisomers by $^{1}H$-$^{15}N$ HMBC experiments. *Magn. Reson. Chem.* **2010,** 48, (8), 612-622.

165. Köck, M.; Junker,J.; Lindel, T., Impact of the 1H,15N-HMBC experiment on the consitutional analysis of alkaloids. *Org. Lett.* **1999,** 1, (13), 2041-2044.

166. Martin, G. E. H., C.E., Long-range 1H-15N Heteronuclear shift correlation at natural abundance. *J. Nat. Prod.* **2000,** 63, 543-585.

167. Williamson, M. P., NMR of proteins. *Nat. Prod. Rep.* **1993,** 10, 207-232.

168. Martin, G. E.; Hadden,A.J. , Long-range 1H-15N Heteronuclear shift correlation. *Ann. Rep. NMR Spectrosc.* **2005,** 55, 1-119.

169. Delso, I.; Tejero, T., 1H-15N HMBC as a valuable tool for the identification and characterization of nitrones. *Tetrahedron Lett.* **2007,** 48, 4101-4104.

170. Morin, R. B.; Gorman, M.; , *Chemistry and Biology of β-Lactams*. New York, 1982.

171. Dürkheimer, W.; Blumbach, J.; Latrell, R.; Scheunemann, K. H., Recent Developments in the Field of β-Lactam Antibiotics. *Angew. Chem. Int. Ed. Engl.* **1985,** 24, 180-202.

172. Alcaide, B.; Almendros, P., 4-Oxoazetidine-2-carbaldehydes as useful building blocks in stereocontrolled synthesis. *Chem. Soc. Rev.* **2001,** 30, 226-240.

173. Palomo, C.; Aizpurua,J. M.; Ganboa, I.; Oiarbide, M., Asymmetric Synthesis of -Lactams Through the Staudinger Reaction and Their Use as Building Blocks of Natural and Nonnatural Products *Curr. Med. Chem.* **2004,** 13, 1837-1872.

174. Marco-Contelles, J., β-Lactam Synthesis by the Kinugasa Reaction. *Angew. Chem. Int. Ed.* **2004,** 43, 2198-2200.

175. Carrasco, E. Auxiliares quirales derivados de carbohidratos. Nuevas aplicaciones. Universdidad de Extremadura, Badajoz, 2008.

176. Dömling, A., Recent Developments in Isocyanide Based Multicomponent Reactions in Applied Chemistry. *Chem. Rev.* **2006,** 106, 17-89.

177. Palomo, C.; Aizpurua, J. M.; Ganboa, I.; Oiarbide, M., Asymmetric Synthesis of â-Lactams by Staudinger Ketene-Imine Cycloaddition Reaction. *Eur. J. Org. Chem.* **1999**, 3223-3235.

178. Gilman, H.; Speeter, M., The Reformatsky Reaction with Benzalaniline. *J. Am. Chem. Soc.* **1943,** 65, 2255-2256.

179. Hart, D. J.; Ha,D.-C., The Ester Enolate-Imine Condensation Route to b-Lactams. *Chem. Rev.* **1989,** 89, 1447-1465.

180. Benaglia, M.; Cinquini, M.; Cozzi, F., The S-Thioester Enolate/Imine Condensation: A Shortcut to β-Lactams. *Eur. J. Org. Chem.* **2000**, 563-572.

181. Toda, F.; Miyamoto, H.; Inoue, M.; Yasaka, S.; Matijasic, I., Enantioselective Photocyclization of Amides to β-Lactam Derivatives in Inclusion Crystals with an Optically Active Host. *J. Org. Chem.* **2000,** 65, 2728-2732.

182. France, S.; Weatherwax, A.; Taggi, A.E.; Lectka, T., Review of asymmetric beta-lactam synthesis. *Acc. Chem. Res.* **2004,** 37, 592-600.

183. Pirrung, M. C.; Sarma, K.D., β-Lactam Synthesis by Ugi Reaction of β-Keto Acids in Aqueous Solution. *Synlett* **2004**, (08), 1425.

184. Seeman, J. I., Effect of Conformational Change on Reactivity in Organic Chemistry. Evaluations, Applications, and Extensions on Curtin-Hammett-Winstein.Holness Kinetics. *Chem. Rev.* **1983,** 83, 84-134.

185. Seeman, J. I., The Curtin-Hammett Principle and the Winstein-Holness Equation. *J. Chem.* **1986,** 63, 42-48.

186. Boulaiz, H.; Alvarez, P.J., Ramirez, A.; Marchal, J.A.; Prados, J.; Rodríguez-Serrano, F.; Perán, M.; Melguizo, C.; Aranega, A., Nanomedicine: Application Areas and Development Prospects. *Int. J. Mol. Sci.* **2011,** 12, (5), 3303-3321.

187. Wijagkanalan, W.; Kawakami, S.; Hashida, M., Designing Dendrimers for Drug Delivery and Imaging: Pharmacokinetic Considerations. *Pharm. Res.* **2011,** 28, 1500-1519.

188. Fischer, M.; Appelhans, D.; Schwarz, S.; Klajnert, B.; Bryszewska, M.; Voit, B.; Rogers, M., Influence of Surface Functionality of Poly(propylene imine) Dendrimers on Protease Resistance and Propagation of the Scrapie Prion Protein. *Biomacromolecules* **2010,** 11, (5), 1314-1325.

189. Boas, U.; Heegard,, P.M.H., Dendrimers in drug research. *Chem. Soc. Rev.* **2004,** 33, 43-63.

190. Grinstaff, M. W., Biodendrimers: New Polymeric Biomaterials for Tissue Engineering. *Chem. Eur. J.* **2002,** 8, 2839-2846.

191. Stiriba, S. E.; Frey, H.; Haag, R., Dendritic Polymers in Biomedical Applications: From Potential to Clinical Use in Diagnostics and Therapy. *Angew. Chem. Int. Ed.* **2002,** 41, 1329-1334.

192. Ciolkowski, M.; Halets, I.; Shcharbin, D.; Appelhans, D.; Voit, B.; Klajnert, B.; Bryszewska, M., Impact of maltose modified poly(propylene imine) dendrimers on liver alcohol dehydrogenase (LADH) internal dynamics and structure. *New J. Chem.* **2012,** 36, 1992-1999.

193. Klajnert, B.; Appelhans, D.; Komber, H.; Morgner, N.; Schwarz, S.; Richter, S.; Brutschy, B.; Ionov, M.; Tonkikh, A.D.; Bryszewska, M.; Voit, B., The Influence of Densely Organized Maltose Shells on the Biological Properties of Poly(propylene imine) Dendrimers: New Effects Dependent on Hydrogen Bonding. *Chem. Eur. J.* **2008,** 14, 7030-7041.

194. Ziemba, B.; Janaszewska, A.; Ciepluch, K.; Krotewicz, M.; Fogel, W.A.; Appelhans, D.; Voit, B.; Brysqewska, M.; Klajnert, B., In vivo toxicity of polypropylenimine dendrimers. *J. Biomed. Mater. Res. Part A* **2011,** 99, 261-268.

195. Dutta, T.; Jain, N.K., Targeting potential and anti-HIV activity of lamivudine loaded mannosylated poly (propyleneimine) dendrimer. *Biochim. Biophys. Acta* **2007,** 70, 681-686.

196. Kumar, P.V; Asthana, A.; Dutta, T.; Jain, N.K., Intracellular macrophage uptake of rifampicin loaded mannosylated dendrimers. *J. Drug Target* **2006,** 14, 546-556.

197. Arima, H.; Chihara, Y., Arizono M, Yamashita S, Wada K, Hirayama F, Uekama K., Enhancement of gene transfer activity mediated by mannosylated dendrimer/alpha-cyclodextrin conjugate (generation 3, G3). *J. Control Release* **2006,** 116, ((1)), 64-74.

198. Kunath, K. v. H., A.; Fischer, D.; Kissel, T., Galactose-PEI-DNA complexes for targeted gene delivery: degree of substitution affects complex size and transfection efficiency. *J. Control Release* **2003,** 88, ((1)), 159-172.

199. Fahmi, A.; Appelhans, D.; Cheval, N.; Pietsch, T.; Bellman, C.; Gindy, N.; Voit, B., Hybrid nanoalloy: Nanofibers fabricated by self-assembling dendrimers mediate in situ CdSe quantum dots and their metallization with discrete gold nanoparticles *Adv. Mat.* **2011,** 23, 3289-3293.

200. Voit, B.; Rossberg, C.; Appelhans, D.; Komber, H.; Krahl, F.; Arndt, K.-F-: Lederer, A., Self-assembly of anionic core-shell architectures into ph-stable particles with defined dimensions as potential carrier systems. *Polym. Preprints* **2011,** 52, 3466-3468.

201. Appelhans, D.; Komber, H.; Abdul-Quadir, M.; Richter, S.; Schwarz, S.; Van der Vlist, J.; Aigner, A.; Müller, M.; Loos, K.; Seidel J.; Arndt, K.F.; Haag, R.; Voit, B., Hyperbranched PEI with Various Oligosaccharide Architectures: Synthesis, Characterization, ATP Complexation, and Cellular Uptake Properties. *Biomacromolecules* **2009,** 10, (5), 1114-1124.

202. Quadir, M. A.; Radowski,M. R.; Kratz, F.; Licha, K.; Hauff, P.; Haag, R., Dendritic multishell architectures for drug and dye transport. *J. Control Release* **2008,** 132, (3), 289-294.

203. Liu, M.; Kono, K.; Fréchet, J. M. J., Water-soluble dendritic unimolecular micelles:: Their potential as drug delivery agents. *Journal of Controlled Release* **2000,** 65, 121-131.

204. Doores, K. J.; Gamblin, D. P.; Davis, B. G., Exploring and Exploiting the Therapeutic Potential of Glycoconjugates. *Chemistry – A European Journal* **2006,** 12, (3), 656-665.

205. Baigude, H.; Katsuraya, K.; Okuyama, K.; Tokunaga, S.; Uryu, T., Synthesis of Sphere-Type Monodispersed Oligosaccharide−Polypeptide Dendrimers. *Macromolecules* **2003,** 36, (19), 7100-7106.

206. Appelhans, D.; Zhong, Y.; Komber, H.; Friedel, P.; Oertel, U.; Scheler, U.; Morgner, N.; Kuckling, D.; Richter, S.; Seidel, J.; Brutschy, B.; Voit, B., Oligosaccharide-Modified Poly(propyleneimine) Dendrimers: Synthesis, Structure Determination, and CuII Complexation. *Macromolecular Bioscience* **2007,** 7, (3), 373-383.

207. Baigude, H.; Katsuraya, K.; Okuyama, K.; Yachi, Y.; Sato, S.; Uryu, T., Synthesis of dicarboxylate oligosaccharide multilayer terminal functionality upon poly(lysine) dendrimer scaffolding. *Journal of Polymer Science Part A: Polymer Chemistry* **2002,** 40, (21), 3622-3633.

208. Baigude, H.; Katsuraya, K.; Okuyama, K.; Hatanaka, K.; Ikeda, E.; Shibata, N.; Uryu, T., Synthesis of spherical and hemispherical sugar-containing poly(ornithine) dendrimers. *Journal of Polymer Science Part A: Polymer Chemistry* **2004,** 42, (6), 1400-1414.

209. Baigude, H.; Katsuraya, K.; Tokunaga, S.; Fujiwara, N.; Satoyama, M.; Magome, T.; Okuyama, K.; Borjihan, G.; Uryu, T., Synthesis of an oligosaccharide–polylysine dendrimer with reducing sugar terminals leading to acquired immunodeficiency syndrome vaccine preparation. *Journal of Polymer Science Part A: Polymer Chemistry* **2005,** 43, (11), 2195-2206.

210. Duncan, R., The dawning era of polymer therapeutics. *Nat. Rev. Drug Discov.* **2003,** 2, 347-360.

211. Moure, A. Modulación química de rutas de señalización celular: Optimización de compuestos hits identificados a partir de quimiotecas. University of Barcelona, Barcelona, 2009.

212. Kleinekofort, W.; Avdiev, J.; Brutschy, B., A new method of laser desorption mass spectrometry for the study of biological macromolecules. *Int. J. Mass. Spectr. Ion Proc.* **1996,** 152, 135-142.

213. Wattenberg, A.; Sobott, F.; Brutschy, B., Detection of intact hemoglobin from aqueous solution with laser desorption mass spectrometry. *Rapid Commun. Mass. Spectrom.* **2000,** 14, 859-861.

214. Morgner, N.; Barth, H. D.; Schimdt, T. L.; Heckel, A.; Scheffer, U.; Gömel, M.; Brutschy, B., Detecting specific ligant binding to nucleic Acids: A test for Ultrasoft mass spectrometry. *Zeit. Phys. Chem.* **2007,** 221, 689-704.

215. Schrödinger, Suite, LLC, New York, NY, 2011/2012.

216. Maestro, version 9.2 and 9.3, Schrödinger, LLC, New York, NY, 2011/2012.

217. MacroModel, version 9.9, Schrödinger, LLC, New York, NY, 2011.

218. Jorgensen, W. L.; Maxwell, D. S.; Tirado-Rives, J., Development and Testing of the OPLS All-Atom Force Field on Conformational Energetics and Properties of Organic Liquids. *J. Am. Chem. Soc.* **1996,** 118, 11225-11236.

219. Still, W. C.; Tempczyk, A.; Hawley, R. C.; Hendrickson, T., Semianalytical treatment of solvation for molecular mechanics and dynamics. *Journal of the American Chemical Society* **1990,** 112, 6127-6129.

220. LigPrep, version 2.5, Schrödinger, *LLC*, New York, NY, 2011.

221. O'Neil, E. J.; Divittorio, K. M.; Smith, B. D., General Procedure for the synthesis of azides. *Org. Lett.* **2007,** 9, 199-202.